Quantum Measurements in Majorana Circuit Quantum Electrodynamics

Von der Fakultät für Mathematik, Informatik und Naturwissenschaften der RWTH Aachen University zur Erlangung des akademischen Grades eines Doktors der Naturwissenschaften genehmigte Dissertation

vorgelegt von

Dipl.-Phys. Christoph Ohm

aus Olpe

Berichter: Jun.-Prof. Dr. Fabian Hassler
Associate Professor Dr. Thomas Schmidt
Univ.-Prof. Dr. David DiVincenzo

Tag der mündlichen Prüfung: 2. Februar 2016

Christoph Ohm
Institute for Quantum Information
RWTH Aachen University
christoph.ohm@rwth-aachen.de

Typeset by $\mathcal{AMS}$-LaTeX and `makeindex`.

Abstract

Quantum computation is a multifaceted field of research aiming for the physical realization of quantum systems and their manipulation. This thesis discusses the combination of two notable approaches in the pursuit of a fully operational quantum computer—circuit quantum electrodynamics and topological quantum computation based on Majorana quasiparticles. In circuit quantum electrodynamics quantum information is stored into small superconducting circuit elements whose interaction with electromagnetic radiation in the range of microwaves allows to process quantum information very efficiently. This approach has proven extremely useful for control and readout of superconducting qubits, i.e., small circuit elements that carry quantum information. Because of remarkably strong light-matter couplings that can be achieved for superconducting qubits in microwave resonators, the circuit quantum electrodynamics architecture is particularly useful to perform highly sensitive quantum measurements.

Superconductivity by itself is an intriguing state of matter that shows a great variety of different phenomena. In particular, the discovery of topological phases in superconductors opened new horizons for quantum computation. One notable system that admits topological superconductivity is a semiconductor-superconductor nanowire with special zero modes occurring at its ends. These so-called Majorana zero modes are remarkably robust against decoherence and therefore well-suited for fault-tolerant quantum computation.

The first part of this thesis examines the coupling of Majorana zero modes to electromagnetic radiation with microwave frequencies. The light-matter coupling mechanism that is considered here arises for Majorana zero modes located at a voltage-biased superconducting tunneling junction. The emission of microwave radiation in presence of Majorana zero modes gives rise to coherent radiation which is emitted at half of the usual Josephson frequency. On the basis of this fractional Josephson radiation, we propose a microwave readout scheme for Majorana qubits. As usual for typical measurements in circuit quantum electrodynamics, the proposed readout implements a quantum non-demolition measurement for Majorana qubit.

In the last part of the thesis we propose a novel scheme for the implementation of measurement-induced entanglement between remote superconducting qubits as required for quantum communication. By detecting a single photon, that passes a Mach-Zehnder interferometric setup, deterministic entanglement with single-shot efficiency is achieved. This scheme essentially relies on the strong coupling between the qubits and the photon.

Zusammenfassung

Quantencomputing ist ein facettenreiches Forschungsfeld, welches die physikalische Realisierung von Quantensystemen und deren Manipulation beabsichtigt. Die vorliegende Arbeit diskutiert die Kombination zweier bemerkenswerter Ansätze in dem Bestreben nach einem vollständig einsatzfähigen Quantencomputer—die Schaltkreis-Quantenelektrodynamik und topologisches Quantencomputing basierend auf Majorana Quasiteilchen. In der Schaltkreis-Quantenelektrodynamik wird Quanteninformation in kleinen supraleitenden Bauelementen eines Schaltkreises gespeichert, deren Wechselwirkung mit elektromagnetischen Feldern im Mikrowellenbereich es erlaubt Quanteninformation in effektiver Weise zu verarbeiten. Wie sich gezeigt hat, ist dieses Verfahren überaus nützlich zur Kontrolle und zum Auslesen supraleitender Qubits, also derjenigen Bauelemente, die Quanteninformation enthalten. Aufgrund der bemerkenswert hohen Licht-Materie Kopplungsstärken, die für supraleitende Qubits in Mikrowellen-Resonatoren erzielt werden können, ist die Schaltkreis-Quantenelektrodynamik-Architektur in besonderem Maße hilfreich um hochempfindliche Quantenmessungen durchzuführen.

Die Supraleitung selbst ist ein faszinierender Materiezustand, der eine Vielzahl unterschiedlicher Phänomene aufzeigt. Insbesondere die Entdeckung topologischer Phasen in der Supraleitung eröffnete neue Horizonte für das Quantencomputing. Ein bemerkenswertes System, in dem topologische Supraleitung auftritt, ist ein halbleitender-supraleitender Nanodraht an dessen Enden spezielle Nullmoden auftreten. Diese sogenannten Majorana-Nullmoden sind bemerkenswert robust gegenüber Dekohärenz und eignen sich daher ideal für fehlertolerantes Quantencomputing.

Im ersten Teil der vorliegenden Arbeit wird die Möglichkeit untersucht Majorana-Nullmoden an Mikrowellenstrahlung zu koppeln. Der hier betrachtete Licht-Materie Kopplungsmechanismus entsteht für Majorana Nullmoden, die sich an einem supraleitenden Tunnelontakt mit angelegter Spannung befinden. Die Emission von Mikrowellen-Strahlung durch die Majorana-Nullmoden resultiert in kohärenter Strahlung, welche mit der halben Josephson-Frequenz abgestrahlt wird. Auf Basis dieser fraktionellen Josephson-Strahlung wird ein Mikrowellen-basiertes Ausleseverfahren für Majorana-Qubits vorgeschlagen. Wie in der Schaltkreis-Quantenelektrodynamik üblich, kann das vorgeschlagene Verfahren ein das Majorana-Qubit auf nicht-invasive Weise auslesen.

Im letzten Teil der Arbeit wird ein neuartiges Verfahren zur Erzeugung von Quantenverschränkung, welche durch Messung induziert wird, zwischen entfernt liegenden supraleitenden Qubits vorgeschlagen, wie es zur Quantenkommunikation benötigt wird. Durch Messung eines einzelnen Photons, welches einen Mach-Zehnder interferometrischen Aufbau durchläuft, wird Quantenverschränkung deterministisch und mittels einer einzelnen Messung erzeugt. Das diskutierte Verfahren beruht im wesentlichen auf der starken Kopplung zwischen den Qubits und dem Photon.

Acknowledgements

When I started as a PhD student at the Institute for Quantum Information (IQI), the institute was founded just a few month ago. For me it was an interesting experience to witness the institute's rapid evolution from the very beginning; while the IQI comprised just a handful of people in the early days, numerous people have come and gone in my time as a graduate student. Truly, it has been an exciting journey in which I had the pleasure to meet many intriguing personalities whose influence, support, and friendship made this work actually possible.

First and foremost I am indebted to Prof. Fabian Hassler for accepting me as his first PhD student and giving me the opportunity to become a member of the IQI. I am grateful for his patience, guidance and help during the four years of my PhD. It has always been a pleasure to experience his passionate nature in discussions about physics, scientific writing, and politics. Thank you, Fabian, for being my mentor. Moreover, I am pleased and honored that Prof. Thomas Schmidt and Prof. David DiVincenzo agreed to referee this PhD thesis. I am most grateful to both of them for being willing and flexible to meet all "rheonomic constraints" imposed during the refereeing process. Furthermore, I want to thank Prof. Markus Morgenstern and Prof. Thomas Schäpers for agreeing to become members of the PhD commission.

Merci beaucoup, grazie mille, and hartelijk bedankt to all members of the IQI; I always appreciated your great colleagueship as well as the open-minded atmosphere at the institute. In particular, in my time as a member of the IQI it was my pleasure to share an office with Michael Hell, Sebastian Mehl, François Konschelle, Jascha Ulrich, Sebastian Rubbert, Manuel Rispler, Dominique Dresen, and Daniel Otten. Thank you, for many enlightening discussions about physics and for creating a friendly working atmosphere. Likewise, I would like to thank Piotr Ćwikliński, Firat Solgun, Norbert Schuch, Giovanni Viola, Lauri Lehman, Nikolas Breuckmann, Gregor Bransky, Susanne Richer, Shabir Barzanjeh, Ben Criger, Fabio Pedrocchi, and Mohsin Iqbal for many of insightful scientific discussions and lots of memorable moments in the institute's coffee area as well as in the bars of Aachen. Indeed, some of these discussions have been a routine—and tremendously helpful—part of my weekly schedule; therefore I want to express my deep appreciation to Nikolas Breuckmann, Jascha Ulrich, and Johannes Keller for numerous hours of obsessively rigorous and yet equally passionate lessons about differential geometry, topology, and excellent textbooks. For taking care of all administrative matters with her kind and gentle nature I want to thank Hélène Barton.

Moreover, I am grateful for being blessed with the help and encouragement of all my close friends not to mention my great-hearted parents-in-law. In addition to that and because of their enormous importance in my life, I also want to include my dear parents Michael and Christiane Ohm together with my sister Julia. Thank

you, for awakening my interest in physics, always supporting me, and giving me the courage to finish this thesis. Above all, I deeply thank my wife Laura for her immense patience and immeasurable love; through all these years of living apart in two different places you have always been close by my side.

Siegen, 2016 Christoph Ohm

Contents

Notation

Electrodynamics

The unit system for electromagnetic fields used throughout this thesis are the Gaussian units of electromagnetism. For a conversion between Gaussian and SI units see Tab. A.1 in Sec. A.4.

Units and Symbols

$e > 0$	Elementary charge
c	Speed of light
$\mu_\mathrm{B} = \hbar e/2m_e c$	Bohr magneton
m_e	Electron mass
$m^* = 2m_e$	Cooper pair mass
$\Phi_0 = hc/2e$	Superconducting magnetic flux quantum
$\alpha = e^2/\hbar c$	Fine structure constant
$G_0 = 2e^2/h$	Conductance quantum
Ψ	Macroscopic wave function
Φ	Magnetic flux (node flux)
φ	Superconducting phase
$\mathcal{H}_\mathrm{BdG}$	Bogoliubov-de Gennes Hamiltonian
$\mathcal{O}, \mathcal{T}, \mathcal{C}, \mathcal{S}, \ldots$	Operators in Nambu space
$\mathcal{P}, \mathcal{P}_{ij}$	Fermionic parity
S^2	Two-dimensional sphere
$\mathbb{Z}_2 = \{0, 1\} \cong \mathbb{Z}/2\mathbb{Z}$	Cyclic group of order 2 (integers modulo two)
$\boldsymbol{a} \wedge \boldsymbol{b}$	Cross product of two spatial vectors $\boldsymbol{a}$ and $\boldsymbol{b}$
$\mathscr{H}$	Hilbert space
$\mathscr{H}_\mathrm{A} \otimes \mathscr{H}_\mathrm{B}$	Tensor product of two Hilbert spaces $\mathscr{H}_\mathrm{A}$ and $\mathscr{H}_\mathrm{B}$
$\mathcal{T} \exp[X(t)]$	Time-ordered exponential of $X(t)$
$\langle X \rangle$	Expectation value of X
$\langle\langle X \rangle\rangle$	Cumulant of X

Acronyms and Abbreviations

BCS	Bardeen-Cooper-Schrieffer
BdG	Bogoliubov-de Gennes
BZ	First Brillouin zone
c.c.	Complex conjugate
EPR	Einstein-Podolsky-Rosen
cavity QED	Cavity quantum electrodynamics
cQED	Circuit quantum electrodynamics
H.c.	Hermitian conjugate
MZM	Majorana zero mode
MZI	Mach-Zehnder interferometer
QP	Quasiparticle poisoning
SNR	Signal to noise ratio
RWA	Rotating wave approximation

Chapter 1

Introduction

Die Ψ-Funktion ist *als Wissen definiert. . . .*
Sie ist vielmehr identisch mit dem Ergebnis,
in dem der Beobachter ein Faktum erkennt.
— C. F. von Weizäcker

1.1. Quantum Mechanics and Information

With his statement "the Ψ-function is defined as knowledge", von Weizäcker expresses his belief that the quantum mechanical wave function Ψ is a subjective quantity that reflects the degree of knowledge an experimenter has about a quantum system. Thus, when performing a measurement the experimenter updates his knowledge in the instant of time, in which the measurement gives him certainty about the state of the system. In turn, the measurement process projects or—as one might say—collapses the quantum mechanical wave function to a quantum state which is compatible with the acquired information about the system. This is the essence of *von Neumanns's projection postulate* which lies at the heart of the probabilistic interpretation of quantum mechanics.

Following the reasoning of von Weizäcker and his colleagues, the wave function should be understood as a measure of uncertainty, which is inherent to the quantum description itself, to find a specific measurement outcome. Viewing the probabilistic interpretation of quantum mechanics from a more information theoretical perspective, one may be drawn to the conclusion that the wave function is a carrier of information which might be transmitted or even processed by the rules of quantum mechanics. Indeed, utilizing quantum mechanics as a resource for information processing has become a new paradigm that led to the development of quantum information theory. Lying at the frontiers between information theory and quantum physics, quantum information science examines the prospects and limitations of using "quantum information". Meanwhile quantum information science has evolved into a diverse field of research covering many subjects like quantum communication, quantum complexity theory, and quantum computation to name just a few. In particular, the field of quantum computation has taken up the challenge to find physical realizations that comply with the demanding technological requests for fault-tolerant quantum information processing. More concretely, this means to design individual quantum systems, whose elementary constituents carry basic units of "quantum information", that are are well-isolated from the environment in order to be coherently controlled.

Quantum bits and quantum computation In classical information processing the fundamental unit of information is carried by a random variable taking the values (states) 0 and 1. The information content of such a random variable is referred to as a bit. Adapting this concept to quantum mechanics, classical information may be represented by two orthogonal quantum states $|0\rangle$ and $|1\rangle$ called logical states or computational basis states. Contrary to the states of a classical bit, quantum mechanics also allows for superpositions of these logical states,

$$|\psi\rangle = \alpha\,|0\rangle + \beta\,|1\rangle\,.$$

Quantum mechanics demands the complex coefficients α and β to be subject of the normalization condition $|\alpha|^2 + |\beta|^2 = 1$. The normalized state $|\psi\rangle$ is a vector in the two-dimensional complex Hilbert space $\mathscr{H}_2 = \mathbb{C}^2$ spanned by the states $|0\rangle$ and $|1\rangle$. Such a quantum mechanical two-state system is defined to be an elementary unit of quantum information—a quantum bit (or *qubit*). Illustrating the manifold of all single qubit states on the *Bloch sphere* reveals the fundamental differences between classical bit and qubits: the set of qubit states $|\psi\rangle$ are represented by all points on the two-dimensional Bloch sphere, whereas the states of a classical bit only correspond to the two poles of the Bloch sphere, see Fig. 1.1.

In order to be able to access every point on the Bloch sphere, qubit states have to be processed via unitary transformations (qubit gates) acting upon the two-state system. Every quantum computation proceeds in three steps beginning by the preparation of an initial quantum state $|\psi_\mathrm{i}\rangle$ (initialization). In the second step the initial state has to be processed to a desired final state $|\psi_\mathrm{f}\rangle$ by the unitary time evolution $U(t)$,

$$|\psi_\mathrm{f}\rangle = U(t)\,|\psi_\mathrm{i}\rangle = \alpha(t)\,|0\rangle + \beta(t)\,|1\rangle$$

with $\mathrm{i}\hbar\frac{\mathrm{d}}{\mathrm{d}t}U(t) = H(t)U(t)$. In analogy to classical information processing, the Hamiltonian $H(t)$ can be seen as the computer program to be run. In order to find the desired unitary time evolution that maps the initial to the final state, the Hamiltonian needs to be designed carefully; even tiny variations in $H(t)$ may lead to an unwanted final state and therefore spoil the entire computation. Finally, in the last stage of the computation, the state $|\psi_\mathrm{f}\rangle$ is read out, i.e., the state is measured yielding either 0 or 1 with probability $|\alpha(t)|^2$ or $|\beta(t)|^2$. Because of its projective nature, the measurement process collapses the quantum superposition $|\psi_\mathrm{f}\rangle$ to one of the states $|0\rangle$ or $|1\rangle$ in accordance with the measurement outcome. This, of course, makes it impossible to gain information about the probability distribution $|\alpha(t)|^2$, $|\beta(t)|^2$ by repeatedly measuring the same qubit without reinitializing its state over and over again.

Even though an experimenter cannot gain full information about the quantum state with a single measurement, the rules of quantum physics allow to run a certain class of computations exponentially faster than any known classical algorithm. A spectacular example is *Shor's algorithm* demonstrating that on a quantum computer is able to factorize prime numbers exponentially faster than any classical computer

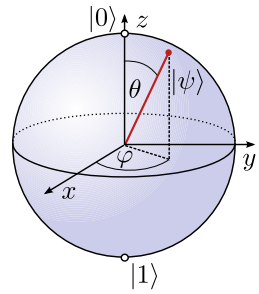

Fig. 1.1.: The Bloch sphere as visualization for the quantum mechanical state space of a two-level system. The computational basis states $|0\rangle$ and $|1\rangle$ are represented by the north and south pole of the sphere. Furthermore, any qubit state is represented as a point on the sphere (red pointer) and can be unambiguously identified by $\alpha = \cos(\theta/2)$ and $\beta = \mathrm{e}^{\mathrm{i}\varphi}\sin(\theta/2)$.

(Shor, 1994). Essentially, this is because the superposition of quantum states allows to perform many[1)] computations in parallel; a quantum computer benefits from the unitarity of the time evolution which takes the coherent sum of all simultaneously performed computations giving rise to what is called *quantum parallelism*, see Nielsen and Chuang (2010).

Entanglement An important aspect of quantum mechanics, which is intrinsic to quantum mechanics and gives rise to the quantum parallelism, is the existence of correlations known as *quantum entanglement*. These non-classical correlations arise by considering composite systems such as multi-qubit quantum devices. For instance, the four-dimensional Hilbert space $\mathscr{H}_\mathrm{A} \otimes \mathscr{H}_\mathrm{B}$ of two qubits A and B is spanned by the tensor product states $|i,j\rangle = |i\rangle_\mathrm{A} \otimes |j\rangle_\mathrm{B}$ with $i,j \in \{0,1\}$. A state is called entangled if it cannot be separated into a product of states which can be independently assigned to A and B. The prime example for such an entangled state living in the composite Hilbert space is the *Bell state*[2)]

$$\left|\Phi^+\right\rangle = \frac{1}{\sqrt{2}}\big(\,|00\rangle + |11\rangle\,\big).$$

For *any* two states $|\psi\rangle_\mathrm{A}$ and $|\phi\rangle_\mathrm{B}$, the Bell state $|\Psi^+\rangle$ cannot be represented as a tensor product, i.e., $|\Phi^+\rangle \neq |\psi\rangle_\mathrm{A} \otimes |\phi\rangle_\mathrm{B}$; for a review on entanglement theory see Horodecki *et al.* (2009).

The irreducibility of entangled states has seemingly paradoxical implications that have challenged generations of physicists. One of the most famous examples is the EPR (Einstein Podolsky Rosen) paradox (Einstein *et al.*, 1935), which intents to demonstrate the absurdity of quantum entanglement by considering spatially separated particles in a (maximally) entangled state as for example $|\Phi^+\rangle$. EPR concluded that quantum mechanics is incomplete, because it fails to be local and realistic.[3)] In fact, almost thirty years after EPR, *J. S. Bell* (1964) put this philosophical question into a mathematical context by demonstrating that two-particle correlations of any

[1)] In fact, exponential many computations in the number of qubits.

[2)] Sometimes also called EPR state.

[3)] Realism means that any measurement result is predetermined before a measurement is performed.

local and realistic theory are incompatible with those of quantum mechanics. Years later, experimental evidences resolved the dispute between local realism and quantum mechanics in favor of quantum mechanics (Freedman and Clauser, 1972; Aspect *et al.*, 1981, 1982).

Despite its counterintuitive predictions, entanglement can be exploited as resource for quantum communication protocols such as quantum teleportation (Bennett *et al.*, 1993) and quantum key distribution (Ekert, 1991). In fact, the quantum key distribution protocol as introduced by *A. K. Ekert* makes a virtue of the EPR paradox by using maximally entangled states in order to guarantee provably secure communication between two distant parties.

Quantum measurements Given the fragility of quantum states, it is important to encode quantum information well-protected from external perturbations. In turn, when it comes to the readout of a qubit, quantum measurements need to be very sensitive in order to accurately extract this information again. In general, the act of measuring a quantum state is characterized by a non-unitary projection of the wave function onto an eigenstate of the measured observable. Formulated in the early days of quantum mechanics, von Neumann's projection postulate is one of the most fundamental principles of quantum mechanics providing a convenient mathematical description for measurements (von Neumann, 1955). However, albeit its mathematical conciseness, the projection postulate merely considers the case of an ideal measurements assumed to happen instantaneously in time.[4)]

With the technological developments in quantum optics during the 1980s, refined experimental techniques offered the possibility to study individual quantum systems. In particular, allowing to measure a single quantum system repeatedly, such experiments revealed further insides into the nature of the measurement process itself. In any case, the projection of the wave function remains as inevitable consequence of the fact that the influence of the meter perturbs the quantum system while measuring it. However, the coupling strength, by which a meter is coupled to the quantum system, decides whether the collapse of the wave function proceeds instantaneously via a *strong projective measurement*, i.e., strictly in the sense of von Neumann or gradually in time via a *weak continuous measurement* (for weakly coupled meters) (Braginsky and Khalili, 1992); as a result of being weakly coupled, the measurement apparatus is required to continuously monitor the quantum system for the amount of time that is needed to obtain full information about the system. Furthermore, in order to prevent measurement-induced back action to obscure the measured quantity (observable), a weak continuous measurement has to be a *quantum non-demolition measurement* which means that the eigenstates of the measured observable coincide

[4)] According to von Weizäcker for example, the collapse of the wave function happens exactly in the moment in which the observer becomes aware of the measurement outcome; even if the interaction with the measurement apparatus has happened long before (von Weizäcker, 1985). Clearly, such an observer-accentuated interpretation—as well as many other interpretations—goes very well together with von Neumann's postulate.

with the stationary states of the quantum system (Braginsky *et al.*, 1980).

The absence of any measurement feedback to the observed quantity implies that a quantum non-demolition measurement is able to determine the quantum state with high accuracy. Such a non-invasive measurement renders the measurement apparatus highly sensitive (with respect to the non-demolition variable). However, since the recorded quantum state is unavoidably altered by measurement-induced detection noise, it gets eventually projected onto an eigenstates of the measured observable. It can be shown that the Heisenberg uncertainty relation requires the minimal amount of time, that is needed to read out the value of the observable, to be limited by the time in which the state collapses to an eigenstate. In other words, this so-called *Heisenberg limit* states that information about the system can be at best extracted as fast as the quantum superposition decays (dephasing), see Braginsky and Khalili (1992); Clerk *et al.* (2010). In fact, there is an intimate relationship between the measurement-induced dephasing rate of a quantum state and the rate of *accessible information* an observer can maximally infer (Clerk *et al.*, 2003).

Nowadays, quantum non-demolition measurements are part of the experimental repertoire and frequently used because of their high sensitivities. Among the most spectacular applications of quantum non-demolition measurements is the non-destructive detection of single photons (Nogues *et al.*, 1999). Furthermore, the increased sensitivity of quantum non-demolition measurements as for example the dispersive readout scheme for superconducting qubits (Blais *et al.*, 2004; Wallraff *et al.*, 2004; Lupascu *et al.*, 2007) makes them very attractive and—especially for weak coupling strengths—indispensable for the purpose of quantum information processing.

1.2. Routes to Implementation: Superconductivity

In principle, every two-state system in the physical world, that can be manipulated in a controlled manner, may serve as a qubit. However, most quantum systems are sensitive to decoherence, i.e., the uncontrollable coupling of qubits to their environment. Indeed, it is one of the major challenges of quantum computation technology to raise coherence times above the typical time scales of gate operations. Moreover, to harness the power of quantum computation, it will be necessary to control hundreds or thousands of connected qubits coherently. Nevertheless, there are several approaches to implement physical qubits such as ions trapped in a laser field or solid state devices employing the electron's charge or spin degree of freedom. Furthermore, an important and promising field is the branch of superconducting qubits which attempts to implement quantum bits by using superconductivity.

Ever since its discovery, superconductivity has been of great importance for the understanding of quantum coherence. Roughly fifty years after its discovery in 1911, the time was ripe to exploit superconductivity for highly sensitive electronic devices; the superconducting tunneling effect, which has been predicted by *B. D. Josephson*

in 1962, opened the possibility to use superconducting devices called *Josephson junctions* (superconducting tunneling junctions) as highly accurate microwave detectors as well as lossless electronic mixers. Furthermore, so called superconducting quantum interference devices (SQUIDs), consisting of two superconducting tunneling junctions in a ring geometry, constitute ultra-sensitive detectors for magnetic fluxes. SQUID devices are capable to resolve fluctuations in the magnetic flux with an accuracy down to a single flux quantum $\Phi_0 = hc/2e$. Because of their high sensitivities, superconducting devices are used as high precision instruments with a multitude of applications, e.g., as detectors for magnetic fields in the human brain (Cohen, 1972) as well as ultra-precise gyroscopes to verify the Lense-Thirring effect (Everitt *et al.*, 2011) just to name a few. Moreover, it has been speculated that Josephson junctions may be even well-suited for the hunt of cold dark matter in form of the hypothetic axion particle (Beck, 2013).

With the ongoing advances of nanoscale fabrication techniques, electrical circuits and superconducting devices could be constructed at sizes that got increasingly smaller. Eventually, the extend of superconducting devices has reached a degree of miniaturization that unfolded their quantum properties. With the observation of coherent quantum superpositions of collective excitations in mesoscopic tunneling junctions in the 1990s, the era of superconducting qubits has begun. Up to the present time, the field of superconducting qubits has made rapid progress. By virtue of various qubit designs, the coherence times of superconducting qubits could be progressively improved. In addition to that, current nanotechnology also offers the flexibility to realize a great variety of qubit architectures. This, of course, gives the opportunity to incorporate other physical components such as microwave resonators or semiconducting devices into the qubit architecture.

Clearly, one of the most exciting examples for the synergy of diverse physical phenomena is the interplay between superconductivity (in form of superconducting qubits) and electromagnetic radiation (microwave fields) in a setup known as *circuit quantum electrodynamics*. By placing superconducting qubits inside a microwave resonator, the interaction between microwave photons and the qubits allows for coherent control and efficient non-demolition readout of the superconducting qubits. Since the early days of quantum mechanics the study of matter interacting with the (quantized) electromagnetic field has been playing a predominant role for the development of quantum mechanics. Being able to access ultra-strong light-matter couplings, circuit quantum electrodynamics raises this story to a new level of precision. By achieving high coupling strengths, circuit quantum electrodynamics is capable to probe quantum phenomena such as entanglement or quantum measurements on a fundamental level involving only a few quantum particles.

Superconductivity bears an enormous potential for quantum computation with applications far beyond circuit quantum electrodynamics. A new world of complex and subtle phenomena emerge in a state known as *topological superconductivity*. Within the last decade, the study of topological phases of matter in all kinds of materials

has attracted a lot of interest in condensed matter physics and quantum information science. *topological quant. comp.* is an approach that uses concepts of topology and its manifestations in physics for the implementation of a quantum computer. As the coupling of a qubit to the environment is hard to control, topological quantum computation circumvents this problem by encoding the quantum information into global properties of a physical system and thus making it insensitive to local perturbations. Several ways of implementing topological quantum computation, ranging from fractional quantum Hall systems to topological superconductors, have been proposed (Kitaev, 2001, 2003; Das Sarma *et al.*, 2005; Nayak *et al.*, 2008). In the case of topological superconductors, Majorana zero modes[5)] occur as mid-gap states localized in vortex cores of two-dimensional samples or at the ends of one-dimensional semiconducting nanowires. Most strikingly, Majorana zero modes obey neither Bose-Einstein nor Fermi-Dirac statistics, but a generalized type of particle statistics known as *non-Abelian exchange statistics*. This makes them very attractive for fault-tolerant quantum computation applications as unitary gates can be simply applied by braiding Majorana quasiparticles. A specific physical system, in which Majorana zero modes are expected to occur, are semiconducting nanowires in proximity to a conventional superconductor in a moderate magnetic field. Crucially, using semiconductor-superconductor hybrid devices allows for practical implementations of Majorana zero modes as well as integrated designs of superconducting and Majorana-based qubits.

1.3. Outline of the thesis

This thesis examines the interplay of superconductivity, electromagnetic radiation, and topological states in form of Majorana-based qubits. More specifically, the main focus of the thesis lies on diverse applications of microwave-based quantum measurement techniques for the purpose of quantum computation. One of the main goals of the thesis is to investigate the possibility of integrating Majorna-based qubits into the framework of circuit quantum electrodynamics dubbed *Majorana circuit quantum electrodynamics*. Another part of the thesis is dedicated to the generation of EPR-like entanglement, i.e., entanglement between remote superconducting qubit via methods of microwave engineering. Results of this thesis that have been published in advance will be explicitly indicated in following as well as in the main text.

Chapters 2 and 3 set the basic background for superconducting qubits, circuit quantum electrodynamics, and Majorana zero modes. Without intending to provide an exhaustive overview of these two fields, Chapters 2 and 3 shall review the basic concepts of circuit quantum electrodynamics and Majorana qubits.

Chapter 4, which is a reprint of the article of Ohm and Hassler (2014), studies the interaction of Majorana zero modes localized at a voltage-biased Josephson junction

[5)] Sometimes simply called Majorana fermions.

with electromagnetic field, even though Majorana zero modes are electrically neutral excitations. This coupling gives rise to coherent radiation that is emitted from the Josephson junction similar to the conventional Josephson radiation. Physical implementations for this kind of light-matter interaction will be discussed. Within a semiclassical analysis of the radiation field, it will be shown that the phase of the radiation field gets locked to the superconducting phase difference and that the radiation is emitted precisely at half the Josephson frequency. In order to confirm the coherence of the radiation and to gain information about the state of the zero modes, correlations of the radiation emitted by two spatially-separated junctions in a dc-SQUID geometry will be discussed. Within this analysis decoherence due to spontaneous state-switches as well as due to quasiparticle poisoning will be taken into account.

Chapter 5 builds on the results of the preceding chapter and describes a microwave-based readout for Majorana qubits. Parts of Ch. 5 have been adapted from Ohm and Hassler (2015b). As quantum information is stored in the topological properties of a Majorana qubit, local noise cannot lead to decoherence. Accordingly, the measurement is challenging as the quantum information is well hidden and thus inherently hard to access. The setup discussed in Ch. 5 measures the state of a Majorana qubit by coupling a transmission line resonator to the Majorana qubit similar to the architecture of circuit quantum electrodynamics. Employing the coupling mechanism described in Ch. 4, photons at half of the Josephson frequency are emitted or absorbed from the qubit when placing it in a microwave resonator. By detuning the system into the dispersive regime, the device allows to read out the qubit by performing quantum non-demolition measurements that may reach the Heisenberg limit. An appealing feature of this technique is the fact that the interaction of the Majorana qubit with the cavity field can be turned on and off at will by changing the dc bias of the Josephson junction.

Chapter 6 discusses the generation of entanglement by using quantum measurements. This chapter is a reprint from the article of Ohm and Hassler (2015a). As on-demand creation of entanglement between distant qubits is desirable for quantum communication devices, Ch. 6 proposes a new entanglement scheme for remote superconducting qubits achieving deterministic entanglement with single-shot efficiency. Within this scheme entanglement is generated by detecting a single photon passing through a Mach-Zehnder interferometer with one transmon qubit in each arm. The entanglement production essentially relies on the fact that superconducting microwave structures allow to achieve strong coupling between the qubit and the photon. By detecting the photon via a photon counter, a parity measurement is implemented and the wave function of the two qubits is projected onto a maximally entangled state. Moreover, due to the indivisible nature of single photons, this scheme promises full security for entanglement-based quantum key distribution. Finally, I want to give a brief outlook for the presented topics in Ch. 7.

Chapter 2

Circuit quantum electrodynamics

The field of circuit quantum electrodynamics (cQED) is the discipline dealing with superconducting qubits and their interaction with microwave photons. Over the past decade this field has became a mature field of quantum technology offering a flexible way of designing scalable architectures for quantum computation and achieving high coherence times.

The basic concepts of cQED are deeply rooted in quantum optics and in particular in cavity quantum electrodynamics. Hence, this chapter begins with a brief review of the main elements of cavity quantum electrodynamics focussing on the ability to manipulate quantum states and engineer entanglement. Although the philosophy of cQED is quite very close to that of cavity quantum electrodynamics, the cQED architecture is composed of completely different constituents—superconducting circuits. Therefore, all basic ingredients of superconducting electronics, including Josephson junctions, quantization of lumped circuit elements, and superconducting waveguides, will be discussed the following section. Equipped with these basic elements, the primary aim of the next section is to introduce the transmon qubit, which is the most common superconducting qubit at the time. Then, in the last section the cQED architecture, in which all the concepts introduced before are united, will be introduced. In the spirit of cavity quantum electrodynamics this architecture allows for the manipulation and the readout of transmon qubits via microwave photons.

2.1. Prelude: Cavity quantum electrodynamics

Since the early days of quantum optics, it has been desired to study the interaction of the quantized light field with a few or even a single atom. Due to the elusive character of individual atoms, this undertaking was unachievable for a long time. Cavity quantum electrodynamics (cavity QED) finally opened the opportunity to realize this situations by trapping single atoms inside a high-quality cavity (optical or microwave) (Meschede *et al.*, 1985; Thompson *et al.*, 1992; An *et al.*, 1994). From its original intention to investigate the interactions of single atoms with quantized radiation modes, cavity electrodynamics has evolved into a field that allows to control and manipulate individual quantum systems at high precision (Berman, 1994; Kimble, 1998; Walther *et al.*, 2006).

In the course of time two branches of cavity QED have been developed: the optical branch uses photons with optical frequencies being captured in between mirrors (Miller *et al.*, 2005; Vahala, 2003), whereas the microwave-based branch of cavity

QED exploits microwave transitions in *Rydberg atoms*, i.e., atoms that are in excited states with a high principal quantum number and uses superconducting cavities to capture single microwave photons (Raimond *et al.*, 2001).

In both cases, the light-matter interaction of the electrons with the radiation field is mediated by the electrical dipole interaction. In general, light-matter interaction of atomic systems is mediated by the atomic dipole Hamiltonian. For an atom consisting of Z electrons bound to the nucleus, the dipole Hamiltonian is given by

$$H_{\mathrm{dip}} = -\boldsymbol{d}\cdot\boldsymbol{E} = e\sum_{i=1}^{Z}\boldsymbol{r}_i\cdot\boldsymbol{E}(\boldsymbol{r}_i) \tag{2.1}$$

where $\boldsymbol{r}_i$ is the position operator of the ith electron and

$$\boldsymbol{E}(t,\boldsymbol{r}) = \mathrm{i}\sum_{k,\lambda}\sqrt{\frac{2\pi\hbar\omega_k}{L^3}}\boldsymbol{\epsilon}_\lambda\,\mathrm{e}^{-\mathrm{i}(\omega_k t-\boldsymbol{k}\cdot\boldsymbol{r})}a_k + \mathrm{H.c.} \tag{2.2}$$

is the electrical field operator for a field inside a cavity of volume L^3, see App. A. Expression (2.1) describes the total interaction of the electric field in the cavity. Most often, only a few atomic transitions are nearly on resonance with a particular cavity mode k, i.e., $\omega_k \approx (E_i - E_j)/\hbar$ where E_i, E_j denote atomic energy levels. Then, all off-resonant atomic transitions do not essentially contribute to (2.1) and therefore can be discarded. This approximation is called the *resonance approximation*. Assuming that only a single atomic transition $i \leftrightarrow j$ to be resonant, the atom can be approximately described as a two-level system $|\psi_i\rangle$ and $|\psi_j\rangle$ coupled to a single cavity mode with frequency ω. Furthermore, by performing a second approximation, known as the *rotating wave approximation* (RWA), the light-matter interaction is reduced only to terms which are energetically favorable. By exploiting these two approximations, a two-level atom coupled to electromagnetic radiation in a cavity QED setup can be modeled by the *Jaynes-Cummings Hamiltonian* (Jaynes and Cummings, 1963)

$$H_{\mathrm{JC}} = \hbar\omega a^\dagger a + \frac{\hbar\Delta}{2}\sigma_z + \hbar(ga\sigma^+ + g^* a^\dagger\sigma^-). \tag{2.3}$$

Here the atomic degrees of freedom are represented by the pseudo-spin operators $\sigma_+ = |\psi_i\rangle\langle\psi_j|$, $\sigma^- = |\psi_j\rangle\langle\psi_i|$, and $\sigma_z = |\psi_i\rangle\langle\psi_i| - |\psi_j\rangle\langle\psi_j|$. Furthermore, the energy splitting between the two levels is denoted by $\Delta = E_i - E_j$ and the effective light-matter coupling strength $g \simeq (E_{\mathrm{zp}}/\hbar)\sum_\lambda \boldsymbol{\epsilon}_\lambda\cdot\boldsymbol{d}$ scales with the zero-point field amplitude $E_{\mathrm{zp}} = (2\pi\hbar\omega/L^3)^{1/2}$. Here $\boldsymbol{d} = -e\,\langle\psi_i|\boldsymbol{r}|\psi_j\rangle$ is the transition dipole moment.

The Jaynes-Cummings model is an exactly solvable model. The Hamiltonian (2.3) acts upon the Hilbert space $\mathscr{H}_{\mathrm{at}}\otimes\mathscr{H}_{\mathrm{cav}}$ which is spanned by the tensor product of the photon number states $|n\rangle$ and the two-dimensional subspace $|\psi_i\rangle, |\psi_j\rangle$. Due to the fact that the light-matter interaction preserves the number of excitation quanta $N_{\mathrm{JC}} = a^\dagger a - \frac{\sigma_z}{2}$ in the system,[1)] the Jaynes-Cummings model is easily solvable. The

[1)] The quantity N_{JC} is a constant of motion, $[H_{\mathrm{JC}}, N_{\mathrm{JC}}] = 0$, and therefore allows to decompose the Hilbert space $\mathscr{H}_{\mathrm{at}}\otimes\mathscr{H}_{\mathrm{cav}}$ into pairs of coupled states.

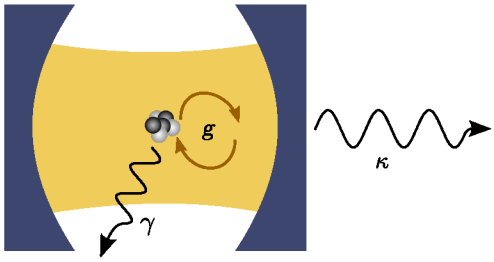

Fig. 2.1.: The cavity QED setup: a single atom (gray and black) placed inside an optical or microwave cavity (blue) coupled to the field mode (yellow) inside the cavity and performing Rabi cycles (brown) due to the light-matter interaction g. Dissipation of the atom is induced by emission into other modes with a rate γ and losses of the cavity field are given by the relaxation rate κ.

eigenstates of H_{JC} are found to be the dressed states

$$|n,\pm\rangle = \cos(\theta)\,|\psi_j\rangle \otimes |n+1\rangle \pm \sin(\theta)\,|\psi_i\rangle \otimes |n\rangle\,. \tag{2.4}$$

The angle $\theta = \frac{1}{2}\arctan[\Omega_n/(\omega-\Delta)]$ is a function of the *Rabi frequency* $\Omega_n = 2g\sqrt{n+1}$ and the level detuning $\omega - \Delta$. When driven on resonance $\omega = \Delta$, the atom-cavity system gets maximally hybridized and performs oscillations with the Rabi-frequency.

In the first place it seem natural that an atom can be approximated as a two-level system, but this approximation, however, works only to a certain extend. This is because at some point relaxation processes in form of other photon-emitting transitions may become important as well. Typically, the life time of an atom is in the regime of 60 ns − 30 ms (Blais *et al.*, 2004). In addition to that, radiation may also leak through imperfect mirrors out of the cavity. This causes a decay of the field inside the cavity with at a characteristic time scale Q/ω_k; the quality factor Q roughly determines the number of photon oscillations before the photon is released from the cavity. Commonly, in cavity QED experiments high-Q cavities with a quality factor of the order $Q \approx 10^7 - 10^8$ are used.

All relaxation processes drive the state of the system out of the considered Hilbert space $\mathscr{H}_{\mathrm{at}} \otimes \mathscr{H}_{\mathrm{cav}}$ of the Jaynes-Cummings model. In order to describe the effective evolution of the two-level atom plus cavity field, the system has to be described in terms of the (reduced) density operator $\rho(t)$ which obeys the *master equation*

$$\frac{\mathrm{d}\rho}{\mathrm{d}t} = -\frac{\mathrm{i}}{\hbar}[H_{\mathrm{JC}},\rho] + \sum_{\mu}\Gamma_\mu\left(J_\mu\rho J_\mu^\dagger - \frac{1}{2}\{J_\mu^\dagger J_\mu,\rho\}\right). \tag{2.5}$$

Equation (2.5) is a master equation in the *Lindblad form*. This form can be derived by considering a quantum Markov process in the limit of weak coupling between the atom-cavity system and its environment (Gardiner and Zoller, 2004). The operators J_μ are arbitrary operators that model the various relaxation processes labeled by the index μ, and Γ_μ are the relaxation rates of the respective relaxation channels. Generically, the evolution of the density operator induces an exponential decay of all observables; the characteristic relaxation rate of the cavity is κ and the relaxation rate γ causes a finite life time of the atomic excitations.

In the presence of dissipation, the evolution of the system is a mixture of two competitive processes—the light-matter interaction and the dissipation induced re-

laxation. In many situations relaxation processes are strongly dominating over effects from the light-matter interaction. An illustrative example is the laser where an ensemble of atoms is collectively emitting radiation. Above the lasing threshold the atomic ensemble is in a nonequilibrium state far from thermal equilibrium that can be only maintained by actively pumping energy into the system (Scully and Lamb, 1967). In contrast, by constructing high-finesse cavities (optical or microwave), cavity QED allows to access the *strong coupling regime* where the light-matter interaction is much stronger than all dissipation-inducing energy scales, $g \gg \kappa, \gamma$. When the light-matter interaction is the dominating energy scale, the quantum nature of the cavity field and the light-matter interaction is revealed. Furthermore, within the strong coupling regime of cavity QED, the validity of the Jaynes-Cummings model (2.3) has been verified, e.g., by the observation of *vacuum Rabi oscillations* (Rempe *et al.*, 1987). Moreover, many experiments have been demonstrating fundamental quantum phenomena such as *Schrödinger cats* (macroscopic quantum superpositions) (Brune *et al.*, 1996), EPR-pair entanglement (Hagley *et al.*, 1997), as well as the non-demolition measurement of single photons (Nogues *et al.*, 1999) which, remarkably, allows to monitor the gradual collapse of the wave function in time (Gleyzes *et al.*, 2007; Guerlin *et al.*, 2007).

To optimize the performance of such quantum protocols it is desirable to engineer the coupling $g \simeq eRE_{\mathrm{zp}}/\hbar$ as strong as possible. To do so one may choose atoms with rather large radii R, called Rydberg atoms, corresponding to large dipole moments $d \simeq eR$. Furthermore, since the zero-point field strength $E_{\mathrm{zp}} = (2\pi\hbar/L^3)^{1/2}$ increases with the cavity volume, it is useful to have small cavities. In total the light-matter coupling has an upper limit which is set by the atomic radius R and the minimal cavity volume set by the cubic wavelength $(2\pi c/\omega)^3$, resulting in the approximate expression

$$g_{3\mathrm{D}} \simeq \omega \frac{R}{\lambda} \left(\frac{\alpha^2}{3}\right)^{\frac{1}{4}} \tag{2.6}$$

where $\alpha = e^2/\hbar c \approx 1/137$ is the fine structure constant. Note that this approximation depends on the shape of the cavity and is therefore different for other geometries. That is to say, by choosing for example a one-dimensional cavity, i.e., a cylindrical cavity with small radius $r < \lambda$, much higher coupling constants can be achieved,

$$g_{1\mathrm{D}} \simeq \omega \frac{R}{r} \left(\frac{2\alpha}{\pi}\right)^{\frac{1}{2}} > g_{3\mathrm{D}}. \tag{2.7}$$

This demonstrates that more specific architectures with one-dimensional cavities such as in circuit QED allow to reach the the strong coupling regime more easily than the conventional cavity QED setting. In addition to such principal matters, cavity QED also involves technical difficulties. Since it is challenging to place individual atoms at the right position, namely at an antinode of the cavity field, it is difficult to keep control about the coupling strength and to address the atomic quantum state.

These technological difficulties make it hard for cavity QED setups to engineer large-scale, highly controllable quantum systems as required for quantum computational purposes.

Just in the spirit of cavity QED, circuit QED attempts to solve these matters by integrating small superconducting tunnel junctions as artificial atoms into one-dimensional superconducting cavities. Importantly, due to the nature of the superconducting state, decoherence is naturally inhibited in these circuits. Furthermore, the possibility to fabricate on-chip circuit designs allows to achieve full control—even for large-scale quantum devices.

2.2. Superconducting electronics in the quantum regime

Common electric circuits used for technology in everyday's life are primarily made of metals like copper or copper-based alloys. There is one thing all these metals have in common: they exhibit electric resistance when a finite voltage is applied. The electrical resistance of a metal microscopically emerges by electron-phonon scattering as well as scattering at lattice defects in the metal. From this microscopical explanation, it should be clear that resistors absorb electrical energy and convert this energy into heat. However, when cooled below a critical temperature, a certain class of metals called superconductors has the remarkable property of loosing their electrical resistance therefore dissipating no energy. The property of superconductors to carry electrical currents with essentially no dissipative losses, makes superconductors ideal candidates for the conduction of currents with intensity as required for quantum devices. Moreover, with the invention of superconducting tunneling junctions, superconducting devices became standard tools in electrical engineering. Since more than two decades, superconducting circuits provide a platform for engineering quantum mechanical devices and validating textbook quantum mechanics.

2.2.1. Classical Josephson junctions

A superconducting tunnel junction, which consists of two superconducting electrodes separated by a thin tunnel barrier. Such a barrier can be realized by a layer of an insulating material, that has been grown between the electrodes, or by a piece of normal conducting metal connecting the electrodes. These variants are abbreviated as S-I-S or S-N-S junctions with S, I, and N abbreviating superconductor, insulator, and normal conducting metal, see Fig. 2.2. Typically, for an S-I-S junction the insulating barriers have a thickness of $d \simeq 1\,\mathrm{nm}$ (Van Duzer and Turner, 1999).

Due to quantum mechanical tunneling, Cooper pairs may pass across the junction from one superconducting electrode to another. This transfer of Cooper pairs means that an electrical current is flowing across the junction without having applied a voltage to the junction. This dissipationless supercurrent is a consequence of the macroscopic phase coherence as described by the Ginzburg-Landau theory. Suppose

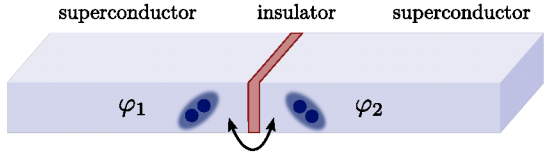

Fig. 2.2.: Josephson junction made of two superconductors (bluish color) separated by an insulating tunnel barrier (red). Cooper pairs (blue dots) are tunneling across the insulating barrier thereby causing a supercurrent $I_c \propto \sin\varphi$ driven by the superconducting phase difference $\varphi = \varphi_1 - \varphi_2$.

each superconducting electrode $i = 1, 2$ has a macroscopic wave function $\Psi_i = |\Psi|e^{i\varphi_i}$ with individual phases φ_i, but each wave function has the same amplitude. Then, the supercurrent follows from the Ginzburg-Landau equations

$$I(\varphi) = I_c \sin\varphi, \tag{2.8}$$

where I_c is the *critical current* and $\varphi = \varphi_1 - \varphi_2$ the *superconducting phase difference* across the junction. The critical current is determined by the modulus of the macroscopic wave function as well as by the length L and the contact area A of the tunneling barrier, $I_c = (e\hbar|\Psi|^2/m_e) \times A/L$. The energy of the junction then reads

$$E(\varphi) = E_J\big(1 - \cos\varphi\big) \tag{2.9}$$

with $E_J = (\hbar/2e)I_c$ being called the Josephson energy. Equation (2.8) constitutes a relation between the supercurrent and the superconducting phase gradient and is a central equation for Josephson junctions. It was first found from microscopic considerations by B. D. Josephson and is also known as the *first Josephson relation*. The first Josephson relation indicates that the supercurrent is driven by a phase difference instead of a voltage drop. This is why supercurrents differ from normal currents; they are driven by gradients of the superconducting phase.

Now suppose a finite bias voltage V_{bias} is applied to the superconducting electrodes of a Josephson junction. In contrast to the electrostatic potentials ϕ_1 and ϕ_2 at the electrodes, the bias voltage is a gauge-invariant quantity. Therefore it is expected to have an effect on the junction's dynamics in form of a relationship to the phase difference φ, which is also a gauge-invariant quantity. Owing to the fact that the macroscopic wave function describes a field carrying charge $-2e$, the sought after relationship takes the form

$$\dot{\varphi} = \frac{2e}{\hbar} V(t) \tag{2.10}$$

and is called the *second Josephson relation*.

The two relations (2.8) and (2.10) fully explain the behavior of an ideal Josephson junction. However, in reality every Josephson junction has a shunting capacitance between the two superconducting electrodes and dissipates energy. To account for these mechanisms the RCSJ (resistively and capacitively shunted junction) model considers a real Josephson junction to consist of an ideal one, a capacitor and a resistor in parallel as shown in Fig. 2.3 (a). The capacitance C of the junction is

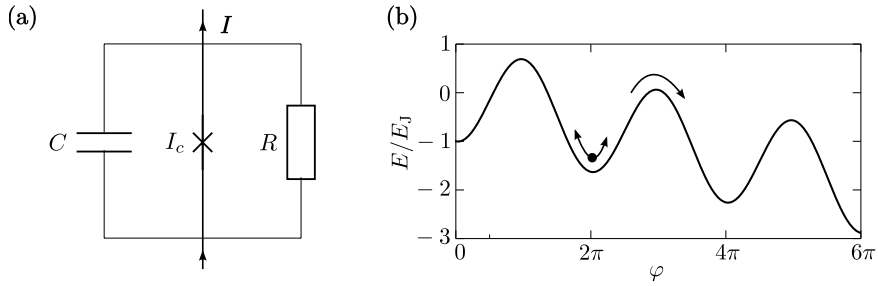

Fig. 2.3.: (a) Circuit representation of a Josephson junction in the RCSJ model. (b) A particle moving in the tilted-washboard potential.

determined by its geometry and the magnitude of the resistance R is of the same scale as the barrier resistance, $R \simeq R_n$. Including effects of the capacitance as well as the resistance the total current traversing a Josephson junction is

$$\begin{aligned} I &= I_c \sin\varphi + \frac{V}{R} + C\dot{V} \\ &= I_c \left(\sin\varphi + \frac{1}{RC\omega_\mathrm{p}^2}\dot{\varphi} + \frac{1}{\omega_\mathrm{p}^2}\ddot{\varphi} \right). \end{aligned} \tag{2.11}$$

In order to eliminate V, Eq. (2.10) has been used. Furthermore, $\omega_\mathrm{p} = \left(2eI_c/\hbar C\right)^{1/2}$ is the plasma frequency of the electric fluid in the Josephson junction. Eq. (2.11) describes the "motion" of the superconducting phase as an particle with mass $\hbar^2 C/4e^2$ moving in the effective potential $V_\mathrm{eff} = -E_\mathrm{J}\cos\varphi - (\hbar I/2e)\varphi$ and subject to the frictional force $(\hbar/2e)^2(1/R)\dot{\varphi}$. Because of its characteristic shape, the effective potential is called the tilted washboard potential, see Fig. 2.3 (b).

So far, the treatment of a Josephson junction was entirely classical, except for the fact that superconductivity itself arises as a quantum effect. However, the constant progress in superconducting technology in the late 1980s allowed to manufacture superconducting circuits small enough to observe the quantum behavior of its macroscopic quantities—current and voltage. Both, current and charge, are quantities that emerge from the collective motion of Cooper pairs in the superconductor and it has been a longstanding question whether these quantities show quantum effects at all (Devoret *et al.*, 1985; Clarke *et al.*, 1988). Although the verification of coherent superpositions had been elusive for over a decade (Bouchiat *et al.*, 1998; Nakamura *et al.*, 1999), these technologies finally allowed to design quantum bits upon these macroscopic degrees of freedom.

2.2.2. Quantizing electrical circuits

The electric fluid in a superconductor, consisting of a large number of Cooper pairs with charge $-2e$, may randomly fluctuate over the extend of the superconductor. In

fact, the local Cooper pair density is given by the squared modulus of the macroscopic wave function $|\Psi(t,\boldsymbol{r})|^2$ being susceptible to the electromagnetic environment of the superconductor. Even so, as long as the frequencies of the electromagnetic perturbations are below the plasma frequency of the superconducting fluid $\omega_\mathrm{p}^2 = 4\pi n_e e^2/m_e$, oscillations of the Cooper pair charge density are strongly suppressed. In that case the dynamical degrees of freedom of the superconductor reduce to a spatially constant charge density and its derivative—the current density. Since the Cooper pair condensate then essentially reacts like a rigid object to electromagnetic influences, the superconductor can be described as a single lumped electric circuit element with charge $Q(t) = -2e\int|\Psi(t,\boldsymbol{r})|^2\mathrm{d}^3r$ and total current $I = \dot{Q}$ (flowing in or out of the superconductor).

With decreasing size of the superconductor its quantum behavior in form of quantum fluctuations of Q and I are revealed. One approach to find the correct quantum description for small superconducting devices is to approximate a Josephson junction formally an electric LC circuit, which is the circuit equivalent of a mechanical spring. The analogy of mechanical systems and electric circuits well known in electrical engineering and because of the harmonic oscillator's omnipresence in physics, this is a very illustrative example how to introduce quantum variables to (superconducting) electronics. For mesoscopic Josephson junctions the characteristic frequencies turn out to be in the regime of microwaves $\omega_\mathrm{p} \approx 2$–$30\,\mathrm{GHz}$ (Schoelkopf and Girvin, 2008).

The LC circuit consists of an inductance L and a capacity C, see Fig. 2.4. Instead of describing the circuit in terms of variables I and V, it is useful to represent the circuit in terms of the charge Q and the node flux to ground

$$\Phi(t) = c\int_{-\infty}^{t} V(t')\mathrm{d}t'. \tag{2.12}$$

According to Eq. (2.10) the node flux is related to the superconducting phase to ground, $\varphi = 2\pi\Phi/\Phi_0$.[2)]

The electric energy of the LC circuit is either stored in form of charge sitting on the capacitor plates $E_\mathrm{C} = Q^2/2C$ or as flux penetrating the inductor with energy $E_\mathrm{L} = \Phi^2/2L$. Then, the total energy $E_\mathrm{C} + E_\mathrm{L}$ must coincide with the Hamiltonian of the LC circuit,

$$H_\mathrm{LC} = \frac{Q^2}{2C} + \frac{\Phi^2}{2L}. \tag{2.13}$$

Because H_LC is quadratic in the variables Q and φ, the LC resonator is the electrical analog of a mechanical quantum harmonic oscillator in one dimension; the oscillation frequency is given by $\omega_\mathrm{LC} = c/\sqrt{LC}$ and the canonically conjugated momentum of Φ is Q/c. For an illustration of this electric-mechanical analogy see Tab. 2.1. At the

[2)] Later, it will be also useful to use variables N (Number of Cooper pairs) and φ (superconducting phase) instead of Q and Φ.

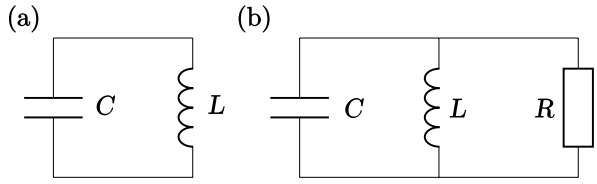

Fig. 2.4.: Electrical circuit diagrams of the (a) LC-resonator and (b) the dissipative LCR-resonator.

quantum level the variables Φ and Q need to become operators and according to the canonical quantization procedure they obey the canonical commutation relation

$$[\Phi, Q] = \mathrm{i}\hbar c. \tag{2.14}$$

For the moment it is assumed that the spectra of Q and Φ are real and continuous just like x and p in the mechanical case.

As known from the quantum harmonic oscillator, it is useful to introduce creation and annihilation operators. With the correspondence between mechanical and electrical quantities the creation and annihilation operators take the form

$$a = \sqrt{\frac{C\omega_{\mathrm{LC}}}{2\hbar c^2}}\left(\Phi + \frac{\mathrm{i}c}{C\omega_{\mathrm{LC}}}Q\right), \qquad a^\dagger = \sqrt{\frac{C\omega_{\mathrm{LC}}}{2\hbar c^2}}\left(\Phi - \frac{\mathrm{i}c}{C\omega_{\mathrm{LC}}}Q\right). \tag{2.15}$$

Then, the spectrum of H_{LC} follows from the algebra $[a, a^\dagger] = 1$ of these ladder operators,

$$E_{\mathrm{LC,n}} = \hbar\omega_{\mathrm{LC}}\left(n + \frac{1}{2}\right). \tag{2.16}$$

The ground state $|0\rangle$, which is determined by the usual condition $a\,|0\rangle = 0$, is given by the wave function

$$\psi_0(\Phi) = \frac{1}{\left(2\pi\Phi_{\mathrm{zp}}^2\right)^{1/4}} \exp\left[-\left(\frac{\Phi}{2\Phi_{\mathrm{zp}}}\right)^2\right] \tag{2.17}$$

in flux representation. The normalization of the wave function $\psi_0(\Phi)$ is determined by the amplitude of its zero-point fluctuations

$$\Phi_{\mathrm{zp}}^2 = \langle 0|\Phi^2|0\rangle = \frac{\hbar c}{2}\sqrt{\frac{L}{C}}. \tag{2.18}$$

By the repeated action of $a^\dagger$ upon the ground state, all eigenstates $\psi_n(\Phi)$ corresponding to higher n-excitations can be generated. These quantum excitations of the LC circuit correspond to collective oscillations of the electric fluid in the LC circuit. In particular, identifying a certain configuration of charge Q and current Φ with the electric and magnetic fields they induce, one can also think of the LC excitations as photons of an resonator with mode frequency ω_{LC}. However, yet the LC circuit has not been coupled explicitly to the electromagnetic environment. Ergo, the photon stays bound to the LC circuit and preserves its energy.

Often, circuit elements are driven by external sources like gate voltages or bias currents. To illustrate the effects of external driving forces, the LC circuit is assumed to be biased by an external current source. The influence of a bias current to the LC circuit is captured by the Hamiltonian

$$H(t) = H_{\mathrm{LC}} - I_{\mathrm{b}}(t)\Phi/c. \tag{2.19}$$

Continuously stimulating the LC circuit, the effect of the external current source is to excite oscillations of the LC resonator. Suppose the LC circuit is initialized in the vacuum state, then the time evolution excites the LC circuit from the vacuum to a coherent state

$$\begin{aligned}
\big|\psi(t)\big\rangle &= \mathcal{T}\exp\left[-\frac{\mathrm{i}}{\hbar}\int_{t_0}^{t}\Big(H_{\mathrm{LC}} - I_{\mathrm{b}}(t)\Phi/c\Big)\mathrm{d}t\right]|0\rangle \\
&= \mathrm{e}^{-\mathrm{i}\zeta(t)}\exp\Big[\lambda(t)a^\dagger - \lambda^*(t)a\Big]\exp\Big[-\mathrm{i}\omega_{\mathrm{LC}}(t-t_0)\,a^\dagger a\Big]\,|0\rangle \\
&= \mathrm{e}^{-\mathrm{i}\zeta(t)-\frac{\mathrm{i}}{2}\omega(t-t_0)}\exp\Big[\lambda(t)a^\dagger - \lambda^*(t)a\Big]\,|0\rangle \\
&= \mathrm{e}^{-\mathrm{i}\zeta(t)-\frac{\mathrm{i}}{2}\omega(t-t_0)}\,|\lambda(t)\rangle
\end{aligned} \tag{2.20}$$

with the time-dependent amplitude of the coherent state[3)]

$$\lambda(t) = -\sqrt{\frac{C\omega_{\mathrm{LC}}}{2\hbar c^2}}\int_{t_0}^{t}\mathrm{e}^{\mathrm{i}\omega_{\mathrm{LC}}(t-t')}\;I_{\mathrm{b}}(t)\mathrm{d}t' \tag{2.21}$$

and the time-dependent phase

$$\zeta(t) = \int_{t_0}^{t}|\lambda(t')|^2\mathrm{d}t'. \tag{2.22}$$

Here, the driving has been considered to be an external classical force that continuously pumps energy in and out of the system without any back action. In general, however, there is a mutual influence of the environment to the system causing noise in the electrical circuits.

2.2.3. Dissipation and noise

Since a device can never be perfectly shielded from its environment, dissipation of energy, i.e., uncontrolled exchange of energy with the environment takes place. For systems of small size, like a single atom for example, the coupling to the environment can often be neglected,[4)] but in macroscopic systems the influence of the environment is generally so strong that its quantum properties disappear (decoherence).

[3)] For further information about coherent states, see App. A.

[4)] Cf. Sec. 2.1.

Tab. 2.1.: Correspondence between mechanical and electrical quantum oscillators.

Mechanical oscillator		Electrical oscillator	
Position	x	Flux	Φ
Momentum	p	Charge	Q
Mass	m	Capacitance	C
Spring constant	k	(inv.) Inductance	L^{-1}
Frequency	$\omega = \sqrt{k/m}$	LC-frequency	$\omega_{\mathrm{LC}} = c/\sqrt{LC}$
Commutation relation	$[x, p] = \mathrm{i}\hbar$		$[\Phi, Q] = \mathrm{i}\hbar c$

The energy of an LC circuit can be, for instance, dissipated by photons that are emitted as radiation into the environment. In any case, energy dissipation leads to damping of the motion as classically modeled by a resistor. In fact, classical Josephson junctions with small capacitances are commonly in the overdamped regime $\omega_{\mathrm{p}} RC \ll 1$. This makes it very challenging to observe quantum phenomena in such macroscopic systems. Furthermore, the mutual influence between environment and quantum system leads to random disturbances acting on the quantum system. This naturally raises the question to which extend quantum phenomena are observable in systems where quantum effects should appear in the collective motion of a macroscopic number of constituents as for instance the Cooper pair condensate in superconductors.

Although quantum dissipation has been studied already in the 1960s from a thermodynamical point of view,[5)] in 1981 *A. O. Caldeira* and *A. J. Leggett* attempted to give an answer to the question whether quantum effects of macroscopic devices such as superconducting tunnel junctions are persistent in presence of dissipation (Caldeira and Leggett, 1981, 1983). To study the influence of an environment to a quantum system, Caldeira and Leggett analyzed the dynamics of a single macroscopic quantum particle linearly coupled to an infinite bath of harmonic oscillators (Caldeira and Leggett, 1983).

Adapted to an LC circuit, the Caldeira-Leggett model is an LC circuit with variables Q and Φ that is coupled to a bath of infinite many LC oscillators. The oscillators of the bath are described by the indexed variables Q_n and Φ_n, where $n \in \mathbb{N}$ may label an infinite amount of externally coupled oscillators. To model the parallel LCR resonator as shown in Fig. 2.4, the flux variable that has to be coupled to the bath environment.[6)] Then, the Caldeira-Leggett Hamiltonian reads

$$H = \frac{Q^2}{2C} + \frac{\Phi^2}{2L} + \sum_n \left(\frac{Q_n^2}{2C_n} + \frac{\Phi_n^2}{2L_n} \right) - \sum_n g_n \Phi_n \Phi \tag{2.23}$$

[5)] See for example Refs. (Magalinskij, 1959; Feynman and Vernon, 1963; Ford *et al.*, 1965).

[6)] For the parallel LCR resonator, it is the charge variable has to be coupled to the bath degrees of freedom.

where L, C are the capacitance and the inductance of the LC-circuit with natural frequency $\omega_{\mathrm{LC}}^2 = c(LC)^{-1}$ and L_n, C_n are the capacitances and inductances of the bath oscillators with individual frequencies $\omega_n = c(L_n C_n)^{-1}$. The couplings g_n between the bath of oscillators and the LC circuit are in principle unknown. Therefore, an arbitrary environment of the LC circuit can be modeled by properly choosing a set of coupling constants g_n. The full dynamics of the LC circuit plus bath system is given by the Heisenberg equations of motion

$$\frac{\dot{Q}}{c} = -\frac{\Phi}{L} + \sum_n g_n \Phi_n, \qquad \dot{\Phi} = \frac{cQ}{C}, \tag{2.24a}$$

$$\frac{\dot{Q}_n}{c} = -\frac{\Phi_n}{L_n} + g_n \Phi, \qquad \dot{\Phi}_n = \frac{cQ_n}{C_n}. \tag{2.24b}$$

The equations of the bath variables can be formally integrated by noticing that the term $\propto \Phi$ acts as an external driving force onto the baths. By introducing creation and annihilation operators for the bath degrees of freedom

$$a_n = \sqrt{\frac{\omega_n C_n}{2\hbar c^2}} \left(\Phi_n + \frac{\mathrm{i}c}{\omega_n C_n} Q_n \right), \quad a_n^\dagger = \sqrt{\frac{\omega_n C_n}{2\hbar c^2}} \left(\Phi_n - \frac{\mathrm{i}c}{\omega_n C_n} Q_n \right) \tag{2.25}$$

the Heisenberg equations (2.24b) decouple into first-order equations driven by the flux variable Φ,

$$\dot{a}_n = -\mathrm{i}\omega_n a_n + \frac{\mathrm{i}c g_n}{\sqrt{2\hbar\omega_n C_n}} \Phi \tag{2.26}$$

with $a_n^\dagger$ obeying the Hermitian conjugate equation. These equations can be formally solved. By using the method of variation of constants, one finds

$$a_n(t) = \mathrm{e}^{-\mathrm{i}\omega_n (t-t_0)} a_n(t_0) - \frac{\mathrm{i}c g_n}{\sqrt{2\hbar\omega_n C_n}} \int_{t_0}^{t} \mathrm{e}^{-\mathrm{i}\omega_n (t-t')} \Phi(t') \mathrm{d}t'. \tag{2.27}$$

Then, by substituting these formal solutions into the Heisenberg equations of the LC circuit Eq. (2.24a), the bath degrees of freedom are effectively integrated out. The effective dynamics of the flux Φ is then determined by the *quantum Langevin equation*

$$\ddot{\Phi} + \omega_{\mathrm{LC}}^2 \Phi + \frac{1}{C} \int_{t_0}^{t} Y(t-t') \dot{\Phi}(t') \mathrm{d}t' = \frac{c}{C} \xi(t), \tag{2.28}$$

where the inhomogeneity

$$\xi(t) = \sum_n \sqrt{\frac{\hbar g_n^2 c^4}{2\omega_n C_n}} \left[\mathrm{e}^{\mathrm{i}\omega_n (t-t_0)} a_n^\dagger(t_0) + \mathrm{e}^{-\mathrm{i}\omega_n (t-t_0)} a_n(t_0) \right] \tag{2.29}$$

is an emergent external force induced by the influence of the bath. This external force $\xi(t)$ may represent an external driving force as well as noise disturbing the LC resonator. In particular, $\xi(t)$ depends only on the initial conditions at time t_0.

Furthermore, the integral term in Eq. (2.28) introduces energy dissipation to the LC circuit as indicated by its proportionality to $\dot{\Phi}$. The integral kernel is given by

$$Y(t) = \sum_n \frac{c^4 g_n^2}{C_n} \cos(\omega_n t) \tag{2.30}$$

and corresponds to the susceptibility of the bath due to fluctuations of the LC circuit. In frequency space the quantum Langevin equation becomes

$$\left[\frac{c}{LC} - \omega^2 + \mathrm{i}\omega \frac{Y(\omega)}{C}\right] \Phi(\omega) = \frac{c}{C}\xi(\omega) \tag{2.31}$$

where $Y(\omega)$ corresponds to the (complex) admittance, which is the inverse impedance of the environment, $Y(\omega) = Z(\omega)^{-1}$. Hence, the environment can be completely described via its admittance and is, due to Eq. (2.30), fully characterized by choosing a set of coupling constants g_n. However, generally nothing is known about these coefficients. Often it is sufficient to assume $c^4 g_n^2/C_n = \text{const.}$, for all n. In this case, known as the *first Markov approximation*, the admittance is frequency independent $Y = R^{-1}$ and renders the quantum Langevin equation local in the time domain (Gardiner and Zoller, 2004).

For such a frequency independent admittance of the bath, the flux is described by

$$\Phi(\omega) = \frac{c}{C\left(\omega_{\mathrm{LC}}^2 - \omega^2 + \mathrm{i}\frac{\omega}{RC}\right)} \xi(\omega) \tag{2.32}$$

in the frequency domain. This is in complete analogy to the classical LRC circuit, where the flux is susceptible to the external sources. However, Φ and ξ are still quantum operators. Since the operator $\xi(t)$ depends only upon the initial conditions of the bath variables at time t_0, the dynamics of Φ and any other observable can be determined by specifying the initial quantum state of the bath. Analogous to the classical case, oscillations of the LC circuit, that are not driven by an external force, are damped within a time scale $\tau = 2RC$.

Often it is assumed that the oscillator bath is in thermal equilibrium. Then, the quantity $\xi(t)$ can be interpreted as a randomly fluctuating stochastic force. As such it is rather defined via its statistical moments than by the initial condition. In order to maintain the system's distribution in thermal equilibrium the statistical moments of the stochastic force have to be characterized by $\langle \xi(t) \rangle = 0$ and

$$\left\langle \xi(t)\xi(t') + \xi(t')\xi(t) \right\rangle = \frac{1}{\pi R} \int_0^\infty \hbar\omega \coth\left(\frac{\hbar\omega}{2k_{\mathrm{B}}T}\right) \cos[\omega(t-t')] \mathrm{d}\omega, \tag{2.33}$$

see Gardiner and Zoller (2004, Ch. 3). In the classical limit, in which the temperature scale much larger than the oscillator energy $\hbar\omega \ll k_{\mathrm{B}}T$, the correlation function

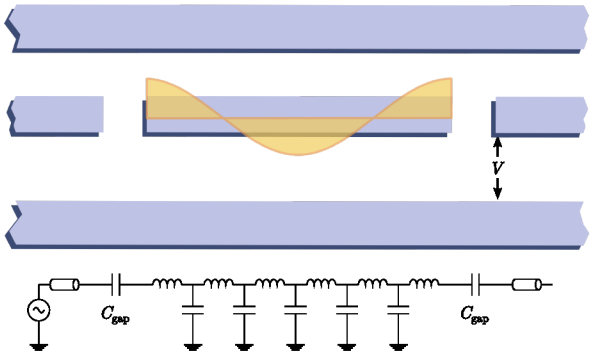

Fig. 2.5.: Schematic illustration of a coplanar waveguide resonator as it is used in the cQED architecture. The superconducting central pin as well as the ground superconducting striplines on the outside are grown onto a dielectric substrate. A voltage V, which is applied between central strip and and the ground plates, builds up an electric field between the striplines that propagate along the transmission line. Standing waves of the electromagnetic field appear inside the stripline resonator, which is formed by the small region in between two gaps interrupting the central stripline. By manufacturing the gaps small enough, a capacitive coupling between the transmission line and the resonator is achieved. Below, the lumped element approximation.

of ξ can be reduced to $\langle \xi(t)\xi(t') \rangle = (2k_{\mathrm{B}}T/R)\delta(t-t')$. Then, by using (2.32) and $V(t) = \dot{\Phi}(t)/c$, this relation can be translated into a correlation function that characterizes thermal fluctuations of the voltage at the resistor

$$\langle V(t)V(t') \rangle = 2Rk_{\mathrm{B}}T\delta(t-t'). \tag{2.34}$$

The resulting thermal noise occuring in electric circuits is known as the *Johnson-Nyquist noise*. The occurrence of the resistance R expresses the fact that thermally induced fluctuations are dissipated in form of heat by the resistor thereby stabilizing the thermal equilibrium state.

So far, the discussion of quantum dissipation was given for the example of an LCR circuit. However, the quantum Langevin equation can be easily extended to describe dissipation for quantum particles moving in a generic potential (Caldeira and Leggett, 1981; Gardiner and Zoller, 2004). In particular, this allows to describe actual Josephson junctions where the quantum particle moves in an periodic potential due to the cosine of the Josephson energy. In the classical limit, in which the phase difference of the junction $\varphi = 2\pi\Phi/\Phi_0$ can be replaced by its average value, the quantum Langevin equation reduces to the tilted-washboard model as introduced in Sec. 2.2.1.

2.2.4. Superconducting transmission lines and microwave resonators

The key concept for dissipation is the notion of an environment, whose influence on the LC circuit is described in terms of the quantum Langevin equation. However,

the environment of a circuit does not necessarily turn electrical energy into heat thereby loosing information in form of thermodynamic entropy; for the purpose of controlling and reading out quantum bits it will be important to add and extract energy controllably. Furthermore, not just the energy, but also information has to be transferred from the quantum bit to the measurement apparatus to obtain knowledge about the qubit. Within the cQED architecture as will be introduced later, superconducting transmission lines are ideally suited to achieve these requirements.

Transmission lines are superconducting wave guides capable to conduct signals of low intensity (down to the single photon level) at a low dissipation rate. Like for common microwave waveguides, the superconducting transmission line is a coaxial cable. A two-dimensional superconducting transmission line consists of three coplanar superconducting strips grown on a dielectric substrate: the center pin and two surrounding ground superconductors, see Fig. 2.5. The working principle of such a two-dimensional transmission line is the same as in a coaxial cable: the signal is transmitted by applying a voltage to the central pin while the surrounding ground superconductors reduced the leakage of radiation outside the wire.

Because of its property to conduct electrical signals between two distant points, a transmission line cannot be described as a single lumped circuit element, but rather as a series of such. Instead of having a single charge degree of freedom and a single flux degree of freedom, a transmission line is characterized by a local flux variable $\Phi(t,x)$ at each point x of the stripline and a charge density (per length) $\varrho(t,x) = \mathfrak{c}\,V(t,x)$ induced by the voltage at position x, $cV(t,x) = \dot{\Phi}(t,x)$. Then the Hamiltonian of a stripline of length L in its continuum version is

$$H_{\mathrm{tl}} = \int_0^L \left(\frac{\varrho^2(t,x)}{2\mathfrak{c}} + \frac{\partial_x \Phi^2(t,x)}{2\mathfrak{l}} \right) \mathrm{d}x. \tag{2.35}$$

Here $\mathfrak{c}$ is the capacity of the strip per length and $\mathfrak{l}$ is the inductance per length. The lumped element approximation corresponding to a discrete version of the continuous model is shown in Fig. 2.5. From the classical Hamiltonian equations for such a string-like object, it follows that electromagnetic signals propagate as waves with phase velocity $v_{\mathrm{p}} = c/\sqrt{\mathfrak{c}\mathfrak{l}}$ through the transmission line. In fact, the electromagnetic fields inside the waveguide is connected to the voltage across the striplines. Hence, the quantization of these wave-like excitations goes hand in hand with the quantization of the electromagnetic field inside, see App. A.

In terms of normal modes, the normal-ordered[7)] Hamiltonian can be written in the form

$$H_{\mathrm{tl}} = \sum_n \hbar\omega_n a_n^\dagger a_n. \tag{2.36}$$

where a_n and $a_n^\dagger$ are creation and annihilation operators of photon states in the transmission line. In this representation the Hamiltonian becomes a collection of in-

[7)] See App. A.

finite many normal modes corresponding to standing waves between the two current nodes at $x = 0$ and $x = L$. Physically, these solutions describe actual photon excitations of the electromagnetic field inside a microwave cavity formed by terminating the end points of a transmission line. Such a microwave cavity formed by a quasi-one-dimensional resonator is also called a *coplanar stripline resonator*. Due to small distances of $\approx 10\,\mu\mathrm{m}$ between the central superconductor and its surrounding ground plates, a coplanar stripline resonator may contain electric fields with large strength of inside. In fact, the zero-point fluctuations of the voltage $V_{0,\mathrm{zp}} \simeq (\hbar\omega_0/cL)^{1/2}$ imply a zero-point field strength of $E_{0,\mathrm{zp}} \approx 0.2\,\mathrm{V/m}$ which is much larger than zero-point fields achieved three-dimensional resonator in cavity QED (Blais *et al.*, 2004).

Often, the length of the transmission line is much larger than other length scales which allows to consider the limit $L \to \infty$. In that case the eigenfrequencies of the stripline form a continuum and the Hamiltonian becomes

$$H_{\mathrm{tl}} = \frac{1}{2\pi} \int_{\mathbb{R}} \hbar\omega_k \, b^\dagger(k) b(k) \, \mathrm{d}k. \tag{2.37}$$

with *distribution-valued* mode operators $b(k)$, $b^\dagger(k)$ obeying the commutation relation

$$[b(k), b^\dagger(k')] = 2\pi\delta(k - k'). \tag{2.38}$$

Whereas the excitations of the lumped circuit elements have been associated with photon-like excitations in the preceding sections, the excitations of an infinite transmission line (or stripline resonator) correspond to photons propagating along the transmission line with a continuous bandwidth. This enables the transport of energy as well as the transmission of microwave signals.

In order to drive a stripline resonator externally, it is connected capacitively to a superconducting transmission line which feeds in microwave signals. This is achieved by manufacturing imperfections in form of little gaps in the central pin of the strip line. These gaps impede the propagation of photon in the transmission line by only transmitting a fraction of the incoming waves into the resonator. The remaining part of the radiation gets reflected back to the transmission line. Because the end points on each side of the gap from a capacitance C_{coup}, coupling between both sides is achieved via the energy that is required to induce an additional amount of charge $C_{\mathrm{coup}}V$ on both capacitor plates. The total charging energy is

$$E_{\mathrm{C}} = -\frac{(Q - C_{\mathrm{coup}}V)^2}{C_\Sigma} \tag{2.39}$$

where Q is the charge on the microwave resonator, C_Σ is the total capacity to ground, and V is the voltage drop between transmission line and resonator. The coupling is mediated by the excess contribution $\propto C_{\mathrm{gap}}VQ$. In terms of creation and annihilation operators such a coupling Hamiltonian generically reads

$$H_{\mathrm{coup}} = \frac{\mathrm{i}\hbar}{2\pi} \sum_n \int_{\mathbb{R}} \sqrt{v_{\mathrm{p}}\kappa_n} \left[a_n^\dagger - a_n\right] \left[b^\dagger(k) + b(k)\right] \mathrm{d}k \tag{2.40}$$

with the coupling constants κ_n depending upon the frequency ω_k as well as the resonator mode. Usually the coupling constants are assumed to be small. In fact, for superconducting striplines typical couplings are of the order of a few MHz (Blais *et al.*, 2004) while microwave frequencies are usually in the GHz regime. Hence, due to the smallness of the coupling constants, the term $\propto a_n^\dagger b^\dagger(k)$ and its Hermitian conjugate can be neglected as rapidly oscillating contributions which cannot drive any transitions. Within this approximation—known as rotating wave approximation—the interaction between microwave resonator and transmission line takes place by the (resonant) exchange of microwave photons and the Hamiltonian reduces to

$$H_{\text{coup}} = \frac{\mathrm{i}\hbar}{2\pi} \sum_n \int_{\mathbb{R}} \sqrt{v_{\text{p}}\kappa_n} \left[a_n b^\dagger(k) - a_n^\dagger b(k) \right] \mathrm{d}k. \tag{2.41}$$

Because of the clear separation of scales, the rotating wave approximation is a very accurate description for the resonator coupling in circuit QED and valid in most situations. Moreover, when a classical microwave signal is applied to the transmission line, the operators $b(k)$ can be replaced by their expectation values $\langle b(k) \rangle \simeq \mathrm{e}^{-\mathrm{i}\omega_k t}\beta(k)$. By virtue of H_{coup}, the microwave signals act as an external driving force that stimulates the field inside the cavity. Assuming the cavity mode was initially in its ground state, driving by classical microwave excites the cavity field into a coherent state, cf. (2.21).

2.3. Superconducting qubits

With the remarkable progress of nanofabrication technology that has allowed to expose quantum properties in superconducting electronics, the development of superconducting qubits has been set off. In the meantime many different designs for superconducting qubits have been developed: the flux qubit, the fluxonium, the Cooper pair box, and the transmon qubit to name just a few. Among these, the transmon qubit is yet the most favorable for quantum computation, because of its simple design as well as its long coherence times. Although the fluxonium is an equal competitor, the improved transmon placed inside of a three-dimensional microwave cavity remains ahead (Devoret and Schoelkopf, 2013). The transmon qubit is essentially a modification of the Cooper pair box which was the prototype of several superconducting qubits. Therefore it is worth to first review the basic physics of the the Cooper pair box before focussing the discussion solely to the transmon regime.

2.3.1. The Cooper pair box

The Cooper pair box is made of a ground superconductor and a small superconducting islands connected by a Josephson junction with Josephson energy E_{J} and finite capacitance C, see Fig. 2.7. In order to be able to tune the Josephson energy, the single Josephson junction is often replaced by a dc-SQUID, which com-

prises two parallel Josephson junctions. Then the effective Josephson energy $E_J = E_{\mathrm{J,max}}|\cos(\pi\Phi_\mathrm{m}/\Phi_0)|$ can be effectively tuned by varying the magnetic flux Φ_m penetrating the dc-SQUID. Essentially, the superconducting island needs to be small enough such that the charging energy $4E_\mathrm{C}$, that is required to add a single Cooper pair, is larger than the characteristic thermal energy of its environment $4E_\mathrm{C} \ll k_\mathrm{B}T$. Since a Cooper pair carries twice the charge of an electron, the charging energy for a Cooper pair is four times larger than for an electron, $4E_\mathrm{C}$. Furthermore, the total amount of charge on the Cooper pair box can be controlled by an external gate voltage V_g connected via a capacitance C_g. The charging energy for a single electron is then given by

$$E_\mathrm{C} = \frac{e^2}{2C_\Sigma} \tag{2.42}$$

where $C_\Sigma = C + C_\mathrm{g}$ is the total capacitance. The gate voltage induces a constant offset charge corresponding to

$$n_\mathrm{g} = \frac{C_\mathrm{g}V_\mathrm{g}}{2e}, \tag{2.43}$$

such that the total energy of the Cooper pair box is given by

$$H_\mathrm{cpb} = 4E_\mathrm{C}(N - n_\mathrm{g})^2 + E_\mathrm{J}(1 - \cos\varphi). \tag{2.44}$$

where $N = -Q/2e$ is the total number of Cooper pairs on the superconducting island and $\varphi = 2\pi\Phi/\Phi_0$ is the superconducting phase difference across the Josephson junction. In the following the constant energy offset E_J shall be neglected for simplicity.

The simplest way to define a two-level system, that can be used as quantum bit, is by manufacturing the Cooper pair box such that the capacitive energy dominates over the Josephson energy $E_\mathrm{C} \gg E_\mathrm{J}$. In this regime, where the supercurrent is obstructed by the Coulomb blockade,[8)] only sequential tunneling of Cooper pairs may happen by changing the gate voltage. Then, by including the Josephson energy the Hamiltonian of the Cooper pair box can be represented in the charge basis

$$H_\mathrm{cpb} = 4E_\mathrm{C}\sum_{n=0}^{\infty}(N - n_\mathrm{g})^2|n\rangle\langle n| - \frac{E_\mathrm{J}}{2}\sum_{n=0}^{\infty}\Big[|n\rangle\langle n+1| + |n+1\rangle\langle n|\Big]. \tag{2.45}$$

The charge basis $\{|n\rangle\}$ forms a complete set of eigenstates of the the Cooper pair number operator with $N|n\rangle = n|n\rangle$. The so-called *charge qubit* can be defined by considering the low energy sector of H_cpb with $n_0 = \min\{|n - n_\mathrm{g}|\}$ and $n_1 = n_0 + 1$. By projecting onto this two-level subsystem, the Hamiltonian can be represented

[8)] For small islands with small capacitances, the tunneling of charge carriers is essentially blocked as long as the gate voltage stays below the charging energy that is required to bring a single charge carrier onto the island. This phenomenon is called Coulomb blockade, because it arises due to the Coulomb repulsion of charge carriers across the capacitor.

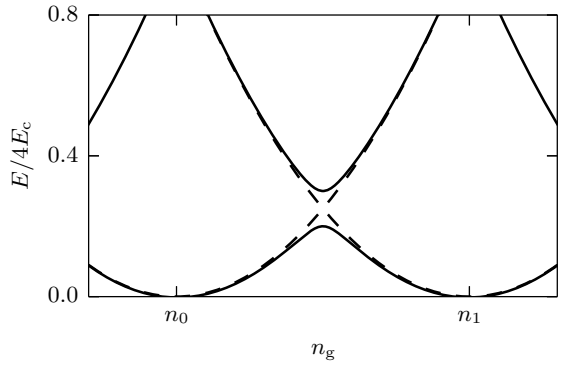

Fig. 2.6.: Cooper pair box spectrum (solid lines) as function of n_g in the charging regime; here $E_J = 0.4E_C$. The Josephson tunneling induces an avoided crossing with a gap size E_J between the parabolic bands (dashed lines) of the charging states $|0\rangle$ and $|1\rangle$.

in terms of the the pseudo-spin operators $\tau_x = \left(|n_0\rangle \langle n_1| + |n_1\rangle \langle n_0| \right)$ and $\tau_z = \left(|n_0\rangle \langle n_0| - |n_1\rangle \langle n_1| \right)$ and reads

$$H_{\text{cpb}} \simeq \Delta\tau_z + \lambda\tau_x \tag{2.46}$$

with $\Delta = 4E_C[n_0^2 - n_1^2 - 2n_g(n_0 - n_1)]/2$ and $\lambda = E_J/2$. The spectrum of H_{cpb} depends parametrically upon the external gate voltage, see Fig. 2.6. In particular, due to the Josephson tunneling contribution, the energy levels avoid to cross. The energy gap between the levels $|n_0\rangle$ and $|n_1\rangle$ is determined by E_J. This means the charge state of the Hamiltonian can be manipulated by driving the gate voltage in an ESR-like fashion, see Bouchiat *et al.* (1998); Nakamura *et al.* (1999). The main disadvantage of the charge qubit is, however, that the spectrum is highly susceptible to fluctuations of the gate voltage. Mesoscopic tunnel junctions are always subject to fluctuations of the offset charge in form of charged two-level systems nearby the junction. The resulting charge noise is of the $1/f$-type, see Zimmerli *et al.* (1992); Visscher *et al.* (1995); Ithier *et al.* (2005). In fact, charge noise is the prime decoherence mechanism for charge qubits and limits the qubits's maximal lifetime up to 10 ns (Devoret and Schoelkopf, 2013).

Moreover, in the regime of smaller capacitances, where $E_C \ll E_J$, the number of Cooper pairs is not a good quantum number anymore. Instead, it is more convenient to express the Hamiltonian in the basis of superconducting phase states $|\varphi\rangle$. In the spirit of Sec. 2.2.2, the correct quantum description of φ and N is supposed to be obtained by postulating the canonical commutation relation (2.14) which translate into

$$[\varphi, N] = \mathrm{i}. \tag{2.47}$$

However, when imposing the above commutation relation there arise some subtleties, that require a closer look. In analogy to the usual quantization procedure, φ and N are supposed to be generators of the one-dimensional group of translations for its

conjugate variable (Weyl, 1927),

$$\exp(-\mathrm{i}\theta N)\varphi\exp(\mathrm{i}\theta N)=\varphi+\theta,\qquad \exp(-\mathrm{i}n\varphi)N\exp(\mathrm{i}n\varphi)=N+n. \tag{2.48}$$

Then, as implied by the *Stone-von Neumann theorem*, both operators φ and N admit the usual Schrödinger representation with $\varphi=-\mathrm{i}\partial_n$, $N=n\in\mathbb{R}$ and vice versa (Reed and Simon, 1980, Ch. VIII). This, however, suggests that the canonical commutation relation is incompatible with the fact that the operator N is bounded from below.[9)] Instead, the *Susskind-Glogower operators*

$$\exp\big(\mathrm{i}\varphi\big)=\sum_{n=0}^{\infty}|n\rangle\langle n+1|,\qquad \exp(-\mathrm{i}\varphi)=\sum_{n=0}^{\infty}|n+1\rangle\langle n| \tag{2.49}$$

turn out to be an appropriate description of the superconducting phase (Susskind and Glogower, 1964). By virtue of the commutation relations

$$[\exp(\mathrm{i}\varphi),N]=\exp(\mathrm{i}\varphi),\qquad [\exp(-\mathrm{i}\varphi),N]=-\exp(-\mathrm{i}\varphi) \tag{2.50}$$

the Susskind-Glogower operators imply the correct translation property

$$\exp\big(\mathrm{i}\varphi\big)\,N\,\exp\big(-\mathrm{i}\varphi\big)=N+1. \tag{2.51}$$

Here the discrete step size of the translation reflects the quantization of the underlying charge which might be the photon number, the electron number, or—as for superconductors—the number of Cooper pairs. Furthermore, in accordance to the tunneling contribution in (2.45), the Susskind-Glogower operators allow to define the Hermitian operator

$$\begin{aligned}\cos(\varphi)&=\frac{1}{2}\big[\exp\big(\mathrm{i}\varphi\big)+\exp\big(-\mathrm{i}\varphi\big)\big]\\&=\frac{1}{2}\sum_{n=0}^{\infty}\Big[|n\rangle\langle n+1|+|n+1\rangle\langle n|\Big]\end{aligned} \tag{2.52}$$

which replaces the cosine contribution of the classical Josephson energy. Then, by defining $\sin(\varphi)=[\exp(\mathrm{i}\varphi)-\exp(-\mathrm{i}\varphi)]/2\mathrm{i}$, the operator of the supercurrent of the Cooper pair box becomes

$$I=-2e\frac{\mathrm{d}N}{\mathrm{d}t}=-2e\frac{\mathrm{i}}{\hbar}[H_{\mathrm{cpb}},N]=-\frac{2e}{\hbar}E_{\mathrm{J}}\sin\varphi. \tag{2.53}$$

[9)] Furthermore, in order to guarantee discreteness of the Cooper pair number operator, the superconducting phase has to be defined as a compact variable whose spectrum is the finite interval $[0,2\pi)$, but there is no well-defined Hermitian phase operator φ: assuming N and φ to be Hermitian observables subject to the commutation relation in (2.47), they obey the uncertainty relation $\Delta\varphi\Delta N\geq\frac{1}{2}$ where the phase uncertainty may become $\Delta\varphi\geq 2\pi$ if ΔN is sufficiently small, see Carruthers and Nieto (1968).

This is nothing else but a quantum version of the first Josephson relation, cf. Eq. (2.8). Hence, the Susskind-Glogower formalism seems perfectly suited to describe the quantum aspects of the superconducting phase. By considering eigenvalues of the Susskind-Glogower operators

$$\left|\mathrm{e}^{\mathrm{i}\theta}\right\rangle = \sum_{n=0}^{\infty} \mathrm{e}^{\mathrm{i}n\theta} \left|n\right\rangle \tag{2.54}$$

with

$$\exp\left(\mathrm{i}\varphi\right) \left|\mathrm{e}^{\mathrm{i}\theta}\right\rangle = \mathrm{e}^{\mathrm{i}\theta} \left|\mathrm{e}^{\mathrm{i}\theta}\right\rangle, \tag{2.55}$$

the formalism even allows to give the notion of states with a well defined phase. However, these eigenvectors do not necessarily form an orthogonal basis, because the Susskind-Glogower operators fail to be proper unitary operators

$$\exp\left(-\mathrm{i}\varphi\right) \exp\left(\mathrm{i}\varphi\right) = \mathbb{1} - |0\rangle\langle 0|. \tag{2.56}$$

Furthermore, as a consequence of the missing unitarity, there is—stricly speaking—no Hermitian generator φ which accurately represents the superconducting phase operator. Nevertheless, in the limit of large particle numbers where all states have none or at least very small overlap with the vacuum state $|0\rangle$, the Susskind-Glogower operators appear to be unitary to a good approximation. In essence, there exists a satisfactory interpretation of the superconducting phase operator φ as a generator of the one-dimensional unitary group of translations $\exp(\mathrm{i}\varphi)$ in the regime of large particle numbers. Hence, the commutation relation (2.47) is—roughly speaking—approximately correct when a sufficient large amount of Cooper pairs is present. Because superconductivity is an emergent phenomenon that arises from the collective motion of a large amount of Cooper paris, canonical commutation relations for the superconducting phase and the Cooper pair number can be clearly imposed to a good approximation. It is thus sufficient to treat the superconducting phase as a compact variable in the following. Furthermore, its canonically conjugated momentum N, which in this approximation has a spectrum that extends to all integers, counts the number of Cooper pairs.[10)]

The discussion above suggests that the Cooper pair box Hamiltonian admits a well-defined phase representation. By going over to this representation, the Hamiltonian of the Cooper pair box assumes the same form as the Hamiltonian of a quantum particle moving in a cosine potential. Then, the Schrödinger equation for the Cooper pair box reads

$$E\psi(\varphi) = \left[4E_{\mathrm{C}}\left(-\mathrm{i}\frac{\partial}{\partial\varphi} - n_{\mathrm{g}}\right)^2 - E_{\mathrm{J}}\cos\varphi\right]\psi(\varphi). \tag{2.57}$$

[10)] By inductively shunting the Cooper pair box, the charge quantization gets explicitly broken. This is due to the additional energy contribution $(2L)^{-1}(\Phi_0/2\pi)^2\varphi^2$ of the inductance L, which renders the Hamiltonian non-periodic in the superconducting phase variable, see Koch *et al.* (2009) for more details of this continuous limit.

Assuming that the superconducting phase is a compact variable, the spectrum of N necessarily encloses all integers $n \in \mathbb{Z}$. This quantization condition is imposed by requiring periodic boundary conditions of the wave function

$$\psi(\varphi + 2\pi) = \psi(\varphi). \tag{2.58}$$

Furthermore, the voltage-induced offset charge n_g can be effectively removed by a gauge transformation. In the co-moving frame with $\psi = \mathrm{e}^{\mathrm{i}n_\mathrm{g}\varphi}\tilde{\psi}$ the Schrödinger equation reduces to *Mathieu's equation*

$$\frac{\mathrm{d}^2\tilde{\psi}}{\mathrm{d}z^2} + [a - 2q\cos(2z)]\,\tilde{\psi} = 0. \tag{2.59}$$

The dimensionless parameters are related to the energy parameters of the Cooper pair box as follows

$$a = \frac{E}{E_\mathrm{C}}, \qquad q = -\frac{E_\mathrm{J}}{2E_\mathrm{C}}, \qquad z = \frac{\varphi}{2}.$$

Being a periodic differential equation, the Mathieu equation admits solutions $F_\nu(z;q)$ and $F_\nu(-z;q)$ of the *Floquet-type* having the property $F_\nu(\pm z + \pi) = \mathrm{e}^{\pm\mathrm{i}\nu\pi}F_\nu(\pm z)$.[11] The index $\nu(a,q)$ is the Floquet characteristic exponent and depends upon the parameters a, q.[12] Furthermore, ν is constrained by the periodic boundary condition (2.58) which translates into the quantization condition

$$\nu(a,q) = 2(k - n_\mathrm{g}), \qquad k \in \mathbb{Z}. \tag{2.60}$$

Then, the inverse relation $a = a_\nu(q)$ defines the so-called *Mathieu characteristic values* and gives the quantized energy spectrum of the Cooper pair box

$$E_n = E_\mathrm{C}\, a_{2(k_n - n_\mathrm{g})}(-E_\mathrm{J}/2E_\mathrm{C}). \tag{2.61}$$

Note, that the series of eigenenergies E_n is not monotonously increasing with k. For convenience, the series k_n introduces an index $n \in \mathbb{N}$ such that the values E_n increase monotonously with n, see Cottet (2002); Koch *et al.* (2007). Then, the eigenfunctions are obtained as

$$\psi_n(\varphi) = \begin{cases} \frac{1}{\sqrt{2\pi}}\mathrm{e}^{\mathrm{i}n_\mathrm{g}\varphi}F_{2(k_n-n_\mathrm{g})}\big(\varphi/2;\,-E_\mathrm{J}/2E_\mathrm{C}\big), & \text{for } k_n \geq 0 \\ \frac{1}{\sqrt{2\pi}}\mathrm{e}^{\mathrm{i}n_\mathrm{g}\varphi}F_{2(k_n-n_\mathrm{g})}\big(-\varphi/2;\,-E_\mathrm{J}/2E_\mathrm{C}\big), & \text{for } k_n < 0 \end{cases}. \tag{2.62}$$

Since the Floquet solutions $F_\nu(\varphi/2)$ and $F_\nu(-\varphi/2)$ are not elementary, the spectrum (2.61) and the wave functions (2.62) generally have to be evaluated numerically.

Nevertheless, analytical results can be obtained in the asymptotic limits $E_\mathrm{C} \gg E_\mathrm{J}$ and $E_\mathrm{C} \ll E_\mathrm{J}$. The charging regime with $E_\mathrm{C} \gg E_\mathrm{J}$ has already been introduced before, see Eq. (2.45) and below. Unfortunately, in this regime charge noise destroys the coherence of the qubit rather fast. Luckily, as will be explained in the next paragraph, it turns out that in the *transmon regime* $E_\mathrm{C} \ll E_\mathrm{J}$ decoherence due to charge noise is heavily suppressed.

[11] For an introduction to *Floquet theory* see for example Grifoni and Hänggi (1998).
[12] The nomenclature is following the book of Abramowitz and Stegun, see Blanch (1970).

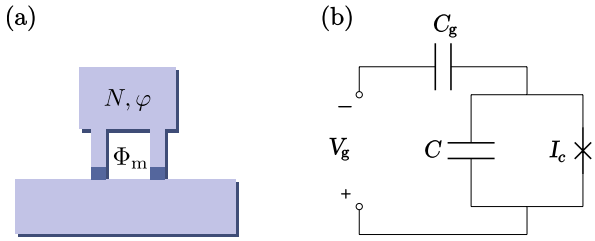

Fig. 2.7.: (a) A Cooper pair box is made of an superconducting island containing N Cooper pairs. The island is separated from the ground superconductor at the bottom by a pair of Josephson junctions (SQUID) penetrated by the magnetic flux Φ_m. The supercurrent flowing through the tunneling junctions is driven by the superconducting phase difference φ. (b) The equivalent circuit representation. The tunneling junction is characterized by a capacitance C and a gate voltage charges the superconducting island with a background charge $n_g = C_g V_g$.

2.3.2. The transmon qubit

With the intention of presenting a "charge-insensitive qubit design derived from the Cooper pair box", Koch *et al.* (2007) introduced the *transmon qubit*. The transmon qubit is a derivative of the Cooper pair box exploiting the regime $E_C \ll E_J$, which has been accomplished experimentally first in 2008 by Schreier *et al.*. This can be realized by shunting the Cooper pair box with a large capacitance C_s whose net effect is to lower the charging energy of a single electron $E_C = e^2/2C_\Sigma$, see Fig. 2.8 (b). With the total capacitance

$$C_\Sigma = C + C_g + C_s, \tag{2.63}$$

the charging energy gets drastically lowered by making C_s large. As shown below, this has the advantage of smoothening the energy band dispersion $E_n(n_g)$ as a function of the background charge n_g. Then, the qubit states $|0\rangle$ and $|1\rangle$ are encoded by the two lowest energy eigenstates corresponding to states which are bound deep in the cosine potential well.

In order to obtain the energy dispersion relation $E_n(n_g)$, Eq. (2.57) is treated by the semiclassical WKB method.[13)] Since Eq. (2.57) represents a single particle Schrödinger equation, the superconducting phase particle can be assumed to be localized at the bottom of the cosine potential at low energies $E \ll E_J$. Since the wave function of such an localized state decays rapidly inside the potential barrier, the periodic boundary condition can be discarded to a good approximation. By doing so, there are in principle infinite many localized ground states of the cosine potential, in which the particle can be trapped as well. Moreover, a particle, that is for instance localized in the potential well at $\varphi = 0$, can be transferred to a neighboring potential well at $\varphi = \pm 2\pi$ via tunneling processes given by the transition amplitude $\langle \varphi = 0 | U(t) | \varphi = \pm 2\pi \rangle \neq 0$. Transitions between two such degenerate ground states

[13)] For an introduction to the WKB method see Landau and Lifshitz (2012); Bender and Orszag (1978).

are non-perturbative quantum effects being called *instantons* (Wen, 2004, Ch. 2). In presence of such instanton-mediated transitions, the localized wave functions in each well hybridize and form a one-dimensional Bloch-like band with dispersion relation

$$E_n(n_\mathrm{g}) = E_n(n_\mathrm{g} = 1/4) + \frac{w_n}{2}\cos(2\pi n_\mathrm{g}). \tag{2.64}$$

The hybridization energy t_n can be approximated by the semiclassical matrix element $\langle 0|H_\mathrm{cpb}|2\pi\rangle$; however, due to the strong oscillatory character of the semiclassical wave functions, it is usually a challenging task to evaluate semiclassical matrix elements. Equivalently, identifying w_m as the peak to peak difference of the energy dispersion and using the asymptotic expansion of the Mathieu characteristic values (Blanch, 1970), the dispersion amplitude becomes

$$\begin{aligned} w_n &= E_n(n_\mathrm{g} = 1/2) - E_n(n_\mathrm{g} = 0) \\ &\sim (-1)^m E_\mathrm{C}\sqrt{\frac{2}{\pi}}\frac{2^{4m+5}}{m!}\left(\frac{E_\mathrm{J}}{2E_\mathrm{C}}\right)\mathrm{e}^{-\sqrt{8E_\mathrm{J}/E_\mathrm{C}}}, \qquad \frac{E_\mathrm{J}}{E_\mathrm{C}} \to \infty; \end{aligned} \tag{2.65}$$

see also (Koch *et al.*, 2007). The exponential decrease of t_n emphasizes its non-perturbative origin and demonstrates that the insensitivity of the energy dispersion to fluctuations in the offset charge n_g in the transmon regime. In fact, it has been shown that by adding a large shunt capacitor, the qubit decoherence times could be considerably increased up to few microseconds (Devoret and Schoelkopf, 2013).

The suppressed susceptibility of the transmon device to charge noise, however, also reduced the controllability of the qubit by charge-based manipulations. Therefore, other means like the circuit QED architecture are required to access the transmon qubit with high accuracy. Furthermore, to set up a well defined two-level system, the transition frequencies $\omega_{nm} = (E_n - E_m)/\hbar$ need to be distinct from each other. In order to have energy spacings, that are not equidistant, a certain amount of anharmonicity as for example in a cosine potential has to be present. By using the asymptotic expressions of the characteristic values, see Blanch (1970), the energies are approximately found to be

$$E_n(n_\mathrm{g} = 1/2) \sim -E_\mathrm{J} + \sqrt{8E_\mathrm{J}E_\mathrm{C}}\left(n + \frac{1}{2}\right) - \frac{E_\mathrm{C}}{4}\left[2\left(n^2 + n\right) + 1\right] + \mathcal{O}(q^{-1/2}), \tag{2.66}$$

as $E_\mathrm{J}/E_\mathrm{C} \to \infty$. Clearly, these are energy levels of a particle that is trapped in one minimum of the cosine potential: by identifying $\omega_\mathrm{p} = \sqrt{8E_\mathrm{J}E_\mathrm{C}}/\hbar$ as the Josephson plasma frequency, the second term corresponds to the excitation spectrum of an harmonic oscillator that arises by expanding the cosine potential to second order around $\varphi = 0$. The last term, which is of the order $\sim E_\mathrm{C}$, arises from quartic corrections. This term introduces anharmonicity to the excitation spectrum and allows to discriminate transitions by their individual frequencies ω_{nm}.[14)] In particular, for the

[14)] Expanding the cosine potential to fourth order in φ, namely

$$E_\mathrm{J}\cos\varphi \sim E_\mathrm{J}\left[1 - \frac{\varphi^2}{2!} + \frac{\varphi^4}{4!} + \mathcal{O}(\varphi^6)\right],$$

first three energy levels E_0, E_1, and E_2 the relative anharmonicity is

$$\alpha_r = \frac{\omega_{12} - \omega_{10}}{\omega_{10}} \sim -\sqrt{\frac{E_C}{8E_J}}, \qquad \frac{E_J}{E_C} \to \infty. \tag{2.67}$$

Though approaching zero in the limit $E_J/E_C \to \infty$, the anharmonicity decays algebraically which means it decays much slower in E_J/E_C than the energy dispersion. Hence, there is a tradeoff between a sufficient flat energy dispersion and a relative anharmonicity that is still large enough to resolve individual transition frequencies. Typically, for transmon qubits it is $E_J/E_C \approx 50$.

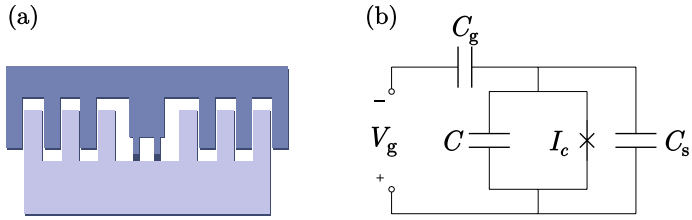

Fig. 2.8.: (a) The basic design of the transmon qubit is the same as for the Cooper pair box: a superconducting island coupled to a ground superconductor via a Josephson junction(s) with energy E_J. Different from the Cooper pair box, the transmon has a large shunt capacitance which allows to access the regime $E_J \gg E_C$. (b) The equivalent circuit diagram. The shunt junction is connected in parallel thereby lowering the charging energy of the island.

2.4. The circuit QED architecture

The cQED architecture has been proposed in 2004 by Blais *et al.* combining superconducting qubits coupled to one-dimensional coplanar stripline resonators in an on-chip architecture, see Fig. 2.9. Within the same year this design has been proven to be capable of accessing the strong coupling regime (Wallraff *et al.*, 2004). This is mainly because of two features: the large dipole moments of superconducting qubits—back in 2004 a Cooper pair box was used—, and the high zero-point field strength of a one-dimensional stripline resonator. The interplay of these two effects allows to reach coupling strengths that are much higher as those in (microwave) cavity QED. During the the last decade cQED has been proven to be very successful as demonstrated by many experiments. Just to name a few: it has been possible to create single microwave photons (Houck *et al.*, 2007) and to engineer entanglement between such a microwave photon and a transmon qubit, e.g., (Eichler *et al.*, 2012).

By coupling the stripline resonator to a superconducting transmission line, one is able to drive the cavity field by applying controlled microwave pulses and to measure the qubit state. Furthermore, the synergy of superconducting wave guides and

and evaluating the total energy in first order perturbation theory yields the same result, even though the perturbation series has zero convergence radius, cf. (Koch *et al.*, 2007).

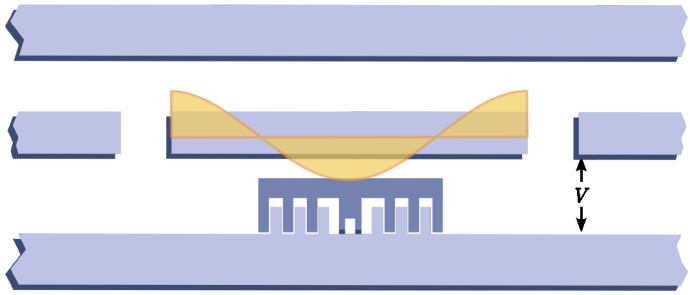

Fig. 2.9.: The cQED architecture: A transmon qubit sensitive to microwave radiation inside a coplanar stripline resonator. In the dispersive regime full sovereignty about the qubit is achieved. This allows for coherent control and readout via microwave radiation that is fed into the cavity from the transmission lines to the right and left of the resonator.

superconducting qubits allows to achieve high coherence times up to 10 µs within cQED using coplanar stripline resonators (Devoret and Schoelkopf, 2013). However, the usage of one-dimensional striplines bears the disadvantage of unavoidably incorporating parasitic capacitances causing unwanted losses of the resonator mode. In particular, these parasitic capacitances arise due to imperfections at the surface of the dielectric substrate on which the stripline resonator is grown (Gao *et al.*, 2008; O'Connell *et al.*, 2008). To avoid such problems, it has been suggested to use three-dimensional superconducting cavities just as in microwave cavity QED long before. In fact, by using three-dimensional cavity architectures, the cavity lifetimes are significantly increased as well as the qubit lifetimes that could be improved to reach 60 µs (Paik *et al.*, 2011).

Nevertheless, in the following a microwave cavity will always considered to be a coplanar stripline resonators as introduced in Sec. 2.2.4. All the other ingredients to be combined into the cQED architecture have been introduced in the preceding sections as well: superconducting electronics and the transmon qubit. In the following the interplay between these elements will be discussed in more detail. In particular, the dispersive readout for transmon qubits with cQED is a spectacular application of the strong coupling light-matter coupling achieved within cQED.

2.4.1. Transmon qubits coupled to a cavity

Just like in cavity QED the light-matter coupling between microwaves and superconducting qubits is mediated via the dipole Hamiltonian. In the language of superconducting electronics, however, the electric field of the resonator mode is replaced by the voltage at the central strip to ground, $V = V_{\mathrm{zp}}(a + a^\dagger)$ where the zero-point field strength is $V_{\mathrm{zp}} = (\hbar\omega_c/2C_c)^{1/2}$. Here ω_c denotes cavity mode and C is the total capacitance of the stripline resonator. To maximize the interaction between the transmon qubit and the cavity field, the qubit has to be placed at an antinode of the field mode. Therefore it is convenient to place the qubit in the middle of the

cavity and couple it to the second harmonic of the cavity. Of course, arrangements other than that are also possible.

The Hamiltonian of this system, comprised of the transmon qubit coupled to the second lowest mode of the stripline resonator, reads

$$H = \hbar\omega_c\, a^\dagger a + 4E_{\mathrm{C}}(N - n_{\mathrm{g}})^2 - E_{\mathrm{J}}\cos(\varphi) - 2e\beta V_{\mathrm{zp}} N(a^\dagger + a) \tag{2.68}$$

where the charge on the superconducting island of the qubit determines an excess energy $\propto N(a^\dagger + a)$. The factor $\beta = C_{\mathrm{g}}/C_\Sigma$ is the leverage arm of the gate, C_{g} is the gate capacitance, and $C_\Sigma = C_{\mathrm{s}} + C_{\mathrm{g}} + C$ is the total capacitance, see Fig. 2.8 (b). Represented in the basis of transmon eigenstates labeled by $|i\rangle$, the Hamiltonian (2.68) assumes the form

$$H = \hbar\omega_c\, a^\dagger a + \sum_i E_i |i\rangle\langle i| + \hbar \sum_{ij} g_{ij} |i\rangle\langle j| (a^\dagger + a) \tag{2.69}$$

with the effective light-matter interaction constants

$$g_{ij} = -\frac{2eV_{\mathrm{zp}}}{\hbar}\beta\langle i|N|j\rangle \tag{2.70}$$

analogously to the procedure in Sec. 2.1. As already argued above, the magnitude of the coupling constants g_{ij} are much larger than in cavity QED. This can be seen by expressing the transition matrix elements in terms of the asymptotic expansion for the wave functions,

$$|\langle i|N|j\rangle| \sim \sqrt{\frac{j+1}{2}} \left(\frac{E_{\mathrm{J}}}{8E_{\mathrm{C}}}\right)^{\frac{1}{4}} \delta_{i,j+1}, \qquad \frac{E_{\mathrm{J}}}{E_{\mathrm{C}}} \to \infty. \tag{2.71}$$

Interestingly, the effective light-matter couplings show an algebraic increase with increasing ratio $E_{\mathrm{J}}/E_{\mathrm{C}}$. In addition to that, the coupling strength can be tuned by varying the magnetic flux inside the loop between formed by the tunneling junctions.

Finally, by applying the rotating wave approximation, the Hamiltonian (2.68) can be reduced to the *generalized Jaynes-Cummings model*

$$H = \hbar\omega_c\, a^\dagger a + \sum_i E_i |i\rangle\langle i| + \hbar \sum_i \left(g_{i,i+1}\, |i\rangle\langle i+1|\, a^\dagger + \mathrm{H.c.}\right); \tag{2.72}$$

cf. (2.3). For a more detailed derivation of the generalized Jaynes-Cummings model, see Koch *et al.* (2007).

In the case of cavity QED, the size of atomic level splittings allowed for the resonance approximation, which reduces the model to only a few resonant transitions. For the transmon, however, this approximation cannot be made. In order to find a way of controlling the qubit states without driving the transmon out of the computational state space, i.e., the subspace spanned by $|0\rangle$ and $|1\rangle$, the influence of the light-matter interaction has to be made small. As will be discussed in the next section this is achieved by tuning the cavity resonance frequency off resonant from the level transitions of the transmon.

2.4.2. Control and readout in the dispersive regime

Using the transmon states $|0\rangle$ and $|1\rangle$ as the computational basis states, coherent manipulation of a general qubit state $\alpha\,|0\rangle+\beta\,|1\rangle$ can be achieved by absorbing (emitting) single photons from (into) the cavity. However, the generalized Jaynes-Cummings interaction also admits transitions to higher excited transmon states bringing the qubit out of its computational subspace. To suppress those unwanted transitions, the rate of absorbing or emitting photons needs to be regularized. This can be achieved by going into the *dispersive regime*, where the detuning between cavity frequency and transition frequency is large, $\Delta_i = \omega_c - \omega_{01} \gg g_{i,i+1}$. In this regime, the light-matter coupling cannot supply the energy, that is required to emit a microwave photon accompanied by a level transition of the transmon. This allows to approximate the influence of the light-matter interaction with methods of perturbation theory.

The dispersive shift

Treating the light-matter interaction as a perturbation of the bare states, the Hamiltonian (2.72) can be split into the non-interacting part

$$H_0 = \hbar\omega_c\, a^\dagger a + \sum_i E_i |i\rangle\langle i| \tag{2.73}$$

and the perturbation part

$$V = \hbar \sum_i \Big(g_{i,i+1}\, |i\rangle\langle i+1|\, a^\dagger + g^*_{i,i+1}\, |i+1\rangle\langle i|\, a \Big). \tag{2.74}$$

By using the method of *Schrieffer-Wolff transformation* (Schrieffer and Wolff, 1966), the full model $H = H_0 + V$ can be mapped onto an effective description of the low energy states which incorporates level-renormalizations due virtual exchange of photons. The effective Hamiltonian H' is obtained by evaluating a canonical transformation of the form $H' = \exp(S)\, H\, \exp(-S)$ where S is an anti-Hermitian operator $S^\dagger = -S$. By employing the *Campbell-Baker-Hausdorff formula*[15] the H' can be determined to an arbitrary order in S. Crucially, to find an effective model, in which the low energy dynamics is only affected via virtual fluctuations, all terms $\propto V$ have to disappear in the expansion. This is accomplished by finding an operator S such that $\lambda[H_0, S] = V$. In particular, for the generalized Jaynes-Cummings model the operator, that fulfills this requirement, turns out to be

$$S = \sum_i \frac{g_{i,i+1}}{\Delta_i} \Big(|i+1\rangle\langle i|\, a - |i+1\rangle\langle i|\, a^\dagger \Big). \tag{2.75}$$

[15] The Campbell-Baker-Hausdorff expansion is given by $\exp(X)\, Y\, \exp(-X) = \sum_n \frac{1}{n!}[X,Y]_n$ where the $(n+1)$th order commutator is recursively defined as $[X,Y]_{n+1} = [X,[X,Y]_n]$ with $[X,Y]_0 = Y$ and $[X,Y]$ the usual commutator. In order to turn the expansion into a convergent series, the operator S needs to depend upon a (set of) small parameter(s).

Here $g_{i,i+1} \in \mathbb{R}$ has been assumed. Since the excitation energy $\Delta_i \gg g_{i,i+1}$ of H_0 is large in the dispersive regime, virtual processes in which a photon is absorbed and re-emitted are very unlikely to happen. This is reflected in the fact that S depends upon the the small parameter $g_{i,i+1}/\Delta_i$ and allows to truncate the transformation in second order. Then the effective Hamiltonian in the dispersive regime is given by

$$H' \approx \frac{\hbar}{2}(\omega_{01} + \chi_{01})\sigma_z + \hbar(\omega_c + \chi\sigma_z)a^\dagger a, \tag{2.76}$$

where the pseudo-spin operators $\sigma_z = |1\rangle\langle 1| - |0\rangle\langle 0|$ and $\sigma_x = |1\rangle\langle 0| + |0\rangle\langle 1|$ are used to describe the qubit degrees of freedom. The parameters

$$\chi_{i,i+1} = \frac{g_{i,i+1}^2}{\Delta_i} = \frac{g_{ij}^2}{(E_{i+1} - E_i)/\hbar - \omega_c} \tag{2.77}$$

induce frequency shifts of the respective qubit transition. The renormalization of the energy levels $\omega_{01} + \chi_{01}$ can be traced back to vacuum fluctuations of the electromagnetic field. This is the cQED analog of the atomic *Lamb shift* (Blais *et al.*, 2004). Additionally, the interaction of the qubit with the electromagnetic field inside the cavity introduces a qubit state dependent shift of the cavity frequency, $\omega_c + \chi\sigma_z$ with $\chi = \chi_{01} - \chi_{12}/2$. This frequency pull is called the *dispersive shift* and can be identified as the *ac Stark effect* in cQED.

For the sake of implementing single-qubit gates, the cavity field is driven by a classical microwave signal $\mathcal{E}(t)$,

$$H_{\text{dr}} = \hbar\mathcal{E}(t)\big[a + a^\dagger\big], \tag{2.78}$$

cf. (2.41). This causes an additional contribution in the Schrieffer-Wolff transformation, which effectively implements a time-dependent interaction $\propto \sigma_x$. To first order in g_{01}/Δ_i, the qubit is driven by the ESR-like interaction

$$H_{\text{qb-dr}} = \hbar\mathcal{E}(t)\frac{g_{01}}{\Delta_1}\sigma_x \tag{2.79}$$

where $\mathcal{E}$ is the complex amplitude of the driving field. Physically, this term becomes relevant when the carrier frequency of the microwave signal is tuned on resonance with the qubit, $\mathcal{E}(t) \simeq \mathrm{e}^{-\mathrm{i}\omega_{01}t} f(t)$. When tuning the driving out of resonance, this term becomes negligible.

In addition to that, the dispersive regime provides ideal conditions for the implementation of a quantum non-demolition measurement: an interaction of the form $\propto \sigma_z a^\dagger a$—as the introduced by the ac Stark effect—commutes with the qubit Hamiltonian and leads to entanglement between the qubit and the cavity field. This can be nicely illustrated by looking at the time evolution of a coherent state $|\lambda\rangle$ in the dispersive regime,

$$\begin{aligned} U(t)\big(\alpha\,|0,\lambda\rangle + \beta\,|1,\lambda\rangle\big) &\simeq \exp\big(-\mathrm{i}\chi t\,\sigma_z a^\dagger a\big)\big(\alpha\,|0\rangle\otimes|\lambda\rangle + \beta\,|1\rangle\otimes|\lambda\rangle\big) \\ &= \alpha\;|0\rangle\otimes\big|\mathrm{e}^{-\mathrm{i}\chi t}\lambda\big\rangle + \beta\;|1\rangle\otimes\big|\mathrm{e}^{\mathrm{i}\chi t}\lambda\big\rangle\,. \end{aligned} \tag{2.80}$$

Then, by detecting whether the induced phase shift is χt or $-\chi t$, the qubit wave function is projected onto $|0\rangle$ or $|1\rangle$ thereby measuring the qubit state.

The dispersive time-evolution is a useful resource of entanglement, which can also be used for various applications other than readout: the preparation of Schrödinger cat states (Brune *et al.*, 1992) and the production of entanglement between distant qubits (Eichler *et al.*, 2012; Riste *et al.*, 2013; Roch *et al.*, 2014). This point will also become important in Ch. 6 where the production of measurement-induced-entanglement of remote transmon qubits will be discussed.

Homodyne readout and measurement back action

For the sake of implementing a qubit readout the (quasi-classical) coherent states $\left|\mathrm{e}^{-\mathrm{i}\chi t}\lambda\right\rangle$ and $\left|\mathrm{e}^{\mathrm{i}\chi t}\lambda\right\rangle$ in (2.80) serve as pointer states of the measurement. Since they may have a considerable overlap $\langle \mathrm{e}^{-\mathrm{i}\chi t}\lambda|\mathrm{e}^{-\mathrm{i}\chi t}\lambda\rangle \neq 0$, their relative phase usually cannot be measured instantaneously. Instead, phase-sensitive detection schemes such as a *homodyne measurement* extract information by weakly interacting with the quantum system. In particular, the homodyne measurement technique resolves the phase by mixing the reflected (or transmitted) radiation from the cavity with a strong coherent state and monitoring the combined signal at a voltmeter. Hence, for the purpose of reading out the qubit the transmission line acts in both directions: stimulating the cavity with radiation, i.e., supplying energy and enabling the transit of quantum information from the cavity to the detector.[16] At the measurement stage the voltmeter records the signal intensity[17]

$$\langle I_{\mathrm{hd}}\rangle = \left\langle V_{\mathrm{hd}}^{(-)} V_{\mathrm{hd}}^{(+)} \right\rangle = \left\langle \left(V_{\mathrm{lo}}^{(-)} + V_{\mathrm{out}}^{(-)}\right)\left(V_{\mathrm{lo}}^{(+)} + V_{\mathrm{out}}^{(+)}\right)\right\rangle. \tag{2.81}$$

The recorded voltage V_{hd} consists of two parts: the measurement signal V_{out} and the local oscillator voltage V_{lo}. Here, the operators $V_\alpha^{(+)} = V_{\mathrm{zp}} a$ and $V_\alpha^{(-)} = V_{\mathrm{zp}} a_\alpha^\dagger$ labeled by $\alpha \in \{\mathrm{hd}, \mathrm{lo}, \mathrm{out}\}$ denote the voltage-counterparts of the electrical field operators $\boldsymbol{E}^{(\pm)}$ for fields inside the transmission line; cf. Sec. A.2.4 of App. A. To be able to resolve the the qubit state dependent phase difference between the coherent states in the superposition (2.80), the intensity difference, i.e., the measurement signal

$$\begin{aligned}\langle \delta I_{\mathrm{hd}}(t)\rangle &= \left\langle V_{\mathrm{hd}}^{(-)} V_{\mathrm{hd}}^{(+)} \right\rangle_{\sigma_z=1} - \left\langle V_{\mathrm{hd}}^{(-)} V_{\mathrm{hd}}^{(+)} \right\rangle_{\sigma_z=-1} \\ &\simeq \left\langle V_{\mathrm{lo}}^{(-)} \Big[\underbrace{V_{\mathrm{out}}^{(+)}\big|_{\sigma_z=1} - V_{\mathrm{out}}^{(+)}\big|_{\sigma_z=-1}}_{\propto \sin(2\chi t)} \Big] \right\rangle + \text{c.c.}\end{aligned} \tag{2.82}$$

has to be discriminated from the background noise $\langle I_{\mathrm{hd}}^2\rangle - \langle I_{\mathrm{hd}}\rangle^2$ which is primarily due to shot noise of the local oscillator. Irradiating the cavity with a single-frequency

[16] A more detailed discussion about input-output theory of cavities as well as the homodyne measurement technique can be found in Secs. A.3.3 and A.3.4 of App. A.

[17] The operator of the signal intensity is defined as $I_{\mathrm{hd}} = V_{\mathrm{hd}}^{(-)} V_{\mathrm{hd}}^{(+)}$.

coherent state $|\alpha_{\rm in}\rangle$, the minimal measurement time is obtained by setting the signal-to-noise ratio to unity,[18)]

$$T = \frac{1}{2\Gamma_{\rm m}} = \frac{\kappa^2}{8\chi^2|\alpha_{\rm in}|^2} \tag{2.83}$$

where κ is the cavity broadening and $\Gamma_{\rm m}$ is the *measurement rate* of the dispersive readout. The occurrence of a finite rate, at which information about the qubit is gained, states that the detector needs to gather statistics for a finite interval of time before the measurement is completed. Therefore, if the dispersive interaction appears to be as small perturbation to the qubit, the interaction-induced phase shift per photon is small $2\chi/\kappa \ll \pi$ and the measurement time is large indicating the weak continuous character of the homodyne readout.

Nevertheless, the wave function is projected onto one of its basis states due to measurement-induced back action of the detector. While recording the homodyne signal, the photon number inside the cavity becomes a randomly altering quantity $n(t) = a^\dagger(t)a(t)$ with $[a(t), a^\dagger(t')] = \mathrm{e}^{-\kappa|t-t'|/2}$ fluctuating around its mean value $\langle n(t)\rangle = |\alpha|^2$ and thus contributes to the dephasing rate of the qubit via the ac Stark interaction $\hbar\chi\sigma_z n(t)$. The measurement-induced dephasing rate can be obtained from the decay of the two-time correlation function

$$\begin{aligned}\langle\sigma^+(t+\tau)\sigma^-(t)\rangle &= \left\langle \exp\left(-\mathrm{i}2\chi\int_0^\tau n(t)\mathrm{d}t\right)\right\rangle \\ &\simeq \exp\left(-2\chi^2\int_0^\tau\int_0^\tau \langle\!\langle n(t)n(t')\rangle\!\rangle\,\mathrm{d}t\mathrm{d}t'\right) \\ &\sim \exp\left(-\frac{8\chi^2|\alpha_{\rm in}|^2}{\kappa^2}\tau\right).\end{aligned} \tag{2.84}$$

For this derivation the cumulant expansion[19)] has been used. Furthermore, it has been assumed that $n(t)$ is described by a Gaussian process whose second cumulant derives to

$$\begin{aligned}\langle\!\langle n(t)n(t')\rangle\!\rangle &= \langle n(t)n(t')\rangle - \langle n\rangle^2 = \mathrm{e}^{-\kappa|t-t'|/2}\,\langle a^\dagger(t)a(t')\rangle \\ &\sim 4\kappa^{-1}\langle n\rangle\,\delta(t-t').\end{aligned}$$

In the long time limit, in which $t - t'$ significantly exceeds the photon lifetime κ^{-1}, the exponential cut-off as introduced by the cavity line width κ can be replaced by a

[18)] Cf. Eq. (A.87) of App. A with a reflection coefficient of $R = \frac{1}{2}$.

[19)] In general, for a single random variable X the cumulant expansion assumes the form $\langle\exp(\mathrm{i}X)\rangle = \exp\left(\sum_k \mathrm{i}^k\langle\!\langle X^k\rangle\!\rangle/k!\right)$ where the double brackets denote the cumulants of X, see Gardiner (2009). These can be given in terms of the usual expectation value by comparing the expansion of the exponential in terms of the statistical moments $\{\langle X^k\rangle\}$ with the cumulant expansion . For the first two cumulants this explicitly yields $\langle\!\langle X\rangle\!\rangle = \langle X\rangle$ (mean value) and $\langle\!\langle X_1X_2\rangle\!\rangle = \langle X_1X_2\rangle - \langle X_1\rangle\langle X_2\rangle$ (covariance). In particular, for a Gaussian process all higher cumulants exactly vanish such that the cumulant expansion is automatically cut off in second order.

δ-function. The measurement-induced dephasing rate is $\Gamma_\phi = -8\chi^2\kappa|\alpha_{\mathrm{in}}|^2$ implying that the dephasing rate is twice as high as the the measurement rate by a factor of two, $\Gamma_\phi = 2\Gamma_{\mathrm{m}}$.

In the case of the transmon qubit, however, the transmission line resonator has been assumed to be a two-sided cavity which means that photons are emitted from the cavity in both directions. Consequently, the phase information carried by a single photon is equally distributed into the transmission and backscattering channels, too. In other words, every single photon, which is not measured by the detector, carries wasted information that is eventually dissipated into the environment. This amount of wasted information demonstrates the ambiguous role of entanglement for the measurement: entanglement of a quantum system with the measurement apparatus, which is a controllable part of the environment, is a necessary ingredient to gain information about a quantum system, whereas entanglement of the quantum system with the rest of the environment wastes the information to be gained.

Chapter 3

Majorana qubits

In a superconductor there are two kinds of excitations: the collective dynamics of the superconducting condensate and particle-like excitations above the superconducting gap. The motion of the superfluid as a hole happens at energy scales whose magnitude is given by the plasma frequency $\hbar\omega_\mathrm{p}$, whereas the motion of individual quasiparticles happens at energies above the superconducting gap Δ. While the last chapter was primarily dealing with the quantum properties of the collective motion of the electric fluid in the superconductor, this chapter will be focussed on a specific type of quasiparticles—Majorana bound states.

In contrast to common quasiparticles, Majorana bound states occur as mid-gap states of a superconductor and have the remarkable property of obeying non-Abelian exchange statistics. Furthermore, the content of quantum information, which can be imprinted in these zero modes, is remarkably robust to decoherence; owing to the topological properties of their host superconductor, Majorana bound states are essentially immune to local perturbations which suggests to use Majorana quasiparticles as qubits for fault-tolerant quantum computation. This poses the question in which materials Majorana zero modes can be realized.

Originally, the occurrence of Majorana quasiparticles has been predicted for the fractional quantum Hall state at filling fraction $\nu = \frac{5}{2}$ (Moore and Read, 1991; Greiter *et al.*, 1992; Read and Green, 2000). Due to some remarkable similarities between the $\nu = \frac{5}{2}$ fractional quantum Hall state and p-wave superconductivity, non-Abelian Majorana quasiparticles are also expected to be found in certain types of superconductors called topological superconductors. However, since both—the $\nu = \frac{5}{2}$ state as well as topological superconductors—are rather challenging to realize experimentally, Majorana-based qubits have to be constructed by other means. One approach towards Majorana bound states, that has attracted a lot of attention in condensed matter physics, is the discovery that topological superconductivity can be mimicked by semiconducting-superconducting nanowires. Having found signs of evidence for Majorana quasiparticles already, first experiments raise the hope to be able to construct topological qubits in the near future. Moreover, the usage of nanoscale technology promises the production of tunable and scalable devices that allow to combine the benefits of topological qubits with those of conventional superconducting qubits.

In the following, the concept of Majorana zero modes (MZMs) shall be introduced from a theoretical perspective. After introducing the notion of a topological superconductor, it will be shown that MZMs inevitably emerge at the edge of such

superconductors. In the second section, it will be demonstrated how topological superconductivity may be implemented and detected by utilizing semiconducting-superconducting hybrid systems. The last section of this chapter deals with the the concept of a Majorana-based qubit. There, it will be discussed how MZMs can be exploited for quantum information processing including hybrid approaches in which topological qubits and superconducting qubits are combined with each other.

3.1. Majorana zero modes

Curiously, Majorana quasiparticle excitations are excitations in superconductors having zero energy. Furthermore, their occurrence is closely tied to a topological superconductor, i.e., a particular superconducting state which exhibits p-wave paring. Therefore it is worth to look a bit more closely into the p-wave pairing state before studying the implementations of MZMs in other systems such as superconductor-semiconductor hybrid devices.

3.1.1. *p*-wave superconductivity

Within BCS theory, the superconducting state is satisfactorily explained by merging electrons pairwise into Cooper pairs; under the action of an attractive interaction the Fermi sea of non-interacting electrons is recast into a condensate of Cooper pairs. With the formation of this superconducting condensate, the binding energy of a Cooper pair introduces the emergent superconducting energy gap which is locked to the Fermi surface.

In its original formulation the BCS theory assumes electrons to be bound in pairs having zero total momentum *and* zero angular momentum. These assumptions give a satisfactory description for all conventional superconductors, the so-called s-wave superconductors whose Cooper pair wave functions are spherically symmetric. However, by hypothesizing possibly different superconducting and superfluid states as for instance for superfluid ^{3}He, the conventional pairing mechanism has been extended to arbitrary orbital angular momenta $\ell = s, p, d, f, \ldots$ not long after BCS (Anderson and Morel, 1960; Balian and Werthamer, 1963). And indeed, these theoretical speculations turned out to be very profitable as the first evidence for unconventional Cooper pairing has been given with the discovery of p-wave pairing in the superfluid phases of ^{3}He (Osheroff *et al.*, 1972). It is also believed that unconventional pairing may also be present in high-temperature superconductors. In particular, *strontium ruthenate* Sr_2RuO_4, whose superconductivity was discovered in 1994 (Maeno *et al.*, 1994), is expected to have p-wave pairing because of similarities to the superfluid A-phase of ^{3}He (Rice and Sigrist, 1995; Baskaran, 1996).[1)]

[1)] For a more detailed discussion about the superconducting state of strontium ruthenate see Maeno *et al.* (2001); Mackenzie and Maeno (2003).

The superfluid phases of ^{3}He unfold a rich spectrum of excitations. In particular, the occurrence of topological defects in ^{3}He allows to observe many exotic effects like domain walls, vortices as well as characteristic quasiparticle excitations such as zero modes (Leggett, 1975; Vollhardt and Wölfle, 1990; Volovik, 2003). Because most of these intriguing effects can be traced back to the absence of spin rotational symmetry (in the A-phase) and the topology of the p-wave pairing state, all these kinds of effects are also to be expected for p-wave superconductors whose symmetry is similar to that of ^{3}He-A.

A simplified model that describes the low-energy sector of a p-wave superconductor and captures these effects—and in particular reveals the emergence of MZMs—has to be described by spin-polarized fermions,

$$H = \int \psi^\dagger(\boldsymbol{r}) \left[-\frac{\hbar^2}{2m_e^*}\nabla^2 - \mu \right] \psi'(\boldsymbol{r})\, \mathrm{d}^3 r + \frac{1}{2} \iint \left[\psi(\boldsymbol{r}) D^*(\boldsymbol{r}-\boldsymbol{r}')\psi(\boldsymbol{r}') + \psi^\dagger(\boldsymbol{r}) D(\boldsymbol{r}-\boldsymbol{r}')\psi^\dagger(\boldsymbol{r}') \right] \mathrm{d}^3 r \mathrm{d}^3 r'. \tag{3.1}$$

Here the electron field operators $\psi(x)$, $\psi^\dagger(x)$ characterize only a single spin direction and obey the *canonical anticommutation relations* $\{\psi(\boldsymbol{r}_1), \psi^\dagger(\boldsymbol{r}_2)\} = \delta(\boldsymbol{r}_1 - \boldsymbol{r}_2)$. Furthermore, μ is the chemical potential, m_e^* is the effective electron mass of the band,[2)] and at low energies the p-wave pairing amplitude assumes the form

$$D(\boldsymbol{r}-\boldsymbol{r}') = -\mathrm{i}\Delta\left[\partial_{x'} - \mathrm{i}\partial_{y'}\right]\delta(\boldsymbol{r}-\boldsymbol{r}'). \tag{3.2}$$

Note that the amplitude $\Delta \in \mathbb{C}$ is a complex number. By considering a clean superconductor, it is convenient to express H in the basis of Bloch functions labeled by their lattice momentum $\boldsymbol{k}$. In $\boldsymbol{k}$-space the Hamiltonian is block-diagonal and reads

$$H = \sum_{\boldsymbol{k}\in \mathrm{BZ}} \xi_{\boldsymbol{k}} c_{\boldsymbol{k}}^\dagger c_{\boldsymbol{k}} + \frac{1}{2}\left[\Delta^*(k_x + \mathrm{i}k_y) c_{-\boldsymbol{k}} c_{\boldsymbol{k}} + \Delta(k_x - \mathrm{i}k_y) c_{\boldsymbol{k}}^\dagger c_{-\boldsymbol{k}}^\dagger \right]. \tag{3.3}$$

with $\xi_{\boldsymbol{k}} = \varepsilon_{\boldsymbol{k}} - \mu$ and $\varepsilon_{\boldsymbol{k}}$ denoting the single particle band energies within the first Brillouin zone (BZ). In terms of momentum states the pairing term transforms into $D(\boldsymbol{r}-\boldsymbol{r}') \mapsto \Delta(k_x - \mathrm{i}k_y)$.[3)]

The ground state of (3.3) is found to be a BCS-like pairing state of the form

$$|\Omega\rangle = \prod_{\boldsymbol{k}} \left(u_{\boldsymbol{k}} + v_{\boldsymbol{k}} c_{\boldsymbol{k}}^\dagger c_{-\boldsymbol{k}}^\dagger \right) |0\rangle = \left(\prod_{\boldsymbol{k}} u_{\boldsymbol{k}} \right) \exp\left(\sum_{\boldsymbol{k}} g_{\boldsymbol{k}} c_{\boldsymbol{k}}^\dagger c_{-\boldsymbol{k}}^\dagger \right) |0\rangle \tag{3.4}$$

where the product and the sum have to be taken over all *distinct pairs* $(\boldsymbol{k}, -\boldsymbol{k})$ and the state $|0\rangle$ denotes the fermionic vacuum with no particles present. Furthermore,

[2)] Not to be confused with the Cooper pair mass $m^* = 2m_e^*$.

[3)] Since this is an approximation valid for long wavelengths, the gap function $\Delta(\boldsymbol{k})$ needs to be regularized for small wavelengths.

by demanding $|u_{\boldsymbol{k}}|^2 + |v_{\boldsymbol{k}}|^2 = 1$ normalization of the pairing state is achieved; note, that the combination $g_{\boldsymbol{k}} = v_{\boldsymbol{k}}/u_{\boldsymbol{k}}$ is the Cooper pair wave function in $\boldsymbol{k}$-space. The last equality in (3.4) expresses the fact that the BCS-like ground state of a p-wave superconductor is a *fermionic Gaussian state*.[4)] In order to find the quasiparticle excitations of H it is convenient to exploit the fact that there is an intimate connection between fermionic Gaussian states forming the fermionic vacuum state for a set of dressed fermionic modes $\beta_{\boldsymbol{k}}$, $\beta_{\boldsymbol{k}}^\dagger$ defined via $\beta_{\boldsymbol{k}}|\Omega\rangle = 0$. Therefore, one seeks fermionic excitations given by the *Bogoliubov transformation*

$$\beta_{\boldsymbol{k}} = u_{\boldsymbol{k}} c_{\boldsymbol{k}} + v_{\boldsymbol{k}} c_{-\boldsymbol{k}}^\dagger, \tag{3.5a}$$

$$\beta_{-\boldsymbol{k}}^\dagger = u_{\boldsymbol{k}} c_{-\boldsymbol{k}}^\dagger - v_{\boldsymbol{k}} c_{\boldsymbol{k}} \tag{3.5b}$$

where the parameters $u_{\boldsymbol{k}}$ and $v_{\boldsymbol{k}}$ have to make sure that the fermionic character of the excitations stays intact, i.e., $\{\beta_{\boldsymbol{k}}, \beta_{\boldsymbol{l}}^\dagger\} = \delta_{\boldsymbol{kl}}$. This translates into the constraint $|u_{\boldsymbol{k}}|^2 + |v_{\boldsymbol{k}}|^2 = 1$.

In addition, the parameters of the Bogoliubov transformation have to be determined such that H is diagonal in terms of the quasiparticle operators $\beta_{\boldsymbol{k}}$, $\beta_{\boldsymbol{k}}$,

$$H = \sum_{\boldsymbol{k}\in \mathrm{BZ}} E_{\boldsymbol{k}} \beta_{\boldsymbol{k}}^\dagger \beta_{\boldsymbol{k}} + E_{\mathrm{gs}} \tag{3.6}$$

with $E_{\boldsymbol{k}}$ denoting the quasiparticle excitation energies and E_{gs} the (non-observable) ground state energy. To find the correct transformation it is convenient to use the method of Bogoliubov-de Gennes (BdG) in which the second-quantized Hamiltonian H is mapped onto a first-quantized matrix $\mathcal{H}_{\mathrm{BdG}}$ called the BdG Hamiltonian,

$$H = \frac{1}{2} \sum_{\boldsymbol{k}\in \mathrm{BZ}} \begin{pmatrix} c_{\boldsymbol{k}}^\dagger \\ c_{-\boldsymbol{k}} \end{pmatrix}^{\mathrm{T}} \underbrace{\begin{pmatrix} \xi(\boldsymbol{k}) & \Delta(k_x - \mathrm{i}k_y) \\ \Delta^*(k_x + \mathrm{i}k_y) & -\xi(-\boldsymbol{k}) \end{pmatrix}}_{\mathcal{H}_{\mathrm{BdG}}(\boldsymbol{k})} \begin{pmatrix} c_{\boldsymbol{k}} \\ c_{-\boldsymbol{k}}^\dagger \end{pmatrix}. \tag{3.7}$$

Then, by translating the Bogoliubov transformation into this matrix description, the parameters $u_{\boldsymbol{k}}$ and $v_{\boldsymbol{k}}$ can be evaluated by solving the *Bogoliubov-de Gennes equation*

$$\mathcal{H}_{\mathrm{BdG}}(\boldsymbol{k})\Psi(\boldsymbol{k}) = E_{\boldsymbol{k}}\Psi(\boldsymbol{k}), \qquad \Psi(\boldsymbol{k}) = \begin{pmatrix} u_{\boldsymbol{k}} \\ v_{\boldsymbol{k}} \end{pmatrix}. \tag{3.8}$$

The normalized two-component spinor $\Psi(\boldsymbol{k})$, whose first (second) component refers to electron (hole) states, is called the *Nambu spinor*.

It is important to understand that even though the BdG equation seems to appear in a first-quantized fashion, it inherently describes a second-quantized model. This is also reflected in the fact that the BdG description carries a build-in redundancy that comes from an artificial doubling of the electron band. More concretely, the self-evident identity $\big(c_{-\boldsymbol{k}}, c_{\boldsymbol{k}}^\dagger\big) = \big[\sigma_x \big(c_{\boldsymbol{k}}, c_{-\boldsymbol{k}}^\dagger\big)^{\mathrm{T}}\big]^\dagger$ has to be reflected in the BdG matrix

[4)] In some sense $|\Omega\rangle$ can be seen as the fermionic analog of the squeezed vacuum state $|0, \zeta\rangle$ of the (bosonic) electromagnetic field as introduced in Sec. A.2.4 of App. A.

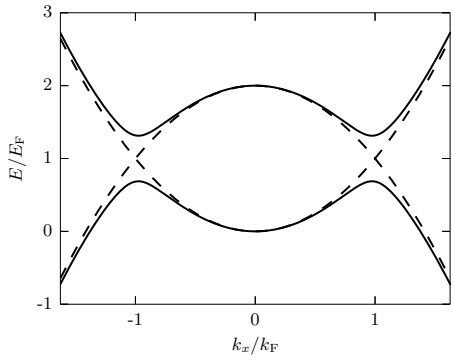

Fig. 3.1.: Bogoliubov-de Gennes excitation spectrum of a p-wave superconductor as a function of k_x at $k_y = 0$. The solid lines indicate the excitation energies $E(k_x) > E_F$ and their particle-hole reversed counterparts $E(k_x) < 0$. While these bands are gapped by the magnitudes of the superconducting pairing Δ, the normal-conducting bands (dashed parabolas) cross at the Fermi level.

description which means one has to impose the particle-hole constraint on the BdG Hamiltonian

$$-\mathcal{H}_{\mathrm{BdG}}(\boldsymbol{k}) = \mathcal{C}^{-1}\,\mathcal{H}_{\mathrm{BdG}}(\boldsymbol{k})\,\mathcal{C} = \sigma_x \mathcal{H}^*_{\mathrm{BdG}}(-\boldsymbol{k})\sigma_x \tag{3.9}$$

as well as on the Nambu spinors

$$\begin{pmatrix} u_{\boldsymbol{k}} \\ v_{\boldsymbol{k}} \end{pmatrix} = \mathcal{C} \begin{pmatrix} u_{\boldsymbol{k}} \\ v_{\boldsymbol{k}} \end{pmatrix} = \begin{pmatrix} v^*_{-\boldsymbol{k}} \\ u^*_{-\boldsymbol{k}} \end{pmatrix}. \tag{3.10}$$

The antiunitary operator $\mathcal{C} = \sigma_x \mathcal{K}$ is the particle-hole symmetry operator that exchanges electron and hole-like states, where $\mathcal{K}$ indicates the complex conjugation in real space. As a consequence of defining $\mathcal{K}$ as the complex conjugation in real space, the momentum vector has to be inverted by the action of $\mathcal{K}$, $\boldsymbol{k} \mapsto -\boldsymbol{k}$.

The solution of the eigenvalue problem (3.3) can be found via a unitary transformation $\mathcal{U}^\dagger \mathcal{H}_{\mathrm{BdG}} \mathcal{U} = \mathrm{diag}(E_{\boldsymbol{k}}, -E_{\boldsymbol{k}})$. Due to the constraint (3.9), the BdG spectrum always contains pairs conjugated eigenvalues $E_{\boldsymbol{k}}$ and $-E_{\boldsymbol{k}}$. In the concrete case of Hamiltonian (3.3), this leads to the excitation energies and the Nambu spinor solutions

$$E_{\boldsymbol{k}} = \sqrt{\xi^2_{\boldsymbol{k}} + |\Delta|^2(k_x^2 + k_y^2)}, \qquad \Psi(\boldsymbol{k}) = \frac{1}{\sqrt{2}} \begin{pmatrix} \left[1 + \xi_{\boldsymbol{k}}/E_{\boldsymbol{k}}\right]^{\frac{1}{2}} \\ \left[1 - \xi_{\boldsymbol{k}}/E_{\boldsymbol{k}}\right]^{\frac{1}{2}} \end{pmatrix}. \tag{3.11}$$

For convenience, the global phase of the Nambu spinor solution has been set here to zero.

3.1.2. Topological superconductivity and the Kitaev chain

By the method of BdG a second-quantized quadratic Hamiltonian is mapped onto the BdG matrix. In fact, this kind of mapping allows to classify all quadratic Hamiltonians within a general classification scheme. Based on *F. J. Dyson's* threefold way, *A. Altland* and *M. R. Zirnbauer* (1997) integrated the superconducting BdG Hamiltonians into a symmetry classification scheme and assigned four independent classes

Tab. 3.1.: Classification of the superconducting BdG Hamiltonians according to Altland and Zirnbauer. The symmetry classes of the BdG Hamiltonians, listed by their Cartan label and the corresponding Lie group, are determined by the discrete symmetries $\mathcal{T}, \mathcal{C}$, and $\mathcal{S}$. Time-reversal symmetry and particle-hole symmetry may occur in two fundamental representations, labeled by their eigenvalues $\mathcal{T}, \mathcal{C} = \pm 1$. The absence of any of these three symmetries is denoted by $\mathcal{T}, \mathcal{C}, \mathcal{S} = 0$. Additionally, the last three columns indicate the nature of the topological invariant for each class in one, two, and three dimensions. In particular, the spin-polarized p-wave superconductor is a representative of class D for which MZMs can be found in one and two dimensions.

Symmetry classification					*Topology*		
Cartan class	Lie group	$\mathcal{T}$	$\mathcal{C}$	$\mathcal{S}$	1D	2D	3D
D	$\mathrm{SO}(2n)$	0	$+1$	0	$\mathbb{Z}_2$	$\mathbb{Z}$	-
C	$\mathrm{Sp}(2n)$	0	-1	0	-	$\mathbb{Z}$	-
DIII	$\mathrm{SO}(2n)/\mathrm{U}(n)$	-1	$+1$	1	$\mathbb{Z}_2$	$\mathbb{Z}_2$	$\mathbb{Z}$
CI	$\mathrm{Sp}(2n)/\mathrm{U}(n)$	$+1$	-1	1	-	-	$\mathbb{Z}$

to them. Strikingly, for each class the time-evolution operator $\exp(-\mathrm{i}\mathcal{H}_{\mathrm{BdG}}t)$ belongs to a characteristic Lie group that fits into Cartan's classification scheme of symmetric spaces.[5)] Within the Altland-Zirnbauer classification, the BdG Hamiltonians are tabulated by their (discrete) inversion symmetries: the time-reversal symmetry $\mathcal{T}$, the sublattice or chiral symmetry $\mathcal{S}$, and the particle-hole symmetry $\mathcal{C}$. An overview of the superconducting classes is given in Tab. 3.1.

Although the symmetry classification exhaustively categorizes all quadratic model Hamiltonians, it was just the starting point for a *topological classification* of symmetry-protected BdG Hamiltonians. For the non-interacting (quadratic) and gapped Hamiltonians, topological phases essentially emerge due to the fact that the time-evolution operator is by its symmetry restrained to a Lie group that is a subgroup of the full unitary group having non-trivial topology. Accordingly, two Hamiltonians are said to be topological equivalent if one can smoothly interpolate between them by changing their parameters without closing the gap, i.e., without changing the symmetry class. This kind of topological order is called symmetry protected topological order and has been classified within the periodic table for topological insulators and superconductors (Schnyder *et al.*, 2008; Kitaev, 2009; Schnyder *et al.*, 2009; Ryu *et al.*, 2010).

This raises the question at which point topology enters the description of a non-interacting, gapped system described by a BdG Hamiltonian. In view of the Majorana edge modes this will be answered on the basis of the topological properties of the spinless p-wave superconductor in symmetry class D. As one can see from Tab. 3.1, a superconductor in symmetry class D admits symmetry protected topological phases only in one and two dimensions. By recognizing that (3.7) defines an entire family

[5)] A symmetric space is a finite-dimensional Riemannian manifold of overall constant curvature.

of BdG Hamiltonians $\mathcal{H}_{\mathrm{BdG}}(\boldsymbol{k})$ labeled by their Bloch momentum $\boldsymbol{k} \in \mathrm{BZ}$, $\mathcal{H}_{\mathrm{BdG}}(\boldsymbol{k})$ defines a mapping from the Brillouin zone into the space of Hermitian 2×2 matrices which can be visualized by a pseudo-Bloch sphere S^2.[6] Then, the BdG Hamiltonian may be represented in terms of Pauli matrices $\boldsymbol{\tau} = (\tau_x, \tau_y, \tau_z)^{\mathrm{T}}$ acting upon the Nambu spinors,

$$\mathcal{H}_{\mathrm{BdG}} = \boldsymbol{h}(\boldsymbol{k}) \cdot \boldsymbol{\tau}. \tag{3.12}$$

The real vector field $\boldsymbol{h}(\boldsymbol{k})$ describes the successive motion of the Nambu spinor on the pseudo-Bloch sphere as function of $\boldsymbol{k}$. As will be illustrated in the following these kinds of mappings can be studied by using topology and in particular homotopy theory which categorizes such mappings into equivalence classes indexed by a so-called topological invariant.

The most prominent and illustrative example is the *Kitaev chain*: a one-dimensional topological superconductor in class D that is defined on a lattice. This model has been proposed in 2001 by *A. Yu. Kitaev* and illustrates how the topology of the BdG mapping gives rise to non-trivial effects. Crucially, this model admits Majorana quasiparticle solutions occurring at the ends of the wire (Kitaev, 2001). The BdG Hamiltonian of the Kitaev chain is given by

$$\mathcal{H}_{\mathrm{BdG}}(k) = \xi(k)\tau_z + \Delta \sin(k)\tau_x \tag{3.13}$$

where $\xi(k) = -t \cos k - \mu$ is the kinetic energy and $\Delta \sin k$ is the p-wave pairing potential on a one-dimensional lattice. In the limit of small k, the Kitaev model reduces to a one-dimensional version of the p-wave superconducting Hamiltonian (3.7). In one dimension the Brillouin zone can be viewed as a circle $k \in \mathrm{BZ}_{1\mathrm{D}} \cong \mathrm{S}^1$ which is, by virtue of the BdG mapping, promoted into closed loops on the pseudo-Bloch sphere. The shape and topology of these closed paths are determined by the parameters in the BdG Hamiltonian; for the Kitaev chain these are t, μ and Δ. For BdG Hamiltonians, however, the built-in particle-hole redundancy has to be taken into account as well. By demanding $\mathcal{C}^{-1}\mathcal{H}_{\mathrm{BdG}}(k)\mathcal{C} = -\mathcal{H}_{\mathrm{BdG}}(k)$ where $\mathcal{C} = \tau_x\mathcal{K}$ is the particle-hole symmetry operator, the vector field is subject to the inversion symmetries

$$h_x(k) = -h_x(-k), \qquad h_y(k) = -h_y(-k), \qquad h_z(k) = h_z(-k).$$

As a consequence of these restrictions, it is sufficient to specify the mapping $\boldsymbol{h}(k)$ on one half of the Brillouin zone only, e.g., $k \in [0, \pi]$. Furthermore, the restrictions on the components h_x and h_y imply that $\boldsymbol{h}(k)$ necessarily passes the north pole or the south pole for $k = 0$ and $k = \pi$. This gives rise to two topologically distinct classes of closed loops:[7] those that are contractible to a single point and those that are non-contractible by connecting the north pole and the south pole, see Fig. 3.2. In order

[6] It is convenient to view the Nambu spinors $\Psi(\boldsymbol{k})$ as unit vectors defined on this pseudo-Bloch sphere where $(1, 0)^{\mathrm{T}}$ is identified with the north pole of the sphere and $(0, 1)^{\mathrm{T}}$ with the south pole.

[7] An intuitive understanding of why there are two topologically distinct types of loops can be given

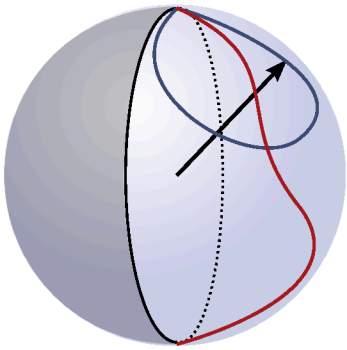

Fig. 3.2.: Closed loops on the pseudo-Bloch sphere for the Nambu spinors. A point on the sphere corresponds to a certain orientation of the Nambu spinor (black arrow). Via the build-in particle-hole constraint, antipodal points are identified with each other. Therefore, only points on one of the two hemispheres (shaded and unshaded regions) describe the independent configurations of the system. Two representatives of loops (blue and red) are shown. The blue loop is topologically trivial, i.e., can be contracted to a single point while the red line is topologically non-trivial.

to define a path, that connects the north pole with the south pole, the parameters of the Kitaev chain have to be chosen such that $|\mu| < t$ whereas for $|\mu| > t$ the loop always remains contractible to a single point. The existence of these two distinct types of loops is expressed by the $\mathbb{Z}_2$ topological invariant $\operatorname{sgn}\big(h_z(0)h_z(\pi)\big) = \pm 1$.[8)]

By changing the homotopy class, the physical behavior changes abruptly. As reflected in the long-range behavior of the Cooper pair wave function, the Kitaev chain admits two distinct phases,

$$g(x) = \frac{1}{2\pi}\int_{\mathrm{BZ}} g_k \, \mathrm{e}^{\mathrm{i}kx}\mathrm{d}k \sim \begin{cases} \mathrm{e}^{-|x|/\xi}, & \text{for } |\mu| > t \\ \text{const.}, & \text{for } |\mu| < t \end{cases}. \tag{3.14}$$

Note that ξ is the superconducting coherence length. For $|\mu| > t$ the system is in the strong pairing phase in which the Cooper pairs are tightly bound, whereas for $|\mu| < t$ the Cooper wave function is essentially constant (in one dimension). Then, the system is in the so-called weak pairing phase. Strikingly, by sweeping through the points $\mu = t$ or $\mu = -t$, the system undergoes a phase transition from strong to weak pairing which is not accompanied with the spontaneous breaking of any symmetry. Instead, the phase transition is accompanied by a change in the topology of the BdG mapping therefore called a *topological phase transition*, see also Refs. (Kitaev, 2001; Read and Green, 2000; Alicea, 2012). As will be shown in the next paragraph, another manifestation of the topological order in the Kitaev chain is the emergence of MZMs living at the ends of the wire.

---

on the level of the Nambu spinors. As the particle-hole constraint identifies all pairs of antipodal points of the pseudo-Bloch sphere, all those pairs describe to the same configuration. The north pole for example corresponds to the same configuration as the south pole. Mathematically speaking, the identification of antipodal points reduces the pseudo-Bloch sphere S^2 to the real projective plane $\mathbb{R}\mathrm{P}^2 \cong \mathrm{S}^2/\mathbb{Z}_2$ whose *first homotopy group* $\pi_1(\mathbb{R}\mathrm{P}^2) \cong \mathbb{Z}_2$ indicates the existence of two inequivalent classes of loops on the constraint pseudo-Bloch sphere.

[8)] In higher dimensions the mapping $\boldsymbol{h}(\boldsymbol{k})$ is characterized by coverings of the pseudo-Bloch sphere with closed surfaces (2D), volumes (3D), etc. This can be formulated in terms of higher homotopy groups and is tabulated in the periodic table of topological insulators and superconductors. For a review on the topic of topological insulators and superconductors, see Hasan and Kane (2010); Qi and Zhang (2011).

3.1.3. Majorana edge states

The occurrence of gapless (conducting) states living at the boundary of a topological material is an intriguing aspect of topological order. The *bulk-boundary correspondence* hypothesizes an intimate relationship between the bulk theory of a topological superconductor (or insulator) and an effective gapless theory on its boundary. In particular, tied to the existence of a topological phase in the bulk material, these edge excitations are exceptionally stable with respect to local perturbations. This is in sharp contrast to regular metallic states whose conductivity are usually suppressed due to the phenomenon of Anderson localization.[9)] The bulk-boundary correspondence is a general concept that applies to most topological materials, but in view of the MZMs only the case of an one-dimensional topological superconductor, as already introduced above, will be considered here.

According to the bulk-boundary correspondence, one has to seek for MZMs at the phase boundary between two topologically distinct sections of the wire. As the Kitaev wire endorses only two topological phases, a phase boundary is the narrow region in space where the system interpolates between the strong and weak pairing phase, see Fig. 3.3. Note, that since the vacuum state is a topologically trivial state too, the material might also be terminated by the vacuum as well. In any case, at the phase boundary between two topologically different regions, the chemical potential necessarily closes the gap by crossing one of the two points $\mu = \pm t$. For concreteness, suppose the chemical potential takes the values $\mu = -2t$ (strong pairing phase) for $x \to -\infty$ and $\mu = 0$ (weak pairing phase) for $x \to \infty$ as depicted in Fig. 3.3. Then, $\mu(x)$ forms a *domain wall* between these two phases by smoothly interpolating between both phases. Hence, the local chemical potential $\mu(x)$ necessarily crosses the point $\mu = -t$ somewhere in the intermediate regions, say at $x = 0$. For such a spatially varying chemical potential, the BdG equation is not translational invariant anymore. Instead, at low energies it assumes the form,[10)]

$$\big[-\big(t+\mu(x)\big)\tau_z + \Delta p_x \tau_x\big]\Psi(x) = E\Psi(x). \tag{3.15}$$

Interestingly, this model admits zero energy solutions which are localized at the phase boundary. Setting the energy to zero, the BdG equation reduces to the homogeneous equations

$$\mathrm{i}\hbar\Delta\frac{\partial v}{\partial x} = -\big(t+\mu(x)\big)u, \qquad \mathrm{i}\hbar\Delta\frac{\partial u}{\partial x} = \big(t+\mu(x)\big)v. \tag{3.16}$$

Eigensolutions of these coupled differential equations are given by two spinors of the form $\Upsilon_1 = (w_1, w_1^*)^{\mathrm{T}}$ and $\Upsilon_2 = \mathrm{i}(w_2, -w_2^*)^{\mathrm{T}}$. In terms of these particle-hole invariant

[9)] Anderson localization implies the absence of charge transport in strongly disordered materials (Anderson, 1958).

[10)] In its effective low-energy approximation the BdG equation reveals a remarkable similarity to the one-dimensional relativistic Dirac equation in which the mass term has a domain wall. This model was first studied by *R. Jackiw* and *C. Rebbi* as a toy model for the low-energy excitations of a Dirac field in presence of soliton solutions of a scalar background field, see Jackiw and Rebbi (1976).

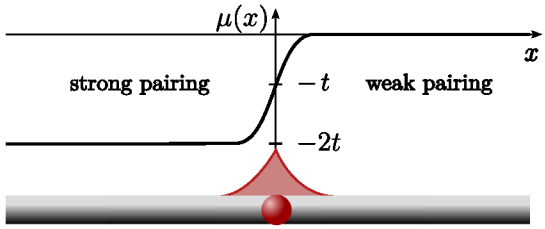

Fig. 3.3.: MZM (red) in a one-dimensional superconductor (gray) bound to a domain wall in form of a position dependent chemical potential $\mu(x)$. For the Kitaev chain the MZMs emerge at the phase boundary which separates topologically non-trivial sections from trivial ones and is strongly localized as indicated by its wave function (also in red).

spinors[11] $\mathcal{C}\Upsilon_{1,2} = \Upsilon_{1,2}$, one can find *only one normalizable solution* of (3.16) that is unique,

$$w_{1,2}(x) \propto \mathrm{e}^{-\mathrm{i}\pi/4} \exp\left[-\frac{1}{\hbar\Delta}\int_0^x \big(t+\mu(x')\big)\mathrm{d}x'\right]. \tag{3.17}$$

Note, that $w_{1,2}$ are exponentially confined to the phase boundary $x = 0$. As a side remark, by the same reasoning it can be shown that MZMs may also occur in two-dimensional p-wave superconductors bound to one-dimensional domain walls or as point-like objects in vortex cores, see Read and Green (2000).

Due their invariance under particle-hole inversion, the localized states (3.17) describe quasiparticles which are their own antiparticles. These states are the MZMs bound to the edges of a superconductor. Re-expressing these zero energy solutions in the language of second quantization, the Majorana quasiparticles are described by *Hermitian operators* of the form

$$\gamma_1 = \int \big[w_1(x)\psi^\dagger(x) + w_1^*(x)\psi(x)\big]\mathrm{d}x, \tag{3.18a}$$

$$\gamma_2 = \mathrm{i}\int \big[w_2(x)\psi^\dagger(x) - w_2^*(x)\psi(x)\big]\mathrm{d}x \tag{3.18b}$$

where $w_{1,2}(x)$ plays the role of a Majorana wave function. Since a wire necessarily has two ends, Majorana bound states always occur in pairs γ_1 and γ_2 that are non-locally separated from each other. Crucially, a set of Hermitian Majorana operators $\gamma_1, \ldots, \gamma_{2N}$ obey the *Clifford algebra*

$$\{\gamma_i, \gamma_j\} = 2\delta_{ij} \tag{3.19}$$

which makes them fundamentally different from usual fermionic particles. However, it is always possible to define a *non-local fermionic mode* by introducing operators

[11] By stressing the similarity between the BdG equations and the relativistic Dirac equation a bit further, the particle-hole constraint (of Nambu spinors) can be transcribed into the *relativistic Majorana condition* which imposes a reality condition on the complex Dirac spinors. In three dimensions for example, this condition reduces the four-component Dirac equation to the relativistic two-component Majorana equation containing only half the degrees of freedom as the original Dirac equation, see for instance (Aste, 2010). A more detailed discussion about similarities and dissimilarities between BdG equations and the relativistic Majorana equation can be found in Wilczek (2009); Chamon *et al.* (2010); Elliott and Franz (2015).

$\beta_0 = \frac{1}{2}(\gamma_1 + i\gamma_2)$ and $\beta_0^\dagger = \frac{1}{2}(\gamma_1 - i\gamma_2)$ recovering the usual fermionic anticommutation relations, $\{\beta_0, \beta_0^\dagger\} = 1$ and $\{\beta_0, \beta_0\} = 0$. This fermionic mode can be either empty or is filled with a fermionic quasiparticle, $\beta_0^\dagger \beta_0 = 0, 1$. As will be discussed in greater detail in Sec. 3.3, this allows to define the notion of a two-level system in which quantum information can be encoded non-locally. Before, the next section will be focussed on the implementation of MZMs in semiconducting nanowires and highlight their experimental characteristics.

3.2. Majorana zero modes in semiconducting nanowires

While the verification of p-wave superconductivity in strontium ruthenate remains elusive, there have been lots of ideas how to imitate the p-wave pairing and generate MZM by other means. Some of these ideas—MZM in the fractional Hall state, in ferromagnetic chains of atoms, as well as in superfluids—have been already mentioned. Another possibility to generate MZMs is the use of semiconductor technology. By the use of superconducting-semiconducting hybrid devices it is possible to imprint superconducting correlations onto semiconducting nano-devices like quantum dots or quantum wires (De Franceschi *et al.*, 2010). Therefore, semiconductor technology appears to be an ideal arena for designing devices that may be able to detect and manipulate MZMs.

The basic question is: how to imitate the p-wave pairing character of topological superconductors? To do so, it seems natural to use a close relative of the topological superconductors—a topological insulator. By virtue of an usual s-wave superconductor, it is possible to induce superconducting pairing on the edge of a topological insulator. Responsible for that is the superconducting *proximity effect*, i.e., the tunneling of Cooper pairs into the topological insulator. Then, as suggested by Fu and Kane (2008), MZMs may occur on the surface between the topological insulator and the superconductor.

Since material challenges still affect the performance of topological insulators (Ortmann *et al.*, 2015), it is desirable to find a way that bypasses the involvement of topological insulators. As shown by Sau *et al.* (2010); Alicea (2010), this can be, indeed, achieved by using two-dimensional semiconductor heterostructures (quantum wires or quantum wells) subject to rather large spin-orbit interaction and a an external magnetic field. These proposals exploit the interplay of two competing interactions—the spin-orbit interaction in form of Rashba and (or) Dresselhaus interactions[12)] and an external magnetic field—generating effective models that effectively emulate p-wave pairing. The superconducting pairing interaction is induced by injecting Cooper pairs from an adjacent s-wave superconductor. In order to generate an effective p-wave pairing amplitude, it is required to use semiconductors with a considerable spin-orbit interaction strength such as InAs or InSb. In particular, MZM are predicted to occur in one-dimensional semiconducting quantum wires (Oreg *et al.*, 2010; Lutchyn *et al.*,

[12)] See Winkler (2003) for example.

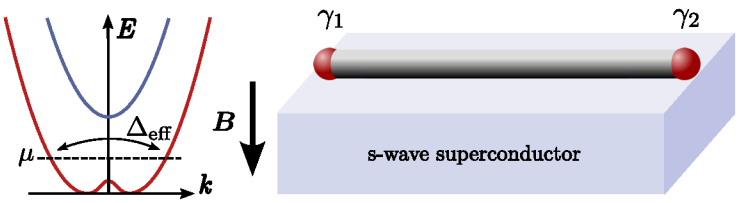

Fig. 3.4.: MZMs γ_1, γ_2 (red dots) occurring at the ends of an one-dimensional semiconducting nanowire on top of an conventional s-wave superconductor. An external magnetic field is applied in the z direction. The effective magnetic field of the Rashba term is pointing transversely to the direction of $\boldsymbol{B}$. This opens a gap in the spectrum shown on the left. In the limit of large magnetic fields the lower band is nearly spin-polarized. By tuning the chemical potential of the wire μ into the gapped region, an effective p-wave pairing Δ_{eff} between spin-polarized pairs of opposite momentum is induced by the proximity effect.

2010). Relative to two-dimensional structures, the use of one-dimensional quantum wires has several advantages. Instead of being bound to vortices somewhere in the 2D quantum well, the MZMs are expected to be found at the edge of the wire (or at the phase boundary between two topologically distinct sections). Furthermore, the confining geometry of a 1D wire suppresses excitations other than MZMs. This is advantageous because such quasiparticles may lead to enhanced decoherence (Franz, 2013).

3.2.1. Emulating p-wave pairing in nanowires

In one-dimensional nanowires MZMs are expected to occur if the Rashba spin-orbit interaction[13)] and the external magnetic field $\boldsymbol{B} = -B\boldsymbol{e}_z$ act in opposite directions. Applying the external magnetic field in z direction the effective magnetic field generated by the Rashba interaction has to be oriented in the xy-plane. Then, for such a nanowire with length L, the Hamiltonian reads

$$H_{\text{wire}} = \sum_{s,s'} \int_0^L \psi_s^\dagger(x) \left[\frac{p_x^2}{2m_e^*} - \mu(x) + \frac{\alpha_{\text{so}}}{\hbar} p_x \sigma_y - \frac{g\mu_{\text{B}} B}{2} \sigma_z \right]_{s,s'} \psi_{s'}(x) \mathrm{d}x. \quad (3.20)$$

Here the parameter α_{so} indicates the strength of the spin-orbit interaction, g the Landè factor in the wire, and m_e^* is the effective mass of the electrons in the wire. The fermionic operators $\psi_s(x)$ describe the electrons in the wire whose spin orientation is labeled by s. Due to the narrow confining geometry of a one-dimensional wire, it can be assumed that all transverse mode excitations labeled by k_y, k_z are gapped out.

In the regime $\alpha_{\text{so}} k_x \ll g\mu_{\text{B}} B$ where the external magnetic field dominates over the Rashba term, the spin bands are energetically split; while spin states with $\downarrow$ are split off by the Zeeman energy $g\mu_{\text{B}}|B|$, the lowest band remains as a spin-polarized band

[13)] Due to the absence of inversion symmetry in InSb and InAs nanowires, Dresselhaus spin-orbit interaction is irrelevant here.

with states $(k_x, \uparrow)$. The influence of the Rashba term on the energy bands is negligibly small in this regime. However, when it comes to the proximity-induced superconductivity, the Rashba interaction in fact plays an important role. The proximity-induced superconducting pairing interaction in the wire is given by

$$H_{\mathrm{sc}} = \Delta \int \left[\psi_{\uparrow}^{\dagger}(x)\psi_{\downarrow}^{\dagger}(x) + \psi_{\downarrow}(x)\psi_{\uparrow}(x)\right] \mathrm{d}x \tag{3.21}$$

where Δ is the proximity-induced superconducting gap parameter. For simplicity Δ is taken to be real here. Generically, Δ is smaller than the superconducting gap of the bulk superconductor, $\Delta < \Delta_{\mathrm{bulk}}$. As the s-wave character of the superconducting pairing term mixes spin up-states in the lower band with spin-down states in the upper band, pairing correlations are energetically not favorable. However, by virtue of the Rashba interaction the eigenstates of both bands are actually admixtures of spin-up and spin-down components.[14)] By projecting onto the lowest energy band, the effective pairing amplitude assumes the form of a p-wave pairing term

$$H_{\mathrm{sc}} \mapsto \Delta_{\mathrm{eff}} \int \left[\tilde{\psi}^{\dagger}\partial_x\tilde{\psi}^{\dagger} - \tilde{\psi}\partial_x\tilde{\psi}\right] \mathrm{d}x. \tag{3.22}$$

As a result of first order perturbation theory, the effective pairing amplitude $\Delta_{\mathrm{eff}} = \Delta\alpha_{\mathrm{so}}/\hbar g\mu_{\mathrm{B}}B$ appears to be weaker than the proximity-induced gap Δ. By defining the effective chemical potential $\mu_{\mathrm{eff}} = \mu + g\mu_{\mathrm{B}}B/2$, the Hamiltonian $H_{\mathrm{wire}} + H_{\mathrm{sc}}$ is a low-energy version of the Kitaev chain; cf. (3.1) by setting $p_y = 0$. In particular, the wire is in the topological phase if $|\mu| < \sqrt{(g\mu_{\mathrm{B}}B/2)^2 - \Delta^2}$, hosting Majorana modes at its ends.

3.2.2. Experimental signatures

So far the discussion has been focused on the theoretical conditions under which MZMs may occur. By virtue of semiconducting-superconducting hybrid devices, experimentalists are set into a position to search for MZMs in devices that can be fabricated via nanoscale technology. Indeed, not long after the nanowire-proposals predicted MZMs, it has been attempted to find signatures of these exotic excitations in semiconductor hybrid systems. In order to identify signatures of MZMs experimentally, there are three characteristic features to look for in nanowires: zero-bias conductance, non-local tunneling, and the fractional Josephson effect as depicted in Fig. 3.5.

Zero-bias conductance

The idea of tunneling spectroscopy is to detect the appearance of MZMs by measuring the electrical conductance properties. This proceeds by probing the electrical

[14)] In first order perturbation theory one finds $\psi_{\uparrow}$ as combination of dressed electron operators $\tilde{\psi}$ and $\tilde{\psi}'$ denoting the lower and the upper band respectively. By projecting into the lower band one finds $\psi_{\downarrow}(x) \approx \left(\alpha_{\mathrm{so}}/g\mu_{\mathrm{B}}|B|\right)\partial_x\tilde{\psi}$, and $\psi_{\uparrow} \approx \tilde{\psi}$. For further details, see for example Alicea (2010).

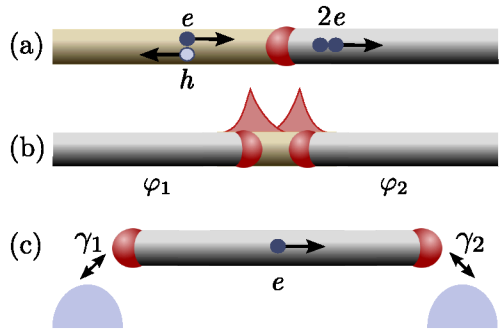

Fig. 3.5.: Three setups for the detection of MZMs. In (a) a MZM gives rise to resonant Andreev reflections resulting in a quantized zero-bias conductance peak. Panel (b) illustrates the fractional Josephson effect; two MZMs form a single Andreev level in the tunneling junction resulting in a 4π periodic current-phase relation as function of $\varphi = \varphi_1 - \varphi_2$. Panel (c) depicts the non-local transfer of electrons though the wire. Via γ_1 electrons from the left lead (left bluish semicircle) can be injected into the wire and immediately extracted into the right lead (right semicircle) via γ_2.

current passing a tunnel barrier that connects a topological (superconducting) section of the nanowire to a metallic section. An electron, incident from the metallic part of the wire, may be either reflected back as an electron or as a hole. The latter process is called *Andreev reflection*[15] and is allowed because in presence of a superconducting pairing term particle conservation is broken; the incident electron, that is absorbed into the superconducting condensate as a Cooper pair, leaves a hole state behind, see Fig. 3.5. This process causes a net charge flow of $2e$ into the superconductor. Strikingly, in presence of a MZM γ_1 sitting close to the tunnel barrier, Andreev reflection is resonantly enhanced if the energy of the incoming electron is on resonance with the zero mode, i.e., if the electron is emitted at the Fermi energy (zero bias voltage). This gives rise to a tunneling conductance that equals precisely one quantum of conductance $G_0 = 2e^2/h$ (Sengupta *et al.*, 2001; Bolech and Demler, 2007; Law *et al.*, 2009). In contrast, if the MZMs were absent, the conductance drops essentially to zero.

In the past years a series of experiments reported on the observation of a conductance anomaly at zero bias voltage (Mourik *et al.*, 2012; Deng *et al.*, 2012; Das *et al.*, 2012; Lee *et al.*, 2012; Finck *et al.*, 2013; Churchill *et al.*, 2013). Although this zero-bias feature is a good indication for the presence of MZMs, it might also be caused by other sub-gap states. Clearly, the infra-gap structure of the nanowire makes it difficult to identify an unambiguous signature of MZMs via tunneling spectroscopy (Flensberg, 2010; Kells *et al.*, 2012).[16]

Non-local tunneling

The presence of MZMs at the ends of a nanowire also manifests as a non-local feature in the transport of electrons through the wire. By coupling the two end modes γ_1 and γ_2 of a nanowire to metallic leads, electrons may be transmitted immediately from one lead to the other (Tewari *et al.*, 2008; Fu, 2010). By injecting electrons

[15] See Nazarov and Blanter (2009).

[16] As a side remark it should be mentioned, that the existence of Majorana end states seems to by confirmed in chains of ferromagnetic atoms (Nadj-Perge *et al.*, 2014).

via tunneling barrier into one of the two end modes γ_1, it can be instantaneously extracted from the other end mode γ_2 at the opposite of the wire with a tunneling rate that is independent of the wire's length. Therefore, it seems that the presence of MZMs gives rise to non-local electron transport regardless of the length of the wire; this phenomenon has been dubbed electron teleportation (Tewari *et al.*, 2008). In fact, in order to observe this teleportation effect, the wire needs to be driven into the Coulomb blockade regime, see Fu (2010).

Confusion about the non-locality of electron transfer processes may arise because of the appearance of two independent length scales. When saying the MZMs are infinitely far apart from each other, the Majorana wave functions are assumed to have an insignificant overlap. In other words, the length of the wire is much larger than the superconducting coherence length, $L \gg \xi$. Within another assumption, the superconductor is treated as a lumped circuit element. This essentially means that the physical size of the superconducting nanowire is small compared to the wave length of characteristic plasma oscillations. Hence, by assuming charging effects to be non-local, it is expected to see also non-local transport signatures in the Coulomb blockade regime. Moreover, it has been argued by Ulrich and Hassler (2015) that non-local electron transport also appears for a floating topological superconductor in the non-interacting case with no Coulomb repulsion present.

The fractional Josephson effect

Another characteristic signature of MZMs is the *fractional Josephson effect*. This effect arises if two MZMs hybridize across a thin tunneling barrier forming a single Andreev bound state.[17] The tunnel coupling of MZMs across the Josephson junction is mediated by the Hamiltonian

$$H_{\text{tun}} = -\frac{\mathrm{i}w}{2}\cos\left(\frac{\varphi}{2}\right)\gamma_1\gamma_2. \tag{3.23}$$

In this expression φ labels the superconducting phase difference, w the overlap of the Majorana wave functions, and γ_1, γ_2 are the Majorana quasiparticle operators at the junction. As indicated by the fractional phase difference $\varphi/2$, the hybridized MZMs give rise to single electron transport across the Josephson junction.[18] Usually, charge transport across the junction is mediated by via second order Andreev processes in which the charge of $2e$ is transferred across the junction. In the presence of two zero modes, however, an electron may be transmitted directly across the superconducting junction. Noticing that the Andreev level can be either filled or empty $\langle -\mathrm{i}\gamma_1\gamma_2\rangle = \pm 1$,

[17] See Nazarov and Blanter (2009).

[18] In Sec. 2.3.1 the Susskind-Glogower operators $\exp(\pm\mathrm{i}\varphi)$ have been introduced as translation operators for the number operator N_{2e}, that counts the number of Cooper pair charges. In the same manner one can define operators $\exp(\pm\mathrm{i}\varphi/2)$ which are associated to single electrons N_e. The correct bookkeeping of charges requires $\left[\exp(\mathrm{i}\varphi/2)\right]^2 = \exp(\mathrm{i}\varphi)$, i.e., the charge of two electrons amounts to the charge of a single Cooper pair; cf. (2.49) in Ch. 2. Hence, charge quantization in multiples of e implies a fundamental periodicity of 4π in the superconducting phase variable.

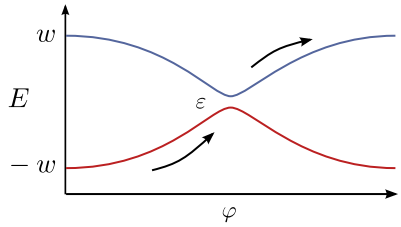

Fig. 3.6.: A finite overlap amplitude of the MZMs on each topological section of the nanowire open a small gap $\simeq \varepsilon$ between the two Andreev levels of the junction (red and blue lines). The resulting current-phase relation is 2π periodic. In presence of a bias voltage, however, Landau-Zener tunneling events restore the 4π periodicity if the voltage-induced drift of the superconducting is sufficiently fast.

the Andreev bound state contributes the amount

$$I_e = \frac{2e}{\hbar}\frac{\partial}{\partial\varphi}\langle H_{\text{tun}}\rangle = \pm\frac{ew}{2\hbar}\sin\left(\frac{\varphi}{2}\right) \tag{3.24}$$

to the total Josephson current. Strikingly, the resulting current-phase relation is 4π periodic therefore called *fractional Josephson effect* (Kitaev, 2001; Kwon *et al.*, 2004; Fu and Kane, 2009).

Experimentally, this peculiar current-phase relation may come to light in form of anomalous Shapiro steps (Kwon *et al.*, 2004; Jiang *et al.*, 2011b); by driving the superconducting phase with a bias voltage of the form $V_{\text{bias}} = V_{\text{dc}} + V_{\text{ac}}\cos(\omega t)$, the supercurrent reveals step-like features—the Shapiro steps—as a function of V_{dc}. Contrary to a regular Josephson junction, if the current-phase relation is 4π periodic, only the even Shapiro steps obeying the (modified) resonance condition $eV_{\text{dc}} = n\hbar\omega$ are expected to occur.[19] In 2012, the experimental proof of anomalous Shapiro steps in an InSb nanowire Josephson junction gave further indication for the existence of MZMs (Rokhinson *et al.*, 2012).

However, the signature of the fractional Josephson effect may be not as definite as one might think. By taking into account the finite length of a nanowire, the MZMs at both ends of each topological section may have a finite overlap amplitude ε. Consequently, these overlap amplitudes open a small gap between the Andreev levels (3.23) at the crossing thereby rendering the current-phase relation 2π periodic. The transition from the usual 2π periodic Josephson effect to the 4π periodic effect takes in fact place in a continuous manner, see Pikulin and Nazarov (2012); San-Jose *et al.* (2012). In essence, the 4π periodicity may be restored in the diabatic regime $eV_{\text{dc}} \gg 4\pi\varepsilon^2/t$ in which the drift of the superconducting phase is fast enough to induce Landau-Zener transitions[20] between the gapped Andreev levels, see Fig. 3.6. In addition to that, the visibility of the anomalous Shapiro effect may be masked by other Andreev bound state channels having a 2π periodic current-phase relation. For a *current biased* Josephson junction, however, it has been shown that the anomalous Shapiro effect remains visible (Domínguez *et al.*, 2012).

[19] For the common Shapiro effect see Tinkham (1996).
[20] See Landau and Lifshitz (2012, §90).

3.3. Quantum computation with MZMs

In the preceding section it has been demonstrated how semiconductor-superconductor hybrid devices may give rise to emergent MZMs. The use of nanoscale technology offers the required flexibility to implement various architectures that are well suited for quantum computational purposes such as networks of nanowires hosting an ensemble of MZMs.

In the following it will be outlined how such an ensemble of MZMs may be used for quantum information processing. The basic blueprint for a single Majorana qubit includes the two important steps: the construction of a non-local state space, that is subject to the fermionic parity constraint, and the implementation of fault-tolerant gates via braiding of quasiparticles. Moreover, finding that the set of topological gates is not sufficient for universal quantum computation, it will be shown that universal computations can be still achieved by utilizing hybrid devices in which topological qubits are combined with superconducting qubits.

3.3.1. Qubit states and fermionic parity

In presence of $2N$ Majorana quasiparticles $\gamma_1, \ldots, \gamma_{2N}$, e.g, hosted by a network of nanowires, the ground state is degenerate if all the MZMs are reasonably far apart from each other. In order to describe the degenerate ground state manifold, it is convenient to make use of an inherent connection between Majorana quasiparticles and regular Dirac fermions. This proceeds by fusing $2N$ Majorana operators into N (non-local) Dirac fermions

$$f_i = \frac{1}{2}\left(\gamma_{2i-1} + \mathrm{i}\gamma_{2i}\right) \tag{3.25}$$

obeying the fermionic algebra $\{f_i, f_j^\dagger\} = \delta_{ij}$ and $\{f_i, f_j\} = 0$. The state space of these fermionic modes is spanned by a complete basis of Fock states

$$|n_1, n_2, \ldots, n_N\rangle = \left(f_N^\dagger\right)^{n_N} \ldots \left(f_1^\dagger\right)^{n_1} |\Omega\rangle \tag{3.26}$$

where $|\Omega\rangle$ is the Fock vacuum which is uniquely defined by requiring $f_i |\Omega\rangle = 0$ for all f_i. For fermionic modes the occupation numbers n_i are restricted to be either zero or one. Accordingly, the dimension of the the ground state space is 2^N. Note that there are $(2N)!/2^N N!$ different possibilities to pair up $2N$ Majorana operators into N Dirac fermions. However, regardless of the actual pairing, all resulting Fock space bases are unitarily equivalent (Nayak *et al.*, 2008).

For fermionic systems and in particular for the purpose of fermionic quantum computation, it is important to consider the *fermionic parity constraint*; since every (fermionic) observable A needs to contain an even number of fermionic operators,[21)]

[21)] In contrast to the bosonic case, classical fermionic fields do not exist; inherently related to the antisymmetric algebra, the classical limit of a fermionic field $\langle f \rangle = \xi$ would be characterized by an

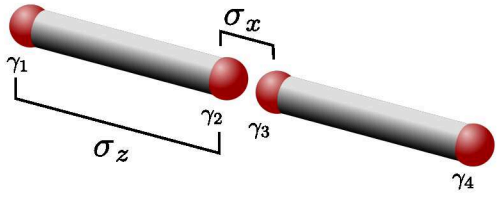

Fig. 3.7.: Four MZMs $\gamma_1, \ldots, \gamma_4$ in a nanowire forming Majorana qubit. The two parities $\mathcal{P}_{12}$ and $\mathcal{P}_{23}$, measuring the occupation number of the fermionic modes formed by fusing γ_1, γ_2 and γ_2, γ_3, define the logical operations σ_z and σ_x respectively. The picture is taken from Hassler (2013).

all observables are subject to the fermionic parity symmetry

$$\mathcal{P} A \mathcal{P} = A. \tag{3.27}$$

The fermionic parity operator $\mathcal{P} = \prod_i \mathcal{P}_i$ is composed of partial parity transformations $\mathcal{P}_i$, each mediating the $\mathbb{Z}_2$ inversion transformation[22)]

$$\mathcal{P}_i \, f_i \, \mathcal{P}_i = \exp\left(\mathrm{i}\pi f_i^\dagger f_i\right) f_i \, \exp\left(-\mathrm{i}\pi f_i^\dagger f_i\right) = -f_i. \tag{3.28}$$

Because of the global parity constraint (3.27), the physical state space admits a decomposition into a direct sum of eigenstates of $\mathcal{P}$. Finding the eigenvalues to be $\mathcal{P} = \pm 1$, the state space decays into two irreducible parity sectors: a state with $\mathcal{P}\,|\psi_+\rangle = |\psi_+\rangle$ is said to have *even fermionic parity* whereas a state with $\mathcal{P}\,|\psi_-\rangle = -\,|\psi_-\rangle$ has *odd fermionic parity*. Physically, the even or odd fermionic parity refers to the total number of fermions modulo two. Because of (3.27) no physical observable is capable to induce transitions between the two parity sectors.[23)] Hence, the constrained state space has dimension 2^{N-1}.

Due to the fermionic parity constraint, it is mandatory to have at least two fermionic modes in order to form a two-level system. Let f_1, f_2 describe two such fermionic modes. Then, within each parity sector of the two modes, a two-level system is spanned by the states

$$|0,0\rangle = |\Omega\rangle\,, \qquad |1,1\rangle = f_1^\dagger f_2^\dagger\,|\Omega\rangle \qquad \text{(even parity sector)}, \tag{3.29a}$$

$$|1,0\rangle = f_1^\dagger\,|\Omega\rangle\,, \qquad |0,1\rangle = f_2^\dagger\,|\Omega\rangle \qquad \text{(odd parity sector)}. \tag{3.29b}$$

This means there have to be at least four Majorana quasiparticles γ_1, γ_2, γ_3, γ_4 in order to define a topological qubit. Since both parity sectors are equivalent, it is sufficient to consider only the case $\mathcal{P} = 1$ for the rest of the section. In the Majorana

anticommuting Graßmann variable ξ (Negele and Orland, 1998, Ch. 1). However, as the notion of a Graßmann-valued classical observable is physically meaningless, any observable must contain on an even number of fermionic operators to make sure it is a real-valued quantity.

[22)] Note, that $\mathcal{P}_i$ appears in many equivalent formulations,

$$\mathcal{P}_i = (-1)^{f_i^\dagger f_i} = \exp\left(\mathrm{i}\pi f_i^\dagger f_i\right) = 1 - 2 f_i^\dagger f_i = -\mathrm{i}\gamma_i\gamma_{i+1}.$$

In particular, the last identity explicitly makes use of the connection between Majorana operators and Dirac fermion operators, $\gamma_{i-1} = f_i^\dagger + f_i$ and $\gamma_i = \mathrm{i}(f_i^\dagger - f_i)$.

[23)] This property is called a superselection rule.

picture it is more convenient to specify the states (3.29) as eigenstates of the fermionic parity operator[24)]

$$\mathcal{P}_{12} = -\mathrm{i}\gamma_1\gamma_2 = 2f_1^\dagger f_1 - 1 = \pm 1. \tag{3.30}$$

For example, the state $|1,1\rangle$ can characterized by $\mathcal{P} = 1$ and $\mathcal{P}_{12}|1,1\rangle = \mathcal{P}_{34}|1,1\rangle = -|1,1\rangle$. In the same manner one finds $\mathcal{P}_{12}|0,0\rangle = |0,0\rangle$ which also shows that $\mathcal{P}_{12}$ acts in the same way as σ_z acts upon the states of a two-level system. Moreover, the action of all Pauli operators can be emulated by looking at different pairings of Majorana operators:

$$\sigma_x \cong -\mathrm{i}\gamma_2\gamma_3 = -\mathrm{i}\gamma_1\gamma_4, \tag{3.31a}$$
$$\sigma_y \cong \mathrm{i}\gamma_1\gamma_3 = -\mathrm{i}\gamma_2\gamma_4, \tag{3.31b}$$
$$\sigma_z \cong -\mathrm{i}\gamma_1\gamma_2 = -\mathrm{i}\gamma_3\gamma_4, \tag{3.31c}$$

see Fig. 3.7. Strikingly, as long as all MZMs $\gamma_1, \ldots, \gamma_4$ are far apart from each other, the logical operations are non-local operations. As a consequence, it is unlikely for logical errors to happen as a result of random fluctuations in the environment. That is to say, quantum information, which has been encoded into a Majorana qubit, is insensitive to local perturbations. This makes Majorana qubits ideally suited for the storage of quantum information (Kitaev, 2001).

When claiming that quantum information can reliably stored into MZMs, it is assumed that the fermionic parity of the qubit is conserved for all times. This requirement, however, is softened when the nanowire is coupled to a noisy (fermionic) environment causing random tunneling of quasiparticles onto the nanowire. Whenever external quasiparticles are captured in a Majorana subgap state, the fermionic parity of the qubit changes and drives the qubit out of its computational state space. These disruptive processes called *quasiparticle poisoning* give rise to a finite decoherence time of the Majorana qubit. As the presence of an adjacent superconductor is indispensable for the occurrence of MZMs, quasiparticle poisoning is an inevitable process that is, de facto, the main source of decoherence for Majorana qubits (Rainis and Loss, 2012; Budich *et al.*, 2012). At finite temperature, also intrinsic quasiparticles in the nanowire living above the proximity-induced superconducting gap may contribute to decoherence by quasi-particle poisoning (Cheng *et al.*, 2012; Schmidt *et al.*, 2012; Konschelle and Hassler, 2013). However, as long as temperatures are kept below the gap, the effect of intrinsic quasiparticles is exponentially suppressed by a factor $\mathrm{e}^{-\Delta_{\mathrm{eff}}/k_{\mathrm{B}}T}$.

3.3.2. Quantum computation with MZMs

So far it has been argued that quantum information, which is stored in Majorana quasiparticle states, is exceptionally insensitive to noise as long as the fermionic

[24)] Knowing that the total parity is $\mathcal{P} = \mathcal{P}_{12}\mathcal{P}_{34} = 1$, it is sufficient to specify only one of the quantities $\mathcal{P}_{12}$ or $\mathcal{P}_{34}$.

parity is conserved. Moreover, Majorana qubits also offer the possibility to process quantum information. In order to promote a Majorana qubit to an active part of the computational process, an experimenter needs to be able to perform three important steps in a controlled manner: initialization, unitary evolution, and readout of the Majorana qubit. Since each of these steps is in principle sensitive to errors, it is desired to benefit from the fault-tolerance of Majorana qubits when executing these steps. Especially when performing gates (unitary evolution), it is profitable to exploit the non-Abelian exchange statistics of MZMs.

Commonly, the rules for particle exchange are dictated either by Bose-Einstein or Fermi-Dirac statistics. In $2+1$ dimensions, however, the topology of configuration spaces turns out to be much richer than in $3+1$ dimensions giving rise to a manifold variety of exchange statistics—the *braiding statistics* (Leinaas and Myrheim, 1977; Wilczek, 1982). While the exchange statistics in $3+1$ dimensions is given by one-dimensional unitary representations of the (finite-dimensional) permutation group $\mathfrak{S}_N$, the exchange statistics of N identical particles in $2+1$ dimensions arise from irreducible unitary representations of the (infinite-dimensional) braid group $\mathfrak{B}_N$.[25)] In particular, the exchange of two MZMs γ_i and γ_j in two dimensions is mediated by the unitary transformation

$$B_{ij}\gamma_i B_{ij}^\dagger = -\gamma_j, \qquad B_{ij}\gamma_j B_{ij}^\dagger = \gamma_i. \tag{3.32}$$

Here $B_{ij} = \exp\left(\frac{\pi}{4}\gamma_i\gamma_j\right) = \frac{1}{\sqrt{2}}(1+\gamma_i\gamma_j)$ is the unitary operator representing the fundamental braid that exchanges γ_i and γ_j (Nayak and Wilczek, 1996; Ivanov, 2001). In contrast to particle exchange in 3+1 dimensions, it matters whether quasiparticles are turned around each other clockwise or counterclockwise, i.e., $B_{ij}^{-1} = B_{ji} \neq B_{ij}$.

Coming back to a single Majorana qubit that involves four zero modes $\gamma_1, \ldots, \gamma_4$, the braiding operation B_{12} acts as follows upon the qubit states

$$B_{12}\,|0,0\rangle = \mathrm{e}^{\mathrm{i}\pi/4}\,|0,0\rangle\,, \qquad B_{12}\,|1,1\rangle = \mathrm{e}^{-\mathrm{i}\pi/4}\,|1,1\rangle\,. \tag{3.33}$$

Hence, B_{12} implements a single qubit rotation by angle $\pi/2$ on the Majorana qubit states. Similarly, other braiding operations such as B_{23}, B_{13}, etc. perform other single qubit rotations. In fact, it is possible to generate all braiding-based gates as a sequence of the two elementary braids

$$B_{12} \cong \exp\left(\mathrm{i}\frac{\pi}{4}\sigma_z\right), \qquad B_{23} \cong \exp\left(\mathrm{i}\frac{\pi}{4}\sigma_x\right). \tag{3.34}$$

For example, a $\pi/2$ rotation around the y axis of the qubit's Bloch sphere $\exp(\mathrm{i}\frac{\pi}{4}\sigma_y) \cong B_{31}$ can be obtained from the sequence $B_{31} = B_{21}B_{23}B_{12}$. Importantly, during the entire process of braiding MZMs, the quasiparticles may be kept far apart from each other thereby guaranteeing topological protection.[26)] However, by virtue of the two

[25)] For more details on the braid group, see the review article by Nayak *et al.* (2008).

[26)] At this point it should be mentioned that the non-Abelian exchange statistics are inherently related to quantum vortices in p-wave superconductors and not to the Majorana quasiparticles

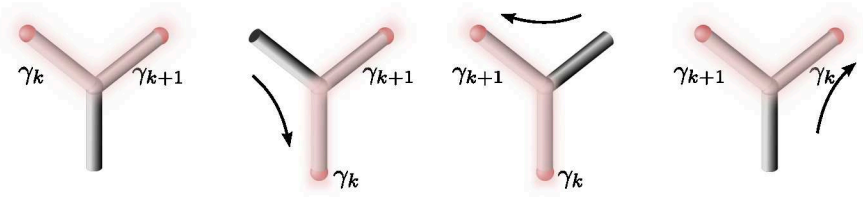

Fig. 3.8.: Exchange of two MZMs γ_k and γ_{k+1} (red dots) in a tri-junction of nanowires. The reddish shaded regions illustrate topological sections of the wire. MZMs can be exchanged in a sequence of four steps, each moving the topological section of the wire to another end. This can be achieved by means of gate voltages or magnetic fluxes, see Alicea *et al.* (2011); Clarke *et al.* (2011); van Heck *et al.* (2012). The Figure is adapted from Hassler (2013).

elementary braiding operations (3.34), it is impossible to generate all unitary operations required for universal quantum computation, but only the subset of Clifford gates (Bravyi and Kitaev, 2005; Ahlbrecht *et al.*, 2009).[27] Therefore, the topologically protected braid operations (3.34) need to be complemented by an additional $\pi/8$-phase gate as well as a controlled-NOT gate in order to find a universal set of gates (Nielsen and Chuang, 2010).

To do so, it seems natural to combine a (topological) Majorana-based qubit with a superconducting qubit by placing the nanowire on top of the superconducting electrodes of the superconducting qubit, see Fig. 3.9. This approach not just provides the possibility to implement the missing quantum gates, but it also offers the big advantage to utilize the machinery of cQED for the sake of reading out the topological qubit. A prominent example, that illustrates the working principle, is the combination of a topological qubit with a superconducting transmon qubit, abbreviated *top-transmon* (Hassler *et al.*, 2011).[28]

The central idea of the top-transmon device is to measure the fermionic parity of the topological qubit via the charging energy of the superconducting qubit. In the transmon regime $E_\mathrm{J}/E_\mathrm{C} \gg 1$, the superconducting qubit is essentially insensitive to the background charge, see Sec. 2.3.2. This changes, if the Josephson energy $E_\mathrm{J} \propto \cos(\pi\Phi_\mathrm{m}/\Phi_0)$ is decreased by tuning the external flux Φ_m that penetrates

theirselves (Beenakker, 2013). Therefore, it is a priori not obvious whether MZMs in one-dimensional nanowires also do obey non-Abelian statistics.

Strictly speaking, in one spatial dimension exchange statistics are ill-defined because particles are not allowed to intersect each other. Nevertheless, by constructing junctions in which three nanowires merge together, it is possible to define protocols for the exchange of quasiparticles, see Fig. 3.8. By using these quasi-two-dimensional networks, it has been shown that MZMs indeed give rise to the exchange rules (3.32) as desired, see Alicea *et al.* (2011); Clarke *et al.* (2011); van Heck *et al.* (2012).

[27] A Clifford gate is an element of the *Clifford group* $\mathscr{C}_{2n}$ which is defined as the normalizer of the *Pauli group* G_n, i.e., $\mathscr{C}_{2n} = \{c \in \mathrm{U}(2^n) \mid c\,G_n\,c^\dagger = G_n\}$. The Pauli group $G_n = G_1 \otimes \ldots \otimes G_1$ itself is the n-fold tensor product of the group $G_1 = \{\pm\mathbb{1}, \pm\mathrm{i}\mathbb{1}, \pm\sigma_x, \pm\mathrm{i}\sigma_x, \pm\sigma_y, \pm\mathrm{i}\sigma_y, \pm\sigma_z, \pm\mathrm{i}\sigma_z\}$ of single qubit gates (single qubit Pauli group), see Nielsen and Chuang (2010, Ch. 10).

[28] Equally, other kinds of superconducting qubits such as a flux qubit (Hassler *et al.*, 2010; Jiang *et al.*, 2011a) or a fluxonium (Pekker *et al.*, 2013) can be coupled to a topological qubit as well.

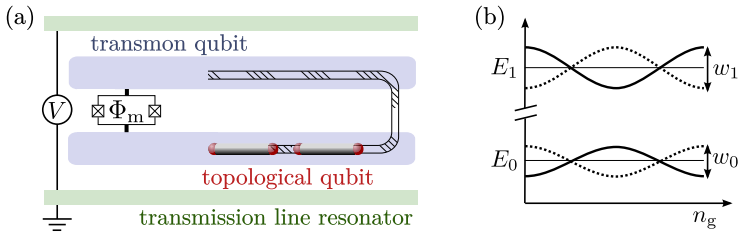

Fig. 3.9.: The top-transmon architecture. (a) sketches the basic setup consisting of a transmon qubit (blue) which is coupled to a transmission line resonator (green). Furthermore, the topological qubit is formed by a nanowire (gray and dashed line) that bridges the two superconducting islands and hosts four MZMs (red dots). For the implementation of qubit rotations, one pair of MZMs has to be moved along the wire to the upper superconducting island. (b) depicts the energy dispersion of the transmon qubit as a function of the background charge. Solid and dashed lines indicate the situation for both parity sectors of the total fermionic parity of the topological qubit. The picture is adapted from Hassler *et al.* (2011).

the split Josephson junction of the transmon. Remember that the band width of the charge dispersion $\propto w_n \sim \exp\left(-\sqrt{E_\mathrm{J}/E_\mathrm{C}}\right)$ scales exponentially with the ratio $E_\mathrm{J}/E_\mathrm{C}$, see Eq. (2.65).[29] This allows to enhance the transmon's sensitivity to the background charge drastically just by tuning $E_\mathrm{J}/E_\mathrm{C}$ properly. In fact, Schreier *et al.* (2008) have demonstrated that w_n can be tuned by two orders of magnitudes. The ability to switch between these two regimes allows to turn the charge sensitivity of the transmon on and off.

For the sake of implementing a non-topological gate, the top-transmon needs to be operated in both regimes. A measurement of the parity $\mathcal{P}_{12} = -\mathrm{i}\gamma_1\gamma_2$ proceeds by maneuvering the pair of MZMs γ_1 and γ_2 along the nanowire from the superconducting ground plate to the superconducting island, see Fig. 3.9. This can be done without affecting the state of the topological qubit by tuning $E_\mathrm{J}/E_\mathrm{C}$ large. Then, by decreasing the ratio $E_\mathrm{J}/E_\mathrm{C}$, the charging energy of the superconducting island gives rise to a finite energy splitting $\propto w_n$ between states $\mathcal{P}_{12} = \pm 1$ differing by a single electron charge.

The net effect of the charge-induced energy splitting emulates a phase gate acting upon the states of the topological qubit. Suppose the transmon qubit is prepared in its ground state ($n = 0$) and the total parity of the topological qubit is $\mathcal{P} = 1$. Then, the state of the topological qubit evolves in time as

$$\alpha\,|0,0\rangle + \beta\,|1,1\rangle \mapsto \alpha \mathrm{e}^{-\mathrm{i}w_0 t/\hbar}\,|0,0\rangle + \beta \mathrm{e}^{\mathrm{i}w_0 t/\hbar}\,|1,1\rangle\,. \tag{3.35}$$

In view of the fact that the interaction can be switched on and off by hand, an arbitrary phase gate—including the missing $\pi/8$ phase gate—is implemented by properly adjusting the duration time of the interaction, see Hassler *et al.* (2011).

The readout of the topological qubit proceeds in a similar way. By irradiating the surrounding transmission line resonator, it is possible to resolve the parity dependent

[29] The index n labels the energy states of the transmon qubit.

energy spacing

$$E_1 - E_0 + \mathcal{P}_{12}\frac{w_0 + w_1}{2} \tag{3.36}$$

between the ground state and the first excited state of the transmon qubit. Here E_0, E_1 denote the (flat dispersion) energies of the superconducting qubit in the transmon regime $E_\mathrm{J}/E_\mathrm{C} \gg 1$ and $\mathcal{P}_{12} = \pm 1$ is the fermionic parity of the MZMs located on top of the superconducting island. In the dispersive regime, the energy splitting (3.36) introduces a parity dependent dispersive shift to the bare frequency of the microwave resonator

$$\chi_{01}(\mathcal{P}_{12}) = \frac{g_{01}^2}{\big[E_1 - E_0 + \mathcal{P}_{12}(w_0 + w_1)/2\big]/\hbar - \omega_c}, \tag{3.37}$$

cf. Eq. (2.77). Here g_{01} is the effective light-matter interaction between the ground state and the first excited state of the transmon qubit, see Sec. 2.4.1. In order to measure the parity $\mathcal{P}_{12}$, the difference $\chi(\mathcal{P}_{12} = 1) - \chi(\mathcal{P}_{12} = -1)$ needs to be resolved, e.g., via a homodyne measurement as outlined in Sec. 2.4.2.

Chapter 4

Coupling Majorana zero modes to electromagnetic radiation

The content of this chapter has been published in:

> Ohm, C. and Hassler, F., 2014: *Majorana fermions coupled to electromagnetic radiation*, New. J. Phys. **16**, 015009.

In order to incorporate MZMs into the framework of cQED, it is important to examine the mechanism that allows to couple MZMs to electromagnetic radiation. Since the superconducting condensate is described by a complex-valued field $\Psi(\boldsymbol{r})$ carrying electrical charge $-2e$, all electrical phenomena of a superconductor are due to the Cooper pair condensate. That is to say, to couple the dynamics of MZMs with the electromagnetic field, the superconducting condensate needs to be involved in some way. This suggests to consider a situation in which MZMs are located at a Josephson junction. In fact, most of the physical phenomena related to superconducting tunnel junctions are governed by the Josephson equations (2.8) and (2.10) which have their microscopic origin in a coherent transfer of charged Cooper pairs through the thin barrier. These equations predict that microwave radiation, also called *Josephson radiation*, is produced by a voltage biased tunnel junction (Josephson, 1962; Lee and Scully, 1971). The microwave radiation is emitted coherently at the Josephson frequency $\omega_{\mathrm{J}} = 2eV/\hbar$ which is given by twice the voltage bias V that is applied across the junction (Yanson *et al.*, 1965; Langenberg *et al.*, 1965).

In contrast to conventional Josephson junctions, single electrons can be transferred coherently in the presence of MZMs (Fu, 2010) leading to a 4π-periodic current-phase relationship (Kitaev, 2001). Because of this, the Josephson effect is dubbed *fractional Josephson effect* (Kitaev, 2001; Fu and Kane, 2009) and its observation would provide a clear evidence of MZMs, see also Ch. 3.

The ac fractional Josephson effect was introduced in the work of Kwon *et al.* (2004) and describes the case of voltage biased Josephson junctions with fractional supercurrents, see also Badiane *et al.* (2011); Pikulin and Nazarov (2012); San-Jose *et al.* (2012); Houzet *et al.* (2013) and Ch. 3 for detailed discussion of the ac effect. As a consequence, non-trivial Shapiro-steps with doubled height in the current-voltage relation emerge providing a signature of the MZMs (Domínguez *et al.*, 2012; Virtanen and Recher, 2013; Rokhinson *et al.*, 2012). Regarding the interaction of MZMs with electromagnetic fields, it has been recently shown that MZMs can be manipulated

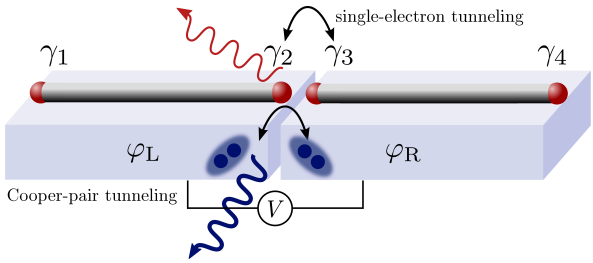

Fig. 4.1.: Two bulk s-wave superconductors (blue cuboids) forming a Josephson junction with superconducting phase difference $\varphi = \varphi_L - \varphi_R$. On top of each of them, there is a semiconducting nanowire (gray cylinders) in the topological phase supporting two MZMs (red spheres) at its ends. We consider the case where the Josephson junction is voltage-biased such that Cooper pairs which move across the junction emit radiation at the Josephson frequency $2eV/\hbar$ with the applied voltage V. This process is indicated by the bold wavy line. Due to the presence of the MZMs, there is the additional process allowed which proceeds via the tunnelling of a single unpaired electron together with the emission of radiation at half the Josephson-frequency indicated by the thin wavy line. In this paper, we will concentrate on the latter process.

by means of microwave driving through weak coupling of microwave radiation to the states of a two Majorana wires (Schmidt *et al.*, 2013a,b). Furthermore, in Ginossar and Grosfeld (2014) the influence of MZMs on the photon coupling of a Majorana-transmon qubit has been investigated. Moreover, it has been proposed to probe the presence of MZMs by measuring the response of a microwave cavity (Cottet *et al.*, 2013).

In this chapter, the focus lies on the radiation that arises from coupling MZMs to the electromagnetic field in a voltage-biased situation. In analogy to the common ac Josephson effect we show that the Majorana-induced Josephson radiation is coherent radiation with a frequency that is half of the Josephson frequency. Furthermore, there is a mutual relationship between the emitted radiation and the state of the MZMs. As a consequence, the system exhibits correlations between the radiation fields emitted from different sources that are situated far away from each other. We will first introduce the coupling of the Majorana zero modes with the electromagnetic field. Then, we proceed outlining different possible realizations of a voltage biased fractional Josephson junction. Subsequently, we derive the semiclassical equation governing the radiation field when the junction is placed in a cavity. Moreover, we will discuss the steady state solution and possible decoherence mechanisms. We will finish with the discussion of correlations of spatially separated radiation sources and show that the superconducting coherence is partially imprinted onto the radiation field. In this respect, the system is closely related to prior work (Recher *et al.*, 2010; Godschalk *et al.*, 2011; Godschalk and Nazarov, 2013a,b) which we will discuss in details below.

4.1. Josephson radiation from Majorana zero modes

4.1.1. Dipole coupling of Majorana zero modes

In topological superconductors, Majorana fermions denoted by γ_j appear as quasiparticles in the middle of the gap. Due to the built-in particle-hole symmetry of superconductors in the mean field description these solutions of the Bogoliubov-de Gennes equation are made-up from equal superpositions of electrons and holes,

$$\gamma_j = \int \left[w_j^*(\boldsymbol{r})\psi(\boldsymbol{r}) + w_j(\boldsymbol{r})\psi^\dagger(\boldsymbol{r}) \right] \mathrm{d}^3 r, \tag{4.1}$$

where $\psi(\boldsymbol{r})$ denotes the fermionic field operator of the electrons and $w(\boldsymbol{r})$ is the wave function of a zero energy solution of the Bogoliubov-de Gennes equation which is localized at either end of the nanowire (Kitaev, 2001; Oreg *et al.*, 2010; Lutchyn *et al.*, 2010). The Majorana operators obey the Clifford algebra $\{\gamma_j, \gamma_k\} = 2\delta_{jk}$. In case the wire is manufactured on top of a Josephson junction additional MZMs have to be taken into account on either side of the Josephson junction (Fu and Kane, 2009). Accordingly, we consider four Majorana bound states in the system denoted by $\gamma_1, \ldots, \gamma_4$, see Fig. 4.1. For the further analysis, it is convenient to introduce two conventional fermionic operators

$$f_{\mathrm{L}} = \frac{1}{2}\left(\gamma_1 + \mathrm{i}\gamma_2\right), \qquad f_{\mathrm{R}} = \frac{1}{2}\left(\gamma_3 + \mathrm{i}\gamma_4\right). \tag{4.2}$$

These fermionic operators account for the parity of the number of electrons on either side of the Josephson junction with the parity given by $\mathcal{P}_x = (-1)^{f_x^\dagger f_x} = \pm 1$, $x =$ L/R. The fermionic Hilbert-space is four dimensional and spanned by the vectors $|\mathcal{P}_{\mathrm{L}}, \mathcal{P}_{\mathrm{R}}\rangle$. It can be generated from the "vacuum" state $|1,1\rangle$ via

$$\begin{aligned} &|1,1\rangle, && |\bar{1},\bar{1}\rangle = f_{\mathrm{L}}^\dagger f_{\mathrm{R}}^\dagger |1,1\rangle, && \text{(even)}, \\ &|\bar{1},1\rangle = f_{\mathrm{L}}^\dagger |1,1\rangle, && |1,\bar{1}\rangle = f_{\mathrm{R}}^\dagger |1,1\rangle, && \text{(odd)} \end{aligned} \tag{4.3}$$

where we have assembled the states according to the total parity $\mathcal{P} = \mathcal{P}_{\mathrm{L}}\mathcal{P}_{\mathrm{R}}$ being even or odd and introduced the shorthand notation $\bar{1} = -1$. It is important to notice that the total parity is conserved such that we only have to consider two out of the four states at one point. Note that for an open system the parity constraint may be violated, e.g., when taking quasiparticle poisoning into account.

Due to the fact that the MZMs are present, an exchange of single electrons between the two sides of the Josephson junction becomes possible which manifests itself in the current-phase relationship having a fundamental period of 4π. Here, we are interested in the Josephson radiation emitted by such a device. For a conventional Josephson junction, the microscopic origin of the ac Josephson effect are Cooper pairs tunneling across the junction thereby transferring a charge $-2e$ and emitting one photon at the Josephson frequency. In the case of the fractional Josephson effect single electron tunneling will lead to the emission of radiation at half the Josephson

frequency. The coupling of the MZMs to the electromagnetic field is provided by a non-vanishing dipole matrix element entering the dipole Hamiltonian

$$H_{\mathrm{dip}} = -\boldsymbol{d}\cdot\boldsymbol{E}; \tag{4.4}$$

here, $\boldsymbol{d} = -e\boldsymbol{r}$ is the dipole operator with $\boldsymbol{r}$ being the position operator and $-e$ is the charge of the electron. As explained in details in Sec. 4.1.2, the dipole operator of the Majorana zero modes for the junction in Fig. 4.1 is given by

$$\boldsymbol{d} = -\frac{\mathrm{i}e}{2}\langle\boldsymbol{r}\rangle\cos\left(\frac{\varphi}{2}\right)\gamma_2\gamma_3, \tag{4.5}$$

with $\varphi = \varphi_{\mathrm{L}} - \varphi_{\mathrm{R}}$ the phase difference across the junction and $\langle\boldsymbol{r}\rangle = \langle w_2|\boldsymbol{r}|w_3\rangle$ the typical distance between the two MZMs 2 and 3. In deriving (4.5), we have taken into account that only γ_2 and γ_3 have a considerable overlap such that the dipole operator only involves the MZMs at the junction. Note that even though the MZMs are charge neutral, the system exhibits a finite dipole matrix element. The reason is that even though the MZMs carry only information about the probability amplitude of chargeless quasiparticles, the charge is provided by the superconducting condensate (Fu, 2010; van Heck *et al.*, 2011). Since the amount of a single electron charge $-e$ (half of a Cooper pair) is transferred from one condensate to the other the dipole matrix element is 4π periodic with respect to the superconducting phase difference.

If we imagine that the junction is placed in a cavity supporting a single mode at frequency ω, the electrical field operator $\boldsymbol{E}$ can be written as

$$\boldsymbol{E} \simeq \sqrt{\frac{\hbar\omega}{V}}\boldsymbol{\epsilon}\left(a + a^\dagger\right) \tag{4.6}$$

with $\boldsymbol{\epsilon}$ the polarization vector and V the volume of the cavity mode. In conclusion, we have the Hamiltonian

$$H_{\mathrm{dip}} = \frac{\mathrm{i}g}{2}\cos\left(\frac{\varphi}{2}\right)\gamma_2\gamma_3(a + a^\dagger) \tag{4.7}$$

describing the interaction of the Majorana zero modes with the electromagnetic radiation with $g \simeq e\sqrt{\hbar\omega/V}\,\boldsymbol{\epsilon}\cdot\langle\boldsymbol{r}\rangle$ the light-matter interaction strength. As the dipole operator is oriented along the nanowire, we need to consider a mode with the electric field having a component along the wire as otherwise the coupling g vanishes. Comparing (4.7) with the pure tunneling contribution of the fractional Josephson effect (Kitaev, 2001; Fu and Kane, 2009) (with tunneling strength w)

$$H_{\mathrm{tun}} = \frac{\mathrm{i}w}{2}\cos\left(\frac{\varphi}{2}\right)\gamma_2\gamma_3 \tag{4.8}$$

shows that there is a close relationship between dipole and tunneling interaction. In both H_{dip} and H_{tun} the Majorana wave functions need to have a considerable overlap such that single fermion transfer is enabled. Indeed, both contributions (4.7)

and (4.8) are complementary in the sense that (4.8) is present at zero bias voltage and (4.7) only becomes important for non-zero bias as the dipole coupling allows for transitions at any energy difference via emission/absorption of a photon carrying the energy surplus. Accordingly, the photon produced by a single electron transfer carries the energy eV which corresponds to half of the Josephson frequency $\omega_{\mathrm{J}}/2$. Therefore it makes sense to call the dipole coupling Hamiltonian H_{dip} the ac analog of the dc Josephson effect.

4.1.2. Dipole operator for Majorana zero modes

The matrix elements of the electric dipole operator in the Majorana ground state manifold are solutions of the BdG equation, $\mathcal{H}_{\mathrm{BdG}}\,\Psi_n(\boldsymbol{r}) = E_n\,\Psi_n(\boldsymbol{r})$ with the Nambu spinor $\Psi_n(\boldsymbol{r}) = (u_n(\boldsymbol{r}), v_n(\boldsymbol{r}))^{\mathrm{T}}$ (Tinkham, 1996). From these solutions $\{\Psi_n\}$ the Bogoliubov quasiparticle operators can be obtained via

$$\beta_n = \int [u_n^*(\boldsymbol{r})\psi(\boldsymbol{r}) + v_n^*(\boldsymbol{r})\psi^\dagger(\boldsymbol{r})]\,\mathrm{d}^3 r, \tag{4.9}$$

with $\beta_n, \beta_n^\dagger$ obeying the canonical anticommutation relations, $\{\beta_m, \beta_n^\dagger\} = \delta_{mn}$. Every BdG Hamiltonian carries a built-in particle hole symmetry which is represented by an operator $\mathcal{C} = \tau_x\mathcal{K}$ that is anticommuting with the BdG Hamiltonian $\{\mathcal{H}_{\mathrm{BdG}}, \mathcal{C}\} = 0$. Here τ_x denotes the first Pauli matrix in Nambu space and $\mathcal{K}$ is the complex conjugation. The operator $\mathcal{C}$ maps a solution of the BdG equation to its particle-hole reversed partner $\Psi_{-n} = \mathcal{C}\,\Psi_n$, which is again a solution of the BdG equation having eigenvalue $-E_n$. In particular, the eigenspace related to solutions at zero energy $\{\Psi_\mu|\ \mathcal{H}_{\mathrm{BdG}}\Psi_\mu = 0\}$ needs to contain an even number of solutions. Given a zero energy solution Ψ_μ, one can choose a different basis which is the eigenbasis of the particle-hole operator via $\Upsilon_{\mu,1} = \Psi_\mu + \mathcal{C}\Psi_\mu$ and $\Upsilon_{\mu,2} = \mathrm{i}(\mathcal{C}\Psi_\mu - \Psi_\mu)$. The new spinors are invariant with respect to electron-hole inversion. With $a = 1, 2$ one finds $\mathcal{C}\Upsilon_{\mu,a} = \Upsilon_{\mu,a}$ which constitutes a condition for MZMs. The new spinors are given by $\Upsilon_{\mu,a} = (w_{\mu,a}, w_{\mu,a}^*)^{\mathrm{T}}$ with components $w_{\mu,1}(\boldsymbol{r}) = u_\mu(\boldsymbol{r}) + v_\mu^*(\boldsymbol{r})$ and $w_{\mu,2} = \mathrm{i}u_\mu(\boldsymbol{r}) - \mathrm{i}v_\mu^*(\boldsymbol{r})$. In the language of second quantization one gets a new set of *Hermitian* operators

$$\gamma_{\mu,1} = \beta_\mu^\dagger + \beta_\mu, \qquad \gamma_{\mu,2} = \mathrm{i}\big(\beta_\mu^\dagger - \beta_\mu\big), \tag{4.10}$$

fulfilling the algebra of Majorana bound states $\{\gamma_{\mu,a}, \gamma_{\nu,b}\} = 2\delta_{\mu\nu}\delta_{a,b}$. The existence of these zero energy modes is guaranteed by the topological structure of the BdG Hamiltonian $\mathcal{H}_{\mathrm{BdG}}(k)$ in presence of (effective) p-wave pairing potentials. Using the reversed Bogoliubov transformation (4.9),

$$\psi(\boldsymbol{r}) = \sum_m \big[u_m(\boldsymbol{r})\beta_m + v_m^*(\boldsymbol{r})\beta_m^\dagger\big], \tag{4.11}$$

it is a straightforward task to represent a second-quantized operator in terms of Bogoliubov quasiparticles. By restricting the general expression on the subspace of

zero energy solutions only, any observable O can be expressed in terms of Majorana operators as follows

$$\begin{aligned} O &= \int \psi^\dagger(\boldsymbol{r}')O(\boldsymbol{r}',\boldsymbol{r})\psi(\boldsymbol{r}')\,\mathrm{d}^3r'\mathrm{d}^3r \\ &= \frac{1}{4}\sum_{\mu,\nu,a,b}\left[\int w^*_{\mu,a}(\boldsymbol{r}')O(\boldsymbol{r}',\boldsymbol{r})w_{\nu,b}(\boldsymbol{r})\,\mathrm{d}^3r'\mathrm{d}^3r\right]\gamma_{\mu,a}\gamma_{\nu,b} \\ &= \frac{\mathrm{i}}{4}\sum_{\mu,\nu,a,b} O_{(\mu,a)(\nu,b)}\gamma_{\mu,a}\gamma_{\nu,b}. \end{aligned} \tag{4.12}$$

The coefficient in front of the Majorana operators is a Hermitian scalar product with respect to the Majorana wave functions $w_{\mu,a}(\boldsymbol{r}')$ and $w_{\nu,b}(\boldsymbol{r})$. This matrix element can only have a finite value where two Majorana wave functions have a considerable overlap. Because the Majorana wave function is spatially localized at the ends of the nanowire finite matrix elements can only appear at Josephson junctions where two Majorana modes are close together. Note, that the matrix elements are antisymmetric in the Majorana basis, $O_{(\mu,a)(\nu,b)} = -O_{(\nu,b)(\mu,a)}$.

Matrix elements between Majorana operators located at two different sides of a Josephson junction acquire a non-trivial phase dependency. This can be derived by performing a gauge transformation of the BdG Hamiltonian. From general principles, it is clear that a non-trivial phase difference $\varphi \neq 0$ cannot be gauged away. Therefore all matrix elements connecting degrees of freedom on both sides of the Josephson junction acquire phase factors $\mathrm{e}^{\pm\mathrm{i}\varphi/2}$ whereas all others become independent of the superconducting phases. In particular, if the operator O connects two MZMs γ_μ, γ_ν across a Josephson junction we obtain the representation

$$O = \frac{\mathrm{i}}{4}\mathrm{e}^{\mathrm{i}\varphi/2}O_{\mu\nu}\gamma_\mu\gamma_\nu + \frac{\mathrm{i}}{4}\mathrm{e}^{-\mathrm{i}\varphi/2}O_{\nu\mu}\gamma_\nu\gamma_\mu \tag{4.13}$$

$$= \frac{\mathrm{i}}{2}\cos\left(\frac{\varphi}{2}\right)O_{\mu\nu}\gamma_\mu\gamma_\nu, \tag{4.14}$$

where the dependence on the superconducting phase keeps track of the charge that is transported across the junction. For the sake of brevity we omitted the indices a, b adding them to μ and ν respectively. Accordingly, for the electrical dipole operator we get the following representation in terms of Majorana operators

$$\boldsymbol{d} = -e\int \psi^\dagger(\boldsymbol{r})\,\boldsymbol{r}\psi(\boldsymbol{r})\,\mathrm{d}^3r = \frac{\mathrm{i}}{2}\sum_{\mu<\nu}\cos\left(\frac{\varphi}{2}\right)\boldsymbol{d}_{\mu\nu}\gamma_\mu\gamma_\nu \tag{4.15}$$

where the matrix elements of the dipole operator are given by

$$\boldsymbol{d}_{\mu\nu} = -e\int \boldsymbol{r}\, w^*_\mu(\boldsymbol{r})w_\nu(\boldsymbol{r})\,\mathrm{d}^3r. \tag{4.16}$$

Note again that these quantities are only non-zero if the Majorana wave functions have some overlap.

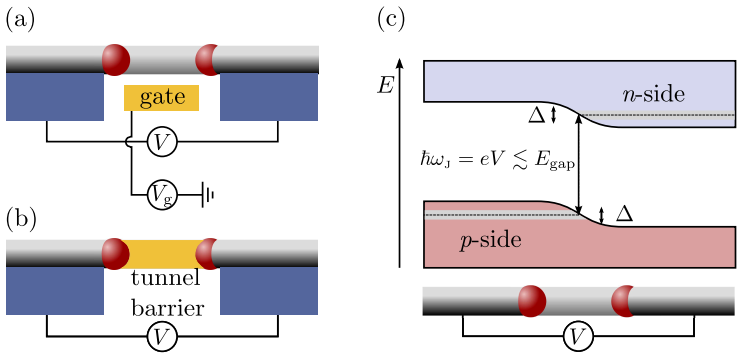

Fig. 4.2.: Possible ways to realize a fractional Josephson junction. (a) A nanowire crossing the two superconductors which is capacitively coupled to a gate at voltage V_g. The gate controls the hybridization strength of the MZMs at the Josephson junction. The bias voltage V shifts the Fermi energies with respect to each other and leads to an ac Josephson effect. Panel (b) shows a similar design with less tunability since the gated part of the nanowire is replaced with a narrow layer of insulator interrupting the semiconducting nanowire. In both of these setups, the radiation frequency is bounded by the superconducting gap and thus typically is in the microwave regime. This limitation can be overcome in the design (c) which shows the band diagram of a p-n junction. The different dopings lead to a pinning of the Fermi-energy in the valence band (left) and the conduction band (right). Around the Fermi-energies a small superconducting gap is opened due to the proximity to the superconductors which leads additionally to two Majorana bound states (red spheres), one in the valence band and one in the conduction band. The junction is operated in the forward bias regime with a potential difference comparable to the band-gap E_{gap}.

4.1.3. Possible realizations for fractional Josephson radiation

As the main ingredient for the present proposal, a Josephson junction where the wave function of the MZMs on either side have sufficient overlap is needed. This junction then needs to be embedded in a cavity to store and amplify the radiation field. Superconducting hybrid devices are very flexible and offer many possibilities to obtain a desired physical effect. Employing this freedom, we present three different designs for realizing fractional Josephson radiation.

A possible setup involves a semiconducting nanowire covered by two conventional s-wave superconductors with a gateable junction in between, see Fig. 4.2 (a). Given the fact that the device is in its topological phase, there are four MZMs formed. An external bias voltage V shifts the Fermi levels of wires with respect to each other and the gate is used to control the Josephson coupling strength, i.e., the size of the Majorana wave function overlap which enters the dipole moment. It is important to note that the bias voltage is bound by the superconducting gap, $eV < |\Delta|$, as otherwise undesired quasiparticles will be generated. Given the typical size of a superconducting gap of the order of a few Kelvin, the resulting Josephson radiation will be in the microwave regime. Obviously, the gated part of the nanowire can be replaced by a narrow, insulating barrier included in the nanowire during the growth process, see Fig. 4.2 (b). Compared to the case (a) discussed above, one would expect

a larger overlap of the wave-function in this case leading to a stronger light-matter interaction g with the drawback that the parameter is not tunable any more.

Inspired by the work of Recher *et al.* (2010), there is another variant that makes use of a superconducting p-n diode, embedding a p-n diode in a semiconducting nanowire, see Fig. 4.2 (c). Doping p- and n-type carriers at the left and right side makes a p-n diode out of the wire and MZMs are formed from the valence and conduction band, respectively. Recent investigations showed that the topological phase of a semiconducting nanowire persists even in presence of material imperfections (large dopant concentrations) (Adagideli *et al.*, 2014). The effect of dopants in the nanowire shifts the chemical potential towards the conduction or valence bands depending on carrier type and concentration. Typically for semiconducting nanowires there are two conduction bands and four hole bands, whereas the light-hole bands are split-off because of the boundary conditions in quasi one-dimensional wires. Light- and heavy-hole bands carry total angular momentum $J = \frac{3}{2}$ with heavy holes being characterized by $m_J = \pm\frac{3}{2}$. Out of the heavy hole states, MZMs for the hole band are formed exactly as for the conventional electron band. Across the p-n junction the bands will bend such that the electro-chemical potential remains constant. By applying reversed bias voltage, i.e., connect the p-type side with the negative pole and the n-type side with the positive pole of a voltage source the junction acts as an insulator up to voltages of the order of the band gap E_{gap}. The corresponding energy diagram is shown in Fig. 4.2 (c). This setup allows to increase the Josephson frequency from the superconducting gap to the band-gap E_{gap} of the semiconductor. For typical semiconductors with rather strong spin-orbit interaction, as for instance InAs, the band gap is of the order of 0.3 eV corresponding to wavelengths of around 4 μm. Hence, the radiation will be emitted in the mid-infrared regime.

Similar devices have been proposed in other systems involving quantum dots and a p-n junction which allows to shift the Josephson frequency into the optical frequency range (Recher *et al.*, 2010; Godschalk *et al.*, 2011). The proposal of Recher *et al.* (2010) discusses incoherent radiation in the emission band close to half the Josephson frequency and additionally coherent emission at the Josephson frequency arising from the coherent transfer of Cooper pairs. On the other hand, the proposal of Godschalk *et al.* (2011) leads to coherent radiation at half the Josephson frequency due to the fact that the device is embedded in a cavity; thus, the device has been named "half-Josephson laser". Although the optical phase of the laser is locked to the superconducting phase difference, decoherence of a half-Josephson laser is induced by spontaneous switches between different states of the quantum dot. Further elaborations have demonstrated that coherence times of emitted light from an array consisting of many emitters placed in a single cavity are exponentially long (Godschalk and Nazarov, 2013a,b). The main difference of these proposals to the present work is the fact that in our case there is no need for quantum dots as the Majorana bound states are formed at the interface without additional confinement. Furthermore, the bound states are automatically aligned with the chemical potential of the

superconductor and thus there is no need for (fine-)tuning of the dot parameters.

4.2. Model for a Josephson junction and dynamics of the radiation

4.2.1. Model

Even though we have advertised three different physical implementation schemes of Josephson radiation from MZMs all of them can be described by a single effective model. This is because in all three setups the physical process leading to radiation is tunneling of single electrons accompanied by the emission of a photon as described by (4.7). Taking additionally the energy of the photons in the cavity as well as possible overlap terms between MZMs on each wire section into account, we arrive at the model Hamiltonian

$$H = \frac{\varepsilon_{\mathrm{L}}}{2}\left(1 - \mathrm{i}\gamma_1\gamma_2\right) + \frac{\varepsilon_{\mathrm{R}}}{2}\left(1 - \mathrm{i}\gamma_3\gamma_4\right) + \hbar\omega a^\dagger a + \frac{\mathrm{i}g}{2}\cos\left(\frac{\varphi(t)}{2}\right)\gamma_2\gamma_3(a + a^\dagger) \tag{4.17}$$

which is the basis for the subsequent analysis; here, the overlap amplitudes are denoted by ε_{L} and ε_{R} for Majorana modes γ_1, γ_2 in the left and γ_3, γ_4 in the right section of the nanowire, respectively. These coefficients are decaying exponentially with the separation $\varepsilon_{\mathrm{L/R}} \propto \mathrm{e}^{-L_{\mathrm{L/R}}/\xi}$, where $L_{\mathrm{L/R}}$ is the length of a particular wire section and ξ is the superconducting coherence length (Kitaev, 2001). Furthermore, it has been assumed that Majorana modes γ_1 and γ_4 are located too far away from each other such that their overlap can be neglected compared to $\varepsilon_{\mathrm{L}}, \varepsilon_{\mathrm{R}}$. The applied bias voltage is taken into account by a time-dependent superconducting phase $\varphi(t) = \varphi(0) + 2eVt/\hbar$. In deriving (4.17), we have neglected all quasiparticle excitations above the superconducting gap which leads to the requirement that $g|\langle a^\dagger + a\rangle| \ll |\Delta|$. Moreover, we have used the fact that we are interested in a situation where the density of states of the cavity is a sharp peaked Lorentzian centered at the frequency $\omega \approx \omega_J/2$ with a small linewidth caused by cavity losses, see Sec. 4.2.2. Because of this, we neglected both the contribution from the dc fractional Josephson effect (4.8) as well as from usual Cooper pair tunneling as those contributions are off resonance. Even though the number of channels by which Cooper pairs emit conventional Josephson radiation is much larger than the single channel emitting radiation at half the Josephson frequency, the emission at the Josephson frequency is suppressed by the factor Q^2 with Q the quality factor of the cavity such that a situation can be reached where the single electron channel dominated the radiation processes. The model Hamiltonian (4.17) describes the dynamics of the Majorana bound states in a Josephson junction as well as dynamics of the radiation field. Note that the superconducting condensate acts as a driving force in this model. It is

convenient to represent (4.17) in terms of a Fock space basis consisting of states $|n\rangle \otimes |N\rangle$ where $|N\rangle$ is the state of the photon mode occupied with N photons and $|n\rangle$ describing the fermionic states as introduced in (4.3).

Next, we assume that the voltage $eV = \hbar\omega_{\text{J}}/2$ is large compared to the other characteristic energies of the system $\varepsilon_{\text{L/R}}, g$, and $\Omega = \omega - \omega_{\text{J}}/2$. We change via the unitary transformation $U = \exp\left(-\frac{\text{i}}{2}\omega_{\text{J}} t\, a^\dagger a\right)$ from (4.17) into a rotating frame where we neglect the rapidly oscillating terms $\propto \exp\left(\pm \text{i}\omega_{\text{J}} t\right)$. Then we end up with the Hamiltonian

$$H_{\text{RWA}} = \frac{\varepsilon_{\text{L}}}{2}\left(1 - \text{i}\gamma_1\gamma_2\right) + \frac{\varepsilon_{\text{R}}}{2}\left(1 - \text{i}\gamma_3\gamma_4\right) + \hbar\Omega b^\dagger b + \frac{\text{i}g}{4}\gamma_2\gamma_3(b + b^\dagger) \tag{4.18}$$

in the rotating wave approximation (RWA); here, we have introduced the new operators $b = \exp\left(i\varphi(0)/2\right) a$ absorbing the superconducting phase at the initial time $t = 0$.

4.2.2. Semiclassical approximation

As we are interested in the resonant regime of small Ω, many photons will accumulate in the cavity due to the driving of the superconducting phase. If the cavity losses are small compared to the pumping rate, many photons will accumulate in the cavity and the radiation field will approach a classical state with a photon number $N = \langle b^\dagger b\rangle \gg 1$. We want to refer to this limit as the semiclassical limit, because the degrees of freedom of the nanowire are still treated quantum mechanically. The semiclassical approximation in (4.18) amounts to replacing b with the complex number $\lambda = \langle b\rangle$. The Hamiltonian H_{RWA} becomes a 4×4 matrix representing the Majorana bound states coupled to a classical field $\lambda(t)$ which is still a dynamical variable of the problem. Even though N is expected to become large, we still want to demand $g\,|\operatorname{Re}\lambda| \ll |\Delta|$ to avoid interaction with the states above the superconducting gap Δ. The equations of motion for $\lambda(t)$ can be derived from the Heisenberg equation of motion for b. This yields the differential equation for the classical radiation field

$$\dot{\lambda} = -\left(\text{i}\Omega + \Gamma\right)\lambda + \frac{g}{2\hbar}\langle\psi(t)|\gamma_2\gamma_3|\psi(t)\rangle, \tag{4.19}$$

where we have introduced the cavity loss rate $\Gamma = \omega_{\text{J}}/2Q$ and the (time-dependent) electronic state $|\psi(t)\rangle$. The state of the nanowire evolves according to

$$|\psi(t)\rangle = \mathcal{T}\exp\left(-\frac{\text{i}}{\hbar}\int_0^t H_{\text{w}}(\lambda)\text{d}t'\right)|\psi(0)\rangle \tag{4.20}$$

where

$$H_{\text{w}}(\lambda) = \frac{\varepsilon_{\text{L}}}{2}(1 - \text{i}\gamma_1\gamma_2) + \frac{\varepsilon_{\text{R}}}{2}(1 - \text{i}\gamma_3\gamma_4) + \frac{\text{i}g}{2}\gamma_2\gamma_3\ \operatorname{Re}\lambda \tag{4.21}$$

is the Hamiltonian of the nanowire driven by the time-dependent field $\lambda(t)$. The two equations (4.19) and (4.20) need to be solved self-consistently. As we are interested in the long-time dynamics where the system approaches a stationary state with $\dot{\lambda} = 0$, we may assume that the radiation field λ changes slowly in time and the system adjusts adiabatically. In this regime, the system remains in its instantaneous eigenstates $|\psi; \lambda\rangle$ which we will assume in the following.

There are four instantaneous eigenstates of H_{W} which we will denote by $|\pm, \mathcal{P}; \lambda\rangle$ with $\mathcal{P} = \pm 1$ labeling the even and odd parity sectors and $\pm$ indicating whether the system is in the upper or lower state respectively. The corresponding eigenenergies are given by

$$E_{\pm,\mathcal{P}} = \frac{1}{2}\left(\varepsilon_{\mathrm{L}} + \varepsilon_{\mathrm{R}} \pm \sqrt{g^2\,\mathrm{Re}(\lambda)^2 + \delta_{\mathcal{P}}^2}\right); \tag{4.22}$$

here, $\delta_{\mathcal{P}} = \varepsilon_{\mathrm{L}} + \mathcal{P}\,\varepsilon_{\mathrm{R}}$ is the size of the avoided crossing, see Fig. 4.3. The validity of the adiabatic approximation is given by

$$|\langle +, \mathcal{P}|\gamma_2\gamma_3|-, \mathcal{P}\rangle| \ll \frac{2g}{\hbar}\,\frac{|\,\mathrm{Re}\,\lambda|}{|\frac{\mathrm{d}}{\mathrm{d}t}\ln(\mathrm{Re}\,\lambda)|} \tag{4.23}$$

which translates to the requirement $\hbar(\Omega^2 + \Gamma^2)^{1/2} \ll g\,|\,\mathrm{Re}\,\lambda|$ by using (4.19).

The initial dynamics of the radiation field before getting close to the stationary state is highly non-adiabatic and the electronic system will switch many times between different eigenstates due to the driving of cavity field. However, we are not interested in the transient dynamics and concentrate on the stationary state of the radiation field which will turn out to be phase locked to the superconducting phase difference, see below. In the adiabatic regime the matrix elements needed in (4.19) can be evaluated explicitly,

$$\langle \pm, \mathcal{P}|\gamma_2\gamma_3|\pm, \mathcal{P}\rangle = \mp \mathrm{i}\frac{g\ \mathrm{Re}\,\lambda}{\sqrt{g^2\ \mathrm{Re}(\lambda)^2 + \delta_{\mathcal{P}}^2}}, \tag{4.24}$$

assuming that the electronic system is in the state $|\psi\rangle = |\pm, \mathcal{P}\rangle$. Plugging the matrix element into the equation of motion (4.19), it becomes a non-linear differential equation for the field amplitude λ. We can see that apart from the trivial stationary solution $\lambda = 0$, there is for each eigenstate the second stationary solution

$$\begin{aligned}\lambda_{\pm,\mathcal{P}} &= \pm\frac{1}{2}\left[\frac{g^2}{4\hbar^2\,(\Omega^2+\Gamma^2)} - 4\frac{\Omega^2+\Gamma^2}{g^2}\left(\frac{\delta_{\mathcal{P}}}{\Omega}\right)^2\right]^{\frac{1}{2}} \mathrm{e}^{\mathrm{i}\arctan(\Gamma/\Omega)} \\ &\approx \pm\frac{g}{4\hbar\sqrt{\Omega^2+\Gamma^2}}\mathrm{e}^{\mathrm{i}\arctan(\Gamma/\Omega)}\end{aligned} \tag{4.25}$$

fulfilling $\dot{\lambda}_{\pm,\mathcal{P}} = 0$. The nontrivial states are stable (and correspondingly the trivial states unstable) if $4|\delta_{\mathcal{P}}|/\Omega \leq g^2/\hbar(\Omega^2 + \Gamma^2)$ which is why we have neglected $\delta_{\mathcal{P}}$ by passing from the first to the second line in (4.25). According to the balance

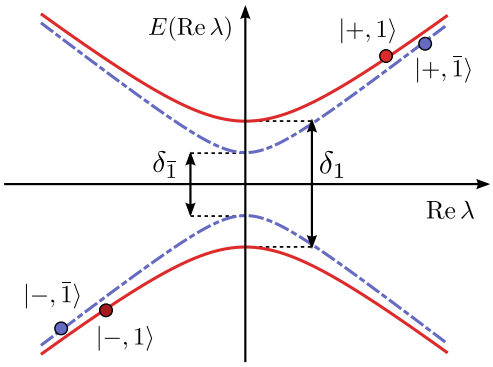

Fig. 4.3.: Spectrum of the electronic system as function of $\mathrm{Re}\,\lambda$. The spectrum has two distinct parity sectors indicated by solid (even) and dashed (odd) spectral-lines differing by their level splitting at zero field, $\delta_{\mathcal{P}} = \varepsilon_{\mathrm{L}} + \mathcal{P}\varepsilon_{\mathrm{R}}$. During the initial time evolution, the radiation field drives the system several times through the avoided crossing until it approaches a stationary state. There is exactly one stationary state of the radiation field, indicated by the dots, associated with each eigenstate of the electronic system.

between driven pumping and cavity losses, the stationary field amplitude depends on the cavity quantities Ω, Γ and the coupling g. Going back to the original non-rotating frame the stationary field configuration describes an oscillating field $\langle a\rangle = \exp[-\mathrm{i}\omega_{\mathrm{J}}t/2 - \mathrm{i}\varphi(0)/2]\lambda_{\pm,\mathcal{P}}$ at frequency $\omega_{\mathrm{J}}/2$, i.e., half of the Josephson frequency. Regarding the phase of the radiation field $\langle a\rangle$, we see that it is *locked* to half of the superconducting phase difference $-\varphi(0)/2$ with an additional phase shift $\arctan(\Gamma/\Omega)$ due to the cavity. Moreover, the sign of the radiation field depends on the fact whether the system is in the upper or lower state but (almost) not on $\mathcal{P}$. This locking mechanism protects the emitted radiation from diffusion of the phase as it is the case for conventional lasers (Scully and Lamb, 1967). This is a consequence of the broken U(1) phase symmetry of the superconductors that is imprinted in the phase of the radiation field. We expect the coherence time of the emitted radiation to be rather long as experiments measuring the relaxation of the persistent current in superconductors have shown that the superconducting coherence lasts for years (Tinkham, 1996). As we show in the next section, these extremely long coherence times cannot be reached in realistic systems due to spontaneous switches of the electronic system as well as quasiparticle poisoning.

4.2.3. Influence of counter-rotating terms

In order to study the effect of the counter-rotating terms that have been neglected in (4.18) the non-rotating stationary solutions are put into the original Hamiltonian (4.17) substituting operator a by $\exp\big(-\mathrm{i}\varphi(t)/2\big)\,\lambda$. The resulting Hamiltonian is given by

$$H = \frac{\varepsilon_{\mathrm{L}} + \varepsilon_{\mathrm{R}}}{2}\mathbb{1}_2 + \frac{\delta_{\mathcal{P}}}{2}\sigma_3 - \frac{g|\lambda|}{2}\cos(\chi)\sigma_1 + \frac{g|\lambda|}{2}\cos(\omega_{\mathrm{J}}t + \varphi(0) - \chi)\sigma_1, \quad (4.26)$$

where the last term represents fast oscillating counter-rotating terms, that have been neglected while going from (4.17) to (4.18). Furthermore, $\chi = \arctan(\Gamma/\Omega)$ is the phase shift due to the cavity and $\sigma_1 = \mathrm{i}\gamma_2\gamma_3, \sigma_3 = -\mathrm{i}\gamma_1\gamma_2$ are Pauli matrices. This is a time-dependent problem with driving frequency ω_{J}. After interchanging σ_1 and

σ_3, we make the ansatz (Nazarov and Blanter, 2009)

$$|\phi\rangle = \exp\left(\mathrm{i}\frac{g|\lambda|}{2\hbar}\int_0^t \cos(\omega_\mathrm{J} t + \varphi(0) - \chi)\mathrm{d}t\,\sigma_3\right)|\tilde{\phi}\rangle \tag{4.27}$$

for the wave function $|\phi\rangle$. This leads to the Schrödinger equation for $|\tilde{\phi}\rangle$

$$\mathrm{i}\hbar\frac{\mathrm{d}}{\mathrm{d}t}\begin{pmatrix}\tilde{\phi}_1\\ \tilde{\phi}_2\end{pmatrix} = \frac{1}{2}\begin{pmatrix}-g|\lambda|\cos\chi & \mathrm{e}^{\mathrm{i}A(t)}\delta_\mathcal{P}\\ \mathrm{e}^{-\mathrm{i}A(t)}\delta_\mathcal{P} & g|\lambda|\cos\chi\end{pmatrix}\begin{pmatrix}\tilde{\phi}_1\\ \tilde{\phi}_2\end{pmatrix} \tag{4.28}$$

with the time-dependent expression

$$A(t) = \frac{g|\lambda|}{2\hbar\omega_\mathrm{J}}\left[\sin\left(\omega_\mathrm{J} t + \varphi(0) - \chi\right) - \sin\left(\varphi(0) - \chi\right)\right]. \tag{4.29}$$

Since the driving frequency is much larger than the largest energy scale in (4.28), $g|\lambda| \ll \hbar\omega_\mathrm{J}$, it is reasonable to perform a time average over one period $T = 2\pi/\omega_\mathrm{J}$. From the resulting time-averaged Schrödinger equation the probability for a state inversion flip is obtained to

$$P_{+\to-}(t) = |\langle\phi_-|\phi_+(t)\rangle|^2 \approx \left(\frac{\delta_\mathcal{P}}{g\,\mathrm{Re}\,\lambda}\right)^2 \sin^2\left(\frac{g\,|\,\mathrm{Re}\,\lambda|}{2\hbar}\,t\right). \tag{4.30}$$

The probability to flip from the upper to the lower state is apparently oscillating in a coherent manner with period $4\pi\hbar/g\,|\,\mathrm{Re}\,\lambda| \ll \Gamma^{-1}$.

4.3. Coherence of the radiation

Switches of the electronic state of the wire are caused by two mechanisms, emission of off-resonant photons and quasiparticle poisoning, that are present even if the stationary state has been reached. Whenever a spontaneous switching event happens, the cavity field will be driven out of its stationary state and eventually will approach another one. Here, we will assume that switches happen instantaneously on the time-scale Γ^{-1} of the cavity. While the system approaches another stable amplitude the time evolution may get non-adiabatic again including many other switching processes as described in Sec. 4.2.1. As noted above, in case the switching process changes the electronic system from the upper to the lower branch (or the other way round), it is accompanied with a change of π of the phase of the radiation field. We will discuss two mechanisms which lead to decoherence: The first process we will discuss conserves the total parity $\mathcal{P}$. By emitting a non-resonant photon that carries the energy of the level splitting $\hbar\tilde{\omega} \simeq g\,|\,\mathrm{Re}\,\lambda|$, a transition between those upper and lower states at fixed parity is possible. The transition rate for such a process can be evaluated by Fermi's golden rule. Using the fact that the density of states of

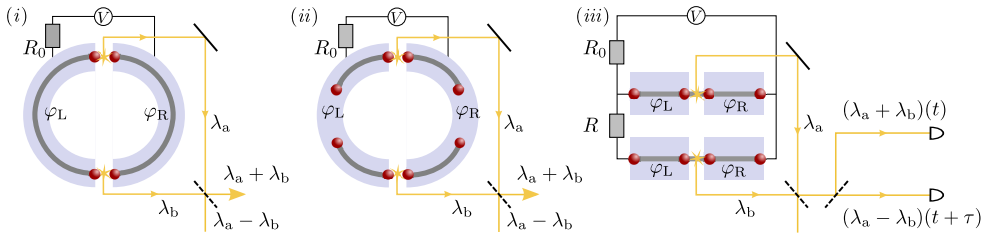

Fig. 4.4.: Three different designs for small networks with two Josephson junctions. In (a), a single semiconducting (circular) nanowire is lying on top two bulk superconductors realizing a dc-SQUID geometry interrupted by two Josephson junctions. In the setup (b), the two fractional Josephson junctions in the dc-SQUID are formed by two distinct nanowires such that there are eight Majorana zero modes in total. In (c), the two fractional Josephson junctions are two independent setups of Fig. 4.1 biased at the same voltage V. Each Josephson junction is surrounded by a cavity which emits coherent radiation indicated by beams of radiation λ_a and λ_b. These radiation fields are subsequently led to interfere by a semitransparent reflector (dashed line). In the main text, we compare the expected coherence of the radiation emitted in these different setups with each other.

the photons in the cavity is Lorentzian, we obtain the approximate transition rate (Godschalk *et al.*, 2011)

$$\Gamma_{\text{F}} = \frac{\Gamma}{8}\left(\frac{\delta_{\mathcal{P}}}{g\,\text{Re}^2\,\lambda}\right)^2, \tag{4.31}$$

where we have assumed that the photon frequency is far detuned, $\tilde{\omega} \gg \Gamma, \Omega$. Given the fact that $\delta_{\mathcal{P}}$ depends exponentially on the separation of the MZMs, we expect that Γ_{F} will most likely be not the dominating process generating decoherence but rather the fact that superconducting devices suffer from *quasiparticle poisoning*. As soon as an extra quasiparticle tunnels on one of the bulk superconductors the parity of the device is changed, see Ch. 3. Additionally, also the upper state might be transformed into the lower state as the quasiparticle changes $\mathcal{P}_{\text{L}}$ or $\mathcal{P}_{\text{R}}$ which do not commute with the Hamiltonian H_{W}. For concreteness, we assume that a quasiparticle tunneling switches the state $|+, \mathcal{P}\rangle$ to the states $|\pm, \bar{\mathcal{P}}\rangle$ with equal probability. Measurements of transmon-type charge qubits have shown that quasiparticle tunneling appears to happen on rather long time scales in the range from microseconds up to milliseconds (Riste *et al.*, 2013). In the following quasiparticle tunneling will be modeled simply by a Γ_{QP}. On top of these spontaneous switches, there are coherent Rabi oscillations with frequency $g\,|\,\text{Re}\,\lambda|$ taking place because of the influence of counter-rotating terms that have been neglected in the RWA, see Sec. 4.2.3 for details.

4.3.1. Autocorrelations and partial coherence

Including the action of both switching mechanisms, the question arises on what time-scale the Josephson radiation remains coherent. In this section we want to address the question of autocorrelations of the radiation emitted by a single Josephson junction, whereas the correlations between different sources are discussed in the next section.

The correlations of the radiation field can be determined from a master equation treatment of the switching processes. The main task of the master equation is to evaluate the vector $\boldsymbol{p}(t)$ whose components are the probabilities $p_\alpha(t)$ for finding the system in a particular state $|\pm, \mathcal{P}\rangle$ at time t given some initial state $\boldsymbol{p}(0)$. The master equation describing the switching events then reads

$$\frac{\mathrm{d}}{\mathrm{d}t}\begin{pmatrix} p_1 \\ p_2 \\ p_3 \\ p_4 \end{pmatrix} = \begin{pmatrix} -\Gamma_\mathrm{F} - \Gamma_\mathrm{QP} & \Gamma_\mathrm{F} & \Gamma_\mathrm{QP}/2 & \Gamma_\mathrm{QP}/2 \\ \Gamma_\mathrm{F} & -\Gamma_\mathrm{F} - \Gamma_\mathrm{QP} & \Gamma_\mathrm{QP}/2 & \Gamma_\mathrm{QP}/2 \\ \Gamma_\mathrm{QP}/2 & \Gamma_\mathrm{QP}/2 & -\Gamma_\mathrm{F} - \Gamma_\mathrm{QP} & \Gamma_\mathrm{F} \\ \Gamma_\mathrm{QP}/2 & \Gamma_\mathrm{QP}/2 & \Gamma_\mathrm{F} & -\Gamma_\mathrm{F} - \Gamma_\mathrm{QP} \end{pmatrix} \cdot \begin{pmatrix} p_1 \\ p_2 \\ p_3 \\ p_4 \end{pmatrix} \tag{4.32}$$

where the index $\alpha \in \{1, 2, 3, 4\}$ labels the states $\{|+, 1\rangle, |-, 1\rangle, |+, \bar{1}\rangle, |-, \bar{1}\rangle\}$. The time evolution of the radiation field is thus given by

$$\langle \Lambda(t) \rangle = \sum_\alpha \mathrm{e}^{-\mathrm{i}\varphi(t)/2} \lambda_\alpha \, p_\alpha(t) \tag{4.33}$$

where the angular brackets indicate the ensemble average and we have assumed that the radiation field is always in its stationary state λ_α which corresponds to demanding that $\Gamma \gg \Gamma_\mathrm{QP}, \Gamma_\mathrm{F}$. In general, correlations can be expressed in terms of the normalized first-order correlation function[1)]

$$g^{(1)}(\tau) = \frac{\langle \Lambda^*(t) \Lambda(t+\tau) \rangle}{\langle |\Lambda|^2 \rangle} \tag{4.34}$$

correlating the signal $\Lambda(t)$ with itself after a time τ. Without the switching processes discussed before, the autocorrelation function equals one indicating coherence with an infinite coherence time. The situation changes when spontaneous switches are taken into account. Then the relative phase factors of λ change randomly by π resulting in a finite coherence time.

Autocorrelations of each beam can be measured by performing a Hanbury Brown-Twiss experiment measuring intensity correlations of the radiation field at the different times t and $t + \tau$. In fact, the first-order autocorrelation function and with that its coherence time can be extracted from the normalized second-order correlation function via

$$g^{(2)} = \frac{\langle \Lambda^*(t) \Lambda^*(t+\tau) \Lambda(t+\tau) \Lambda(t) \rangle}{\langle |\Lambda|^2 \rangle^2} = 1 + |g^{(1)}(\tau)|^2 \tag{4.35}$$

where the last identity is valid for a classical radiation field as we are considering (Loudon, 1973). The solution of the master equation for $\boldsymbol{p}$ yields in the steady state the first-order correlation function

$$g^{(1)}(\tau) = \exp\left(-\frac{\mathrm{i}}{2} \omega_\mathrm{J} \tau - \frac{\tau}{\tau_\mathrm{c}} \right) \tag{4.36}$$

[1)] Cf. Sec. A.3 in App. A.

where $\tau_c = (2\Gamma_F + \Gamma_{QP})^{-1}$ is the coherence time. The reason for the factor two of Γ_F compared to Γ_{QP} is the fact that the former process leads every time to a switch of the upper to the lower state whereas for the former process this happens only with a probability of 50%.

Another effect which leads to decoherence are thermal fluctuations of the bias voltage. Since there is a finite resistance R_0 associated to the circuit that connects the ideal voltage source with the Josephson junction, cf. Fig. 4.4, there is a Johnson-Nyquist noise characterized by $\langle\langle V(t)V(t+\tau)\rangle\rangle = 2R_0 k_B T\delta(\tau)$ at any finite temperature T. As the first-order correlation function is proportional to the complex phase factor $e^{i[\varphi(t)-\varphi(t+\tau)]/2}$ and thus depends on $V(t)$, the thermal noise leads to decoherence. Using the fact that the thermal noise is Gaussian, the expectation value of the complex phase factor assumes the form

$$\left\langle e^{i[\phi(t)-\phi(t+\tau)]/2}\right\rangle = e^{-i\omega_J\tau/2} \tag{4.37a}$$

$$e^{-\langle\langle[\varphi(t)-\varphi(t+\tau)]^2\rangle\rangle/8} = \exp\left(-\frac{i}{2}\omega_J\tau - \frac{e^2R_0}{\hbar^2}k_B T\tau\right). \tag{4.37b}$$

Consequently, the normalized autocorrelation function is given by

$$g^{(1)}(\tau) = \exp\left[-\frac{i}{2}\omega_J\tau - \left(\tau_c^{-1} + \frac{e^2R_0}{\hbar^2}k_B T\right)\tau\right] \tag{4.38}$$

with a reduced coherence time due to the finite resistance R_0.

4.3.2. Correlations of different sources

So far, we have discussed the dynamics and stationary properties of the emitted Josephson radiation of a single junction. In this section, we want to expand the setup and take possible coherence between different emitters into account. Due to the phase locking, we expect that the radiation fields are ideally perfectly correlated with each other (Recher *et al.*, 2010). Hence, it should be possible to observe correlations between two radiation fields even if these junctions are spatially-separated from each other.

Here, we want to determine the correlation between different radiation sources for the three setups illustrated in Fig. 4.4. We will label the properties associated with two radiation sources by a and b. The coherence will show up in the second-order correlation function

$$g^{(2)}_{ab}(\tau) = \frac{\langle\Lambda_a^*(t)\Lambda_b^*(t+\tau)\Lambda_b(t)\Lambda_a(t+\tau)\rangle}{\langle|\Lambda_a|^2\rangle\langle|\Lambda_b|^2\rangle} \tag{4.39}$$

measuring correlations between two radiation fields λ_a, λ_b. The function $g^{(2)}_{ab}(\tau)$ is part of the intensity correlator $\langle|\Lambda_a(t)\pm\Lambda_b(t)|^2\,|\Lambda_a(t+\tau)\pm\Lambda_b(t+\tau)|^2\rangle$ and thus can be measured by correlating the intensities after the beamsplitters, see Fig. 4.4 (c).

The first setup, we analyze is shown in Fig. 4.4 (a). There is a single circular nanowire placed on a superconducting ring interrupted by two Josephson junctions

(dc-SQUID geometry). Each of these junctions implements a source as discussed above. For simplicity, we assume both junctions to be equal, i.e., $g_\mathrm{a} = g_\mathrm{b} = g$, $\Omega_\mathrm{a} = \Omega_\mathrm{b} = \Omega$, and $\Gamma_\mathrm{a} = \Gamma_\mathrm{b} = \Gamma$. In total there will be four MZMs in the system and the equations of motion assume the form

$$\begin{aligned}\dot{\lambda}_\mathrm{a} &= -(\mathrm{i}\Omega + \Gamma)\lambda_\mathrm{a} \pm \mathrm{i}\frac{g^2}{4\hbar}\frac{\mathrm{Re}(\lambda_\mathrm{a} - \mathcal{P}\lambda_\mathrm{b})}{\sqrt{\delta_\mathcal{P}^2 + g^2\,\mathrm{Re}^2(\lambda_\mathrm{a} - \mathcal{P}\lambda_\mathrm{b})}},\\ \dot{\lambda}_\mathrm{b} &= -(\mathrm{i}\Omega + \Gamma)\lambda_\mathrm{b} \pm \mathrm{i}\frac{g^2}{4\hbar}\frac{\mathrm{Re}(\lambda_\mathrm{b} - \mathcal{P}\lambda_\mathrm{a})}{\sqrt{\delta_\mathcal{P}^2 + g^2\,\mathrm{Re}^2(\lambda_\mathrm{a} - \mathcal{P}\lambda_\mathrm{b})}},\end{aligned} \tag{4.40}$$

with $\mathcal{P}$ the total fermion parity of the system, as before. The stationary solutions are given by (4.25) with the additional constraint $\lambda_\mathrm{b} = -\mathcal{P}\lambda_\mathrm{a}$ which correlates both field amplitudes λ_a and λ_b by the parity constraint. Hence the dc-SQUID geometry exhibits a strong correlation between different stationary fields for arbitrary spatial separation. In particular, the constraint implies that the relative phase between λ_a and λ_b can only be changed by changing the total fermion parity of the system, i.e., quasiparticle poisoning. Indeed, we obtain the result

$$g^{(2)}_\mathrm{ab}(\tau) = \exp(-2\Gamma_\mathrm{QP}\tau) \tag{4.41}$$

for the case (a). Note that this result is independent of the resistance R_0 of the voltage source.[2)] The case (a) shows very robust correlations but we expect it to be rather challenging to realize experimentally as a circular nanowire is required. Therefore, we want to analyze the situation where the two emitters are formed by two different nanowires, see Fig. 4.4 (b). In contrast to the last case, there are in total eight MZMs involved in this case—four on each nanowire. As a result, there is no parity constraint relating the phase of the field of one emitter to the field of the other emitter in the stationary state. Instead, the Hamiltonian of the wires separates into two parts $H_\mathrm{a} + H_\mathrm{b}$ with only the common superconducting phase providing correlations. Thus, the stationary state of the radiation fields in the rotating frame are individually given by (4.25). In the laboratory frame, the states evolve according to $\mathrm{e}^{-\mathrm{i}\varphi(t)/2}\lambda_\mathrm{a/b}$ with the common superconducting phase difference $\varphi(t)$ which is expected to lead to partial coherence of the sources. Indeed, calculating the correlation function for this case, we obtain

$$g^{(2)}_\mathrm{ab}(\tau) = \exp[-2(2\Gamma_\mathrm{F} + \Gamma_\mathrm{QP})\tau] \tag{4.42}$$

which is decaying with the typical time scale τ_c of the spontaneous switching events. As above, the result is independent of the resistance R_0.

The last case (c) differs from (b) by the fact that the radiation-emitting junctions do not share common superconductors but only a common voltage source. In this

[2)] Interestingly, for case (a) one can also obtain a non-vanishing cross-correlation $g^{(1)}_\mathrm{ab}(\tau) = \exp(-\mathrm{i}\omega_\mathrm{J}\tau/2 - \tau/\tau_\mathrm{c})$, because it behaves essentially like an autocorrelation according to the constraint $\lambda_\mathrm{b} = -\mathcal{P}\lambda_\mathrm{a}$.

case, the phase difference φ_{a} will differ from φ_{b} which leads to decoherence of the two radiation fields evolving according to $\mathrm{e}^{-\mathrm{i}\varphi_{\mathrm{a/b}}(t)/2}\lambda_{\mathrm{a/b}}$ in the laboratory frame. In fact, the diffusion of the difference $\varphi_{\mathrm{a}} - \varphi_{\mathrm{b}}$ will be governed by the resistance R, cf. Fig. 4.4 (c). Because of that the second-order correlation function

$$g^{(2)}_{\mathrm{ab}}(\tau) = \exp\left[-2(2\Gamma_{\mathrm{F}} + \Gamma_{\mathrm{QP}})\tau - \frac{e^2 R}{\hbar^2} k_{\mathrm{B}} T \tau\right] \tag{4.43}$$

shows an additional decay compared to (4.42).

4.4. Conclusions

To summarize, in this chapter we have analyzed the possibility to couple MZMs to electromagnetic fields in a Josephson junction Ch. 4. It has been shown that partially coherent Josephson radiation is emitted at half of the Josephson frequency. The coherence of the emitted radiation is limited due to rare spontaneous switches of the relative phase flipping randomly between values $0, \pi$. Due to the coupling of the MZMs to the superconductor, there are only two phase differences allowed. This leads to a fixed phase of the radiation field different from conventional lasers where the optical phase is slowly diffusing (Scully and Lamb, 1967). Even though the phases are in principle locked, decoherence of the radiation is induced by spontaneous switches as well as by frequency fluctuations.

Furthermore, we have analyzed the correlations between two emitters, which are spatially-separated but share the same superconductors. The temporal correlations of the two emitters provide information about the state of the MZMs inside the wire. In particular, by considering a dc-SQUID geometry the global fermionic parity constraint as well as the pinning of the Josephson frequency can be clearly identified by means of second-order correlation functions. In addition, we have suggested a possible way to access these correlations experimentally.

As the radiation field carries lots of information about the state of the nanowire, the interaction of MZMs with electromagnetic radiation can be used to address and manipulate Majorana-based qubits in a microwave resonator. By operating the device in *resonance* with the microwave cavity $\omega \approx \frac{\omega_{\mathrm{J}}}{2}$, the setups considered in this chapter primarily work as emitters for coherent radiation. For the purpose of manipulating the states of a topological qubit, it may be preferred to use weak electromagnetic fields containing only a few photons. As will be discussed in the next chapter, this allows to measure the state of a Majorana non-invasively.

Chapter 5

Readout of Majorana qubits

The results of this chapter have been published in:

> Ohm, C. and Hassler, F., 2015: *Microwave readout of Majorana qubits*, Phys. Rev. B **91**, 085406.

The possibility to couple Majorana zero modes to electromagnetic radiation opens new perspectives for quantum computation with topological Majorana-based qubits; even though the main intention of topological quantum computation is to encode quantum information into global properties of the system, a readout for a topological qubit can only be executed by accessing this global information and thereby breaking the topological protection. In the context of the fractional quantum Hall state, it has been suggested that the readout can be executed by interference experiments (Stern and Halperin, 2006; Bonderson *et al.*, 2006). This was later adapted to topological superconductors where the Aharonov-Casher effect allows to read out the Majorana qubit by interfering fluxons (Hassler *et al.*, 2010; Sau *et al.*, 2011; Hassler *et al.*, 2011; Pekker *et al.*, 2013).

Recently, several works have reported that it is possible to couple MZMs in semiconducting nanowires directly to electromagnetic radiation. While some of the proposals primarily aimed at identifying the signature of MZMs in microwave signals (Trif and Tserkovnyak, 2012; Cottet *et al.*, 2013; Ohm and Hassler, 2014), others use the microwave coupling mechanism to implement controlled qubit manipulations (Schmidt *et al.*, 2013a,b; Ginossar and Grosfeld, 2014; Yavilberg *et al.*, 2015). Among different types of coupling mechanisms, it has been shown in the previous chapter how coherent radiation can be emitted at half of the Josephson frequency. The effect arises in a voltage-biased Majorana Josephson junction and can be understood as the so-called *fractional Josephson radiation* (Domínguez *et al.*, 2012). Tuning a microwave cavity on resonance, the Josephson junction then acts as a light source for coherent radiation (Ohm and Hassler, 2014). In this chapter, we want to employ the fractional Josephson radiation in order to implement a readout scheme for Majorana qubits. Instead of tuning the microwave cavity on resonance, we envision a setup in the dispersive regime allowing for a quantum non-demolition measurement. As the fractional Josephson radiation arises from single-electron transport due to the presence of MZMs, it allows for a direct readout of the Majorana qubit without involving intermediate interference steps. Coupling of the readout device to the Majorana qubit can be turned on and off at will via control of the external bias voltage.

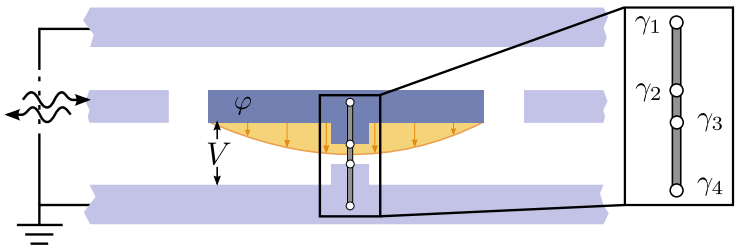

Fig. 5.1.: The measurement setup involves three strips of superconducting electrodes. The two outer strips are grounded. The left part forms a transmission line (indicated by wavy-lines), whereas the darker center region is a strip-line microwave resonator. A semiconducting nanowire bridging the center strip to the lower strip in a moderate magnetic field implements a Majorana Josephson junction hosting four localized MZMs $\gamma_1, \ldots, \gamma_4$ (white dots). The junction is characterized by a time-dependent superconducting phase difference $\varphi(t)$ generated by a voltage $V = \hbar\dot{\varphi}/2e$. The voltage V consists of a dc component V_0 by which the measurement can be turned on and off and an ac component induced by the microwave radiation in the transmission line.

In Sec. 5.1 we briefly introduce and review the coupling mechanism that leads to fractional Josephson radiation. We continue by introducing the effective model for a dispersive readout in Sec. 5.2. We then study the susceptibility of the system to coherent radiation introduced by coupling the cavity to a transmission line resonator (Sec. 5.3). Finally in Sec. 5.4, we compute the measurement times for a homodyne measurement scheme as well as for an intensity measurement showing that both methods profit from phase coherence. While this is always the case for the homodyne measurement, in the present situation, the MZMs lead to squeezing of the radiation, thereby also rendering the intensity measurement phase-sensitive.

5.1. Setup

A prominent way to emulate a topological superconductor in order to create MZMs is to employ nanowires having strong spin-orbit interaction in combination with an external magnetic field as well as proximity-induced Cooper pairing (Oreg *et al.*, 2010; Lutchyn *et al.*, 2010). In its topological phase, the nanowire hosts a pair of MZMs at its ends. Being zero energy modes of superconductors, MZMs are characterized by quasiparticle operators that are Hermitian, $\gamma_j = \gamma_j^\dagger$, and fulfill the Clifford algebra $\{\gamma_j, \gamma_k\} = 2\delta_{jk}$. In a superconductor, the fermion number is strongly fluctuating, and only the fermion parity $\mathcal{P} = \pm 1 = (-1)^N$, with N the total number of fermions, remains a good quantum number. In a one-dimensional topological superconductor, one can also define the fermion parity of a topological section as the product of the two Majorana end mode operators (Kitaev, 2001). As the total fermion parity in a closed system is conserved, a qubit can only be realized in a system having two topological segments and thus four Majorana zero modes $\gamma_1, \gamma_2, \gamma_3, \gamma_4$. Denoting the fermion parities of the segment between γ_1 and γ_2 (γ_3 and γ_4) by $\mathcal{P}_{12} = \mathrm{i}\gamma_1\gamma_2$

($\mathcal{P}_{34} = \mathrm{i}\gamma_3\gamma_4$), the ground-state manifold is spanned by the states $|11\rangle$, $|\bar{1}1\rangle$, $|1\bar{1}\rangle$, and $|\bar{1}\bar{1}\rangle$, with $\mathcal{P}_x|p_{12}p_{34}\rangle = p_x|p_{12}p_{34}\rangle$, $p_x = \pm 1$, $x \in \{12, 34\}$. The states $|11\rangle$, $|\bar{1}\bar{1}\rangle$ are characterized by an even number of fermions having the parity $\mathcal{P} = \mathcal{P}_{12}\mathcal{P}_{34} = 1$, whereas the states with an odd number of fermionic particles $|1\bar{1}\rangle, |1\bar{1}\rangle$ have parity $\mathcal{P} = -1$.[1)] Most importantly, keeping the total fermion parity fixed, the MZMs form a two-level system (Majorana qubit) with the two states $|p_{12}, \mathcal{P}p_{12}\rangle$ distinguished by $p_{12} = \pm 1$. The Pauli operators for the Majorana qubit are accordingly given by $\sigma_z = \mathcal{P}_{12} = \mathrm{i}\gamma_1\gamma_2$ and $\sigma_x = \mathrm{i}\gamma_2\gamma_3$ (Beenakker, 2013).

A single segment of a topological superconductor interrupted by a tunneling junction (a Majorana Josephson junction), such as that formed, for example, by a semiconducting nanowire bridging two superconductors, is a natural place to realize four MZMs; see Fig. 5.1. Two MZMs are situated at the ends of the nanowire, while two additional ones are formed on either side of the tunnel junction with the overlap tunable by the phase difference across the junction (Fu and Kane, 2008). A distinctive feature of such a Majorana Josephson junction is the ability to coherently transport single electrons (and not only Cooper pairs) between the two superconductors (Kitaev, 2001; Fu and Kane, 2009). Such an event changes the fermion parity on either side of the wire and thus acts like a σ_x on the Majorana qubit.

In the following, we consider the situation in which such a Majorana Josephson junction is embedded in a strip line resonator and coupled to its resonator modes via a dipole interaction Hamiltonian. Hence the system can be described by the total Hamiltonian

$$H = H_0 + H_c + H_{\mathrm{dip}}. \tag{5.1}$$

The first term $H_0 = \frac{1}{2}\hbar\delta_{\mathcal{P}}\sigma_z$ arises due to finite overlap amplitudes of the MZMs on each wire (Ohm and Hassler, 2014). This results in a small energy splitting $\hbar\delta_{\mathcal{P}}$ whose value in principle depends on the total fermion parity $\mathcal{P}$. The strip-line resonator with the resonance frequency ω_c is described by the Hamiltonian $H_c = \hbar\omega_c a^\dagger a$, with a the annihilation operators of the cavity mode fulfilling the canonical commutation relation $[a, a^\dagger] = 1$. Applying a voltage bias to the Majorana Josephson junction allows for single electron transfer that is accompanied by the emission/absorption of photons carrying the residual energy of the transition. The interaction of the Majorana Josephson junction with the electromagnetic environment is given by the dipole Hamiltonian (Ohm and Hassler, 2014)

$$H_{\mathrm{dip}} = -\boldsymbol{d}\cdot\boldsymbol{E} = -2\hbar g\cos\left[\frac{\varphi(t)}{2}\right](a + a^\dagger)\sigma_x; \tag{5.2}$$

here, $\varphi(t)$ is the superconducting phase difference across the junction, which is related to the voltage by $V = \hbar\dot{\varphi}/2e$. The voltage consists of two parts $V = V_0 + V_{\mathrm{ac}}$, with V_0 the dc voltage bias and a part due to the cavity field $V_{\mathrm{ac}} = V_{\mathrm{zp}}(a + a^\dagger)$, which determines the light-matter interaction constant $g \simeq eV_{\mathrm{zp}}/\hbar$. Here the strength of

[1)] We introduce the shorthand notation $\bar{1} = -1$.

the vacuum fluctuations, $V_{\rm zp} = (\hbar\omega_c/C)^{1/2}$, of the cavity is given by its total capacitance C to ground. The physical significance of σ_x is to implement the parity changes on either side, and $a^{(\dagger)}$ refers to the absorption (emission) of a photon. For the sake of implementing a qubit readout via microwave radiation, a superconducting transmission line is capacitively coupled to the cavity acting as a bus for the information to be read out; see Fig. 5.1.

5.2. Model

5.2.1. The dispersive interaction model

As explained below, the measurement setup will be active when the dc voltage has a value $V_0 \approx \hbar\omega_c/e$. Without the applied dc bias voltage, the superconducting phase difference φ is constant up to quantum fluctuations due to the oscillator. Thus in this case, the first factor in Eq. (5.2) is almost constant and the second term becomes ineffective as emission or absorption of a photon requires the energy $\hbar\omega_c$. Tuning the dc voltage close to the value $\hbar\omega_c/e$ leads to the superconducting phase difference of the form

$$\varphi(t) = \varphi_0 + \omega_{\rm J} t + \varphi_{\rm ac}, \tag{5.3}$$

where we have introduced the Josephson frequency $\omega_{\rm J} = 2eV_0/\hbar$ and the initial phase difference φ_0. The last term originates from the cavity mode and is given by $\varphi_{\rm ac} = (2eV_{\rm zp}/\hbar\omega_c)\,{\rm i}(a - a^\dagger)$ since $\varphi_{\rm ac}$ and $V_{\rm ac}$ are canonically conjugate variables.[2)] Its magnitude can be estimated as $\varphi_{\rm ac} \simeq n^{1/2}eV_{\rm zp}/\hbar\omega_c = (ne^2/\hbar\omega_c C)^{1/2}$, where n denotes the number of photons in the cavity. In the following, we assume that the capacity is large enough such that $\omega_c C \gg ne^2/\hbar$, which corresponds to weak coupling ($n^{1/2}g \ll \omega_c$).[3)] As a result, we can approximately set $\varphi(t) = \varphi_0 + \omega_{\rm J} t$. The combined dynamics of the Majorana qubit and the cavity is described by Hamiltonian (5.1), which is driven at half of the Josephson frequency due to the time-dependent superconducting phase in (5.3). By going to the interaction picture with respect to the Hamiltonian $H = \frac{1}{2}\hbar\omega_{\rm J} a^\dagger a$, the time evolution is determined by slowly varying variables $\tilde{a} = {\rm e}^{{\rm i}\omega_{\rm J} t/2} a$ corresponding to operators in a rotating frame. By neglecting off-resonant contributions, which appear as fast oscillating terms in the rotating frame, the Hamiltonian (5.1) maps to the time-independent quantum Rabi problem

$$H = \tfrac{1}{2}\hbar\delta_{\mathcal{P}}\sigma_z + \hbar\Omega\tilde{a}^\dagger\tilde{a} - \hbar g\sigma_x({\rm e}^{{\rm i}\varphi_0/2}\tilde{a} + {\rm e}^{-{\rm i}\varphi_0/2}\tilde{a}^\dagger), \tag{5.4}$$

where $\Omega = \omega_c - \omega_{\rm J}/2 \ll \omega_c$ is the detuned frequency in the rotating frame.[4)] In the following, we are interested in the regime of large detuning $\Omega \gg g, \delta_{\mathcal{P}}$ that is

[2)] The operator corresponding to the classical variable $\dot{\varphi}_{\rm ac}$ is given by $({\rm i}/\hbar)[H_c, \varphi_{\rm ac}] = 2eV_{\rm ac}/\hbar$ in the Schrödinger picture.

[3)] Later, we will see that we even need to require that $\sqrt{n}g \ll \Omega$.

[4)] Note that contrary to the conventional case (Gardiner and Zoller, 2004) due to the driving with a bias voltage the problem does not map to the Jaynes-Cummings problem in the rotating frame.

characterized by weak exchange of energy between the qubit and the cavity, therefore called the dispersive regime (Boissonneault *et al.*, 2009). In this case, perturbation theory in the small parameter g/Ω is a well-controlled approximation as long as the number of photons n in the cavity does not exceed the critical value Ω^2/g^2. Using the technique of Schrieffer-Wolff transformation, see below, we obtain the effective Hamiltonian

$$H = \hbar(\Omega + \chi\sigma_z)\,\tilde{a}^\dagger\tilde{a} + \frac{\hbar}{2}(\delta_{\mathcal{P}} + \chi)\sigma_z + \frac{\hbar\chi}{2}\sigma_z\big(\mathrm{e}^{\mathrm{i}\varphi_0}\tilde{a}^2 + \mathrm{e}^{-\mathrm{i}\varphi_0}\tilde{a}^{\dagger 2}\big) \tag{5.5}$$

up to second order in g/Ω. Due to virtual processes, the interaction shifts the cavity frequency and furthermore introduces the anomalous (quadrature squeezing) terms $\propto \tilde{a}^2, \tilde{a}^{\dagger 2}$ which arise due to counter-rotating terms of the transversal coupling (Zueco *et al.*, 2009). Note that the frequency shift as well as the squeezing amplitude are determined by the parameter $\chi = -2g^2\delta_{\mathcal{P}}/\Omega^2 \ll \Omega$. Most importantly, both effects depend on the qubit state σ_z. To simplify the notation, we introduce the shifted cavity frequency $\tilde{\Omega} = \Omega + \chi\sigma_z$ with a small shift compared to the bare frequency Ω. Therefore, the qubit state can be extracted by detecting the relative cavity shift $\pm\chi$ with respect to the undressed cavity frequency. For the case of homodyne detection, which we will discuss below, the measurement will be due to the first term of Eq. (5.5). On the contrary, for the intensity measurement, the last term will dominate.

5.2.2. Schrieffer-Wolff transformation

Before proceeding with the dispersive readout, we briefly sketch the Schrieffer-Wolff transformation that maps the quantum Rabi Hamiltonian (5.4) to the dispersive Hamiltonian (5.5). The quantum Rabi Hamiltonian (5.4) can be split into two parts: a free evolution $H_0 + H_c$ and coupling between the Majorana qubit and the cavity mode H_{dip}. For further convenience it is useful to introduce the auxiliary operators

$$I_\pm = \mathrm{e}^{\mathrm{i}\varphi_0/2}\sigma_+\tilde{a} \pm \mathrm{e}^{-\mathrm{i}\varphi_0/2}\sigma_-\tilde{a}^\dagger, \tag{5.6a}$$

$$J_\pm = \mathrm{e}^{\mathrm{i}\varphi_0/2}\sigma_+\tilde{a}^\dagger \pm \mathrm{e}^{-\mathrm{i}\varphi_0/2}\sigma_-\tilde{a} \tag{5.6b}$$

with $\sigma_\pm = \frac{1}{2}(\sigma_x \pm \mathrm{i}\sigma_y)$. In terms of these operators the coupling Hamiltonian reads

$$H_{\mathrm{dip}} = \hbar g(I_+ + J_+). \tag{5.7}$$

The technique of Schrieffer-Wolff transformation proceeds by translating the Hamiltonian H to a new frame of reference via a unitary transformation $\exp(\lambda\Theta)$ that depends upon the small parameter λ and the anti-Hermitian operator $\Theta = -\Theta^\dagger$. Relying on the assumption that λ is small, the transformed Hamiltonian can be expanded in powers of λ. By virtue of the Campbell-Baker-Hausdorff relation one finds the converted Hamiltonian

$$\exp(-\lambda\Theta)H\exp(\lambda\Theta) = H + \lambda[H,\Theta] + \frac{\lambda^2}{2}[\,[H,\Theta],\Theta] + \mathcal{O}(\lambda^3). \tag{5.8}$$

Determining the parameters of the transformation such that $\lambda[H,\Theta] = -H_{\mathrm{dip}}$, the contribution of the coupling Hamiltonian cancels to first order in λ. This can be achieved by choosing

$$\lambda = -\frac{g}{\Omega - \delta_{\mathcal{P}}}, \qquad \Theta = I_- - \left(\frac{\Omega - \delta_{\mathcal{P}}}{\Omega + \delta_{\mathcal{P}}}\right) J_-. \tag{5.9}$$

The residual second order effective Hamiltonian is then obtained by substituting (5.9) into (5.8) and making use the commutation relations

$$[I_+, I_-] = \left(\tilde{a}^\dagger \tilde{a} + \tilde{a}\,\tilde{a}^\dagger\right)\sigma_z + 1, \tag{5.10a}$$
$$[J_-, J_+] = \left(\tilde{a}^\dagger \tilde{a} + \tilde{a}\,\tilde{a}^\dagger\right)\sigma_z - 1, \tag{5.10b}$$
$$[J_+, I_-] = [J_-, I_+] = \left(\mathrm{e}^{-\mathrm{i}\varphi}\tilde{a}^{\dagger 2} + \mathrm{e}^{\mathrm{i}\varphi}\tilde{a}^2\right)\sigma_z, \tag{5.10c}$$
$$[(H_0 + H_c), I_\pm] = \hbar(\Omega - \delta_{\mathcal{P}})I_\pm, \tag{5.10d}$$
$$[(H_0 + H_c), J_\pm] = \hbar(\Omega + \delta_{\mathcal{P}})I_\mp. \tag{5.10e}$$

Since the cavity is tuned far off-resonant $\delta_{\mathcal{P}}/\Omega \ll 1$, the second order effective Hamiltonian can be expanded in the small parameter $\delta_{\mathcal{P}}/\Omega$ thereby arriving at the dispersive Hamiltonian (5.5).

5.3. Methods: Transmission line coupling

The measurement of the Majorana qubit is performed by observing the shift in the cavity frequency, cf. (5.5), by probing the cavity via the transmission line. We want to take into account that the detector is not ideal in the sense that it does not capture every photon. For that purpose, we couple the resonator to two independent waveguides ($j \in \{1,2\}$), with the idea that the photons in the waveguide with $j = 1$ are measured while the other photons are lost. The transmission lines are modeled by the Hamiltonian

$$H_{\mathrm{tl}} = \frac{1}{2\pi}\sum_j \int \hbar\omega b_j^\dagger(\omega) b_j(\omega)\,\mathrm{d}\omega \tag{5.11}$$

with operators $b_j^\dagger(\omega), b_j(\omega)$ creating and annihilating microwave photons at the frequency ω fulfilling the commutation relation $[b_j(\omega), b_k^\dagger(\omega')] = 2\pi\delta_{jk}\delta(\omega - \omega')$. The cavity field is coupled to the waveguides by the Hamiltonian

$$H_\kappa = \frac{\mathrm{i}\hbar}{2\pi}\sum_j \sqrt{\kappa_j}\int [a^\dagger b_j(\omega) - b_j^\dagger(\omega) a]\,\mathrm{d}\omega; \tag{5.12}$$

here, the coupling parameters $\kappa_j > 0$ denote the decay rate of the cavity photons in the j-th transmission line. In the following, we will introduce the efficiency $\eta = \kappa_1/(\kappa_1 + \kappa_2)$ of the detector which denotes the fraction of detected photons. Neglecting spin-flip errors induced by off-resonant interaction of the qubit with the

radiation,[5] the combined qubit-cavity Hamiltonian H commutes with σ_z rendering the measurement to be a quantum non-demolition measurement. In this case, the interaction of the resonator with the transmission lines can be described by the quantum Langevin equations[6]

$$\begin{aligned}\frac{\mathrm{d}\tilde{a}}{\mathrm{d}t} &= \frac{\mathrm{i}}{\hbar}[H + H_\kappa, \tilde{a}] - \frac{1}{2}\sum_j \kappa_j \tilde{a} \\ &= -\mathrm{i}\tilde{\Omega}\tilde{a} - \mathrm{i}\chi\sigma_z \mathrm{e}^{-\mathrm{i}\varphi_0}\tilde{a}^\dagger - \sum_j \Big[\sqrt{\kappa_j}\,\tilde{a}_{\mathrm{in},j} + \frac{1}{2}\kappa_j \tilde{a}\Big],\end{aligned} \tag{5.13}$$

where the input field, defined as

$$\tilde{a}_{\mathrm{in},j}(t) = \frac{1}{2\pi}\int \mathrm{e}^{-\mathrm{i}\nu t} b_j(\omega_\mathrm{J}/2 + \nu)\,\mathrm{d}\nu, \tag{5.14}$$

satisfies the commutation relation $[\tilde{a}_{\mathrm{in},j}(t), \tilde{a}^\dagger_{\mathrm{in},k}(t')] = \delta_{jk}\delta(t-t')$. The output field is then given by the boundary condition $\tilde{a}_{\mathrm{out},1}(t) = \tilde{a}_{\mathrm{in},1}(t) + \sqrt{\kappa_1}\tilde{a}(t)$ at the interface to the transmission line 1. The stochastic differential equations (5.13) can be solved for $\tilde{a}$ by going to frequency space with $\tilde{a}(\nu) = \int \mathrm{e}^{\mathrm{i}\nu t}\tilde{a}(t)\,\mathrm{d}t$. The solution is given by the linear relation

$$\tilde{a}_{\mathrm{out},1}(\nu) = \sum_j \Big[u_j(\nu)\tilde{a}_{\mathrm{in},j}(\nu) + v_j(\nu)\tilde{a}^\dagger_{\mathrm{in},j}(-\nu)\Big] \tag{5.15}$$

between the input and the output fields. In our case, the annihilation operator of the output field is a coherent superposition of annihilation as well as creation operators of the input field. This can be traced back to the anomalous terms in (5.5). All the relevant information about the scattering of microwaves is encoded into the functions

$$u_1(\nu) = \frac{(\frac{1}{2}\kappa_2 - \mathrm{i}\nu)^2 - (\frac{1}{2}\kappa_1 - \mathrm{i}\tilde{\Omega})^2 - \chi^2}{(\frac{1}{2}\kappa - i\nu)^2 + \tilde{\Omega}^2 - \chi^2}, \tag{5.16a}$$

$$v_1(\nu) = \frac{\mathrm{i}\kappa_1\chi\mathrm{e}^{-\mathrm{i}\varphi_0}}{(\frac{1}{2}\kappa - \mathrm{i}\nu)^2 + \tilde{\Omega}^2 - \chi^2}, \tag{5.16b}$$

$$u_2(\nu) = -\frac{\sqrt{\kappa_1\kappa_2}\left[\frac{1}{2}\kappa - \mathrm{i}(\nu + \tilde{\Omega})\right]}{(\frac{1}{2}\kappa - \mathrm{i}\nu)^2 + \tilde{\Omega}^2 - \chi^2}, \tag{5.16c}$$

$$v_2(\nu) = \frac{\mathrm{i}\sqrt{\kappa_1\kappa_2}\,\chi\mathrm{e}^{-\mathrm{i}\varphi_0}}{(\frac{1}{2}\kappa - \mathrm{i}\nu)^2 + \tilde{\Omega}^2 - \chi^2}, \tag{5.16d}$$

where $\kappa = \kappa_1 + \kappa_2$ is the total line width of the cavity. Note that they satisfy the identity $\sum_j(|u_j|^2 - |v_j|^2) = 1$ which translates the canonical commutation relation from $\tilde{a}_\mathrm{in}$ to $\tilde{a}_\mathrm{out}$.

[5] In the dispersive frame also spin-flip terms $\propto \sigma_+, \sigma_-$ are induced. These contributions can be regarded to be small as they only appear in first order of g/Ω.

[6] Cf. Sec. A.3.3 in App. A.

In the following, we will only consider the situation where the resonator is fed by a coherent state at frequency $\nu_{\rm in}$ with $\langle \tilde{a}_{\rm in,1}\rangle = {\rm e}^{-{\rm i}\nu_{\rm in}t}\alpha_{\rm in}$. For the second transmission line, we take the vacuum state as an input state that is valid in the low temperature limit at temperatures $k_{\rm B}T \ll \hbar\omega_c$. The radiation reflected back into the first transmission line, which will be subsequently measured, is characterized by its mean output signal

$$\langle \tilde{a}_{\rm out,1}(\nu)\rangle = u_1(\nu)\alpha_{\rm in}\delta(\nu-\nu_{\rm in}) + v_1(\nu)\alpha_{\rm in}^*\delta(\nu+\nu_{\rm in}) \tag{5.17}$$

as well as by the correlation functions

$$\begin{aligned} \langle\!\langle \tilde{a}^\dagger_{\rm out,1}(\nu)\tilde{a}_{\rm out,1}(\nu')\rangle\!\rangle &= 2\pi\,|v_1(\nu)|^2\,\delta(\nu-\nu'), \\ \langle\!\langle \tilde{a}_{\rm out,1}(\nu)\tilde{a}_{\rm out,1}(\nu')\rangle\!\rangle &= 2\pi\,u_1^*(\nu)v_1^*(-\nu)\,\delta(\nu+\nu'); \end{aligned} \tag{5.18}$$

here and below, the double brackets denote the (co-)variance defined as $\langle\!\langle AB\rangle\!\rangle = \langle AB\rangle - \langle A\rangle\langle B\rangle$. The squeezing term of Eq. (5.5) leads to the fact that both correlators in (5.18) are nonzero.

5.4. Majorana qubit readout

The qubit readout proceeds via the measurement of the ac voltage component $\propto a_{\rm out,1}$ that is reflected back from the cavity into the transmission line 1. As the ac voltage component oscillates at microwave frequencies, the signal frequency needs to be downconverted, which can be achieved by means of a homodyne measurement technique as well as by measuring the intensity which is the squared modulus of the voltage. Both schemes will be discussed in the following. To keep the discussion simple, we will discuss only the case in which the frequency of the input signal is given by $\nu_{\rm in} = \Omega + \chi$, i.e, it is on resonance with the cavity given that the qubit is in the state $\sigma_z = 1$.

5.4.1. Homodyne detection

The standard homodyne measurement[7)] technique converts high-frequency signals down to a zero frequency signal by mixing the voltage to be measured, $V_{\rm out} = V_{\rm zp}(a_{\rm out,1} + a^\dagger_{\rm out,1})$, with a local oscillator, $V_{\rm lo} = V_{\rm zp}\,{\rm Re}(\alpha_{\rm lo}{\rm e}^{-{\rm i}\omega_{\rm J}t/2-{\rm i}\nu_{\rm in}t})$, where both voltages oscillate at the same frequency $\omega_{\rm J}/2+\nu_{\rm in}$; see Fig. 5.2. The mixer outputs the intensity $I_{\rm hd} = (V_{\rm lo}+V_{\rm out})^2$, which can be subsequently measured at the voltmeter. We assume that due to the attenuator, the amplitude of the local oscillator is much larger than the output of the cavity, $|\alpha_{\rm lo}| \gg |\alpha_{\rm in}|$. In this case, the leading contribution to $I_{\rm hd}$ is the mixed term $2V_{\rm lo}V_{\rm out}$ as the product $V_{\rm lo}^2$ carries no information about the qubit state. For the measurement of the qubit state $\sigma_z = \pm 1$, it is thus necessary to distinguish the intensities $I_{\rm hd}|_{\sigma_z=\pm1}$ corresponding to the fact

[7)] See also Sec. A.3.4 in App. A.

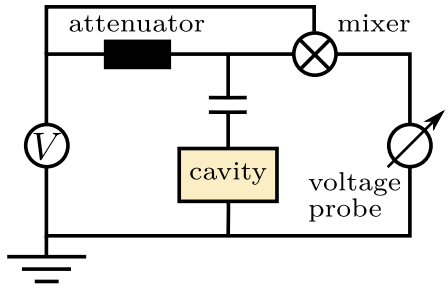

Fig. 5.2.: Electric circuit for implementing the homodyne readout: The gray box symbolizes the microwave cavity of Fig. 5.1. The cavity is coupled via the capacitance C to the microwave signal generated by the voltage source and subsequently attenuated (black box). The output signal of the resonator is then mixed with the input signal to down-convert the frequency and in the end the dc component is measured. It is important that while the input signal is attenuated the local oscillator strength remains unsuppressed therefore dominantly contributing to the output of the mixer.

that the qubit is in one of the two states. Introducing the difference of the intensities $\delta I_{\mathrm{hd}} = I_{\mathrm{hd}}|_{\sigma_z=1} - I_{\mathrm{hd}}|_{\sigma_z=\bar{1}}$ as our signal strength, we derive the result

$$|\delta I_{\mathrm{hd}}| \simeq \eta|\alpha_{\mathrm{in}}||\alpha_{\mathrm{lo}}| \left|\frac{\chi}{\Omega}\right| \left|16\frac{\Omega}{\kappa}\sin(\varphi_{\mathrm{lo}}-\varphi_{\mathrm{in}}) + \sqrt{\frac{\omega_{\mathrm{J}}}{\omega_c-1}}\left[\frac{\kappa}{\Omega}\sin(\varphi_{\mathrm{lo}}-\varphi_{\mathrm{in}}+\varphi_0) - 4\cos(\varphi_{\mathrm{lo}}-\varphi_{\mathrm{in}}+\varphi_0)\right]\right| \tag{5.19}$$

$$\lesssim \eta|\alpha_{\mathrm{in}}||\alpha_{\mathrm{lo}}| \left|\frac{\chi}{\kappa}\right| \tag{5.20}$$

valid to first order in $\chi/\Omega \ll 1$. Note that the intensities, as is typical for homodyne detection, are dependent on the phase $\varphi_{\mathrm{in/lo}}$ of the corresponding signals with $\alpha_{\mathrm{in/lo}} = |\alpha_{\mathrm{in/lo}}|\mathrm{e}^{\mathrm{i}\varphi_{\mathrm{in/lo}}}$. In going from (5.19) to (5.20), we have optimized the phase φ_{lo} so as to have the maximum signal. To remain in the dispersive limit taking the cavity broadening κ into account, we have to require that $\kappa/\Omega \ll 1$ such that the first term of (5.19) that originates from the first term in Eq. (5.5) is dominating and thus gives in the optimal case $\varphi_{\mathrm{lo}} - \varphi_{\mathrm{in}} = \frac{\pi}{2}$.

In order to determine the measurement time T, we have to compare the magnitude of the signal $S_{\mathrm{hd}} = \delta I_{\mathrm{hd}}\, T$ to the noise

$$N_{\mathrm{hd}}^2 = \int_0^T\int_0^T \langle\!\langle I_{\mathrm{hd}}(t')I_{\mathrm{hd}}(t)\rangle\!\rangle \,\mathrm{d}t\,\mathrm{d}t' \simeq T|\alpha_{\mathrm{lo}}|^2; \tag{5.21}$$

here, we have used the fact that $|\alpha_{\mathrm{lo}}| \gg |\alpha_{\mathrm{in}}|$ such that the noise is dominated by the local oscillator. The minimal measurement time T_0 is given by a signal-to-noise ratio $S_{\mathrm{hd}}/N_{\mathrm{hd}} = 1$. Employing Eqs. (5.20) and (5.21), we obtain

$$T_{0,\mathrm{hd}} \simeq \frac{\kappa^2}{\eta^2|\alpha_{\mathrm{in}}|^2\chi^2}. \tag{5.22}$$

Note that the measurement time is inversely proportional to the number of photons $|\alpha_{\rm in}|^2$ which are sent in per unit of time. This is a common behavior for measurement setups at low temperatures that are limited by shot noise. The factor χ/κ which enters quadratically is there due to the fact that we have to distinguish the qubit induced frequency shift χ relative to the spectral broadening κ of the cavity. In order to determine the minimal measurement time, we have to remember that the number of photons in the cavity has to be smaller than the critical value Ω^2/g^2 in order for the Schrieffer-Wolff approximation to be applicable. This translates to the bound $|\alpha_{\rm in}|^2 \lesssim \Omega^2\kappa/\eta g^2$ on the input field strength and thus to

$$T_{0,\rm hd} \gtrsim \frac{\kappa g^2}{\eta\Omega^2\chi^2} \simeq \frac{\kappa}{\eta\delta_{\mathcal{P}}\chi}. \tag{5.23}$$

As we did not assume any relation between κ and χ, the measurement time can be made arbitrarily small by decreasing κ/χ.

5.4.2. Intensity measurement

Another route to achieve down-conversion is to mix the signal with itself, i.e., to measure the intensity $I_{\rm int} = V_{\rm out}^2$. Calculating the difference of intensities between the two qubit states yields

$$|\delta I_{\rm int}| \simeq \eta|\alpha_{\rm in}|^2 \frac{|\kappa_1-\kappa_2|}{\kappa}\left|\frac{\chi}{\Omega}\right| \times \left|\frac{\kappa}{\Omega}\sin(\varphi_0+2\varphi_{\rm in}) - 4\cos(\varphi_0+2\varphi_{\rm in})\right| \tag{5.24}$$

$$\lesssim \eta|\alpha_{\rm in}|^2 \frac{|\kappa_1-\kappa_2|}{\kappa}\left|\frac{\chi}{\Omega}\right| \tag{5.25}$$

to first nonvanishing order in χ/Ω. In going from (5.24) to (5.25), we have again chosen the optimal value of the phases of the incoming signal which is $\varphi_{\rm in} = \frac{\pi}{4} - \frac{1}{2}\varphi_0$ in the relevant limit $\kappa \ll \Omega$.

Surprisingly, the first term in $\delta I_{\rm int}$ appears in first order in χ/Ω and not only to second order, as one would generically expect. The reason for this can be traced back to the fact that the term is due to the squeezing term in (5.5), which makes the intensity measurement phase-sensitive by acting as a parametric amplifier operated below the threshold; cf. Ch. 4. In this way, in our setup the intensity measurement itself is phase sensitive and not only the homodyne detection. To zeroth order in χ/Ω, the noise is given by

$$N_{\rm int}^2 \simeq T|\,\alpha_{\rm in}|^2|u_1(\nu_{\rm in})|^2 \simeq T|\,\alpha_{\rm in}|^2\frac{(\kappa_1-\kappa_2)^2}{\kappa^2}. \tag{5.26}$$

Comparing the noise to the signal leads to the expression

$$T_{0,\rm int} \simeq \frac{\Omega^2}{\eta^2|\alpha_{\rm in}|^2\chi^2} \gtrsim \frac{g^2}{\eta\kappa\chi^2} \simeq \frac{\Omega^2}{\kappa^2}T_{0,\rm hd} \tag{5.27}$$

for the minimal time of measurement. Even though the intensity measurement in our case is better than in a typical situation without parametric driving, comparing

it to the homodyne detection, we conclude that due to the additional (large) factor Ω^2/κ^2 the homodyne detection scheme is always more efficient.

5.4.3. Decoherence

As long as the external bias voltage is switched off, there is no coupling to the electromagnetic field, but nevertheless the Majorana qubit as an open quantum system may suffer from uncontrollable interaction with its environment. Due to a finite overlap of MZMs on the nanowire, the qubit may be affected by dephasing errors $\propto \delta_{\mathcal{P}}\sigma_z$ as well as by external tunneling of quasiparticles onto the junction (Rainis and Loss, 2012). The latter process is also called quasiparticle poisoning (QP). An erroneous interaction $\propto \sigma_z$ results in dephasing of the qubit with an intrinsic dephasing rate $\Gamma_\delta \simeq \delta_{\mathcal{P}}^{-1}$, whereas the dephasing caused by QP arises due to global parity switches (Budich *et al.*, 2012). QP of the MZM can also be generated by driving-induced transitions to the quasiparticle continuum above the gap (Houzet *et al.*, 2013). We assume this mechanism to be negligible here as the transparency of the Josephson junction is considered to be relatively small. Other sources of decoherence such as nonequilibrium fluctuations of the nanowire's chemical potential (Konschelle and Hassler, 2013) or thermal effects (Cheng *et al.*, 2012; Schmidt *et al.*, 2012), may also be included, but here we want to focus only on QP and effects due to finite splitting.

We wish to describe QP by a simple model where each of the mid gap states $|p_{12}p_{34}\rangle$ can be changed to an arbitrary state in the opposite parity sector via quasiparticle tunneling processes. For simplicity, it is assumed that all these processes happen with the same rate Γ_{QP}. The density matrix fulfills the Lindblad equation

$$\frac{\mathrm{d}\rho}{\mathrm{d}t} = -\frac{\mathrm{i}}{\hbar}[H,\rho] + \sum_{i=0}^{8}\Gamma_i\left(J_i\rho J_i^\dagger - \frac{1}{2}\{J_i^\dagger J_i,\rho\}\right) \tag{5.28}$$

with jump operators J_i implementing dephasing due to finite energy splitting of MZMs ($i=0$) and QP-induced jump processes $i\in\{1,\dots,8\}$. In particular, we have for the intrinsic dephasing $\Gamma_0=\Gamma_\delta$, $J_0=\sigma_z$. The QP is modeled by $\Gamma_i=\Gamma_{\text{QP}}, i\geq 1$ with the jump operators J_i given by the eight possibilities to change the parity, e.g., $J_1=|11\rangle\langle\bar{1}1|,\dots$, see Ch. 4.

In equation (5.28), the diagonal elements decouple, which results in an exponential decay of the qubits expectation value

$$\sigma_z(t) = \mathrm{Tr}[\sigma_z\rho(t)] = e^{-2\Gamma_{\text{QP}}t}\sigma_z(0), \tag{5.29}$$

with $\sigma_z(0)$ denoting the expectation value of σ_z at time $t=0$. The dephasing time can be inferred from the correlation function $\langle\sigma_+(\tau)\sigma_-(0)\rangle$, which, neglecting fast

oscillating terms as well as sub-leading terms of the order χ/Ω, evaluates to

$$\begin{aligned}\langle\sigma_+(t)\sigma_-(0)\rangle &= \left\langle \exp\left[-2\mathrm{i}\int_0^t \varepsilon(t')\mathrm{d}t' - \Gamma_{\mathrm{QP}}t - \Gamma_\delta t\right]\right\rangle \\ &= \exp\left[-2\mathrm{i}\langle\varepsilon\rangle t - \Gamma_\phi t\right]. \end{aligned} \tag{5.30}$$

The dephasing rate

$$\Gamma_\phi = \Gamma + \frac{8\eta\chi^2|\alpha_{\mathrm{in}}|^2}{\pi\kappa^2} \tag{5.31}$$

consists of two parts. The first part given by $\Gamma = \Gamma_{\mathrm{QP}} + \Gamma_\delta$ is dephasing due to the Lindblad equation. The second source of decoherence is the fluctuation of the instantaneous qubit frequency $\varepsilon(t) \approx \frac{1}{2}\delta_{\mathcal{P}} + \chi\left[\langle\tilde{a}^\dagger(t)\tilde{a}(t)\rangle + \frac{1}{2}\right]$ around its mean frequency $\langle\varepsilon\rangle = \frac{1}{2}\delta_{\mathcal{P}} + \chi(\eta|\alpha_{\mathrm{in}}|^2/\kappa + \frac{1}{2})$ due to the fact that the number of photons in the cavity $\langle\tilde{a}^\dagger(t)\tilde{a}(t)\rangle$ changes in time. A necessary requirement for a good readout is that the dephasing time is dominated by the measurement setup which means that

$$\Gamma \ll \frac{\eta\chi^2|\alpha_{\mathrm{in}}|^2}{\kappa^2} \simeq \eta^{-1}T_{0,\mathrm{hd}}^{-1} \lesssim \frac{\Omega^2\chi^2}{\kappa g^2}. \tag{5.32}$$

In order to reach the quantum limit for the homodyne detection, the $\lesssim$ signs in (5.32) have to be equalities and $\eta = 1$ such that $\Gamma_\phi = T_{0,\mathrm{hd}}^{-1}$ and thus all dephasing is due to the measurement. Note that in the case of intensity measurement, the quantum limit cannot be achieved as $T_{0,\mathrm{int}}^{-1} \gg T_{0,\mathrm{hd}}^{-1}$.

To see the limit of the homodyne detection, it is interesting to discuss the ideal situation without QP, $\Gamma_{\mathrm{QP}} = 0$, such that only intrinsic dephasing mechanisms are present. In this case, the necessary condition Eq. (5.32) for quantum-limited measurement implies that $\Gamma_\delta \ll \Omega^2\chi^2/\kappa g^2$ which can be simplified to $\chi/\kappa \gg 1$. Thus, in order to be able to reach the quantum limit, we need the immediately evident result that the shift of the cavity due to the qubit state has to be much larger than the cavity broadening. In this parameter range, every photon carries a sufficient amount of information, which allows for a quantum-limited measurement.

5.5. Conclusions

In this chapter we have demonstrated how the embedding of a semiconducting nanowire bridging two superconductors in a microwave cavity can be utilized for the measurement of the Majorana qubit due to the four MZMs at the ends and the interface. The measurement proceeds by probing the transmission lines capacitively coupled to the cavity. In the dispersive regime of large qubit cavity detuning, the system implements a quantum non-demolition measurement. It has been shown that the dispersive frequency shift can be either detected by a homodyne or alternatively

by an intensity measurement. Although the intensity measurement contains an unusually large amount of coherence, it turns out not to be sufficient in order to compete with the dephasing time of the qubit. In contrast, with the homodyne measurement technique one is even able to push the measurement time towards the quantum limit. Thus, the microwave homodyne readout of the Majorana qubit promises to be a new scheme having the main advantages of providing a mechanism directly coupling microwave radiation to the topological qubit. Furthermore, the readout process can be turned on and off at will by simply changing the dc bias voltage.

Chapter 6

Entangling distant transmon qubits by a single photon

The results of this chapter have been submitted for publication. The content of this chapter is available on:

> Ohm, C. and Hassler, F., 2015: *Measurement-induced entanglement of two transmon qubits by a single photon*: arXiv:1508.05104.

Quantum entanglement is a resource for quantum information theory with lots of applications. In order to use its full potential for quantum computation, reliable protocols for the production of entanglement are required. Typically, entanglement protocols are making use of local interactions between the qubits to be entangled. For the purpose of quantum communication, however, entanglement generation is more challenging as the two conversational partners are spatially separated from each other. A convenient method to overcome this problem is the use of *measurement-induced entanglement*.

6.1. Measurement-induced entanglement in cQED

The pioneering works of Yurke and Stoler (1992a,b) and Żukowski *et al.* (1993) have shown that entanglement can not only be transferred via direct interactions, but also by performing a measurement such that the wave function is projected onto an entangled state. This method, known as entanglement swapping, is based on the indistinguishability of the quantum states compatible with the measurement outcome and constitutes one of the key ingredients used for quantum repeaters (Briegel *et al.*, 1998). Moreover, the genesis of entanglement by performing a measurement has been first proposed for atoms in a quantum optical framework (Cabrillo *et al.*, 1999; Plenio *et al.*, 1999). Since then, measurement-induced entanglement of remote quantum systems has been experimentally demonstrated for diverse atomic setups (Chou *et al.*, 2005; Moehring *et al.*, 2007; Hofmann *et al.*, 2012) as well as for solid state qubit devices such as nitrogen vacancy centers (Bernien *et al.*, 2013) and superconducting qubits (Roch *et al.*, 2014).

To our knowledge, none of these schemes is capable of generating on-demand entanglement in a fast and secure fashion with single-shot efficiency as desired for

quantum communication protocols. The main obstacle is that the light-matter interaction is weak in the range of optical frequencies. To overcome this problem most quantum optical entangling-schemes exploit the photon polarization degree of freedom, whereas other proposals suggest to use more challenging concepts such as NOON-states (Huang and Moore, 2008). Furthermore, since the emission of optical photons is an undirected process, all these settings suffer from a low photon collection efficiency.

In contrast, in circuit quantum electrodynamics (cQED), which deals with superconducting qubits and their interaction to microwave radiation, it has been possible to reach the strong coupling regime in which the light-matter coupling is stronger than typically induced dissipation scales (Wallraff *et al.*, 2004). Even though microwave photons are typically unpolarized, present cQED-implementations accomplished measurement-induced entanglement of superconducting qubits with sufficient efficiency via coherent states, either with the qubits placed inside a single cavity (Riste *et al.*, 2013) or in separate resonators (Roch *et al.*, 2014). Due to the lack of erasure of the which-path information, these protocols only offer a maximal efficiency of 50%. More recently, it has been understood that employing additionally a nonlinear element maximum efficiency is achievable (Roy *et al.*, 2015; Silveri *et al.*, 2015). The quantum mechanical state projection is caused in all these cases by a weak continuous measurement (Hutchison *et al.*, 2009; Lalumière *et al.*, 2010). Because of that, entanglement emerges only rather slowly with the wave function gradually collapsing in time. Furthermore, the usage of semi-classical radiation, involving signals with many photons, allows for the generation of multi-partite entanglement (Helmer and Marquardt, 2009; Bishop *et al.*, 2009). In turn, the possibility of such multipartite entanglement bears the risk of eavesdropping and therefore renders the Ekert protocol for quantum key distribution insecure (Ekert, 1991).

Here, we propose a novel scheme for entangling superconducting transmon qubits over a distance by using a strong projective measurement of a single microwave photon. The photon propagates through a Mach-Zehnder interferometer (MZI) containing two transmon qubits to be entangled. Relying on the discreteness of photonic Fock states as well as the ability of cQED to access the strong coupling regime, our scheme prohibits eavesdropping during the entanglement generation as required for a secure key distribution. Within the last decade, cQED has become a mature field of quantum engineering technology promising integrated and scalable circuits suitable for quantum computation. In particular, the generation of single microwave photons in superconducting circuits (Houck *et al.*, 2007) and moreover the controlled creation of entanglement between microwave photons and transmon qubits has been reported (Eichler *et al.*, 2012). These promising attempts towards well-controlled microwave photonics encouraged us to suggest an entanglement protocol taking advantage of the high efficiencies in cQED combined with single-shot (projective) measurements.

In the following we will first explain the generation of entanglement by introducing the interferometric apparatus and discuss the procedure under ideal conditions.

Subsequently, a more general analysis clarifys the conditions under which maximal entanglement is achieveable. Specifically, we will discuss the case of entanglement generated by a Lorentzian-shaped single-photon wave packet as well as the entanglement in case of non-identical cavities.

6.2. Deterministic Entanglement by a Mach-Zehnder interferometer

Suppose a single photon traverses the MZI setup as depicted in Fig. 6.1. At the first beamsplitter, an incoming photon is split into two partial waves $|\psi_{\mathrm{ph}}\rangle = (|1_{\mathrm{A}}, 0_{\mathrm{B}}\rangle + |0_{\mathrm{A}}, 1_{\mathrm{B}}\rangle)/\sqrt{2}$, each traversing one arm (A or B) of the interferometer. After having passed the second beamsplitter, the partial waves are recombined and the photon escaped into one of the two output channels C and D, see Fig. 6.1. If both partial waves acquire a relative phase difference of $\varphi = 0$ while passing the MZI, i.e., if both partial waves accumulate exactly the same phase in both arms A and B, the photon is transmitted into channel C with certainty. On the other hand, if the partial waves accumulate a relative phase difference of $\varphi = \pi$, the photon is transmitted into mode D. Due to this single-photon interference effect, the MZI distinguishes between certain qubit states: by placing two dispersively interacting transmon qubits A and B in each arm of the interferometer as shown in Fig. 6.1, each partial wave picks up an individual phase due to scattering from these distinct qubits. If the qubits are initialized in a state spanned by the subspace $|\uparrow_{\mathrm{A}}, \uparrow_{\mathrm{B}}\rangle$, $|\downarrow_{\mathrm{A}}, \downarrow_{\mathrm{B}}\rangle$, the scattering phases on are identical in both arms and the photon is transmitted into channel C. If on the other hand, the qubits are in a state spanned by $|\uparrow_{\mathrm{A}}, \downarrow_{\mathrm{B}}\rangle$, $|\downarrow_{\mathrm{A}}, \uparrow_{\mathrm{B}}\rangle$ and if the scattering induces a relative phase difference of $\varphi = \pi$, then the photon is transmitted only into channel D. Hence, the interference of the partial waves allows for a parity-selective transmission of the photon through the MZI, discriminating the states $|\uparrow_{\mathrm{A}}, \uparrow_{\mathrm{B}}\rangle$, $|\downarrow_{\mathrm{A}}, \downarrow_{\mathrm{B}}\rangle$ with even parity from the states $|\uparrow_{\mathrm{A}}, \downarrow_{\mathrm{B}}\rangle$, $|\downarrow_{\mathrm{A}}, \uparrow_{\mathrm{B}}\rangle$ with odd parity. As a consequence of this parity-selective single-photon interference, the MZI can be used to measure the qubit parity $P = \sigma_{z,\mathrm{A}}\sigma_{z,\mathrm{B}}$. Once the photon is registered in one of the detectors C or D, the wave function collapses onto a state with definite parity, $P = 1$ (even parity) or $P = -1$ (odd parity). Furthermore, such a parity measurement is useful for entanglement preparation like other solid-state implementations suggest (Ruskov and Korotkov, 2003; Beenakker *et al.*, 2004; Trauzettel *et al.*, 2006; Williams and Jordan, 2008; Haack *et al.*, 2010), but here entanglement is accomplished with single-shot efficiency. The protocol proceeds as follows: we initialize the qubits in the superposition

$$|+_j\rangle = \frac{1}{\sqrt{2}}(|\uparrow_j\rangle + |\downarrow_j\rangle) \tag{6.1}$$

for each qubit $j = \mathrm{A}, \mathrm{B}$. This state is—among other possibilities—a suitable choice and due to the dispersive interaction $\propto \sigma_{z,j} a_j^\dagger a_j$ each partial wave of the photon

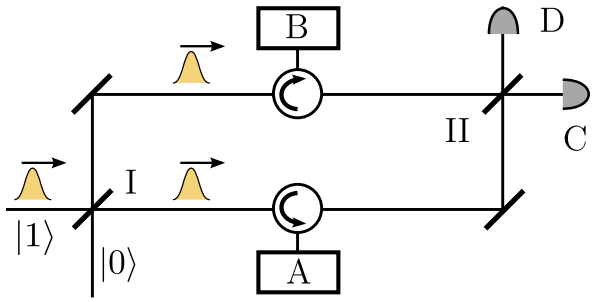

Fig. 6.1.: Mach-Zehnder interferometer made of two 50:50 beamsplitters (I and II). Each arm of the interferometer is coupled to a microwave resonator (A and B) which in turn is dispersively coupled to a transmon qubit. A single-photon wave packet that is send into the MZI causes a click in one of the two detectors at the outputs. The projective measurement due to the photon counters implements a party measurement on the transmon qubits. As a result, irrespective of which photon detector (C or D) clicks, the wave function is projected on a maximally entangled two-qubit state.

introduces state-dependent scattering phases $\varphi_\uparrow$ and $\varphi_\downarrow$ to the qubit: within each arm the state is mapped to

$$\frac{1}{\sqrt{2}}(|\uparrow_j\rangle + |\downarrow_j\rangle) \mapsto \frac{1}{\sqrt{2}}(\mathrm{e}^{\mathrm{i}\varphi_\uparrow}\,|\uparrow_j\rangle + \mathrm{e}^{\mathrm{i}\varphi_\downarrow}\,|\downarrow_j\rangle). \tag{6.2}$$

Crucially, we demand the phase difference to be $\varphi_\downarrow - \varphi_\uparrow = \pi$ in order to make the MZI parity-discriminating. Note that such a large difference between the scattering phases can only be implemented within the strong coupling regime. After the photon is reflected off the cavities, it carries information about the qubit state as well as about the path it has taken. As this makes the states distinguishable we use the second beamsplitter (II) to erase the which-path information of the photon. In terms of the output Fock modes C and D the resulting state reads

$$\frac{1}{\sqrt{2}}\big(\,|\Phi^-\rangle\,|1_\mathrm{C}, 0_\mathrm{D}\rangle + |\Psi^-\rangle\,|0_\mathrm{C}, 1_\mathrm{D}\rangle\,\big).$$

Recasting the final state in terms of the Bell states

$$|\Phi^-\rangle = \frac{1}{\sqrt{2}}\,(|\uparrow_\mathrm{A}, \uparrow_\mathrm{B}\rangle - |\downarrow_\mathrm{A}, \downarrow_\mathrm{B}\rangle) \qquad \text{with } P = 1, \tag{6.3a}$$

$$|\Psi^-\rangle = \frac{1}{\sqrt{2}}\,(|\uparrow_\mathrm{A}, \downarrow_\mathrm{B}\rangle - |\downarrow_\mathrm{A}, \uparrow_\mathrm{B}\rangle) \qquad \text{with } P = -1, \tag{6.3b}$$

reveals the parity-selectivity of the MZI and shows furthermore that, due to the missing which-path information, the parity measurement is not able to distinguish in which arm the photon has scattered. Hence, the state projection leaves the qubits in an entangled state no matter in which detector the photon is registered. Taking the measurement outcome as starting point, every other entangled two-qubit state can be prepared by means of single qubit gates. In this sense, the protocol accomplishes deterministic entanglement with single-shot efficiency.

6.3. Model

In the following, we will look at this scheme on a more formal level that allows to discuss imperfections. The crucial part of the photon propagation is the scattering process with the cavities and the qubits inside of these. In order to describe the cavity-qubit subsystems, we assume for simplicity that each qubit j is coupled to a single cavity mode with frequency ω_c. The qubit states are separated by an energy splitting $\hbar\Delta$ which is considered to be far detuned from the resonance frequencies of the cavities, $\omega_c \gg \Delta$. In this regime, the light-matter coupling gives rise to a qubit-state dependent renormalization of the cavity frequency—the dispersive shift $\chi\sigma_{z,j}$. Accordingly, each cavity-qubit subsystem is then described by the Hamiltonian

$$H_j = \hbar\omega_c a_j^\dagger a_j + \frac{\hbar\Delta}{2}\sigma_{z,j} + \hbar\chi\sigma_{z,j}a_j^\dagger a_j, \tag{6.4}$$

where $a_j, a_j^\dagger$ are creation and annihilation operators of the cavity modes obeying the canonical commutation relations $\left[a_j, a_l^\dagger\right] = \delta_{jl}$. A photon $b_{\mathrm{in},j}(k)$, incident to arm j of the MZI with wave number $k > 0$ and frequency $\omega_k = c|k|$, induces a qubit-state dependent phase shift after being scattered off the cavity. This process is completely characterized by the reflection coefficient

$$r(\omega_k; \sigma_{z,j}) = \frac{\mathrm{i}(\omega_c + \chi\sigma_{z,j} - \omega_k) - \kappa/2}{\mathrm{i}(\omega_c + \chi\sigma_{z,j} - \omega_k) + \kappa/2} \tag{6.5}$$

which relates incoming and outgoing modes of the MZI by $b_{\mathrm{out},j} = r_j(\omega_k; \sigma_{z,j})b_{\mathrm{in},j}$ (Walls and Milburn, 2008). In (6.5), κ denotes the spectral broadening of the cavities. Due to the occurrence of the $\sigma_{z,j}$ terms, the qubit states $|\uparrow_j\rangle$ and $|\downarrow_j\rangle$ accumulate the relative phase difference $\varphi = \arg[r(\omega_k; \sigma_z = 1)] - \arg[r(\omega_k; \sigma_z = -1)]$ while the photon passes the interferometer. To achieve maximal entanglement between the qubits, it is crucial to generate a relative π phase shift, i.e., we would like to adjust the parameters of the device such that

$$\pi = \arg\left[r(\omega_k; \sigma_{z,j} = 1)\right] - \arg\left[r(\omega_k; \sigma_{z,j} = -1)\right] \tag{6.6}$$

for both qubits A and B. Condition (6.6) can be fulfilled by tuning the photon frequency to be

$$\Omega = \omega_c \pm \frac{1}{2}\sqrt{4\chi^2 - \kappa^2}. \tag{6.7}$$

Note that these frequency sweet spots do only exist in the strong coupling regime where $2\chi \geq \kappa$. For convenience we will only consider one solution in (6.7) and omit the other one; this particular choice will be of no importance for the following analysis as long as we consistently stick to it. Recombining the two arms of the interferometer, the second beamsplitter acts as linear transformation upon the outgoing modes A, B and defines the output modes C, D via

$$\begin{pmatrix} c_{\mathrm{out}} \\ d_{\mathrm{out}} \end{pmatrix} = \frac{1}{\sqrt{2}}\begin{pmatrix} 1 & \mathrm{e}^{\mathrm{i}\theta} \\ -1 & \mathrm{e}^{\mathrm{i}\theta} \end{pmatrix}\begin{pmatrix} b_{\mathrm{out,A}} \\ b_{\mathrm{out,B}} \end{pmatrix}. \tag{6.8}$$

The phase shift $\theta = k(\ell_B - \ell_A)$ keeps track of to the individual path lengths ℓ_j the photon has to take in each arm of the interferometer. As we will see later, this parameter turns out to be useful to prevent disturbing interferences that negatively affect the degree of entanglement. Finally, after passing II, the photon is absorbed by one of the detectors C and D thereby projecting the transmon qubits onto an entangled state.

6.4. Detailed analysis

Several erroneous mechanisms may spoil the production of full entanglement and lead to limitations of our scheme: the shape of the photon wave packet, the fine tuning of cavity parameters, dissipative photon propagation due to leaky cavities or imperfect circulators, and efficiency of microwave photon counters. In the following the effect of all these mechanisms will be discussed, but since only the first two points are inherent to the entanglement protocol, the discussion will be focused primarily on the intrinsic aspects. Therefore the latter points, arising because of (extrinsic) technological limitations, are discussed first.

6.4.1. Technological challenges

If the circuit elements or the circulators are leaky, there is a finite probability for the photon to transmit into unwanted channels. For instance, by considering a two-sided cavity with loss coefficients κ_1 and κ_2 on each side of the cavity, the reflection coefficient assumes the modified form

$$r(\omega_k;\sigma_z) = \frac{\mathrm{i}(\omega_c + \chi\sigma_z - \omega) - (\kappa_1 - \kappa_2)/2}{\mathrm{i}(\omega_c + \chi\sigma_z - \omega) + (\kappa_2 + \kappa_1)/2};$$

a similar expression holds for the reflection coefficient on the other side of the cavity. Clearly, leakage of the photon into unwanted channels, present for $\kappa_2 \neq 0$, causes the reflection amplitude to have modulus less than one $|r(\omega_k;\sigma_z)|^2 < 1$. This lowers the photon count efficiency as well as the entanglement of the obtained state.

The most serious experimental problem is the detection of single microwave photons. Although there are several theoretical and experimental advancements towards working microwave photon detectors (Romero *et al.*, 2009; da Silva *et al.*, 2010; Govia *et al.*, 2012; Bozyigit *et al.*, 2011; Chen *et al.*, 2011), it remains a challenging task to build microwave photon counters working with single shot efficiency. However, given the rapid progress in the field of cQED in the last decade, we are confident that the technological challenges will be addressed in the near future.

6.4.2. Fidelities in non-ideal setups

For a non-ideal setup, the photon measurement yields—depending on the outcome—projected states $|\Psi^m\rangle$ and $|\Phi^m\rangle$ that generally deviate from a Bell state. In order to

quantify the degree of entanglement, we determine the fidelity of the outcome after the measurement and the wanted Bell state; the fidelity is a measure of distance between states in Hilbert space and is defined as $F[\psi,\phi] = |\langle\psi|\phi\rangle|^2$ for two arbitrary pure states $|\psi\rangle$ and $|\phi\rangle$, see Nielsen and Chuang (2010). Specifically, we are interested in the fidelities $F[\Phi^{\mathrm{m}}, \Phi^-]$ or $F[\Psi^{\mathrm{m}}, \Psi^-]$, depending on the measurement outcome. If these quantities take the value one, the projected state is the sought-after Bell state. In the following we study how intrinsic errors affect the entanglement production.

Generally, a single traveling photon is emitted as a wave packet, i.e., a superposition of various frequencies. This, however, means that it becomes impossible to fulfill Eq. (6.6) for a generic photon state. Furthermore, also the cavities are not necessarily identical which results in differing reflection coefficients $r_{\mathrm{A}} \neq r_{\mathrm{B}}$. In order to consider single photon wave packets it is convenient to introduce wave packet operators

$$B_j^\dagger = \frac{1}{2\pi}\int f(k)\, b_j^\dagger(k)\,\mathrm{d}k \tag{6.9}$$

that create single photons with a certain wave profile $f(k)$ from the vacuum state in arm j of the interferometer. To ensure that these wave packets carry the intensity of one photon, the envelope function has to be normalized to one, $\frac{1}{2\pi}\int |f(k)|^2 \mathrm{d}k = 1$. Accordingly, the state of an incoming photon, which has been split by beamsplitter I, can be represented as

$$|\psi_{\mathrm{ph}}\rangle = \frac{1}{\sqrt{2}}(B_{\mathrm{A}}^\dagger + B_{\mathrm{B}}^\dagger)\,|0\rangle\,. \tag{6.10}$$

After the photon has scattered with the qubits inside the MZI, the two modes $b_{\mathrm{out,A}}$ and $b_{\mathrm{out,B}}$ of arms A and B are converted into the output modes

$$c_{\mathrm{out}} = \frac{1}{\sqrt{2}}\left(b_{\mathrm{out,A}} + \mathrm{e}^{\mathrm{i}\theta} b_{\mathrm{out,B}}\right), \tag{6.11a}$$

$$d_{\mathrm{out}} = \frac{1}{\sqrt{2}}\left(-b_{\mathrm{out,A}} + \mathrm{e}^{\mathrm{i}\theta} b_{\mathrm{out,B}}\right) \tag{6.11b}$$

by the second beamsplitter (II) to erase the which-path information of the photon. The phase shift $\theta = k(\ell_{\mathrm{B}} - \ell_{\mathrm{A}})$ arises due to the difference of the optical paths of the photon in the interferometer. Then, by detecting the photon in one of the output modes C or D, the total wave function $|\psi\rangle = |\psi_{\mathrm{qb}}\rangle \otimes |\psi_{\mathrm{ph}}\rangle$ is projected onto one of the states

$$|\Phi^{\mathrm{m}}\rangle = \frac{c_{\mathrm{out}}(t)\,|\psi\rangle}{\langle\psi|c_{\mathrm{out}}^\dagger c_{\mathrm{out}}|\psi\rangle^{\frac{1}{2}}}, \qquad \text{or} \qquad |\Psi^{\mathrm{m}}\rangle = \frac{d_{\mathrm{out}}(t)\,|\psi\rangle}{\langle\psi|d_{\mathrm{out}}^\dagger d_{\mathrm{out}}|\psi\rangle^{\frac{1}{2}}}.$$

In particular, the projected wave functions can be represented as

$$|\Phi^{\mathrm{m}}\rangle = \frac{1}{\sqrt{N_\Phi}}\sum_{\sigma,\sigma'}\left(f_{\sigma,\mathrm{A}} + f_{\sigma',\mathrm{B}}\right)|\sigma_{\mathrm{A}}, \sigma'_{\mathrm{B}}\rangle\,, \tag{6.12a}$$

$$|\Psi^{\mathrm{m}}\rangle = \frac{1}{\sqrt{N_\Psi}}\sum_{\sigma,\sigma'}\left(f_{\sigma,\mathrm{A}} - f_{\sigma',\mathrm{B}}\right)|\sigma_{\mathrm{A}}, \sigma'_{\mathrm{B}}\rangle \tag{6.12b}$$

with normalization constants N_Φ and N_Ψ. All information about the shape of the photon wave packet as well as the cavity detuning, i.e., the differences between the two cavities is encoded into the linear coefficients which are given by

$$f_{\sigma,j} = \frac{1}{2\pi} \int \mathrm{e}^{-\mathrm{i}(\omega_k t - k x_j)} r_j(\omega_k; \sigma_j) f(k)\, \mathrm{d}k. \tag{6.13}$$

Here $x_j = \ell_j + \ell_0$ denotes the total distance, that has been taken by the photon from I through arm j to the detectors; ℓ_j is the path length of arm j and ℓ_0 is the distance from II to the detectors. For simplicity it is assumed that both detectors have the same distance to II. From the general expressions (6.12) the ideal case is easily recovered: if the photon frequency is emitted exactly at the sweet spot $\omega_k = \Omega$ and if both cavities are identical, the projected states are equal to the favored Bell states $|\Phi^\mathrm{m}\rangle = |\Phi^-\rangle$ and $|\Psi^\mathrm{m}\rangle = |\Psi^-\rangle$.

However, if the conditions for the ideal case cannot be fulfilled, the projected state is not a maximally entangled state. This deviation can be quantified in terms of the fidelities

$$F[\Phi^\mathrm{m}, \Phi^-] = \frac{1}{2|N_\Phi|} \left|(f_{\uparrow,\mathrm{A}} + f_{\uparrow,\mathrm{B}}) - (f_{\downarrow,\mathrm{A}} + f_{\downarrow,\mathrm{B}})\right|^2, \tag{6.14a}$$

$$F[\Psi^\mathrm{m}, \Psi^-] = \frac{1}{2|N_\Psi|} \left|(f_{\uparrow,\mathrm{A}} - f_{\downarrow,\mathrm{B}}) - (f_{\downarrow,\mathrm{A}} - f_{\uparrow,\mathrm{B}})\right|^2. \tag{6.14b}$$

So far, the discussion has been focussed on the general expressions of the fidelities. For the sake of concreteness, we compute how the fidelity is affected by a single-photon wave packet with Lorentzian wave profile as well as for non-identical cavities in the following.

6.4.3. Lorentzian wave packet

As single microwave photons are usually produced from the controlled decay of a microwave resonator, it is a natural choice to consider the envelope function of the photon to be a Lorentzian wave packet

$$f(k) = \frac{\sqrt{c\Gamma}}{\mathrm{i}(\omega_k - \Omega) - \Gamma/2} \tag{6.15}$$

with spectral broadening Γ and the mean frequency tuned to Ω. Importantly, the relative weight factor η between qubit states $|\uparrow_j\rangle$ and $|\downarrow_j\rangle$, which is implied by the dispersive interaction, can be represented as a coherent sum over all frequency components in the wave packet. While the central frequency component of the photon wave packet $\omega_k = \Omega$ reveals a relative phase factor of $e^{\mathrm{i}\pi}$, all other frequency components induce relative phase factors deviating from this value. By averaging coherently over all these contributions the resulting weight factor η has modulus less than one, $|\eta| < 1$, and an average phase $\varphi = \arg(\eta) \neq \pi$ which generally differs from π.

Since both cavities are taken to be equal in this case, the linear coefficients are symmetric with respect to exchange of the cavities, $f_{\sigma,\mathrm{A}} = f_{\sigma,\mathrm{B}}$. Therefore, we will

omit the index j in the following. The coefficients take two independent values $f_\uparrow$ and $f_\downarrow = \eta f_\uparrow$ where η is a complex factor. Moreover, for a Lorentzian wave packet these coefficients $f_\uparrow$, $f_\downarrow$, and η can be evaluated explicitly. In the limit of large cavity damping as compared to the photon line width $\Gamma/\kappa \ll 1$, the η-factor becomes time-independent and reads

$$\eta(\Gamma) = \prod_{\nu=1}^{2} \frac{\mathrm{i}[\omega_c + (-1)^\nu \chi - \Omega] - \Gamma/2 + (-1)^\nu \kappa/2}{\mathrm{i}[\omega_c + (-1)^\nu \chi - \Omega] - \Gamma/2 + (-1)^{\nu-1} \kappa/2}. \tag{6.16}$$

Here the difference between the optical path lengths has been set to zero, $\theta = 0$.

Accordingly, for the Lorentzian wave packet the fidelity is a function of the photon spectral width Γ. Assuming $2\chi > \kappa$,[1] $\theta = 0$, and focussing to the limit $\Gamma/\kappa \ll 1$ we find the fidelity

$$F[\Phi^{\mathrm{m}}, \Phi^-] \simeq 1 - 2\left[1 - \left(\frac{\kappa}{2\chi}\right)^2\right]\left(\frac{\Gamma}{\kappa}\right)^2, \tag{6.17}$$

see Fig. 6.2. Equation (6.17) holds if the photon has been registered in the detector C. For the reciprocal measurement outcome we find, due to parity-selective interference amplitudes, $F[\Psi^{\mathrm{m}}, \Psi^-] = 1$ irrespective of the line width. This is due to the fact that both cavities have been assumed to be identical. This implies that states with even parity obtain the same phase when interacting with the photon in both arms,

$$\begin{aligned} &\frac{1}{\sqrt{2}} |{\uparrow_{\mathrm{A}}}{\uparrow_{\mathrm{B}}}\rangle \otimes \big(|0_{\mathrm{A}}, 1_{\mathrm{B}}\rangle + |1_{\mathrm{A}}, 0_{\mathrm{B}}\rangle \big) \\ \mapsto\ &\mathrm{e}^{\mathrm{i}\varphi_\uparrow} \frac{1}{\sqrt{2}} |{\uparrow_{\mathrm{A}}}{\uparrow_{\mathrm{B}}}\rangle \otimes \big(|0_{\mathrm{A}}, 1_{\mathrm{B}}\rangle + |1_{\mathrm{A}}, 0_{\mathrm{B}}\rangle \big) = \mathrm{e}^{\mathrm{i}\varphi_\uparrow} |{\uparrow_{\mathrm{A}}}{\uparrow_{\mathrm{B}}}\rangle \otimes |1_{\mathrm{C}}\rangle \end{aligned}$$

and similar for $|{\downarrow_{\mathrm{A}}}{\downarrow_{\mathrm{B}}}\rangle$. As a consequence of having the same phase, the partial waves of the photon, that have scattered with the even parity states, are transmitted with certainty into output channel C. In other words, as the even parity states destructively interfere in the output mode D, the wave function has to be projected onto the odd Bell state $|\Psi^-\rangle$ if the photon has been registered in D. Note that the entanglement production due to this parity-selective interference effect is merely probabilistic. However, as Γ/κ approaches zero, the fidelity (6.17) becomes unity thereby achieving full, deterministic entanglement, i.e., for any measurement outcome.

6.4.4. Cavity detuning

Moreover, in a realistic setup the cavities will always be fabricated slightly differently. As a consequence, the frequency sweet spots of cavity A and B differ from each other, i.e., $\Omega_{\mathrm{A}} \neq \Omega_{\mathrm{B}}$. This implies that we can, at best, tune the (central) frequency of the photon to fulfill Eq. (6.6) on one side, say Ω_{A}. Then, according to (6.7) the

[1] In the case $2\chi = \kappa$, the first non-vanishing contributions of Eqs. (6.17) and (6.20) appear to forth order in Γ/κ and $\delta\omega/\kappa$.

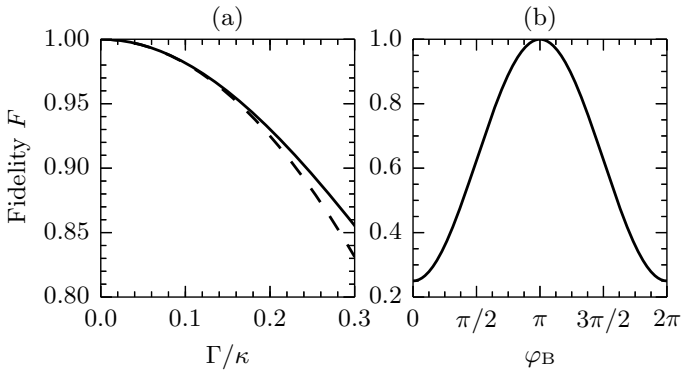

Fig. 6.2.: Fidelities $F[\Psi^m, \Psi^-]$ of the protocol for the two two intrinsic error mechanisms as discussed in the main text. In (a), the fidelity $F[\Psi^m, \Psi^-]$ is shown as function of the spectral broadening in case a Lorentzian-shaped photon wave packet passing the MZI (for $\chi = 2\kappa$). The solid line is obtained numerically whereas the dashed line corresponds to Eq. (6.17); both results agree in the regime $\Gamma \ll \kappa$. In (b), the fidelity (6.19) is shown as a function of the parameter φ_B, quantifying the detuning of cavity B, while assuming that cavity A is perfectly tuned. The ideal case corresponds to $\varphi_B = \pi$ with fidelity $F = 1$.

dispersive interaction induces a relative weight factor $\eta_A = f_{\downarrow,A}/f_{\uparrow,A} = e^{i\pi}$ between states $|\uparrow_A\rangle$ and $|\downarrow_A\rangle$ of qubit A. Since the other cavity cannot fulfill Eq. (6.7) at the same time, it induces a distinct relative weight factor $\eta_B = f_{\downarrow,B}/f_{\uparrow,B} = e^{i\varphi_B} \neq -1$ where φ_B is a function of the parameters $\omega_{c,B}$, χ_B, and κ_B.

Furthermore, due to the detuning of the cavities, another relative weight factor $\eta_{AB} = f_{\uparrow,B}/f_{\uparrow,A} \neq 1$ similar to η_A and η_B has to be taken into account. Since we neglect the influence of a finite line width of the photon here, all linear coefficients $f_{\sigma,j}$ and their corresponding η-factors are complex phase factors with modulus one. Fortunately, the influence of η_{AB} on the fidelity can be balanced out by appropriately adjusting the optical path lengths inside the MZI. Using (6.13) we find

$$\eta_{AB} = \frac{f_{\uparrow,B}}{f_{\uparrow,A}} = \frac{r_B(\Omega_A;\uparrow)}{r_A(\Omega_A;\uparrow)}\, e^{i\Omega_A(\ell_B-\ell_A)/c}. \tag{6.18}$$

Hence, by choosing the phase of the interferometer $\theta = k(\ell_B - \ell_A)$ properly, φ_B remains the only parameter that cannot be controlled in situ.

Expressed as a function of φ_B, the fidelity reads

$$F[\Phi^m, \Phi^-] = F[\Psi^m, \Psi^-] = \frac{1}{8}\left[5 - 3\cos(\varphi_B)\right]. \tag{6.19}$$

When the parameters of both cavities coincide φ_B takes the value π and we recover the ideal case as indicated by a unit fidelity.

To be more specific, we want to discuss the case where cavities A and B only differ by their resonance frequency $\delta\omega = \omega_{c,B} - \omega_{c,A} \neq 0$ with all other parameters identical. Expanding φ_B in terms of the small parameter $\delta\omega/\kappa$ we find $\varphi_B \approx \pi +$

$4\sqrt{1-\kappa^2/4\chi^2}\,\delta\omega/\kappa$ for $\chi > \kappa/2$. Hence, the fidelity is

$$F[\Phi^{\mathrm{m}}, \Phi^{-}] \simeq 1 - 3\left[1 - \left(\frac{\kappa}{2\chi}\right)^2\right]\left(\frac{\delta\omega}{\kappa}\right)^2. \tag{6.20}$$

Equations (6.17) and (6.20) suggest to tune the cavities in both cases such that κ is sufficiently large as compared to the photon line width and the cavity detuning. However, since Eq. (6.7) sets an upper limit $\chi \geq \kappa/2$ for the magnitude of κ, the optimal implementation is a tradeoff between κ being larger than the photon line width and the cavity detuning, but still smaller than the dispersive shift.

6.5. Conclusions

In summary, we have proposed a novel method to entangle distant transmon qubits by single-shot photon measurements. Relying on the ability to access the strong coupling regime as well as the discrete nature of the Fock state microwave photons, this scheme represents a parity meter based upon strong projective measurements as opposed to previous approaches involving weak continuous measurements. We have analyzed the entanglement protocol under non-ideal conditions by demonstrating the sensitivity of the entanglement in terms of the fidelity for a photon, emitted with a finite line width, as well as for inaccurate parameter fine tuning of the cavities. Furthermore, we have argued that for an optimal implementation the magnitude of the cavity broadenings have to be on an intermediate scale limited from above by the light-matter coupling strength. Although the lack of high efficiency microwave photon counters remains a technological challenge for the entanglement protocol, we believe our method has potential applications for high-speed quantum communication protocols and rehabilitates a secure quantum key distribution for cQED implementations.

Chapter 7

Outlook

This thesis is dedicated to the interplay of two exciting and promising approaches of quantum computation: circuit quantum electrodynamics and Majorana-based topological quantum computation. Regarding their physical realizations, however, both fields are at very different stages of development presently.

Since 2004 when the first experiments of cQED have been carried out, the rapid evolution of cQED allowed for a significant increase in the coherence times of superconducting qubits. Furthermore, due to its functional design and its high degree of controllability, the framework of cQED has become an integral part for the quantum information processing with superconducting qubits. Nowadays cQED has approached a level of maturity that allows to focus on more advanced applications such as in quantum communication, demonstration of multi-qubit entanglement and even simple routines for error-correction (Schoelkopf and Girvin, 2008).

In view of these developments we proposed a scheme that aims for the implementation of EPR-like correlations between superconducting qubits as required for fast and secure quantum communication, see Ch. 6. Promising deterministic entanglement with single-shot efficiency for remote qubits, the presented entanglement protocol might get adapted for an efficient entanglement generation in large-scale quantum devices. However, relying on the controlled manipulation of a single microwave photon, this scheme is beyond the scope of present microwave technology. Therefore future research will have to investigate the influence of technological limitations on the fidelity of the proposed entanglement protocol. Nonetheless, given the progress of microwave photon production and detection techniques in cQED over the last years (Houck *et al.*, 2007; Bozyigit *et al.*, 2011; Chen *et al.*, 2011), the current technological challenges might be overcome in the near future.

As compared to superconducting qubits, the development of (topological) Majorana-based qubits in semiconducting nanowires is currently still at a very early stage. Although first experimental signatures have indicated the existence of Majorana modes in semiconducting nanowires, devices capable to manipulate the state of MZMs are not available so far. Nevertheless, recent progress on the fabrication of semiconducting nanowire devices integrated into superconducting circuit elements (de Lange *et al.*, 2015; Larsen *et al.*, 2015) marks one step of many others towards the physical realization of Majorana qubits. As required for several Majorana qubit architectures, the implementation of the fractional Josephson effect would be a key achievement in this undertaking. Once accomplished, it will be possible to probe qubit architectures in the laboratory to figure out whether the current models accu-

rately capture the physics of Majorana modes in hybrid devices. In expectation of these exciting experimental prospects, further research will be stimulated focussing on the design of refined architectures for Majorana qubits. Time will tell whether Majorana-based quantum computation in superconducting circuits is a profitable approach that enriches and complements the possibilities in superconducting qubits.

Appendix A

Electromagnetic radiation

This appendix addresses some topics in electrodynamics ranging from the quantization of the electromagnetic field to basic concepts of quantum optics.

A.1. Classical electromagnetism and radiation

Subsuming electrical and magnetic phenomena under what is known as electromagnetism is one of the most important breakthroughs in the physics of the 19th century; all phenomena of classical electromagnetism are captured by *Maxwell's equations*,

$$\nabla \cdot \boldsymbol{B} = 0, \qquad \nabla \wedge \boldsymbol{E} - \frac{1}{c}\frac{\partial \boldsymbol{B}}{\partial t} = 0, \tag{A.1a}$$

$$\nabla \cdot \boldsymbol{D} = 4\pi\rho, \qquad \nabla \wedge \boldsymbol{H} - \frac{1}{c}\frac{\partial \boldsymbol{D}}{\partial t} = \frac{4\pi}{c}\boldsymbol{j}. \tag{A.1b}$$

Sources of the electromagnetic field are the electrical charge density $\rho(t, \boldsymbol{r})$ and the electric current density $\boldsymbol{j}(t, \boldsymbol{r})$. In the vacuum, i.e., in the absence of charge and electrical currents the dielectric displacement field $\boldsymbol{D}(t, \boldsymbol{r})$ and the magnetic field $\boldsymbol{H}(t, \boldsymbol{r})$ (macroscopic fields) can be identified with the electrical field $\boldsymbol{E}(t, \boldsymbol{r})$ and the magnetic induction field $\boldsymbol{B}(t, \boldsymbol{r})$ (microscopic fields) via $\boldsymbol{D} = \boldsymbol{E}$ and $\boldsymbol{H} = \boldsymbol{B}$. In the presence of dielectric and magnetizable materials the relations $\boldsymbol{D}(\boldsymbol{E})$ and $\boldsymbol{H}(\boldsymbol{B})$ between macroscopic and microscopic fields become more complex because of the influence of polarization induced charge and current distributions, that have to be taken into account. Combining (A.1) with Newton's equations of motion and the Lorentz force, the resulting set of coupled equations describes a complete theory of charged classical particles interacting with the electromagnetic field.

The extraordinary success of Maxwell's theory lies in the prediction of electromagnetic waves, which travel precisely at the speed of light c. In order to derive the wave equation for electromagnetic radiation, it is convenient to recast Maxwell's equations in terms of the electromagnetic potentials: the vector potential $\boldsymbol{A}$ and the scalar potential ϕ. The homogeneous Maxwell equations are solved by introducing the electromagnetic potentials

$$\boldsymbol{B} = \nabla \wedge \boldsymbol{A}, \qquad \boldsymbol{E} = -\nabla\phi - \frac{1}{c}\frac{\partial \boldsymbol{A}}{\partial t}. \tag{A.2}$$

Furthermore, in terms of the potentials $\boldsymbol{A}, \phi$ the inhomogeneous Maxwell equations

(A.1b) take the form

$$-\nabla^2\phi - \frac{1}{c}\frac{\partial}{\partial t}\nabla\cdot\boldsymbol{A} = 4\pi\rho, \tag{A.3a}$$

$$-\nabla^2\boldsymbol{A} + \frac{1}{c^2}\frac{\partial^2\boldsymbol{A}}{\partial t^2} + \nabla\left(\nabla\cdot\boldsymbol{A} + \frac{1}{c}\frac{\partial\phi}{\partial t}\right) = \frac{4\pi}{c}\boldsymbol{j}. \tag{A.3b}$$

Since the potential fields $\boldsymbol{A}$ and ϕ are defined from differential expressions, they are ambiguously defined; for any set of electromagnetic potentials $(\boldsymbol{A},\phi)$ satisfying (A.2) the transformation

$$\boldsymbol{A}' = \boldsymbol{A} + \nabla\chi, \qquad \phi' = \phi - \frac{1}{c}\frac{\partial\chi}{\partial t} \tag{A.4}$$

maps $(\boldsymbol{A},\phi)$ to a new set of potentials $(\boldsymbol{A}',\phi')$ which describe the same physics, i.e., leaving the physical fields $\boldsymbol{E},\boldsymbol{B}$ invariant. These redundant fields are called *gauge equivalent* and the transformation rule is accordingly called a *gauge-transformation*. Although the physics is not changed by a gauge transformation, it is desirable to work within the gauge, in which Maxwell's equations look most convenient. In particular, to find the wave equation for the vector potential it is useful to work in the *Coulomb gauge*,[1)] characterized by the gauge condition $\nabla\cdot\boldsymbol{A} = 0$. In the Coulomb gauge Maxwell's equations reduce to

$$\nabla^2\boldsymbol{A} - \frac{1}{c^2}\frac{\partial^2\boldsymbol{A}}{\partial t^2} = \frac{4\pi}{c}\boldsymbol{j}_\mathrm{t}, \qquad -\nabla^2\phi = 4\pi\rho, \tag{A.5}$$

where the *transversal current* is defined as divergence-free part of the total current, $\nabla\cdot\boldsymbol{j}_\mathrm{t} = 0$. More explicitly, it is

$$\boldsymbol{j}_\mathrm{t} = \boldsymbol{j} - \frac{1}{4\pi}\nabla\frac{\partial\phi}{\partial t}. \tag{A.6}$$

Without any electromagnetic sources, the scalar potential vanishes, $\phi = 0$, and the vector potential obeys the homogeneous wave equation

$$\nabla^2\boldsymbol{A} - \frac{1}{c^2}\frac{\partial^2\boldsymbol{A}}{\partial t^2} = 0. \tag{A.7}$$

A solution to (A.7) can be found by expanding the vector potential in terms of frequency modes. In view of the following sections, it is convenient to split the vector potential into two parts

$$\boldsymbol{A}(t,\boldsymbol{r}) = \boldsymbol{A}^{(+)}(t,\boldsymbol{r}) + \boldsymbol{A}^{(-)}(t,\boldsymbol{r}) \tag{A.8}$$

containing either only positive or only negative frequencies

$$\boldsymbol{A}^{(+)} = \sum_{k,\lambda}\alpha_{k,\lambda}\boldsymbol{u}_{k,\lambda}(\boldsymbol{r})\,\mathrm{e}^{-\mathrm{i}\omega_k t}, \qquad \boldsymbol{A}^{(-)} = \sum_{k,\lambda}\alpha^*_{k,\lambda}\boldsymbol{u}^*_{k,\lambda}(\boldsymbol{r})\,\mathrm{e}^{\mathrm{i}\omega_k t}. \tag{A.9}$$

[1)] In the literature the Coulomb gauge is also known as *radiation gauge* or *transversal gauge* (Jackson, 1999, Ch. 6).

The positive and negative frequency parts of the vector potential are complex conjugates of each other, $\boldsymbol{A}^{(+)\,*} = \boldsymbol{A}^{(-)}$, making sure that the vector is a real vector field. Each frequency component in (A.9) is characterized by a mode function $\boldsymbol{u}_{k,\lambda}$ or $\boldsymbol{u}^*_{k,\lambda}$ and weighted by a complex amplitude $\alpha_{k,\lambda}$ or $\alpha^*_{k,\lambda}$. In order for $\boldsymbol{A}$ to fulfill (A.7), the mode functions have to satisfy the *Helmholtz equation*

$$(\nabla^2 - \boldsymbol{k}^2)\,\boldsymbol{u}_{k,\lambda}(\boldsymbol{r}) = 0, \tag{A.10}$$

subject to the condition $\boldsymbol{u}_k(\boldsymbol{r}) = 0$ at the boundary of the domain V. As is well known from the theory of partial differential equations, the solutions $\boldsymbol{u}_{k,\lambda}$ of the Helmholtz equation can be chosen to form a complete set of orthogonal functions over the domain V. Assuming V to be a cube with spatial extend L in every direction, the mode functions read

$$\boldsymbol{u}_{k,\lambda}(\boldsymbol{r}) = \frac{1}{\sqrt{L^3}}\boldsymbol{\epsilon}_\lambda\, \mathrm{e}^{\mathrm{i}\boldsymbol{k}\cdot\boldsymbol{r}}, \tag{A.11}$$

where $\boldsymbol{k} = (k_x, k_y, k_z)$ is the wave vector with components $k_i = 2\pi n_i/L$, $n_i \in \mathbb{Z}$ and $\boldsymbol{\epsilon}_\lambda \in \mathbb{R}^3$ is the polarization vector. Due to the Coulomb gauge condition, $\boldsymbol{\epsilon}_\lambda \cdot \boldsymbol{k} = 0$, there are only two independent polarization vectors $\boldsymbol{\epsilon}_1, \boldsymbol{\epsilon}_2$ with $\boldsymbol{\epsilon}_\lambda \cdot \boldsymbol{\epsilon}_{\lambda'} = \delta_{\lambda,\lambda'}$. On account of the solution (A.11) the Helmholtz equation (A.10) leads to the linear dispersion relation for electromagnetic waves

$$\omega_k = c\,\|\boldsymbol{k}\|\,. \tag{A.12}$$

Gathering all ingredients together the full mode expansion of the vector potential reads

$$\boldsymbol{A}(t,\boldsymbol{r}) = \frac{1}{\sqrt{L^3}}\sum_{k,\lambda}\left[\boldsymbol{\epsilon}_\lambda \alpha_{k,\lambda}\mathrm{e}^{-\mathrm{i}(\omega_k t - \boldsymbol{k}\cdot\boldsymbol{r})} + \boldsymbol{\epsilon}^*_\lambda \alpha^*_{k,\lambda}\mathrm{e}^{\mathrm{i}(\omega_k t - \boldsymbol{k}\cdot\boldsymbol{r})}\right]. \tag{A.13}$$

Furthermore, with $\boldsymbol{E} = -\frac{1}{c}\partial_t \boldsymbol{A}$ and $\boldsymbol{B} = \nabla \wedge \boldsymbol{A}$ the electric and magnetic fields can be represented as

$$\boldsymbol{E}(\boldsymbol{r},t) = \frac{\mathrm{i}}{\sqrt{L^3}}\sum_{k,\lambda}\frac{\omega_k}{c}\left[\boldsymbol{\epsilon}_\lambda \alpha_{k,\lambda}\mathrm{e}^{-\mathrm{i}(\omega_k t - \boldsymbol{k}\cdot\boldsymbol{r})} - \boldsymbol{\epsilon}^*_\lambda \alpha^*_{k,\lambda}\mathrm{e}^{\mathrm{i}(\omega_k t - \boldsymbol{k}\cdot\boldsymbol{r})}\right], \tag{A.14a}$$

$$\boldsymbol{B}(\boldsymbol{r},t) = \frac{\mathrm{i}}{\sqrt{L^3}}\sum_{k,\lambda}\boldsymbol{k} \wedge \left[\boldsymbol{\epsilon}_\lambda \alpha_{k,\lambda}\mathrm{e}^{-\mathrm{i}(\omega_k t - \boldsymbol{k}\cdot\boldsymbol{r})} - \boldsymbol{\epsilon}^*_\lambda \alpha^*_{k,\lambda}\mathrm{e}^{\mathrm{i}(\omega_k t - \boldsymbol{k}\cdot\boldsymbol{r})}\right]. \tag{A.14b}$$

With the mode expansions (A.13) and (A.14) the propagation of any electromagnetic signal can be can be resolved by expressing the initial field $\boldsymbol{A}(t_0,\boldsymbol{r})$ at some time t_0 in terms of the complex mode amplitudes $\alpha_{k,\lambda}$ and $\alpha^*_{k,\lambda}$.

A.2. Quantization of the electromagnetic field

Maxwell's equations predict the existence of electromagnetic radiation, emerging from mutually induced time-dependent electric and magnetic fields. It turns out that

this mechanism of cyclic induction describes nothing else but a system of coupled harmonic oscillators—the field modes. As the quantization of a system consisting of many harmonic oscillators is well known, the quantization of the electromagnetic field follows by promoting the mode amplitudes to be oscillators and postulate canonical commutation relations for conjugate variables. Guided by this idea, *P. A. M. Dirac* (1927) presented a quantum theory of electromagnetic radiation, which brought Einstein's light quanta in line with the principles of Schödinger's wave mechanics.

There are several ways of quantizing Maxwell's equations, but Dirac's method of normal mode quantization appears most convenient for the purpose of describing electromagnetic radiation in a non-relativistic theory. The key issue of quantizing electromagnetism in a relativistic fashion is the compatibility with gauge invariance; it turns out that the gauge cannot be completely fixed without loosing a manifestly Lorentz-covariant description of the system (Sexl and Urbantke, 2001). By not fixing a gauge for the electromagnetic potentials, gauge-redundant field configurations give rise to an over-counting of dynamical degrees of freedom in the quantization procedure. To avoid these problems, methods of constrained quantization need to be applied for a Lorentz-covariant description of electromagnetism (Peskin and Schroeder, 1995).

A.2.1. Quantization in the Coulomb gauge

A guiding line for every quantization method is the action principle; according to the quantum principle the action of an mechanical system can be determined with an uncertainty, that corresponds to a cell with volume $\Delta S \simeq 2\pi\hbar$ in phase space. For the electromagnetic field the action reads

$$S[\boldsymbol{A}, \dot{\boldsymbol{A}}] = \int \mathcal{L}\big(\boldsymbol{A}, \dot{\boldsymbol{A}}\big)\, \mathrm{d}^3 r\, \mathrm{d}t; \tag{A.15}$$

with $\boldsymbol{E} = -\frac{1}{c}\partial_t \boldsymbol{A} - \nabla\phi$, $\boldsymbol{B} = \nabla \wedge \boldsymbol{A}$, and the Lagrangian density of the free electromagnetic field (Jackson, 1999; Landau and Lifshitz, 2009)

$$\mathcal{L} = \frac{1}{8\pi}\left[\boldsymbol{E}^2(t, \boldsymbol{r}) - \boldsymbol{B}^2(t, \boldsymbol{r})\right]. \tag{A.16}$$

In absence of of any charges, i.e., with $\rho(t, \boldsymbol{r}) = 0$ the scalar potential can be set to zero, $\phi(t, \boldsymbol{r}) = 0$. Then the canonically conjugate field $\pi_i(t, \boldsymbol{r})$ of the i-th component of the vector potential turns out to be $\pi_i = -\frac{1}{4\pi c} E_i$. Following the principles of Hamiltonian mechanics, the Hamiltonian of the electromagnetic field, whose domain is a finite volume V, follows to be

$$H_{\mathrm{em}} = \int\limits_V \Big(\dot{\boldsymbol{A}} \cdot \boldsymbol{\pi} - \mathcal{L}\Big)\, \mathrm{d}^3 r = \frac{1}{8\pi} \int\limits_V \left(\boldsymbol{E}^2 + \boldsymbol{B}^2\right) \mathrm{d}^3 r. \tag{A.17}$$

In order to find a quantum description for electromagnetic radiation, the field observables $\boldsymbol{E}$ and $\boldsymbol{B}$ have to be replaced by quantum mechanical observables, i.e.,

Hermitian operators acting upon a Hilbert space. For that purpose it is profitable to work with the normal mode expansions (A.14); in the quantum regime the mode amplitudes $\alpha_{k,\lambda}$, $\alpha^*_{k,\lambda}$ have to be treated as fluctuating quantities. Therefore the complex amplitudes are promoted to operators acting upon a unitary space. Since H_{em} is quadratic in the fields, every k-mode is formally equivalent to a separate harmonic oscillator with frequency ω_k. Therefore, the field quantization proceeds by introducing creation and annihilation operators $a_{k,\lambda}$, $a^\dagger_{k,\lambda}$ for every k-mode as a replacement for the classical amplitudes $\alpha_{k,\lambda}$, $\alpha^*_{k,\lambda}$. Normalized to the magnitude of their zero-point fluctuations,[2)] the quantum fields assume the mode expansions

$$\boldsymbol{A}(t,\boldsymbol{r}) = \sum_{k,\lambda} \sqrt{\frac{2\pi\hbar c^2}{\omega_k L^3}} \left[\boldsymbol{\epsilon}_\lambda \, \mathrm{e}^{-\mathrm{i}(\omega_k t - \boldsymbol{k}\cdot\boldsymbol{r})} \, a_k + \boldsymbol{\epsilon}^*_\lambda \, \mathrm{e}^{\mathrm{i}(\omega_k t - \boldsymbol{k}\cdot\boldsymbol{r})} \, a^\dagger_k\right], \tag{A.18a}$$

$$\boldsymbol{E}(t,\boldsymbol{r}) = \mathrm{i}\sum_{k,\lambda} \sqrt{\frac{2\pi\hbar\omega_k}{L^3}} \left[\boldsymbol{\epsilon}_\lambda \, \mathrm{e}^{-\mathrm{i}(\omega_k t - \boldsymbol{k}\cdot\boldsymbol{r})} \, a_k - \boldsymbol{\epsilon}^*_\lambda \, \mathrm{e}^{\mathrm{i}(\omega_k t - \boldsymbol{k}\cdot\boldsymbol{r})} \, a^\dagger_k\right]. \tag{A.18b}$$

Similar to the one-dimensional harmonic oscillator in quantum mechanics, the state space for the quantum fields can be generated by postulating canonical commutations relations for the creation and annihilation operators

$$\left[a_{k,\lambda}, a^\dagger_{k',\lambda'}\right] = \delta_{\lambda,\lambda'}\delta_{kk'}\mathbb{1}, \qquad \left[a_{k,\lambda}, a^\dagger_{k',\lambda'}\right] = \left[a^\dagger_{k,\lambda}, a^\dagger_{k',\lambda'}\right] = 0. \tag{A.19}$$

The term canonical commutation relation stems from the quantum harmonic oscillator, where the commutation relation between creation and annihilation operators are tightly connected to the canonical relation $[x,p] = \mathrm{i}\hbar$ between position and momentum operators of the oscillator. In fact, for the electromagnetic field the field operators $\boldsymbol{A}(t,\boldsymbol{r})$ and $\boldsymbol{E}(t,\boldsymbol{r})$ play the same role as position and momentum operators for a mechanical system. However, due to the Coulomb gauge condition $\nabla\cdot\boldsymbol{A} = 0$ the vector potential is a purely transversal field. Therefore it is not possible to realize canonical commutation relations for fields at equal times. Instead, the canonically conjugated fields $\boldsymbol{A}$ and $\boldsymbol{E}$ obey the *modified* equal-time commutation relations

$$-\frac{1}{4\pi c}[A_i(t,\boldsymbol{r}), E_j(t,\boldsymbol{r}')] = \mathrm{i}\hbar\left(\delta_{ij} - \frac{\partial_i\partial_j}{\nabla^2}\right)\delta(\boldsymbol{r}-\boldsymbol{r}'). \tag{A.20}$$

The nonlocal differential operator $\partial_i\partial_j/\nabla^2$ is defined via its Fourier-transform in position space and its occurrence is rooted in the nonlocal character of the Coulomb gauge. For a detailed discussion on causality and locality in the Coulomb gauge and for further literature see Jackson (1999, Ch. 6).

[2)] From the quantum harmonic oscillator it is well known that the zero-point fluctuations of every mode contribute half a quantum $\hbar\omega_k/2$ to the ground state energy. For a single k-mode with polarization λ the ground state energy is $\langle H_{\mathrm{em}}\rangle_{\mathrm{gs}} = \hbar\omega_k/2$. Furthermore, in the ground state it is $\langle H_{\mathrm{em}}\rangle_{\mathrm{gs}} = L^3\langle \boldsymbol{E}^2_{k,\lambda}\rangle_{\mathrm{gs}}/4\pi$ as follows from the *virial theorem* for the harmonic oscillator. Hence, the magnitude of the zero-point fluctuations per mode and polarization is found to be $\langle \boldsymbol{E}^2_{k,\lambda}\rangle_{\mathrm{gs}} = 2\pi\hbar\omega_k/L^3$.

Expressing the Hamiltonian (A.17) in terms of the mode expansion (A.18) yields

$$H_{\mathrm{em}} = \sum_{k,\lambda} \hbar\omega_k \left(a^\dagger_{k,\lambda} a_{k,\lambda} + \frac{1}{2} \right). \tag{A.21}$$

This representation of H_{em} clearly suggests that the electromagnetic field is a collection of uncoupled harmonic oscillators—the field modes. The spectrum of H_{em} is therefore characterized by the occupation of each mode oscillator, where each oscillator quantum is interpreted as a particle-like excitation of the electromagnetic field above its ground state—a *photon*. For each photon, that has been added to the vacuum, the energy $\hbar\omega_k$ has to be payed. Accordingly, the system is in its ground state if no photons are present. However, the ground state energy

$$E_{\mathrm{zp}} = \sum_k \frac{\hbar\omega_k}{2} = \frac{\hbar c}{2} \sum_k \|\boldsymbol{k}\| \tag{A.22}$$

appears to be an infinite number. By considering the electromagnetic field as an infinite bunch of quantum harmonic oscillators, where each oscillator contributes half an elementary quantum to the ground state energy, it is clear that E_0 grows to infinity. Even so, an observer can only measure the excitations above the ground state such that E_{zp} is in principle inaccessible to the observer. In fact, one has the freedom to choose the origin of the energy scale. Therefore, by simply translating energy scale by an amount of $-E_{\mathrm{zp}}$, the spectrum of H_{em} is well defined and characterized by its photon excitations above the zero-point energy only. The origin of this peculiarity lies in the ordering of creation and annihilation operators; by substituting the field operators (A.18) into the classical energy functional (A.17) the operator ordering corresponds to

$$\frac{1}{8\pi} \int \left(\boldsymbol{E}^2 + \boldsymbol{B}^2 \right) \mathrm{d}^3 r \longmapsto \sum_{\lambda,k} \frac{\hbar\omega_k}{2} \left(a^\dagger_{k,\lambda} a_{k,\lambda} + a_{k,\lambda} a^\dagger_{k,\lambda} \right) \tag{A.23}$$

To avoid the vacuum energy to appear, the operators need be brought to an order where all the $a_{k,\lambda}$'s are to the right of all the $a^\dagger_{k,\lambda}$'s. This ordering is called *normal order* and a normal-ordered operator $:O:$ is denoted by colons. For example it is

$$:a_{k_1,\lambda_1} a^\dagger_{k_2,\lambda_2} a_{k_3,\lambda_3}: = a^\dagger_{k_2,\lambda_2} a_{k_1,\lambda_1} a_{k_3,\lambda_3}. \tag{A.24}$$

Because any normal-ordered observable has vanishing vacuum expectation value, the normal order seems to be physically meaningful. In particular, this means the vacuum energy has been subtracted from the normal-ordered Hamiltonian, $\langle 0|:H_{\mathrm{em}}:|0\rangle = 0$. Later, it will be also important to obtain normal-ordered expectation values of physical observables such as the intensity of the electric field or intensity correlations. A convenient way of representing normal-ordered observables

is to use the operators

$$\boldsymbol{E}^{(+)}(t,\boldsymbol{r}) = \mathrm{i}\sum_{k,\lambda}\sqrt{\frac{2\pi\hbar\omega_k}{L^3}}\boldsymbol{\epsilon}_\lambda\,\mathrm{e}^{-\mathrm{i}(\omega_k t-\boldsymbol{k}\cdot\boldsymbol{r})}\,a_k, \tag{A.25a}$$

$$\boldsymbol{E}^{(-)}(t,\boldsymbol{r}) = -\mathrm{i}\sum_{k,\lambda}\sqrt{\frac{2\pi\hbar\omega_k}{L^3}}\boldsymbol{\epsilon}_\lambda^*\,\mathrm{e}^{\mathrm{i}(\omega_k t-\boldsymbol{k}\cdot\boldsymbol{r})}\,a_k^\dagger, \tag{A.25b}$$

containing solely $a_{k,\lambda}$'s or $a_{k,\lambda}^\dagger$'s. The decomposition (A.25) follows in analogy to the separation of positive and negative frequencies for the vector potential (A.9).

A.2.2. The continuous limit

Before discussing the state space and its properties in more detail, the quantum description of electromagnetic radiation shall be widened to quantum fields extending over an infinitely large volume, $V = \mathbb{R}^3$. As the size of the finite volume V increases, the difference between two sequential wave numbers $\Delta k_i = 2\pi/L$ becomes smaller and smaller. In the limit of $L \to \infty$ the sum over all k converges to the integral

$$\lim_{L\to\infty}\sum_{\{k_x,k_y,k_z\}} f(\boldsymbol{k})\Delta k_x\Delta k_y\Delta k_z = \int_{\mathbb{R}^3} f(\boldsymbol{k})\,\mathrm{d}^3k. \tag{A.26}$$

Furthermore, as the k-space becomes continuous, the operator $a_\lambda(\boldsymbol{k})^\dagger a_\lambda(\boldsymbol{k})\Delta k^3$ counts the number of field quanta with polarization λ within a k-space volume Δk^3. Accordingly, the mode operators have to be replaced by

$$a_{k,\lambda} \xrightarrow{L\to\infty} \left(\frac{2\pi}{L}\right)^{\frac{3}{2}} a_\lambda(\boldsymbol{k}). \tag{A.27}$$

Note that in the continuous case the mode operators have units $\mathrm{m}^{3/2}$ and the canonical commutation relations translate into $\left[a_\lambda(\boldsymbol{k}), a_{\lambda'}^\dagger(\boldsymbol{k}')\right] = (2\pi)^3\delta_{\lambda\lambda'}\delta(\boldsymbol{k}-\boldsymbol{k}')$. Consequently, the field operators assume the form

$$\boldsymbol{A}^{(+)}(t,\boldsymbol{r}) = \frac{1}{(2\pi)^3}\sum_\lambda\int\sqrt{\frac{2\pi\hbar c^2}{\omega_k}}\boldsymbol{\epsilon}_\lambda\,\mathrm{e}^{-\mathrm{i}(\omega_k t-\boldsymbol{k}\cdot\boldsymbol{r})}\,a_\lambda(\boldsymbol{k})\,\mathrm{d}^3k. \tag{A.28}$$

All other field operators follow from the identity $\boldsymbol{A}^{(-)} = \left[\boldsymbol{A}^{(+)}\right]^\dagger$ and $\boldsymbol{A} = \boldsymbol{A}^{(+)} + \boldsymbol{A}^{(-)}$ as well as from the relation between vector potentials and physical fields (A.2). Finally, by using all the replacements discussed the Hamiltonian becomes

$$H_{\mathrm{em}} = \sum_\lambda\int\hbar\omega_k\left(a_\lambda^\dagger(\boldsymbol{k})a_\lambda(\boldsymbol{k}) + \frac{1}{2}\right)\mathrm{d}^3k \tag{A.29}$$

in the case of an infinite volume.

A.2.3. Photons and the state space

The quantized electromagnetic field can be characterized by the occupation of its eigenmodes. The corresponding ladder operators $a_{k,\lambda}$ and $a^\dagger_{k,\lambda}$ replace the complex amplitudes of the classical expressions. Equipped with the algebraic relations (A.19) the operators $a_{k,\lambda}, a^\dagger_{k,\lambda}$ are capable to generate the Hilbert space of the quantum field by their properties of raising and lowering the eigenvalues of the number operators $n_{k,\lambda} = a^\dagger_{k,\lambda} a_{k,\lambda}$ counting the occupation number of quanta in each mode. In analogy to the quantum harmonic oscillator, the action of the operators $a^\dagger_{k,\lambda}$ adds a quantum of electromagnetic radiation with polarization λ in mode $\boldsymbol{k}$ to a state with quantum number n_i and maps it to a state with $n_i + 1$ quanta. Due to the discreteness of these field excitations, these "light quanta" are associated with particles called *photons*. For definiteness there must be a vacuum state $|0\rangle$,[3] with zero occupation number, i.e.,

$$a_{k,\lambda} |0\rangle = 0, \qquad \forall\ a_{k,\lambda}. \tag{A.30}$$

Then, a state with an arbitrary number of photons is generated by letting act a series creation operators upon this uniquely defined vacuum state $|0\rangle$

$$|n_1, \ldots, n_i, \ldots\rangle = \frac{1}{\sqrt{\prod_i n_i}} a^\dagger_{k_1,\lambda_1} \ldots a^\dagger_{k_i,\lambda_i} \ldots |0\rangle\,, \tag{A.31}$$

where n_i denotes the photon number of mode $i \cong (k_i, \lambda_i)$ with polarization λ_i and wave vector $\boldsymbol{k}_i$. The states defined in (A.31) are called *Fock states* and their total particle number is measured by the operator $N = \sum_i n_i$. Furthermore, the factor $1/\sqrt{\prod_i n_i}$ is the normalization of the Fock state. As (A.31) suggests, the electromagnetic field may contain an arbitrary amount of photons. However, the notion of a photon as a particle differs a lot from the classical picture of a particle for two reasons:

I) A single photon may be in an arbitrary superposition of single photon states[4]

$$|1\mathrm{ph}\rangle = \frac{1}{(2\pi)^3} \sum_\lambda \int f_\lambda(\boldsymbol{k}) a^\dagger_\lambda(\boldsymbol{k}) |0\rangle \, \mathrm{d}^3k.$$

In order for these states to fulfill the normalization condition $\langle 1\mathrm{ph}|1\mathrm{ph}\rangle = 1$, the envelope function $f_\lambda(\boldsymbol{k})$ is subject to the constraint $\frac{1}{(2\pi)^3} \sum_\lambda \int |f_\lambda(\boldsymbol{k})|^2 \, \mathrm{d}^3k = 1$. At first glance this superposition might look like a classical superposition of monochromatic waves, but in fact quantum theory dictates the collapse of this superposition when the photon has been measured. Instead, a coherent superposition of monochromatic waves is characterized by a macroscopic amplitude and therefore indestructible with respect to single photon detection events.

[3] Sometimes also called the *Fock vacuum*.

[4] Here considered in the continuous limit.

II) Photons are indistinguishable particles. This means there are $(N+K-1)!/K!(N-1)!$ possibilities to distribute N indistinguishable photons onto K modes. As the which-photon-in-which-mode information is experimentally inaccessible, states containing N identical photons have to be indistinctive with respect to these redundant configurations. Because the states $|n_1,\dots,n_K\rangle$ only indicate how many photons occupy a single mode, but do not specify which photon is in which mode, the indistinguishability of photons is already built into the Fock states by the way they are constructed.

It is clear from (A.31) that arbitrary superpositions of states are still legitimate states and by construction these states are already symmetric with respect to particle exchange. Furthermore, there may be superpositions between states having different particle numbers N. A general superposition therefore reads

$$|\Psi\rangle = \sum_{n_1,n_2,\dots} \alpha_{n_1,n_2,\dots}\,|n_1,n_2,\dots\rangle \tag{A.32}$$

and is a state in the *bosonic Fock space*

$$\mathscr{F}_{\mathrm{B}} = \bigoplus_{N=0}^{\infty} \underbrace{\mathscr{H}\vee\ldots\vee\mathscr{H}}_{N\ \text{times}} = \mathbb{C}\oplus\mathscr{H}\oplus(\mathscr{H}\vee\mathscr{H})\oplus\ldots \tag{A.33}$$

The bosonic Fock space is the direct sum of all totally symmetric N-particle Hilbert spaces $\mathscr{H}\vee\ldots\vee\mathscr{H}$, where the symbol $\vee$ is the symmetric tensor product, which is defined via $|a\rangle\vee|b\rangle = \frac{1}{\sqrt{2}}\big(|a\rangle\otimes|b\rangle + |b\rangle\otimes|a\rangle\big)$, for $|a\rangle\in\mathscr{H}_a, |b\rangle\in\mathscr{H}_b$. The space containing no particles is the one-dimensional span of the vacuum state, $\mathrm{span}(|0\rangle)\cong\mathbb{C}$. It can be shown that the Fock states (A.31) form a complete orthogonal basis of the bosonic Fock space, see Negele and Orland (1998, Ch. 1).

A.2.4. Observables and states of the electromagnetic field

The normal ordering procedure allows to express all observables of the electromagnetic field without counting the infinite vacuum contributions. To study the measurable quantities in a systematic way, it is useful to recast the expectation values of normal-ordered observables in terms of field-correlation functions $G^{(n)}$. The nth-order correlation functions defined by[5)]

$$\begin{aligned} &G^{(n)}(x_1,\dots,x_n,x_{n+1},\dots,x_{2n}) \\ &= \big\langle\Psi\big|\boldsymbol{E}^{(-)}(x_1)\dots\boldsymbol{E}^{(-)}(x_n)\boldsymbol{E}^{(+)}(x_{n+1})\dots\boldsymbol{E}^{(+)}(x_{2n})\big|\Psi\big\rangle, \end{aligned} \tag{A.34}$$

where $x_i = (t_i,\boldsymbol{r}_i)$ is a shorthand notation for time and space coordinates of the ith field operator. Two examples, that will be of importance in the following are

[5)] For a statistical mixture with density matrix ρ, the expectation value has to be computed by the trace, i.e., $G^{(n)}(x_1,\dots,x_{2n}) = \mathrm{Tr}\big[\rho\boldsymbol{E}^{(-)}(x_1)\dots\boldsymbol{E}^{(+)}(x_{2n})\big]$.

intensity of the electric field[6)]

$$\langle I(t,\boldsymbol{r})\rangle = \left\langle \boldsymbol{E}^{(-)}(t,\boldsymbol{r})\boldsymbol{E}^{(+)}(t,\boldsymbol{r})\right\rangle \tag{A.35}$$

as well as the (normal-ordered) squared intensity of the electric field

$$\langle :I(t,\boldsymbol{r})I(t+\tau,\boldsymbol{r}):\rangle = \left\langle \boldsymbol{E}^{(-)}(t,\boldsymbol{r})\boldsymbol{E}^{(-)}(t+\tau,\boldsymbol{r})\boldsymbol{E}^{(+)}(t+\tau,\boldsymbol{r})\boldsymbol{E}^{(+)}(t,\boldsymbol{r})\right\rangle. \tag{A.36}$$

In order to obtain concrete values of for all these expressions, the state of the electromagnetic field has to be known. In fact, the state of the fields significantly determines its physical behavior—classical or quantum. In the following, the properties of the most important types of states shall be discussed: Fock states, coherent states, and squeezed states. To do so, it will be sufficient to reduce the discussion to a fields with a single mode of frequency ω (the associated wave vector is $\boldsymbol{k}$) and with only one polarization degree of freedom. This single mode is characterized by the creation and annihilation operators a and $a^\dagger$. Sometimes it will be also helpful to make use of the *quadrature operators* $X_1 = (a^\dagger + a)$ and $X_2 = \mathrm{i}(a^\dagger - a)$. The quadrature operators obey the commutation relation $[X_1, X_2] = 2\mathrm{i}$ and therefore form a suitable set of canonical conjugate variables for a single field mode. Most of the properties discussed here can also be found in quantum optics textbook, see for example Mandel and Wolf (1995); Schleich (2001); Walls and Milburn (2008).

Fock states

As discussed above, the Fock states are generated by letting act a product of creation operators upon the vacuum state generating a state with definite particle number

$$N\,|n\rangle = n\,|n\rangle\,, \tag{A.37}$$

where n denotes the eigenvalue of the photon number operator $N = a^\dagger a$. Being in a particle number state implies that the conjugated phase is not well defined, cf. Susskind-Glogower operators in Sec. 2.3.1. Consequently, it is

$$\langle n|a|n\rangle = \langle n|a^\dagger|n\rangle = 0, \tag{A.38a}$$

$$\langle n|X_j|n\rangle = 0 \qquad \text{for } j \in \{1,2\}, \tag{A.38b}$$

$$\langle n|:X_j^2:|n\rangle = \langle n|X_j^2|n\rangle - 1 = 2n. \tag{A.38c}$$

[6)] The intensity of the electrical field is defined by the normal-ordered expression $I(t,\boldsymbol{r}) = \boldsymbol{E}^{(-)}(t,\boldsymbol{r})\boldsymbol{E}^{(+)}(t,\boldsymbol{r})$.

Moreover, for a Fock state $|n\rangle$ with occupation number n the field correlation functions can be obtained in a systematic way. For $\ell \leq n$ one finds

$$\begin{aligned} G^{(\ell)} &= \langle n | \boldsymbol{E}^{(-)}(t_1, \boldsymbol{r}_1) \dots \boldsymbol{E}^{(+)}(t_{\ell+1}, \boldsymbol{r}_{\ell+1}) \dots | n \rangle \\ &= \left(\frac{2\pi\hbar\omega}{L^3} \right)^{\ell} \left\langle n \middle| \left(a^\dagger\right)^{\ell} (a)^{\ell} \middle| n \right\rangle \prod_{i=1}^{\ell} \mathrm{e}^{-\mathrm{i}[\omega(t_{\ell+i}-t_i) - \boldsymbol{k}\cdot(\boldsymbol{r}_{\ell+i}-\boldsymbol{r}_i)]} \\ &= \left(\frac{2\pi\hbar\omega}{L^3} \right)^{\ell} \frac{n!}{(n-\ell)!} \prod_{i=1}^{\ell} \mathrm{e}^{-\mathrm{i}[\omega_k(t_{\ell+i}-t_i) - \boldsymbol{k}\cdot(\boldsymbol{r}_{\ell+i}-\boldsymbol{r}_i)]} \end{aligned} \tag{A.39}$$

whereas all other correlation functions vanish, i.e., for $\ell > n$ one finds $G^{(\ell)} = 0$.

Coherent states

A very important class of states is the class of coherent states, which are states of minimal uncertainty. Furthermore, coherent states are considered as semi-classical states, because they may develop a macroscopic intensity $\langle I \rangle \gg 2\pi\hbar\omega/L^3$ while the quantum fluctuations remain minimal. In order to produce states fulfilling the minimal uncertainty relation, the coherent states are generated by *displacing* the vacuum state $|0\rangle$ to another state $|\alpha\rangle$ with complex amplitude $\alpha \in \mathbb{C}$; cf. Fig. A.1 (a). Such a mapping is mediated by the unitary *displacement operator*

$$D(\alpha) = \exp\left(\alpha a^\dagger - \alpha^* a\right). \tag{A.40}$$

The displacement operator has the following properties

$$D^{-1}(\alpha) = D^\dagger(\alpha) = D(-\alpha) \qquad \text{(unitarity)}, \tag{A.41}$$

$$D^\dagger(\alpha)\, a\, D(\alpha) = a + \alpha \qquad \text{(translation)}. \tag{A.42}$$

Especially due to the translation property (A.42), the set of conjugate operators $(a, a^\dagger)$ is furnished with a unitary representation of translations in the complex plane by the set of displacement operators $\{D(\alpha) | \alpha \in \mathbb{C}\}$. Using the defining property of coherent states

$$|\alpha\rangle = D(\alpha)\,|0\rangle \tag{A.43}$$

one finds that $|\alpha\rangle$ is an eigenstate of the annihilation operator with eigenvalue α. This is because

$$\begin{aligned} & \alpha\,|\alpha\rangle = a\,|\alpha\rangle \\ \Leftrightarrow \quad & 0 = D(-\alpha)[a-\alpha]D^\dagger(-\alpha)D(-\alpha)\,|\alpha\rangle \\ \Leftrightarrow \quad & 0 = D^\dagger(\alpha)[a-\alpha]D(\alpha)\,|0\rangle \\ \Leftrightarrow \quad & 0 = a\,|0\rangle\,. \end{aligned}$$

In other words, since coherent obey essentially the same equations as the ground state they are also Gaussian states, i.e., states whose wave function is a Gaussian function. Using these basic properties of coherent states, it follows

$$\langle\alpha|a|\alpha\rangle = \alpha, \tag{A.44a}$$
$$\langle\alpha|n|\alpha\rangle = \langle\alpha|a^\dagger a|\alpha\rangle = |\alpha|^2, \tag{A.44b}$$
$$\langle\alpha|n^2|\alpha\rangle = |\alpha|^4 + |\alpha|^2, \tag{A.44c}$$
$$\langle\alpha|X_1|\alpha\rangle = 2\,\mathrm{Re}(\alpha), \tag{A.44d}$$
$$\langle\alpha|X_2|\alpha\rangle = 2\,\mathrm{Im}(\alpha), \tag{A.44e}$$
$$\langle\alpha|X_1^2|\alpha\rangle = 4\,\mathrm{Re}(\alpha)^2 + 1, \tag{A.44f}$$
$$\langle\alpha|X_2^2|\alpha\rangle = 4\,\mathrm{Im}(\alpha)^2 + 1. \tag{A.44g}$$

From these properties it follows that $\langle n^2\rangle - \langle n\rangle^2 = \langle n\rangle$ as expected for Poissonian statistics. Indeed, representing a coherent state in the basis of Fock states

$$|\alpha\rangle = \mathrm{e}^{-|\alpha|^2/2} \sum_{n=0}^{\infty} \frac{\alpha^n}{\sqrt{n!}} |n\rangle = \mathrm{e}^{-|\alpha|^2/2} \sum_n \frac{(\alpha a^\dagger)^n}{n!} |0\rangle \tag{A.45}$$

reveals a Poissonian distribution $P(n) = |\langle n|\alpha\rangle|^2 = \mathrm{e}^{-|\alpha|^2}|\alpha|^2/n!$ for measuring n photons being present in the coherent state. Furthermore, coherent states fulfill the minimum uncertainty relation

$$\langle\!\langle X_1^2\rangle\!\rangle \, \langle\!\langle X_2^2\rangle\!\rangle = 1 \tag{A.46}$$

where the second order cumulant $\langle\!\langle AB\rangle\!\rangle = \langle AB\rangle - \langle A\rangle\langle B\rangle$ coincides with the (co)-variance of A (and B). The correlation functions for the electromagnetic field in a coherent state read

$$\begin{aligned} G^{(\ell)} &= \big\langle\alpha\big|\boldsymbol{E}^{(-)}(t_1,\boldsymbol{r}_1)\ldots\boldsymbol{E}^{(+)}(t_{\ell+1},\boldsymbol{r}_{\ell+1})\ldots\big|\alpha\big\rangle \\ &= \left(\frac{2\pi\hbar\omega}{L^3}\right)^{\ell} |\alpha|^{2\ell} \prod_{i=1}^{\ell} \mathrm{e}^{-\mathrm{i}[\omega_k(t_{\ell+i}-t_i)-\boldsymbol{k}\cdot(\boldsymbol{r}_{\ell+i}-\boldsymbol{r}_i)]}. \end{aligned} \tag{A.47}$$

Note that this expression holds for all ℓ. Therefore (A.47) is significantly different from (A.39) and reveals the fundamental different nature of coherent states in comparison to the Fock states.

These fundamental differences between Fock states and coherent states are also reflected in the classical limit with $\langle N\rangle \to \infty$. This is due to the fact that coherent states always keep minimal uncertainty, see (A.46), whereas the quantum fluctuations of Fock states grow quadratically with the photon number n, $\langle\!\langle X_1^2\rangle\!\rangle_n \langle\!\langle X_2^2\rangle\!\rangle_n \sim 4n^2$ as $n \to \infty$. In other words, only coherent states reveal the correct classical limit in the sense that *all* quantum fluctuations become negligible as the complex amplitude becomes large enough. This enables coherent states to develop a well defined phase in the limit $\langle n\rangle = |\alpha|^2 \to \infty$ and therefore gives rise to the emergence of classical trajectories, see Glauber (1963) and references therein.

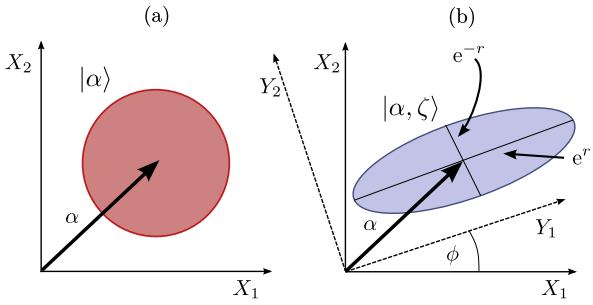

Fig. A.1.: (a) Coherent state with complex amplitude α. (b) Squeezed state with squeezing parameter $\zeta = r\mathrm{e}^{2\mathrm{i}\phi}$ originating from a coherent state with amplitude α by $|\alpha,\zeta\rangle = S(\zeta)\,|\alpha\rangle$.

Squeezed states

Another class of minimum uncertainty states are the so called *squeezed states*. For such a state the Heisenberg uncertainty relation demands $\langle\!\langle X_1^2\rangle\!\rangle\langle\!\langle X_2^2\rangle\!\rangle = 1$, but it does not require that each of these variances has to be (at least) equal to one as in the case of coherent states. While coherent states correspond to spherical shaped phase space quasi-probability distributions, squeezed states rather correspond to elliptical shaped phase space distributions, see Fig. A.1. As their name already suggests, squeezed states arise from coherent states by a squeezing operation which densifies the variance in direction of a particular quadrature while stretching the variance of the other.

By introducing the unitary operators $U_\mathrm{r}(\phi) = \exp(\mathrm{i}\phi\, a^\dagger a)$, the quadratures can be rotated in the X_1X_2-plane[7)]

$$\begin{aligned} Y_1 + \mathrm{i}Y_2 &= U_\mathrm{r}^\dagger(\phi)\,[X_1 + \mathrm{i}X_2]\,U_\mathrm{r}(\phi) \\ &= \mathrm{e}^{-\mathrm{i}\phi}(X_1 + \mathrm{i}X_2) \end{aligned} \tag{A.48}$$

Here ϕ denotes the angle of the rotation. Equivalently, rotations in the X_1X_2-plane can be represented as

$$\begin{pmatrix} Y_1 \\ Y_2 \end{pmatrix} = \begin{pmatrix} \cos\phi & \sin\phi \\ -\sin\phi & \cos\phi \end{pmatrix} \cdot \begin{pmatrix} X_1 \\ X_2 \end{pmatrix}. \tag{A.49}$$

As an entire class of quadratures arises by rotations, the squeezing operation may be applied to each of these rotated quadrature operators. This allows to generate squeezing in an arbitrary direction. However, in any case the Heisenberg uncertainty relation is required to remain intact, $\langle\!\langle Y_1^2\rangle\!\rangle\langle\!\langle Y_2^2\rangle\!\rangle = 1$.

The general *squeezing operator* is composed of the squeezing operation and a rotation in the quadrature plane,

$$S(\zeta) = \exp\left[\frac{1}{2}\left(\zeta^* a^2 - \zeta a^{\dagger 2}\right)\right] = U_\mathrm{r}^\dagger(\phi)\exp\left[\frac{r}{2}\left(a^2 - a^{\dagger 2}\right)\right]U_\mathrm{r}(\phi) \tag{A.50}$$

[7)] As a subgroup of the symplectic group Sp(2), the group of two-dimensional rotations SO(2) ≅ U(1) preserve the canonical commutation relation $[Y_1, Y_2] = 2\mathrm{i}$ of the quadratures. In addition to that, the group of transformations SO(2) ≅ U(1) also preserves the normal ordering of observables. Therefore it is impossible to turn an annihilation operator $a = \frac{1}{2}(X_1 + \mathrm{i}X_2)$ into a creation operator $a^\dagger = \frac{1}{2}(X_1 - \mathrm{i}X_2)$ by means of a two-dimensional rotation.

where $\zeta = re^{2i\phi} \in \mathbb{C}$ is the complex *squeezing amplitude* and $r = |\zeta|$ is the *squeezing parameter* (Walls and Milburn, 2008). The squeezing operator has the following properties

$$S^\dagger(\zeta) = S^{-1}(\zeta) \qquad \text{(unitary)}, \tag{A.51}$$

$$S^{-1}(\zeta) = S(-\zeta) \qquad \text{(inverse squeezing)}. \tag{A.52}$$

Furthermore, the squeezing operation has the following conjugation properties

$$S^\dagger(\zeta)\, a\, S(\zeta) = \cosh(r)\, a - e^{-2i\phi} \sinh(r)\, a^\dagger, \tag{A.53a}$$

$$S^\dagger(\zeta)\, a^\dagger\, S(\zeta) = \cosh(r)\, a^\dagger - e^{2i\phi} \sinh(r)\, a, \tag{A.53b}$$

$$S^\dagger(\zeta)\, D(\alpha)\, S(\zeta) = D(\beta) \quad \text{with} \quad \beta = \alpha \cosh r - \alpha^* e^{-2i\phi} \sinh r, \tag{A.53c}$$

$$S^\dagger(\zeta) \left[Y_1 + iY_2\right] S(\zeta) = e^{-r}\, Y_1 + ie^{r}\, Y_2. \tag{A.53d}$$

Equation (A.53d) reveals the squeezing character of the S operation; by letting act $S(\zeta)$ upon the *rotated quadratures* Y_1 and Y_2, the quadrature Y_1 is scaled by the factor e^{-r} (squeezed) and Y_2 is scaled by the factor e^{r} (stretched). Hence, the modulus of the complex squeezing amplitude $\zeta = re^{2i\phi}$ specifies the amount of squeezing whereas the complex phase of the squeezing amplitude divided by two indicates the direction in which the squeezing operator acts. Note, that the conjugated quadratures $\tilde{Y}_1 = S^\dagger Y_1 S = e^{-r} Y_1$ and $\tilde{Y}_2 = S^\dagger Y_2 S = e^{r} Y_2$ are still canonical variables obeying $[\tilde{Y}_1, \tilde{Y}_2] = 2i$. This shows that the squeezing operation constitutes a *symplectic transformation* which is composed of a pure rotation in the X_1X_2-plane and a directional scaling transformation. In fact, it can be shown that the entire symplectic group in two dimensions $\mathrm{Sp}(2) \cong \mathrm{SL}(2)$ can be covered by the set of squeezing transformations and rotations.[8)]

So far, only the squeezing operation as such has been considered. Since squeezed states are supposed to be states with minimal uncertainty relation, they can be constructed from coherent states. By the unitarity of the S operators it follows

$$\begin{aligned}\langle\alpha|\tilde{Y}_i|\alpha\rangle &= \langle\alpha|S(\zeta)\, Y_i\, S^\dagger(\zeta)|\alpha\rangle = \langle\alpha|S^\dagger(-\zeta)\, Y_i\, S(-\zeta)|\alpha\rangle \\ &= \langle\alpha, -\zeta|Y_i|\alpha, -\zeta\rangle\end{aligned} \tag{A.54}$$

where the *squeezed state*

$$\begin{aligned}|\alpha, \zeta\rangle &= S(\zeta)\,|\alpha\rangle = S^\dagger(-\zeta) D(\alpha)\,|0\rangle = D(\beta) S^\dagger(-\zeta)\,|0\rangle \\ &= D(\beta)\,|0, \zeta\rangle\end{aligned} \tag{A.55}$$

originates by displacing the so called squeezed vacuum state $|0, \zeta\rangle = S^\dagger(-\zeta)\,|0\rangle$. Then, it follows that squeezed states fulfill the minimal uncertainty relation

$$\begin{aligned}1 &= \langle\!\langle Y_1^2 \rangle\!\rangle \langle\!\langle Y_2^2 \rangle\!\rangle \\ &= \Big(\langle\alpha, \zeta|Y_1^2|\alpha, \zeta\rangle - \langle\alpha, \zeta|Y_1|\alpha, \zeta\rangle^2\Big)\Big(\langle\alpha, \zeta|Y_1^2|\alpha, \zeta\rangle - \langle\alpha, \zeta|Y_1|\alpha, \zeta\rangle^2\Big).\end{aligned} \tag{A.56}$$

[8)] Cf. Fulton and Harris (1991, Lecture 11): the generators of the Lie algebra $\mathfrak{sl}_2$ can be identified as $H = a^\dagger a$, $X = a^{\dagger 2}$, and $Y = a^2$.

For a squeezed state one finds the following properties

$$\langle \alpha, \zeta | X_1 + \mathrm{i} X_2 | \alpha, \zeta \rangle = 2\alpha, \tag{A.57a}$$

$$\langle\!\langle Y_1^2 \rangle\!\rangle = \mathrm{e}^{-2r} \qquad \Rightarrow \qquad \langle\!\langle Y_2^2 \rangle\!\rangle = \mathrm{e}^{2r}, \tag{A.57b}$$

$$\langle \alpha, \zeta | a^\dagger a | \alpha, \zeta \rangle = |\alpha|^2 + \sinh^2 r, \tag{A.57c}$$

$$\langle\!\langle a^\dagger a \rangle\!\rangle = |\alpha \cosh r - \alpha^* \mathrm{e}^{2\mathrm{i}\phi} \sinh r|^2 + 2\cosh^2(r)\sinh^2(r). \tag{A.57d}$$

The last two identities show that the particle content of a squeezed state is different from the particle content of the a coherent with the same complex amplitude.

In particular, this is also true for the squeezed vacuum. Represented in terms of the Fock basis, the squeezed vacuum reads

$$|0, \zeta\rangle = \frac{1}{\sqrt{\cosh r}} \sum_{n=0}^{\infty} \frac{\sqrt{2n!}}{2^n n!} \left(\mathrm{e}^{-2\mathrm{i}\phi} \tanh r\right)^n |2n\rangle \tag{A.58}$$

and is therefore a superposition of an infinite amount of Fock states. That the squeezing operation changes the particle content of a state is deeply connected to its nature. This follows from the identities (A.53a) and (A.53b) in which the squeezing operation mixes creation and annihilation operators. Such a transformation is generally known as *Bogoliubov transformation*,

$$b \;\; = S(\zeta)\, a\, S(\zeta) = ua + va^\dagger, \tag{A.59a}$$

$$b^\dagger = S(\zeta)\, a^\dagger\, S(\zeta) = u^* a^\dagger + v^* a. \tag{A.59b}$$

The Bogoliubov transformation defines a new set of bosonic operators b and $b^\dagger$ obeying the commutation relation $[b, b^\dagger] = 1$. Since the commutation rule of b and $b^\dagger$ restricts all configurations (u, v) to lie on a hyperbola with $|u|^2 - |v|^2 = 1$, the coefficients admit in accordance to (A.53a) and (A.53b) the parametrization

$$u = \mathrm{e}^{\mathrm{i}\phi_1} \cosh r, \tag{A.60a}$$

$$v = \mathrm{e}^{\mathrm{i}\phi_2} \sinh r. \tag{A.60b}$$

Defining a new set of creation an annihilation operators, one would expect to have another set of number states determined by

$$b\,|0_b\rangle = 0 \tag{A.61}$$

and the commutation relation $[b, b^\dagger] = 1$. This implies the existence of at least two vacuum states: either $|0_a\rangle$ (formerly denoted $|0\rangle$ and annihilated by a) or $|0_b\rangle$.[9] It is convenient to choose the ground state of the considered Hamiltonian to be the

[9] This has far-reaching consequences in relativity: paradoxically, the vacuum state of a quantum field is seen as a thermal state from the perspective of an accelerated observer. This sort of black body radiation is called *Unruh radiation* (Unruh, 1976) and arises due to the fact that an accelerated observer can only infer the state of the quantum field in a region of spacetime which is separated from the rest by an event horizon. Due to the occurrence of such an event horizon in accelerated

actual vacuum state. This choice also defines a normal ordering operation, which is generically damaged by a Bogoliubov transformation.

With the set of the new operators b and $b^\dagger$ one can also define coherent states. As before, coherent states emerge from the displacement of the vacuum state

$$|\beta_b\rangle = \exp\left(\beta b^\dagger - \beta^* b\right)|0_b\rangle\,. \tag{A.62}$$

As a result the states $|\beta\rangle$ are eigenstates of the operator b,

$$b\,|\beta_b\rangle = \beta\,|\beta_b\rangle\,. \tag{A.63}$$

There is an intimate relation between squeezed states and coherent states. Looking more closely at the states $|\beta_b\rangle$, their connection to squeezed states in the basis of a-modes can be inferred from

$$\begin{aligned}
&\beta\,|\beta_b\rangle = b\,|\beta_b\rangle \\
\Leftrightarrow\quad &\beta S^\dagger(\zeta)\,|\beta_b\rangle = S^\dagger(\zeta) b S(\zeta) S^\dagger(\zeta)\,|\beta_b\rangle \\
\Leftrightarrow &\beta\big\{S(-\zeta)\,|\beta_b\rangle\,\big\} = a\big\{S(-\zeta)\,|\beta_b\rangle\,\big\}.
\end{aligned}$$

In the next step, one has to find the action of a on the state $|\varkappa\rangle = S(-\zeta)\,|\beta_b\rangle$,

$$\begin{aligned}
&\beta\,|\varkappa\rangle = a\,|\varkappa\rangle \\
\Leftrightarrow\quad &0 = D^\dagger(\beta)\,[a-\beta]\,D(\beta)D^\dagger(\beta)\;|\varkappa\rangle \\
\Leftrightarrow\quad &0 = a\,D^\dagger(\beta)\;|\varkappa\rangle \\
\Leftrightarrow\quad &|0_a\rangle = D^\dagger(\beta)\;|\varkappa\rangle \\
\Leftrightarrow\quad &|\beta_b\rangle = S(\zeta)\,|\beta_a\rangle = |\beta_a,\zeta\rangle\,.
\end{aligned}$$

In particular, for $\beta = 0$ one finds the definition of the squeezed vacuum $|0_b\rangle = S(\zeta)\,|0_a\rangle = |0,\zeta\rangle$ as introduced before. This means that the coherent states of the b-modes are the squeezed states of the a-modes. Therefore, the states $|\beta_b\rangle$ are also called *two-photon coherent states* (Yuen, 1976).

Requiring non-linear optical media for their generation, squeezed states are experimentally difficult to realize, but extremely useful for applications that require high-sensitive interferometric devices. The prime example, in which squeezed states are used, is the search for gravitational waves (Caves, 1981).

---

reference frames, an observer resting in the accelerated frame rather experiences a mixed state than the (pure) vacuum state. A similar effect also exists for the event horizon of a black hole in curved spacetime. In this case the thermal radiation, which originates from the Schwarzschild horizon, is called *Hawking radiation* (Hawking, 1974). Because of their formal analogy to the phenomenon of parametric amplification, it has recently been proposed to simulate such relativistic effects by using methods of cQED, i.e., with superconducting circuits, Josephson parametric amplifiers, and microwave cavities, see Nation *et al.* (2012).

A.3. Quantum optics

With the invention of a new type of radio interferometry by *R. Hanbury Brown* and *R. Q. Twiss* (1956b), it has been questioned whether the effect of intensity correlations—at the time observed for classical radiation—is compatible with quantum mechanics (Hanbury Brown and Twiss, 1956a; Brannen and Ferguson, 1956). In a seminal paper *E. Purcell* (1956) has demonstrated that the quantum description of light in terms of photons is indeed in full accordance with the *Hanbury Brown and Twiss effect* and therefore with Maxwell's equations. This was the birth of *quantum optics* and set off further developments whose climax was reached with the theoretical works of *R. Glauber* (1963), *E. C. G. Sudarshan* (1963) on quantum optical coherence theory as well as *L. Mandel* (1958) on the statistics of photon detection. Nowadays, the field of quantum optics has become a diverse and manifold field of research with many subfields. Among them are cavity QED, the study of open quantum systems, quantum information theory (in parts) and many more.

A.3.1. Quantum optical fields

So far, it has been avoided to speak about light or microwaves, because these terms only comprise a small fraction of the entire spectrum of electromagnetic radiation. While optical electromagnetic waves are characterized by frequencies in the range of 3–30 THz, microwaves frequencies are in the range of 3–30 GHz. In both cases the bandwidth is considerably smaller than the magnitude of the used frequencies. This allows to make the useful approximation for the electric field

$$\begin{aligned}\boldsymbol{E}^{(+)}(t,\boldsymbol{r}) &\approx \frac{\mathrm{i}}{(2\pi)^3}\sqrt{2\pi\hbar\Omega}\sum_{\lambda}\int \boldsymbol{\epsilon}_\lambda \mathrm{e}^{-\mathrm{i}(\omega_k t-\boldsymbol{k}\cdot\boldsymbol{r})}a_\lambda(\boldsymbol{k})\mathrm{d}^3k \\ &= \mathrm{i}\Omega\boldsymbol{A}^{(+)}(t,\boldsymbol{r}) \end{aligned} \tag{A.64}$$

where Ω is the *carrier frequency* of the wave. Within this approximation the factors $\sqrt{\omega}$ have been replaced by the constant factors $\sqrt{\Omega}$. This is particularly useful for the evaluation of integral expressions of the field correlation functions.

In the following the propagation of optical fields will be directed in a particular direction by waveguides. The electromagnetic modes inside a hollow waveguide with a quasi-one-dimensional geometry (cylindrical, rectangular, etc.) are unbounded in the direction pointing along the waveguide and strongly confined by the waveguide in the transverse direction. For concreteness, the longitudinal direction of the wire is taken to be parallel to the z direction. Due to the strong confinement of the fields imposed by the waveguide, the transverse wave numbers $k_x, k_y \simeq 1/\ell$, related to the transverse extend of the waveguide $\simeq \ell$, take discrete values. In the following they are assumed to be fixed. Hence, traveling fields inside the waveguide can be characterized by their longitudinal wave number k. Moreover, for signals emitted at high frequencies $\omega/ck_{x/y} \simeq \ell\Omega/c \gg 1$ the (one-dimensional) dispersion relation of a waveguide becomes approximately linear,

$$ck = \sqrt{\omega^2 - c^2(k_x^2 + k_y^2)} \approx \omega.$$

Within this approximation it is useful to introduce quasi-one-dimensional field operators

$$a(t,z) = \mathrm{e}^{-\mathrm{i}k_\Omega(ct-z)} \frac{1}{2\pi} \int \mathrm{e}^{-\mathrm{i}k(ct-z)} a(k)\mathrm{d}k. \tag{A.65}$$

These distribution-valued operators have dimension $\mathrm{m}^{-1/2}$ and obey the commutation relations

$$\left[a(t,z), a^\dagger(t',z')\right] = \delta(t-t')\delta(z-z') \tag{A.66}$$

which are local in space and time. For the sake of simplicity the polarization degree of freedom has been neglected here. Furthermore, often it is convenient to describe the dynamics of the fields in a frame rotating at frequency Ω.

A.3.2. Degree of optical coherence

The importance of the field correlation functions $G^{(n)}(t_1, \boldsymbol{r}_1, \ldots)$ for the evaluation of physical observables has been emphasized in the previous section. Moreover, in quantum optics one often also intends to characterize the quantum properties of the electromagnetic fields. Therefore, the measurement of field correlation functions itself is of particular interest since these reveal the statistics of the fields and their sources. One term that plays a predominant role in this discussion is the degree of optical coherence. In the following the significance of the most common correlation functions—the normalized correlation functions of first and second order—will be discussed. For the sake of simplicity, the shorthand notation $x_i = (t_i, \boldsymbol{r}_i)$ will be used instead of denoting time and space coordinates separately.

First-order correlation function

The normalized first-order correlation function is defined by

$$g^{(1)}(x_1, x_2) = \frac{G^{(1)}(x_1, x_2)}{\sqrt{G^{(1)}(x_1, x_1) G^{(1)}(x_2, x_2)}} \tag{A.67}$$

in which $G^{(1)}(x_1, x_2) = \left\langle \boldsymbol{E}^{(-)}(x_1) \boldsymbol{E}^{(+)}(x_2) \right\rangle$ is a quadratic field correlation function. From the Cauchy-Schwartz inequality it follows that

$$\left| g^{(1)}(x_1, x_2) \right| \leq 1. \tag{A.68}$$

The first-order correlation function $g^{(1)}(x_1, x_2)$ is intimately related to the occurrence of interference patterns in a double-slit experiment. A calculation of the intensity on

the screen behind two slits gives

$$\begin{aligned} I &= \left\langle \left[\boldsymbol{E}^{(-)}(x_1) + \boldsymbol{E}^{(-)}(x_2)\right]\left[\boldsymbol{E}^{(+)}(x_1) + \boldsymbol{E}^{(+)}(x_2)\right]\right\rangle \\ &= G^{(1)}(x_1, x_1) + G^{(1)}(x_2, x_2) \\ &\quad + 2\sqrt{G^{(1)}(x_1, x_1)G^{(1)}(x_2, x_2)}\left|g^{(1)}(x_1, x_2)\right|\cos[\Delta\phi(x_1, x_2)]. \end{aligned} \tag{A.69}$$

Hence, the interference fringe becomes most visible if $g^{(1)}(x_1, x_2)$ is maximal. In turn, there is no interference patters for $\left|g^{(1)}(x_1, x_2)\right| = 0$. Hence, the higher the value of $g^{(1)}(x_1, x_2)$, the better the visibility of the interference pattern. Since the discussion here includes space and time coordinates of the fields, the first-order correlation function is capable to characterize the spatial as well as temporal coherence properties. By considering $g^{(1)}(x_1, x_2)$ at a fixed position $\boldsymbol{r}_1 = \boldsymbol{r}_2$ in space, a temporal decay $\left|g^{(1)}(t_1, t_2)\right| \sim \mathrm{e}^{-(t_1 - t_2)/\tau_\mathrm{c}}$ with $t_1 > t_2$ indicates the existence of a finite coherence time τ_c. A similar definition holds for the coherence length by considering different space coordinates at a fixed point in time.

Second-order correlation function

In analogy to the first-order correlation, the normalized second-order correlation function is defined by

$$g^{(2)}(x_1, x_2) = \frac{G^{(2)}(x_1, x_2, x_2, x_1)}{G^{(1)}(x_1, x_1)G^{(1)}(x_2, x_2)} \tag{A.70}$$

with the property $g^{(2)} \geq 0$. Since the definition of $g^{(2)}$ makes use of the intensity correlation

$$\begin{aligned} G^{(2)}(x_1, x_2, x_2, x_1) &= \left\langle \boldsymbol{E}^{(-)}(x_1)\boldsymbol{E}^{(-)}(x_2)\boldsymbol{E}^{(+)}(x_2)\boldsymbol{E}^{(+)}(x_1)\right\rangle \\ &= \left\langle :I(x_1)I(x_2):\right\rangle, \end{aligned} \tag{A.71}$$

it suggests a close relationship to the intensity-intensity correlations of the Hanbury Brown and Twiss interferometer. The study of intensity correlations exposes properties of the light source by which the measured radiation has been emitted. In the original paper of Hanbury Brown and Twiss (1956a) intensity correlations of chaotic light, i.e., radiation that has been emitted by thermal light sources have been considered.[10] In this situation the fields $\boldsymbol{E}^{(\pm)}$ can be treated as Gaussian-distributed variables which allow for the decomposition

$$g^{(2)}_\mathrm{chaotic}(t_1, t_2) = 1 + \left|g^{(1)}(t_1, t_2)\right|^2 \tag{A.72}$$

of the second-order correlation function. For thermal fields one finds $g^{(2)}(t, t) = 2$ indicating non-trivial correlations of the intensities. Interestingly, for a coherent light

[10] For the following discussion it is implicitly assumed, that all correlation functions are evaluated at a fixed position in space with $\boldsymbol{r}_1 = \boldsymbol{r}_2$.

field as produced by a laser for example, this enhancement of correlations disappears entirely with

$$g^{(2)}_{\text{coherent}}(t_1, t_2) = 1; \tag{A.73}$$

such a field is said to be *second order coherent*. Furthermore, the Hanbury Brown and Twiss correlation are also able to distinguish between classical and quantum light sources. For classical fields the second-order correlation function is supposed to be strictly greater or equal than one at a single time, $g^{(2)}(t, t) \geq 1$. This limitation, however, is weakened by quantum mechanical fields. In situations in which photons are sequentially emitted as for example fluorescent light from the decay of two-level atoms, the second order correlation functions may even reach the absolute minimum $g^{(2)}(t, t) \geq 0$.

A field that exhibits an enhancement or a reduction of intensity correlations at the same time is said to be *bunched* or *antibunched*, respectively. This terminology has its origin in experiments in which sequential streams of photons are measured. If the intensity correlations are enhanced the photons tend to clump together. In contrast, for $|g^{(2)}(t, t)| < 1$ a sequence of single photon detections reveals the tendency of photons to avoid each other. Owing to their bosonic exchange statistics, beams of photons naturally produce bunched statistics, but there are also situations in which photon beams appear to be antibunched. Such situations generically arise when beams of photons are sequentially emitted in processes in which the fermionic exchange statistics of electrons plays a predominant role, e.g., the fluorescence of two-level atoms.

In optical coherence theory this classification scheme of first and second order coherence can be generalized to nth order coherence. The normalized nth-order correlation function is defined as

$$g^{(n)}(x_1, \ldots, x_{2n}) = \frac{G^{(n)}(x_1, \ldots, x_{2n})}{\prod_{i=1}^{2n} \sqrt{G^{(1)}(x_i, x_i)}} \tag{A.74}$$

and a field is said to be nth order coherent if $\left|g^{(n)}(x_1, \ldots, x_{2n})\right| = 1$. For further reading about optical coherence theory, interference patterns and the Hanbury Brown and Twiss effect, see Loudon (1973); Mandel and Wolf (1995); Puri (2001); Walls and Milburn (2008).

A.3.3. Photon scattering: input output theory for cavities

Experimentally, it is often impossible to directly determine the statistical properties of a field inside a cavity. Instead, a scattering approach is pursued to reveal information about properties of the field inside the cavity. The basic principle of such a cavity scattering is illustrated in Fig. A.2: incoming radiation stimulates the cavity, interacts with the internal degrees of freedom, and gets scattered into one of the output channels modeled by waveguides (transmission lines).

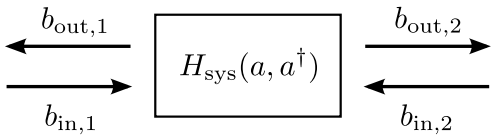

Fig. A.2.: Schematic illustration of the cavity scattering. Photons coming from two channels (transmission lines) $b_{\text{in},1}$ and $b_{\text{in},2}$ are scattered into the output modes $b_{\text{out},1}$ and $b_{\text{out},2}$ of the respective channels.

A coplanar stripline resonator naturally forms a two-sided cavity connected with two scattering channels $j = 1, 2$, but in principle nothing forbids to take an arbitrary amount of scattering channels into account. For the sake of simplicity, here only a single mode of the cavity field is considered. The cavity subsystem is then characterized by an Hamiltonian $H_{\text{sys}}(a, a^\dagger)$, which describes the dynamics of a single cavity mode with operators $a, a^\dagger$ and its potential interaction with additional degrees of freedom, e.g., a transmon qubit inside the cavity. In fact, for most applications of cQED the system Hamiltonian H_{sys} coincides with the dispersive Hamiltonian (2.76) describing the intertwined time evolution of a transmon qubit and the cavity field. However, with an eye on Ch. 5, it will be convenient to keep the discussion more general; the only relevant information here is the dependence of H_{sys} upon the cavity operators.

Processes, in which incident photons are fed into the cavity and re-emitted into one of the waveguides, are fully captured by the Hamiltonian

$$H_{\text{tot}} = H_{\text{sys}} + \sum_j \left(H_{\text{tl},j} + H_{\text{cp},j}\right). \tag{A.75}$$

Describing a directional motion, each waveguide (transmission line) j is considered to be described by a one-dimensional continuum of modes

$$H_{\text{tl},j} = \frac{1}{2\pi} \int \hbar\omega_k \, b_j^\dagger(k) b_j(k) \, \mathrm{d}k \tag{A.76}$$

as introduced in Sec. 2.2.4. According to (2.41), the coupling between each of these scattering channels and the cavity is given by

$$H_{\text{cp},j} = \frac{\mathrm{i}\hbar}{2\pi} \int_{\mathbb{R}} \sqrt{v_{\text{p}}\kappa_j} \left[a b_j^\dagger(k) - a^\dagger b_j(k)\right] \mathrm{d}k \tag{A.77}$$

where the channel-specific couplings κ_j characterize the degree of hybridization between the cavity and its environment. Due to these couplings, radiation leaks from the cavity into each connected channel thereby broadening the cavity frequency with a Lorentzian line shape.

Far apart from the cavity, i.e., for $|x| \to \infty$, the incoming and outgoing photons are freely propagating in the waveguides. This suggests the definition of the time-dependent input and output fields

$$b_{\text{in},j}(x,t) = \frac{\sqrt{v_{\text{p}}}}{2\pi} \int \mathrm{e}^{-\mathrm{i}[\omega_k(t+T)-kx]} \, b_{\text{in},j}(k) \, \mathrm{d}k, \tag{A.78a}$$

$$b_{\text{out},j}(x,t) = \frac{\sqrt{v_{\text{p}}}}{2\pi} \int \mathrm{e}^{-\mathrm{i}[\omega_k(t-T)-kx]} \, b_{\text{out},j}(k) \, \mathrm{d}k. \tag{A.78b}$$

In the remote past $t = -T$ (or the far future $t = T$), the operators $b_{\mathrm{in},j}(k) = b_j(k)|_{t=-T}$ (or $b_{\mathrm{out},j}(k) = b_j(-k)|_{t=T}$) describe non-interacting photon states—depending on the sign of k—either propagating towards the cavity or away from it. In other words, in the limit $T \to \infty$ these operators generate suitable sets of asymptotic scattering states for incoming and outgoing photons, cf. Fig. A.2. For simplicity, the incoming states of a transmission line are chosen to have positive wave number, whereas the outgoing states are labeled by negative wave numbers. Furthermore, the spatial coordinates will be omitted in the following. Only the point $x = 0$, where the transmission line is connected to the cavity, shall be considered instead.

In order to find the scattering amplitude of a photon to scatter from one channel to another, the full time evolution $\lim_{T\to\infty} U(T, -T)$ has to be evaluated. Therefore, one attempts to solve the Heisenberg equations of motion

$$\dot{b}_j = -\mathrm{i}\omega_k b_j(k) + \sqrt{v_\mathrm{p}\kappa_j}\, a_j, \tag{A.79a}$$

$$\dot{a} = \frac{\mathrm{i}}{\hbar}[H_\mathrm{sys}, a_j] - \frac{\sqrt{v_\mathrm{p}\kappa_j}}{2\pi}\int b_j(k)\,\mathrm{d}k. \tag{A.79b}$$

These equations can be partially integrated by introducing the formal solution

$$b_j(k) = \mathrm{e}^{-\mathrm{i}\omega_k(t-t_0)} b_j(k)\big|_{t_0} + \sqrt{v_\mathrm{p}\kappa_j}\int_{t_0}^{t} \mathrm{e}^{-\mathrm{i}\omega_k(t-t')} a(t')\,\mathrm{d}t'. \tag{A.80}$$

In complete analogy to the procedure in Sec. 2.2.3, the effective equation of motion is found to be the quantum Langevin equation. To do so, one substitutes (A.80) into (A.79b) and chooses the boundary conditions to be either specified at $t_0 = -T$ or $t_0 = T$. Then, by performing the limit $T \to \infty$ and assuming all couplings κ_j to be frequency-independent, one finds the two Langevin equations:

$$\dot{a} = \frac{\mathrm{i}}{\hbar}[H_\mathrm{sys}, a] - \sum_j \left(\sqrt{\kappa_j}\, b_\mathrm{in}(t) + \frac{\kappa_j}{2} a\right), \tag{A.81a}$$

$$\dot{a} = \frac{\mathrm{i}}{\hbar}[H_\mathrm{sys}, a] - \sum_j \left(\sqrt{\kappa_j}\, b_\mathrm{out}(t) - \frac{\kappa_j}{2} a\right), \tag{A.81b}$$

both correctly describing the dynamics of the cavity mode. While the first equation is specified by an *initial condition* at $t_0 = -T$, the second equation describes the propagation of the system as specified by a *final condition* at $t_0 = T$. As both pictures have to be equivalent for a consistent scattering theory, the input-output boundary conditions

$$b_{\mathrm{out},j}(t) - b_{\mathrm{in},j}(t) = \sqrt{\kappa_j}\, a(t) \tag{A.82}$$

are found by combining both equations (A.81a) and (A.81b). Together with one of the above equations (A.81), the boundary conditions (A.82) relate n incoming field

modes to n outcoming field modes in form of the unitary *scattering matrix*

$$\begin{pmatrix} b_{\text{out},1} \\ \vdots \\ b_{\text{out},n} \end{pmatrix} = \begin{pmatrix} r_{11} & \dots & t_{1n} \\ \vdots & \ddots & \vdots \\ t_{n1} & \dots & r_{nn} \end{pmatrix} \begin{pmatrix} b_{\text{in},1} \\ \vdots \\ b_{\text{in},n} \end{pmatrix}. \tag{A.83}$$

The matrix elements characterize the frequency-dependent reflection and transmission coefficients r_{ii} and t_{ij}. For a specific H_{sys}, the reflection and transmission coefficients can be found by explicitly solving the quantum Langevin and using the generic boundary conditions, see Gardiner and Collett (1985); Walls and Milburn (2008).

A.3.4. Homodyne detection

For the homodyne measurement scheme the signal to be detected b is mixed with a strong harmonic signal b_{lo}—the *local oscillator*. By mixing these two fields the measurement becomes phase-sensitive with respect to the measurement signal b. Additionally, choosing the frequency of the local oscillator such that it coincides with the carrier frequency of b, the mixed signal gets effectively down-converted to zero frequency.[11)] Subsequently, the mixed signal is measured by a photodetector. Here it is sufficient to outline the concept of a homodyne measurement schematically as depicted in Fig. A.3.

Suppose the local oscillator is prepared to be in a coherent state with large amplitude $|\alpha_{\text{lo}}|\mathrm{e}^{\mathrm{i}\phi_{\text{lo}}}$ compared to the measurement signal b. At the beam splitter both fields b and b_{lo} are combined into the mixed output modes to be measured

$$\begin{aligned} c &= \sqrt{R}\, b + \mathrm{i}\sqrt{1-R}\, b_{\text{lo}}, \\ d &= -\mathrm{i}\sqrt{1-R}\, b + \sqrt{R}\, b_{\text{lo}}. \end{aligned}$$

Here it has been assumed that the beam splitter causes a relative phase shift of $\frac{\pi}{2}$ between the two modes b_{lo}, b and $R < 1$ is the reflection coefficient of the beamsplitter. Then, the photodetector records the intensity[12)] of one of the beam splitter's outputs, either c or d (the homodyne measurement signals). If c is measured, the photodetector records the field intensity

$$\begin{aligned} \langle I(t)\rangle &\propto \langle c^\dagger c\rangle \\ &= (1-R)|\alpha_{\text{lo}}|^2 + R\langle b^\dagger b\rangle + \sqrt{R(1-R)}\,|\alpha_{\text{lo}}|\,\langle X_{\phi_{\text{lo}}+\pi/2}(t)\rangle. \end{aligned} \tag{A.84}$$

Assuming $R \ll 1$ to be small, the measurement record essentially consists of the bare intensity of the local oscillator and a term that is proportional to the expectation value of the quadrature operator

$$X_\theta = \mathrm{e}^{\mathrm{i}(\omega t-\theta)} b + \mathrm{e}^{-\mathrm{i}(\omega t-\theta)} b^\dagger. \tag{A.85}$$

[11)] If the frequencies are different, the measurement is called a *heterodyne measurement* .
[12)] Cf. Eq. (A.35) in Sec. A.2.4.

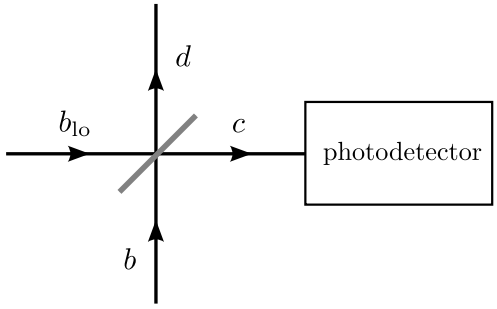

Fig. A.3.: Homodyne detection scheme in quantum optical language. At the beam splitter the measurement signal b is mixed with the local oscillator b_{lo} which is prepared in a coherent state. The beam splitter introduces the two output modes c, d where the intensity of one of these (here c) is measured by a photodetector. Choosing the local oscillator frequency to be equal to the carrier frequency of b, the signal is down-converted to zero frequency.

By tuning ϕ_{lo}, the measurement quadrature $X_{\phi_{\mathrm{lo}}+\pi/2}$ may be rotated such that the measurement signature $\langle X_{\phi_{\mathrm{lo}}+\pi/2}\rangle$ is maximal indicating the alignment of the measurement quadrature $X_{\phi_{\mathrm{lo}}+\pi/2}$ with the direction of $\langle b\rangle$ in the plane of quadratures. Then, at this point the sought-after phase of b coincides with $\phi_{\mathrm{lo}}+\pi/2$.

In practice, the measured signal is always accompanied by noise. Therefore, the signature of $\langle X_{\phi_{\mathrm{lo}}+\pi/2}\rangle$ has to be discriminated from the background fluctuations. If the measurement signal is in a single-frequency coherent state with amplitude $|\alpha_{\mathrm{sig}}|\mathrm{e}^{\mathrm{i}\phi}$, the signal-to-noise ratio can be explicitly determined: considering only shot noise, which is primarily induced by quantum fluctuations of the local oscillator,

$$\begin{aligned}
&\int_0^T\int_0^T \langle\!\langle I(t)I(t')\rangle\!\rangle \,\mathrm{d}t'\mathrm{d}t \\
&\propto \int_0^T\int_0^T \left\langle a^\dagger(t)a(t)a^\dagger(t')a(t')\right\rangle \mathrm{d}t'\mathrm{d}t - \left[\int_0^T \left\langle a^\dagger(t)a(t)\right\rangle \mathrm{d}t\right]^2 \\
&= \int_0^T\int_0^T \left\langle a^\dagger(t)a^\dagger(t')a(t)a(t')\right\rangle \mathrm{d}t'\mathrm{d}t + \int_0^T \left\langle a^\dagger(t)a(t)\right\rangle \mathrm{d}t - \left[(1-R)|\alpha_{\mathrm{lo}}|^2T\right]^2 \\
&= (1-R)|\alpha_{\mathrm{lo}}|^2T
\end{aligned} \tag{A.86}$$

the signal-to-noise ratio becomes

$$\begin{aligned}
\mathrm{SNR} &= \left[\sqrt{R(1-R)}\,|\alpha_{\mathrm{lo}}|\int_0^T \langle X_{\phi_{\mathrm{lo}}+\pi/2}\rangle \mathrm{d}t\right]^2 \Big/ \int_0^T\int_0^T \langle\!\langle I(t)I(t')\rangle\!\rangle \,\mathrm{d}t'\mathrm{d}t \\
&= 4R|\alpha_{\mathrm{sig}}|^2\cos^2(\phi_{\mathrm{lo}}+\pi/2-\phi)\,T.
\end{aligned} \tag{A.87}$$

The signal-to-noise ratio increases linearly with the measurement time T demonstrating that the measurement resolution increases in time as expected for shot noise. Furthermore, the proportionality factor $4R|\alpha_{\mathrm{sig}}|^2\cos^2(\phi_{\mathrm{lo}}+\pi/2-\phi)$ depends upon the signal strength $|\alpha_{\mathrm{sig}}|$ as well as upon its phase ϕ. This illustrates the phase-sensitivity of the homodyne detection scheme: the homodyne measurement is most

efficient if the measurement quadrature is aligned with the complex amplitude of the signal $\phi = \phi_{\mathrm{lo}} + \pi/2$.

In the microwave regime there are no beam splitters and photodetectors. Instead, beam splitters are implemented by directional couplers and the photodetectors are replaced by voltage probes measuring the voltage to ground of the stripline.

A.4. Gaussian units of electromagnetism

The definition of current, inductance, and magnetic flux are chosen such that $\dot{Q} = I$ and the energy of an inductor becomes $E = LI^2/2c^2 = \Phi^2/2L$.

Tab. A.1.: Conversion between Gaussian and SI units.

Quantity	Gaussian	SI
Speed of light	c	$\frac{1}{\sqrt{\varepsilon_0\mu_0}}$
Charge density (or charge)	ρ (or Q)	$\frac{1}{\sqrt{4\pi\varepsilon_0}}\rho$ (or Q)
Current density (or current)	$\boldsymbol{j}$ (or I)	$\frac{1}{\sqrt{4\pi\varepsilon_0}}\boldsymbol{j}$ (or I)
Magnetic flux density	$\boldsymbol{B}$	$\sqrt{\frac{4\pi}{\mu_0}}\boldsymbol{B}$
Magnetic field	$\boldsymbol{H}$	$\sqrt{4\pi\mu_0}\boldsymbol{H}$
Electric field (or voltage)	$\boldsymbol{E}$ (or V)	$\sqrt{4\pi\varepsilon_0}\boldsymbol{E}$ (or V)
Electric displacement	$\boldsymbol{D}$	$\sqrt{\frac{4\pi}{\varepsilon_0}}\boldsymbol{D}$
Magnetic flux (node flux)	Φ	$\sqrt{\frac{4\pi}{\mu_0}}\Phi$
Capacitance	C	$\frac{1}{4\pi\varepsilon_0}C$
Resistance (or impedance)	R (or Z)	$4\pi\varepsilon_0 R$ (or Z)
Inductance	L	$\frac{4\pi}{\mu_0}L$

Bibliography

Adagideli, İ., Wimmer, M., and Teker, A., 2014: *Effects of Electron Scattering on the Topological Properties of Nanowires: Majorana Fermions from Disorder and Superlattices*, Phys. Rev. B **89**, 144506.

Ahlbrecht, A., Georgiev, L. S., and Werner, R. F., 2009: *Implementation of Clifford Gates in the Ising-Anyon Topological Quantum Computer*, Phys. Rev. A **79**, 032311.

Alicea, J., 2010: *Majorana Fermions in a Tunable Semiconductor Device*, Phys. Rev. B **81**, 125318.

Alicea, J., 2012: *New Directions in the Pursuit of Majorana Fermions in Solid State Systems*, Rep. Prog. Phys. **75**, 076501.

Alicea, J., Oreg, Y., Refael, G., von Oppen, F., and Fisher, M. P. A., 2011: *Non-Abelian Statistics and Topological Quantum Information Processing in 1D Wire Networks*, Nat Phys **7**, 412–417.

Altland, A. and Zirnbauer, M. R., 1997: *Nonstandard Symmetry Classes in Mesoscopic Normal-Superconducting Hybrid Structures*, Phys. Rev. B **55**, 1142–1161.

An, K., Childs, J. J., Dasari, R. R., and Feld, M. S., 1994: *Microlaser: A laser with One Atom in an Optical Resonator*, Phys. Rev. Lett. **73**, 3375–3378.

Anderson, P. W., 1958: *Absence of Diffusion in Certain Random Lattices*, Phys. Rev. **109**, 1492–1505.

Anderson, P. W. and Morel, P., 1960: *Generalized Bardeen-Cooper-Schrieffer States and Aligned Orbital Angular Momentum in the Proposed Low-Temperature Phase of Liquid* He^3, Phys. Rev. Lett. **5**, 136–138.

Aspect, A., Dalibard, J., and Roger, G., 1982: *Experimental Test of Bell's Inequalities Using Time-Varying Analyzers*, Phys. Rev. Lett. **49**, 1804–1807.

Aspect, A., Grangier, P., and Roger, G., 1981: *Experimental Tests of Realistic Local Theories via Bell's Theorem*, Phys. Rev. Lett. **47**, 460–463.

Aste, A., 2010: *A Direct Road to Majorana Fields*, Symmetry **2**, 1776–1809.

Badiane, D. M., Houzet, M., and Meyer, J. S., 2011: *Nonequilibrium Josephson Effect through Helical Edge States*, Phys. Rev. Lett. **107**, 177002.

Balian, R. and Werthamer, N. R., 1963: *Superconductivity with Pairs in a Relative p Wave*, Phys. Rev. **131**, 1553–1564.

Baskaran, G., 1996: *Why is* Sr_2RuO_4 *Not a High Tc Superconductor? Electron Correlation, Hund's Coupling and p-Wave Instability*, Physica B **223–224**, 490 – 495.

Beck, C., 2013: *Possible Resonance Effect of Axionic Dark Matter in Josephson Junctions*, Phys. Rev. Lett. **111**, 231801.

Beenakker, C. W. J., 2013: *Search for Majorana Fermions in Superconductors*, Annu. Rev. Con. Mat. Phys. **4**, 113.

Beenakker, C. W. J., DiVincenzo, D. P., Emary, C., and Kindermann, M., 2004: *Charge Detection Enables Free-Electron Quantum Computation*, Phys. Rev. Lett. **93**, 020501.

Bell, J. S., 1964: *On the Einstein Podolsky Rosen Paradox*, Physics **1**, 195–200.

Bender, C. M. and Orszag, S. A., 1978: *Advanced Mathematical Methods for Scientists and Engineers* (McGraw-Hill, New York).

Bennett, C. H., Brassard, G., Crépeau, C., Jozsa, R., Peres, A., and Wootters, W. K., 1993: *Teleporting an Unknown Quantum State via Dual Classical and Einstein-Podolsky-Rosen Channels*, Phys. Rev. Lett. **70**, 1895–1899.

Berman, P. R. (Ed.), 1994: *Cavity Quantum Electrodynamics* (Academic Press, Boston).

Bernien, H., *et al.*, 2013: *Heralded Entanglement between Solid-State Qubits Separated by Three Metres*, Nature **497**, 86–90.

Bishop, L. S., *et al.*, 2009: *Proposal for Generating and Detecting Multi-Qubit GHZ States in Circuit QED*, New J. Phys. **11**, 073040.

Blais, A., Huang, R.-S., Wallraff, A., Girvin, S. M., and Schoelkopf, R. J., 2004: *Cavity Quantum Electrodynamics for Superconducting Electrical Circuits: An Architecture for Quantum Computation*, Phys. Rev. A **69**, 062320.

Blanch, G., 1970: *Mathieu Functions*, in *Handbook of Mathematical Functions*, edited by Abramowitz, M. and Stegun, I. (Dover Publications, New York), 7th ed., Chap. 20.

Boissonneault, M., Gambetta, J. M., and Blais, A., 2009: *Dispersive Regime of Circuit QED: Photon-Dependent Qubit Dephasing and Relaxation Rates*, Phys. Rev. A **79**, 013819.

Bolech, C. J. and Demler, E., 2007: *Observing Majorana Bound States in p-Wave Superconductors Using Noise Measurements in Tunneling Experiments*, Phys. Rev. Lett. **98**, 237002.

Bonderson, P., Kitaev, A., and Shtengel, K., 2006: *Detecting Non-Abelian Statistics in the $\nu = 5/2$ Fractional Quantum Hall State*, Phys. Rev. Lett. **96**, 016803.

Bouchiat, V., Vion, D., Joyez, P., Esteve, D., and Devoret, M. H., 1998: *Quantum Coherence with a Single Cooper Pair*, Physica Scripta **1998**, 165.

Bozyigit, D., *et al.*, 2011: *Antibunching of Microwave-Frequency Photons Observed in Correlation Measurements Using Linear Detectors*, Nat. Phys. **7**, 154–158.

Braginsky, V. B. and Khalili, F. Y., 1992: *Quantum Measurement* (Cambridge University Press, Cambridge).

Braginsky, V. B., Vorontsov, Y. I., and Thorne, K. S., 1980: *Quantum Nondemolition Measurements*, Science **209**, 547–557.

Brannen, E. and Ferguson, H. I. S., 1956: *The Question of Correlation between Photons in Coherent Light Rays*, Nature **178**, 481.

Bravyi, S. and Kitaev, A. Yu., 2005: *Universal Quantum Computation with Ideal Clifford Gates and Noisy Ancillas*, Phys. Rev. A **71**, 022316.

Briegel, H.-J., Dür, W., Cirac, J. I., and Zoller, P., 1998: *Quantum Repeaters: The Role of Imperfect Local Operations in Quantum Communication*, Phys. Rev. Lett. **81**, 5932–5935.

Brune, M., Hagley, E., Dreyer, J., Maître, X., Maali, A., Wunderlich, C., Raimond, J. M., and Haroche, S., 1996: *Observing the Progressive Decoherence of the "Meter" in a Quantum Measurement*, Phys. Rev. Lett. **77**, 4887–4890.

Brune, M., Haroche, S., Raimond, J. M., Davidovich, L., and Zagury, N., 1992: *Manipulation of Photons in a Cavity by Dispersive Atom-Field Coupling: Quantum-Nondemolition Measurements and Generation of "Schrödinger Cat" States*, Phys. Rev. A **45**, 5193–5214.

Budich, J. C., Walter, S., and Trauzettel, B., 2012: *Failure of Protection of Majorana Based Qubits against Decoherence*, Phys. Rev. B **85**, 121405.

Cabrillo, C., Cirac, J. I., García-Fernández, P., and Zoller, P., 1999: *Creation of Entangled States of Distant Atoms by Interference*, Phys. Rev. A **59**, 1025–1033.

Caldeira, A. and Leggett, A., 1983: *Quantum Tunnelling in a Dissipative System*, Annals of Physics **149**, 374 – 456.

Caldeira, A. O. and Leggett, A. J., 1981: *Influence of Dissipation on Quantum Tunneling in Macroscopic Systems*, Phys. Rev. Lett. **46**, 211–214.

Carruthers, P. and Nieto, M. M., 1968: *Phase and Angle Variables in Quantum Mechanics*, Rev. Mod. Phys. **40**, 411.

Caves, C. M., 1981: *Quantum-Mechanical Noise in an Interferometer*, Phys. Rev. D **23**, 1693–1708.

Chamon, C., Jackiw, R., Nishida, Y., Pi, S.-Y., and Santos, L., 2010: *Quantizing Majorana Fermions in a Superconductor*, Phys. Rev. B **81**, 224515.

Chen, Y.-F., Hover, D., Sendelbach, S., Maurer, L., Merkel, S. T., Pritchett, E. J., Wilhelm, F. K., and McDermott, R., 2011: *Microwave Photon Counter Based on Josephson Junctions*, Phys. Rev. Lett. **107**, 217401.

Cheng, M., Lutchyn, R. M., and Das Sarma, S., 2012: *Topological Protection of Majorana Qubits*, Phys. Rev. B **85**, 165124.

Chou, C. W., de Riedmatten, H., Felinto, D., Polyakov, S. V., van Enk, S. J., and Kimble, H. J., 2005: *Measurement-Induced Entanglement for Excitation Stored in Remote Atomic Ensembles*, Nature **438**, 828–832.

Churchill, H. O. H., Fatemi, V., Grove-Rasmussen, K., Deng, M. T., Caroff, P., Xu, H. Q., and Marcus, C. M., 2013: *Superconductor-Nanowire Devices from Tunneling to the Multichannel Regime: Zero-Bias Oscillations and Magnetoconductance Crossover*, Phys. Rev. B **87**, 241401.

Clarke, D. J., Sau, J. D., and Tewari, S., 2011: *Majorana Fermion Exchange in Quasi-One-Dimensional Networks*, Phys. Rev. B **84**, 035120.

Clarke, J., Cleland, A. N., Devoret, M. H., Esteve, D., and Martinis, J. M., 1988: *Quantum Mechanics of a Macroscopic Variable: The Phase Difference of a Josephson Junction*, Science **26**, 992–997.

Clerk, A. A., Devoret, M. H., Girvin, S. M., Marquardt, F., and Schoelkopf, R. J., 2010: *Introduction to Quantum Noise, Measurement, and Amplification*, Rev. Mod. Phys. **82**, 1155–1208.

Clerk, A. A., Girvin, S. M., and Stone, A. D., 2003: *Quantum-Limited Measurement and Information in Mesoscopic Detectors*, Phys. Rev. B **67**, 165324.

Cohen, D., 1972: *Magnetoencephalography: Detection of the Brain's Electrical Activity with a Superconducting Magnetometer*, Science **11**, 664–666.

Cottet, A., 2002: *Implementation of a Quantum Bit in a Superconductor* (PhD thesis, University of Paris).

Cottet, A., Kontos, T., and Douçot, B., 2013: *Squeezing Light with Majorana Fermions*, Phys. Rev. B **88**, 195415.

da Silva, M. P., Bozyigit, D., Wallraff, A., and Blais, A., 2010: *Schemes for the Observation of Photon Correlation Functions in Circuit QED with Linear Detectors*, Phys. Rev. A **82**, 043804.

Das, A., Ronen, Y., Most, Y., Oreg, Y., Heiblum, M., and Shtrikman, H., 2012: *Zero-Bias Peaks and Splitting in an Al-InAs Nanowire Topological Superconductor as a Signature of Majorana Fermions*, Nature Phys. **8**, 887.

Das Sarma, S., Freedman, M., and Nayak, C., 2005: *Topologically Protected Qubits from a Possible Non-Abelian Fractional Quantum Hall State*, Phys. Rev. Lett. **94**, 166802.

De Franceschi, S., Kouwenhoven, L., Schönenberger, C., and Wernsdorfer, W., 2010: *Hybrid Superconductor-Quantum Dot Devices*, Nature Nanotech. **5**, 703.

de Lange, G., van Heck, B., Bruno, A., van Woerkom, D. J., Geresdi, A., Plissard, S. R., Bakkers, E. P. A. M., Akhmerov, A. R., and DiCarlo, L., 2015: *Realization of Microwave Quantum Circuits Using Hybrid Superconducting-Semiconducting Nanowire Josephson Elements*, Phys. Rev. Lett. **115**, 127002.

Deng, M. T., Yu, C. L., Huang, G. Y., Larsson, M., Caroff, P., and Xu, H. Q., 2012: *Anomalous Zero-Bias Conductance Peak in a Nb–InSb Nanowire–Nb Hybrid Device*, Nano Lett. **12**, 6414.

Devoret, M. H., Martinis, J. M., and Clarke, J., 1985: *Measurements of Macroscopic Quantum Tunneling out of the Zero-Voltage State of a Current-Biased Josephson Junction*, Phys. Rev. Lett. **55**, 1908–1911.

Devoret, M. H. and Schoelkopf, R. J., 2013: *Superconducting Circuits for Quantum Information: An Outlook*, Science **339**, 1169–1174.

Dirac, P. A. M., 1927: *The Quantum Theory of the Emission and Absorption of Radiation*, Proc. Royal Soc. (London) A **114**, 243–265.

Domínguez, F., Hassler, F., and Platero, G., 2012: *Dynamical Detection of Majorana Fermions in Current-Biased Nanowires*, Phys. Rev. B **86**, 140503.

Eichler, C., Lang, C., Fink, J. M., Govenius, J., Filipp, S., and Wallraff, A., 2012: *Observation of Entanglement between Itinerant Microwave Photons and a Superconducting Qubit*, Phys. Rev. Lett. **109**, 240501.

Einstein, A., Podolsky, B., and Rosen, N., 1935: *Can Quantum-Mechanical Description of Physical Reality Be Considered Complete?*, Phys. Rev. **47**, 777–780.

Ekert, A. K., 1991: *Quantum Cryptography Based on Bell's Theorem*, Phys. Rev. Lett. **67**, 661–663.

Elliott, S. R. and Franz, M., 2015: *Colloquium : Majorana Fermions in Nuclear, Particle, and Solid-State Physics*, Rev. Mod. Phys. **87**, 137–163.

Everitt, C. W. F., *et al.*, 2011: *Gravity Probe B: Final Results of a Space Experiment to Test General Relativity*, Phys. Rev. Lett. **106**, 221101.

Feynman, R. P. and Vernon, F. L., 1963: *The Theory of a General Quantum System Interacting with a Linear Dissipative System*, Annals of Physics **24**, 173.

Finck, A. D. K., Van Harlingen, D. J., Mohseni, P. K., Jung, K., and Li, X., 2013: *Anomalous Modulation of a Zero-Bias Peak in a Hybrid Nanowire-Superconductor Device*, Phys. Rev. Lett. **110**, 126406.

Flensberg, K., 2010: *Tunneling Characteristics of a Chain of Majorana Bound States*, Phys. Rev. B **82**, 180516.

Ford, G. W., Kac, M., and Mazur, P., 1965: *Statistical Mechanics of Assemblies of Coupled Oscillators*, J. Math. Phys. **6**, 504.

Franz, M., 2013: *Majorana's Wires*, Nature Nanotech. **8**, 149.

Freedman, S. J. and Clauser, J. F., 1972: *Experimental Test of Local Hidden-Variable Theories*, Phys. Rev. Lett. **28**, 938–941.

Fu, L., 2010: *Electron Teleportation via Majorana Bound States in a Mesoscopic Superconductor*, Phys. Rev. Lett. **104**, 056402.

Fu, L. and Kane, C. L., 2008: *Superconducting Proximity Effect and Majorana Fermions at the Surface of a Topological Insulator*, Phys. Rev. Lett. **100**, 096407.

Fu, L. and Kane, C. L., 2009: *Josephson Current and Noise at a Superconductor/Quantum-Spin-Hall-Insulator/Superconductor Junction*, Phys. Rev. B **79**, 161408.

Fulton, W. and Harris, J., 1991: *Representation Theory: A First Course* (Springer-Verlag, Berlin).

Gao, J., Daal, M., Vayonakis, A., Kumar, S., Zmuidzinas, J., Sadoulet, B., Mazin, B. A., Day, P. K., and Leduc, H. G., 2008: *Experimental Evidence for a Surface Distribution of Two-Level Systems in Superconducting Lithographed Microwave Resonators*, Appl. Phys. Lett. **92**, 152505.

Gardiner, C., 2009: *Stochastic Methods: A Handbook for the Natural and Social Sciences* (Springer-Verlag, Berlin), 4th ed.

Gardiner, C. W. and Collett, M. J., 1985: *Input and Output in Damped Quantum Systems: Quantum Stochastic Differential Equations and the Master Equation*, Phys. Rev. A **31**, 3761.

Gardiner, C. W. and Zoller, P., 2004: *Quantum Noise* (Springer-Verlag, Berlin), 3rd ed.

Ginossar, E. and Grosfeld, E., 2014: *Microwave Transitions as a Signature of Coherent Parity Mixing Effects in the Majorana-Transmon Qubit*, Nat. Commun. **5**, 4772.

Glauber, R. J., 1963: *Coherent and Incoherent States of the Radiation Field*, Phys. Rev. **131**, 2766–2788.

Gleyzes, S., Kuhr, S., Guerlin, C., Bernu, J., Deleglise, S., Busk Hoff, U., Brune, M., Raimond, J.-M., and Haroche, S., 2007: *Quantum Jumps of Light Recording the Birth and Death of a Photon in a Cavity*, Nature **446**, 297–300.

Godschalk, F., Hassler, F., and Nazarov, Yu. V., 2011: *Proposal for an Optical Laser Producing Light at Half the Josephson Frequency*, Phys. Rev. Lett. **107**, 073901.

Godschalk, F. and Nazarov, Yu. V., 2013a: *Lasing at Half the Josephson Frequency with Exponentially Long Coherence Times*, Phys. Rev. B **87**, 094511.

Godschalk, F. and Nazarov, Yu. V., 2013b: *Optical Stabilization of Voltage Fluctuations in Half-Josephson Lasers*, Europhys. Lett. **103**, 28005.

Govia, L. C. G., Pritchett, E. J., Merkel, S. T., Pineau, D., and Wilhelm, F. K., 2012: *Theory of Josephson Photomultipliers: Optimal Working Conditions and Back Action*, Phys. Rev. A **86**, 032311.

Greiter, M., Wen, X.-G., and Wilczek, F., 1992: *Paired Hall States*, Nucl. Phys. B **374**, 567–614.

Grifoni, M. and Hänggi, P., 1998: *Driven Quantum Tunneling*, Physics Reports **304**, 229–354.

Guerlin, C., Bernu, J., Deleglise, S., Sayrin, C., Gleyzes, S., Kuhr, S., Brune, M., Raimond, J.-M., and Haroche, S., 2007: *Progressive Field-State Collapse and Quantum Non-Demolition Photon Counting*, Nature **448**, 889–893.

Haack, G., Förster, H., and Büttiker, M., 2010: *Parity Detection and Entanglement with a Mach-Zehnder Interferometer*, Phys. Rev. B **82**, 155303.

Hagley, E., Maître, X., Nogues, G., Wunderlich, C., Brune, M., Raimond, J. M., and Haroche, S., 1997: *Generation of Einstein-Podolsky-Rosen Pairs of Atoms*, Phys. Rev. Lett. **79**, 1–5.

Hanbury Brown, R. and Twiss, R. Q., 1956a: *Correlation between Photons in Two Coherent Beams of Light*, Nature **177**, 27 – 29.

Hanbury Brown, R. and Twiss, R. Q., 1956b: *A Test of a New Type of Stellar Interferometer on Sirius*, Nature **178**, 1046 – 1048.

Hasan, M. Z. and Kane, C. L., 2010: *Colloquium : Topological Insulators*, Rev. Mod. Phys. **82**, 3045–3067.

Hassler, F., 2013: *Majorana Qubits*, in *Lecture Notes of the 44th IFF Spring School: Quantum Information Processing*, edited by DiVincenzo, D. P. (Forschungszentrum Jülich GmbH), Chap. B 2.

Hassler, F., Akhmerov, A. R., and Beenakker, C. W. J., 2011: *The Top-Transmon: A Hybrid Superconducting Qubit for Parity-Protected Quantum Computation*, New J. Phys. **13**, 095004.

Hassler, F., Akhmerov, A. R., Hou, C.-Y., and Beenakker, C. W. J., 2010: *Anyonic Interferometry without Anyons: How a Flux Qubit Can Read Out a Topological Qubit*, New J. Phys. **12**, 125002.

Hawking, S. W., 1974: *Black Hole Explosions?*, Nature **248**, 30.

Helmer, F. and Marquardt, F., 2009: *Measurement-Based Synthesis of Multiqubit Entangled States in Superconducting Cavity QED*, Phys. Rev. A **79**, 052328.

Hofmann, J., Krug, M., Ortegel, N., Gérard, L., Weber, M., Rosenfeld, W., and Weinfurter, H., 2012: *Heralded Entanglement between Widely Separated Atoms*, Science **337**, 72–75.

Horodecki, R., Horodecki, P., Horodecki, M., and Horodecki, K., 2009: *Quantum Entanglement*, Rev. Mod. Phys. **81**, 865–942.

Houck, A. A., *et al.*, 2007: *Generating Single Microwave Photons in a Circuit*, Nature **449**, 328–331.

Houzet, M., Meyer, J. S., Badiane, D. M., and Glazman, L. I., 2013: *Dynamics of Majorana States in a Topological Josephson Junction*, Phys. Rev. Lett. **111**, 046401.

Huang, Y. P. and Moore, M. G., 2008: *On-Demand Generation of Entanglement of Atomic Qubits via Optical Interferometry*, Phys. Rev. A **77**, 032349.

Hutchison, C. L., Gambetta, J. M., , Blais, A., and Wilhelm, F. K., 2009: *Quantum Trajectory Equation for Multiple Qubits in Circuit QED: Generating Entanglement by Measurement*, Can. J. Phys. **87**, 225–231.

Ithier, G., *et al.*, 2005: *Decoherence in a Superconducting Quantum Bit Circuit*, Phys. Rev. B **72**, 134519.

Ivanov, D. A., 2001: *Non-Abelian Statistics of Half-Quantum Vortices in p-Wave Superconductors*, Phys. Rev. Lett. **86**, 268–271.

Jackiw, R. and Rebbi, C., 1976: *Solitons with Fermion Number* 1/2, Phys. Rev. D **13**, 3398–3409.

Jackson, J. D., 1999: *Classical Electrodynamics* (Wiley, New York), 3rd ed.

Jaynes, E. and Cummings, F., 1963: *Comparison of Quantum and Semiclassical Radiation Theories with Application to the Beam Maser*, Proc. IEEE **51**, 89–109.

Jiang, L., Kane, C. L., and Preskill, J., 2011a: *Interface between Topological and Superconducting Qubits*, Phys. Rev. Lett. **106**, 130504.

Jiang, L., Pekker, D., Alicea, J., Refael, G., Oreg, Y., and von Oppen, F., 2011b: *Unconventional Josephson Signatures of Majorana Bound States*, Phys. Rev. Lett. **107**, 236401.

Josephson, B., 1962: *Possible New Effects in Superconductive Tunnelling*, Physics Letters **1**, 251 – 253.

Kells, G., Meidan, D., and Brouwer, P. W., 2012: *Low-Energy Subgap States in Multichannel p-Wave Superconducting Wires*, Phys. Rev. B **85**, 060507.

Kimble, H. J., 1998: *Strong Interactions of Single Atoms and Photons in Cavity QED*, Physica Scripta **1998**, 127.

Kitaev, A. Yu., 2001: *Unpaired Majorana Fermions in Quantum Wires*, Phys.-Usp. **44**, 131.

Kitaev, A. Yu., 2003: *Fault-Tolerant Quantum Computation by Anyons*, Ann. Phys. (NY) **303**, 2.

Kitaev, A. Yu., 2009: *Periodic Table for Topological Insulators and Superconductors*, AIP Conference Proceedings **1134**, 22–30.

Koch, J., Manucharyan, V., Devoret, M. H., and Glazman, L. I., 2009: *Charging Effects in the Inductively Shunted Josephson Junction*, Phys. Rev. Lett. **103**, 217004.

Koch, J., Yu, T. M., Gambetta, J., Houck, A. A., Schuster, D. I., Majer, J., Blais, A., Devoret, M. H., Girvin, S. M., and Schoelkopf, R. J., 2007: *Charge-Insensitive Qubit Design Derived from the Cooper Pair Box*, Phys. Rev. A **76**, 042319.

Konschelle, F. and Hassler, F., 2013: *Effects of Nonequilibrium Noise on a Quantum Memory Encoded in Majorana Zero Modes*, Phys. Rev. B **88**, 075431.

Kwon, H.-J., Sengupta, K., and Yakovenko, V. M., 2004: *Fractional ac Josephson Effect in p- and d-Wave Superconductors*, Eur. Phys. J. B **37**, 349.

Lalumière, K., Gambetta, J. M., and Blais, A., 2010: *Tunable Joint Measurements in the Dispersive Regime of Cavity QED*, Phys. Rev. A **81**, 040301.

Landau, L. D. and Lifshitz, E. M., 2009: *Klassische Feldtheorie*, Vol. 2 of *Lehrbuch der Theoretischen Physik* (Verlag Harri Deutsch, Frankfurt am Main), 12th ed.

Landau, L. D. and Lifshitz, E. M., 2012: *Quantenmechanik*, Vol. 3 of *Lehrbuch der Theoretischen Physik* (Verlag Harri Deutsch, Frankfurt am Main), 9th ed.

Langenberg, D. N., Scalapino, D. J., Taylor, B. N., and Eck, R. E., 1965: *Investigation of Microwave Radiation Emitted by Josephson Junctions*, Phys. Rev. Lett. **15**, 294.

Larsen, T. W., Petersson, K. D., Kuemmeth, F., Jespersen, T. S., Krogstrup, P., Nygård, J., and Marcus, C. M., 2015: *Semiconductor-Nanowire-Based Superconducting Qubit*, Phys. Rev. Lett. **115**, 127001.

Law, K. T., Lee, P. A., and Ng, T. K., 2009: *Majorana Fermion Induced Resonant Andreev Reflection*, Phys. Rev. Lett. **103**, 237001.

Lee, E. J. H., Jiang, X., Aguado, R., Katsaros, G., Lieber, C. M., and De Franceschi, S., 2012: *Zero-Bias Anomaly in a Nanowire Quantum Dot Coupled to Superconductors*, Phys. Rev. Lett. **109**, 186802.

Lee, P. A. and Scully, M. O., 1971: *Theory of Josephson Radiation. I. General Theory*, Phys. Rev. B **3**, 769.

Leggett, A. J., 1975: *A Theoretical Description of the New Phases of Liquid* ^{3}He, Rev. Mod. Phys. **47**, 331–414.

Leinaas, J. M. and Myrheim, J., 1977: *On the Theory of Identical Particles*, Nuovo Cimento Soc. Ital. Fis. B **37B**.

Loudon, R., 1973: *The Quantum Theory of Light* (Oxford University Press).

Lupascu, A., Saito, S., Picot, T., de Groot, P. C., Harmans, C. J. P. M., and Mooij, J. E., 2007: *Quantum Non-Demolition Measurement of a Superconducting Two-Level System*, Nat. Phys **3**, 119–125.

Lutchyn, R. M., Sau, J. D., and Das Sarma, S., 2010: *Majorana Fermions and a Topological Phase Transition in Semiconductor-Superconductor Heterostructures*, Phys. Rev. Lett. **105**, 077001.

Mackenzie, A. P. and Maeno, Y., 2003: *The Superconductivity of* Sr_2RuO_4 *and the Physics of Spin-Triplet Pairing*, Rev. Mod. Phys. **75**, 657–712.

Maeno, Y., Hashimoto, H., Yoshida, K., Nishizaki, S., Fujita, T., Bednorz, J. G., and Lichtenberg, F., 1994: *Superconductivity in a Layered Perovskite without Copper*, Nature **372**, 532–534.

Maeno, Y., Rice, T. M., and Sigrist, M., 2001: *The Intriguing Superconductivity of Strontium Ruthenate*, Physics Today **54**, 42.

Magalinskij, V. B., 1959: *Dynamical Model in the Theory of the Brownian Motion*, Zh. Eksperim. i Teor. Fiz. **36**, 1942.

Mandel, L., 1958: *Fluctuations of Photon Beams and Their Correlations*, Proceedings of the Physical Society **72**, 1037.

Mandel, L. and Wolf, E., 1995: *Optical Coherence and Quantum Optics* (Cambridge University Press, Cambridge).

Meschede, D., Walther, H., and Müller, G., 1985: *One-Atom Maser*, Phys. Rev. Lett. **54**, 551–554.

Miller, R., Northup, T. E., Birnbaum, K. M., Boca, A., Boozer, A. D., and Kimble, H. J., 2005: *Trapped Atoms in Cavity QED: Coupling Quantized Light and Matter*, Journal of Physics B: Atomic, Molecular and Optical Physics **38**, S551.

Moehring, D. L., Maunz, P., Olmschenk, S., Younge, K. C., Matsukevich, D. N., Duan, L. M., and Monroe, C., 2007: *Entanglement of Single-Atom Quantum Bits at a Distance*, Nature **449**, 68–71.

Moore, G. and Read, N., 1991: *Nonabelions in the Fractional Quantum Hall Effect*, Nucl. Phys. B **360**, 362 – 396.

Mourik, V., Zuo, K., Frolov, S. M., Plissard, S. R., Bakkers, E. P. A. M., and Kouwenhoven, L. P., 2012: *Signatures of Majorana Fermions in Hybrid Superconductor-Semiconductor Nanowire Devices*, Science **336**, 1003.

Nadj-Perge, S., Drozdov, I. K., Li, J., Chen, H., Jeon, S., Seo, J., MacDonald, A. H., Bernevig, B. A., and Yazdani, A., 2014: *Observation of Majorana Fermions in Ferromagnetic Atomic Chains on a Superconductor*, Science **346**, 602–607.

Nakamura, Y., Pashkin, Y. A., and Tsai, J. S., 1999: *Coherent Control of Macroscopic Quantum States in a Single-Cooper-Pair Box*, Nature **398**, 786–788.

Nation, P. D., Johansson, J. R., Blencowe, M. P., and Nori, F., 2012: *Colloquium : Stimulating Uncertainty: Amplifying the Quantum Vacuum with Superconducting Circuits*, Rev. Mod. Phys. **84**, 1–24.

Nayak, C., Simon, S. H., Stern, A., Freedman, M., and Das Sarma, S., 2008: *Non-Abelian Anyons and Topological Quantum Computation*, Rev. Mod. Phys. **80**, 1083–1159.

Nayak, C. and Wilczek, F., 1996: $2n$*-Quasihole States Realize* $2n-1$*-Dimensional Spinor Braiding Statistics in Paired Quantum Hall States*, Nucl. Phys. B **479**, 529–553.

Nazarov, Yu. V. and Blanter, Ya. M., 2009: *Quantum Transport* (Cambridge University Press, New York).

Negele, J. W. and Orland, H., 1998: *Quantum Many-Particle Systems* (Westview Press).

Nielsen, M. A. and Chuang, I. L., 2010: *Quantum Computation and Quantum Information* (Cambridge University Press, Cambridge).

Nogues, G., Rauschenbeutel, A., Osnaghi, S., Brune, M., Raimond, J. M., and Haroche, S., 1999: *Seeing a Single Photon without Destroying It*, Nature **400**, 239–242.

O'Connell, A. D., *et al.*, 2008: *Microwave Dielectric Loss at Single Photon Energies and Millikelvin Temperatures*, Appl. Phys. Lett. **92**, 112903.

Ohm, C. and Hassler, F., 2014: *Majorana Fermions Coupled to Electromagnetic Radiation*, New J. Phys. **16**, 015009.

Ohm, C. and Hassler, F., 2015a: *Measurement-Induced Entanglement of Two Transmon Qubits by a Single Photon*: arXiv:1508.05104.

Ohm, C. and Hassler, F., 2015b: *Microwave Readout of Majorana Qubits*, Phys. Rev. B **91**, 085406.

Oreg, Y., Refael, G., and von Oppen, F., 2010: *Helical Liquids and Majorana Bound States in Quantum Wires*, Phys. Rev. Lett. **105**, 177002.

Ortmann, F., Roche, S., and Valenzuela, S. O. (Eds.), 2015: *Topological Insulators: Fundamentals and Perspectives* (Wiley-VCH, Weinheim).

Osheroff, D. D., Richardson, R. C., and Lee, D. M., 1972: *Evidence for a New Phase of Solid* He^3, Phys. Rev. Lett. **28**, 885–888.

Paik, H., *et al.*, 2011: *Observation of High Coherence in Josephson Junction Qubits Measured in a Three-Dimensional Circuit QED Architecture*, Phys. Rev. Lett. **107**, 240501.

Pekker, D., Hou, C.-Y., Manucharyan, V. E., and Demler, E., 2013: *Proposal for Coherent Coupling of Majorana Zero Modes and Superconducting Qubits Using the* 4π *Josephson Effect*, Phys. Rev. Lett. **111**, 107007.

Peskin, M. E. and Schroeder, D. V., 1995: *An Introduction to Quantum Field Theory* (Westview Press, Boulder).

Pikulin, D. I. and Nazarov, Yu. V., 2012: *Phenomenology and Dynamics of a Majorana Josephson Junction*, Phys. Rev. B **86**, 140504.

Plenio, M. B., Huelga, S. F., Beige, A., and Knight, P. L., 1999: *Cavity-Loss-Induced Generation of Entangled Atoms*, Phys. Rev. A **59**, 2468–2475.

Purcell, E. M., 1956: *The Question of Correlation between Photons in Coherent Light Rays*, Nature **178**, 1449–1450.

Puri, R. R., 2001: *Mathematical Methods of Quantum Optics* (Springer-Verlag, Berlin).

Qi, X.-L. and Zhang, S.-C., 2011: *Topological Insulators and Superconductors*, Rev. Mod. Phys. **83**, 1057–1110.

Raimond, J. M., Brune, M., and Haroche, S., 2001: *Manipulating Quantum Entanglement with Atoms and Photons in a Cavity*, Rev. Mod. Phys. **73**, 565–582.

Rainis, D. and Loss, D., 2012: *Majorana Qubit Decoherence by Quasiparticle Poisoning*, Phys. Rev. B **85**, 174533.

Read, N. and Green, D., 2000: *Paired States of Fermions in Two Dimensions with Breaking of Parity and Time-Reversal Symmetries and the Fractional Quantum Hall Effect*, Phys. Rev. B **61**, 10267–10297.

Recher, P., Nazarov, Yu. V., and Kouwenhoven, L. P., 2010: *Josephson Light-Emitting Diode*, Phys. Rev. Lett. **104**, 156802.

Reed, M. and Simon, B., 1980: *Functional Analysis*, Vol. I of *Methods of Modern Mathematical Physics* (Academic, San Diego).

Rempe, G., Walther, H., and Klein, N., 1987: *Observation of Quantum Collapse and Revival in a One-Atom Maser*, Phys. Rev. Lett. **58**, 353–356.

Rice, T. M. and Sigrist, M., 1995: Sr_2RuO_4*: An Electronic Analogue of 3 He?*, J. Phys. Cond. Matter **7**, L643.

Riste, D., Dukalski, M., Watson, C. A., de Lange, G., Tiggelman, M. J., Blanter, Y. M., Lehnert, K. W., Schouten, R. N., and DiCarlo, L., 2013: *Deterministic Entanglement of Superconducting Qubits by Parity Measurement and Feedback*, Nature **502**, 350–354.

Roch, N., Schwartz, M. E., Motzoi, F., Macklin, C., Vijay, R., Eddins, A. W., Korotkov, A. N., Whaley, K. B., Sarovar, M., and Siddiqi, I., 2014: *Observation of Measurement-Induced Entanglement and Quantum Trajectories of Remote Superconducting Qubits*, Phys. Rev. Lett. **112**, 170501.

Rokhinson, L. P., Liu, X., and Furdyna, J. K., 2012: *The Fractional a.c. Josephson Effect in a Semiconductor-Superconductor Nanowire as a Signature of Majorana Particles*, Nature Phys. **8**, 795.

Romero, G., García-Ripoll, J. J., and Solano, E., 2009: *Microwave Photon Detector in Circuit QED*, Phys. Rev. Lett. **102**, 173602.

Roy, A., Jiang, L., Stone, A. D., and Devoret, M. H., 2015: *Remote Entanglement by Coherent Multiplication of Concurrent Quantum Signals*, Phys. Rev. Lett. **115**, 150503.

Ruskov, R. and Korotkov, A. N., 2003: *Entanglement of Solid-State Qubits by Measurement*, Phys. Rev. B **67**, 241305.

Ryu, S., Schnyder, A. P., Furusaki, A., and Ludwig, A. W. W., 2010: *Topological Insulators and Superconductors: Tenfold Way and Dimensional Hierarchy*, New J. Phys. **12**, 065010.

San-Jose, P., Prada, E., and Aguado, R., 2012: *ac Josephson Effect in Finite-Length Nanowire Junctions with Majorana Modes*, Phys. Rev. Lett. **108**, 257001.

Sau, J. D., Lutchyn, R. M., Tewari, S., and Das Sarma, S., 2010: *Generic New Platform for Topological Quantum Computation Using Semiconductor Heterostructures*, Phys. Rev. Lett. **104**, 040502.

Sau, J. D., Tewari, S., and Das Sarma, S., 2011: *Probing Non-Abelian Statistics with Majorana Fermion Interferometry in Spin-Orbit-Coupled Semiconductors*, Phys. Rev. B **84**, 085109.

Schleich, W., 2001: *Quantum Optics in Phase Space* (Wiley-VHC, Berlin).

Schmidt, M. J., Rainis, D., and Loss, D., 2012: *Decoherence of Majorana Qubits by Noisy Gates*, Phys. Rev. B **86**, 085414.

Schmidt, T. L., Nunnenkamp, A., and Bruder, C., 2013a: *Majorana Qubit Rotations in Microwave Cavities*, Phys. Rev. Lett. **110**, 107006.

Schmidt, T. L., Nunnenkamp, A., and Bruder, C., 2013b: *Microwave-Controlled Coupling of Majorana Bound States*, New J. Phys. **15**, 025043.

Schnyder, A. P., Ryu, S., Furusaki, A., and Ludwig, A. W. W., 2008: *Classification of Topological Insulators and Superconductors in Three Spatial Dimensions*, Phys. Rev. B **78**, 195125.

Schnyder, A. P., Ryu, S., Furusaki, A., and Ludwig, A. W. W., 2009: *Classification of Topological Insulators and Superconductors*, AIP Conference Proceedings **1134**, 10–21.

Schoelkopf, R. J. and Girvin, S. M., 2008: *Wiring Up Quantum Systems*, Nature **451**, 664–669.

Schreier, J. A., *et al.*, 2008: *Suppressing Charge Noise Decoherence in Superconducting Charge Qubits*, Phys. Rev. B **77**, 180502.

Schrieffer, J. R. and Wolff, P. A., 1966: *Relation between the Anderson and Kondo Hamiltonians*, Phys. Rev. **149**, 491–492.

Scully, M. O. and Lamb, W. E., 1967: *Quantum Theory of an Optical Maser. I. General Theory*, Phys. Rev. **159**, 208.

Sengupta, K., Žutić, I., Kwon, H.-J., Yakovenko, V. M., and Das Sarma, S., 2001: *Midgap Edge States and Pairing Symmetry of Quasi-One-Dimensional Organic Superconductors*, Phys. Rev. B **63**, 144531.

Sexl, R. U. and Urbantke, H. K., 2001: *Relativity, Groups, Particles* (Springer-Verlag, Wien).

Shor, P. W., 1994: *Algorithms for Quantum Computation: Discrete Logarithms and Factoring*, in *Proceedings of the 35th Annual Symposium on Foundations of Computer Science* (IEEE Press, Los Alamitos), (pp. 124).

Silveri, M., Zalys-Geller, E., Hatridge, M., Leghtas, Z., Devoret, M. H., and Girvin, S. M., 2015: *Theory of Remote Entanglement via Quantum-limited Phase-Preserving Amplification*: arXiv:1507.00732.

Stern, A. and Halperin, B. I., 2006: *Proposed Experiments to Probe the Non-Abelian $\nu = 5/2$ Quantum Hall State*, Phys. Rev. Lett. **96**, 016802.

Sudarshan, E. C. G., 1963: *Equivalence of Semiclassical and Quantum Mechanical Descriptions of Statistical Light Beams*, Phys. Rev. Lett. **10**, 277–279.

Susskind, L. and Glogower, J., 1964: *Quantum Mechanical Phase and Time Operator*, Physics **1**, 49–61.

Tewari, S., Zhang, C., Das Sarma, S., Nayak, C., and Lee, D.-H., 2008: *Testable Signatures of Quantum Nonlocality in a Two-Dimensional Chiral p-Wave Superconductor*, Phys. Rev. Lett. **100**, 027001.

Thompson, R. J., Rempe, G., and Kimble, H. J., 1992: *Observation of Normal-Mode Splitting for an Atom in an Optical Cavity*, Phys. Rev. Lett. **68**, 1132–1135.

Tinkham, M., 1996: *Introduction to Superconductivity* (McGraw-Hill, New York), 2nd ed.

Trauzettel, B., Jordan, A. N., Beenakker, C. W. J., and Büttiker, M., 2006: *Parity Meter for Charge Qubits: An Efficient Quantum Entangler*, Phys. Rev. B **73**, 235331.

Trif, M. and Tserkovnyak, Y., 2012: *Resonantly Tunable Majorana Polariton in a Microwave Cavity*, Phys. Rev. Lett. **109**, 257002.

Ulrich, J. and Hassler, F., 2015: *Majorana-Assisted Nonlocal Electron Transport through a Floating Topological Superconductor*, Phys. Rev. B **92**, 075443.

Unruh, W. G., 1976: *Notes on Black-Hole Evaporation*, Phys. Rev. D **14**, 870–892.

Vahala, K. J., 2003: *Optical Microcavities*, Nature **424**, 839–846.

Van Duzer, T. and Turner, C. W., 1999: *Principles of Superconductive Devices and Circuits* (Prentice Hall, Upper Saddle River), 2nd ed.

van Heck, B., Akhmerov, A. R., Hassler, F., Burrello, M., and Beenakker, C. W. J., 2012: *Coulomb-Assisted Braiding of Majorana Fermions in a Josephson Junction Array*, New J. Phys. **14**, 035019.

van Heck, B., Hassler, F., Akhmerov, A. R., and Beenakker, C. W. J., 2011: *Coulomb Stability of the 4π-Periodic Josephson Effect of Majorana Fermions*, Phys. Rev. B **84**, 180502(R).

Virtanen, P. and Recher, P., 2013: *Microwave Spectroscopy of Josephson Junctions in Topological Superconductors*, Phys. Rev. B **88**, 144507.

Visscher, E. H., Verbrugh, S. M., Lindeman, J., Hadley, P., and Mooij, J. E., 1995: *Fabrication of Multilayer Single-Electron Tunneling Devices*, Appl. Phys. Lett. **66**, 305.

Vollhardt, D. and Wölfle, P., 1990: *The Superfluid Phases of Helium 3* (Taylor & Francis, London).

Volovik, G. E., 2003: *The Universe in a Helium Droplet*, Vol. 117 of *International series of monographs on physics* (Clarendon Press).

von Neumann, J., 1955: *Mathematical Foundations of Quantum Mechanics* (Princeton University Press, Princeton).

von Weizäcker, C. F., 1985: *Aufbau der Physik* (Hanser, München).

Wallraff, A., Schuster, D. I., Blais, A., Frunzio, L., Huang, R. S., Majer, J., Kumar, S., Girvin, S. M., and Schoelkopf, R. J., 2004: *Strong Coupling of a Single Photon to a Superconducting Qubit Using Circuit Quantum Electrodynamics*, Nature **431**, 162–167.

Walls, D. F. and Milburn, G. J., 2008: *Quantum Optics* (Springer-Verlag).

Walther, H., Varcoe, B. T. H., Englert, B.-G., and Becker, T., 2006: *Cavity Quantum Electrodynamics*, Rep. Prog. Phys. **69**, 1325–1382.

Wen, X.-G., 2004: *Quantum Field Theory of Many-Body Systems* (Oxford University Press).

Weyl, H., 1927: *Quantenmechanik und Gruppentheorie*, Z. Phys. **46**, 1–46.

Wilczek, F., 1982: *Magnetic Flux, Angular Momentum, and Statistics*, Phys. Rev. Lett. **48**, 1144–1146.

Wilczek, F., 2009: *Majorana Returns*, Nat. Phys. **5**, 614–618.

Williams, N. S. and Jordan, A. N., 2008: *Entanglement Genesis under Continuous Parity Measurement*, Phys. Rev. A **78**, 062322.

Winkler, R., 2003: *Spin–Orbit Coupling Effects in Two-Dimensional Electron and Hole Systems* (Springer-Verlag, Berlin).

Yanson, I. K., Svistuno, V. M., and Dmitrenko, I. M., 1965: *Experimental Observation of Tunnel Effect for Cooper Pairs with Emission of Photons*, JETP Lett. **21**, 650.

Yavilberg, K., Ginossar, E., and Grosfeld, E., 2015: *Fermion Parity Measurement and Control in Majorana Circuit Quantum Electrodynamics*, Phys. Rev. B **92**, 075143.

Yuen, H. P., 1976: *Two-Photon Coherent States of the Radiation Field*, Phys. Rev. A **13**, 2226.

Yurke, B. and Stoler, D., 1992a: *Bell's-Inequality Experiments Using Independent-Particle Sources*, Phys. Rev. A **46**, 2229–2234.

Yurke, B. and Stoler, D., 1992b: *Einstein-Podolsky-Rosen Effects from Independent Particle Sources*, Phys. Rev. Lett. **68**, 1251–1254.

Zimmerli, G., Eiles, T. M., Kautz, R. L., and Martinis, J. M., 1992: *Noise in the Coulomb Blockade Electrometer*, Appl. Phys. Lett. **61**, 237–239.

Zueco, D., Reuther, G. M., Kohler, S., and Hänggi, P., 2009: *Qubit-Oscillator Dynamics in the Dispersive Regime: Analytical Theory beyond the Rotating-Wave Approximation*, Phys. Rev. A **80**, 033846.

Żukowski, M., Zeilinger, A., Horne, M. A., and Ekert, A. K., 1993: *"Event-Ready-Detectors" Bell Experiment via Entanglement Swapping*, Phys. Rev. Lett. **71**, 4287–4290.

Index

S

T

U

V

W

Z

List of Publications

- Ohm, C. and Hassler, F., 2014: *Majorana fermions coupled to electromagnetic radiation*, New. J. Phys. **16**, 015009. [Chapter 4]
- Ohm, C. and Hassler, F., 2015: *Microwave readout of Majorana qubits*, Phys. Rev. B **91**, 085406. [Chapter 5]
- Ohm, C. and Hassler, F., 2015: *Measurement-induced entanglement of two transmon qubits by a single photon*: arXiv:1508.05104. [Chapter 6]